



Engineering for Particle Accelerators

The fundamentals of large-scale linear accelerator engineering

Vyacheslav Yakovlev, Fermilab

U.S. Particle Accelerator School (USPAS)

Education in Beam Physics and Accelerator Technology

15 July, 2024

Engineering for Particle Accelerators

Instructors: Vyacheslav Yakovlev, Timergali Khabiboulline, Thomas Nicol, and Miao Yu, Fermilab, Batavia

One-week course at USPAS 2024, Rohnert Park, July 15-19, 2024

Purpose and Audience:

The purpose of this course is to give an engineering foundation to the development of modern particle accelerators. This course is suitable for graduate students, senior undergraduate students, and engineers interested in particle accelerator design and development. The course will focus on large-scale proton superconducting linear particle accelerators.

Prerequisites

Undergraduate-level electromagnetism, classical mechanics, RF and mechanical engineering courses.

It is the responsibility of the student to ensure that he or she meets the course prerequisites or has equivalent experience.

Engineering for Particle Accelerators

Objectives

Students will learn basic principles of the engineering design of large-scale proton superconducting linear particle accelerators. Upon completing this course, students will be familiar with the principles, approach, and basic technique of the design of the main components in superconducting linear accelerators and be able to perform basic analysis on their performance.

Instructional Method

The course will consist of lectures and daily homework assignments on the fundamentals of engineering of superconducting linear particle accelerators.

Engineering for Particle Accelerators

Course Content

* The course will cover the fundamentals of superconducting accelerator engineering and provide examples and exercises in the practical design of the main accelerator components.

* Topics will include:

- general accelerator layout and parameter optimization; operational regime dependent technology selection;
- general cryomodule design issues, challenges, principles, and approaches;
- RF optimization and design of superconducting RF cavities and components;

Engineering for Particle Accelerators

- cavity processing recipes and procedures; engineering issues and challenges of SRF cavity mechanical design and fabrication;
- problems and techniques for design of focusing elements for superconducting accelerator applications (room-temperature and superconducting);
- diagnostics and alignment;
- cavity and cryomodule testing and commissioning.

Engineering for Particle Accelerators

Reading Requirements

It is ***recommended*** that students re-familiarize themselves with the fundamentals of electrodynamics at the level of

“Classical Electrodynamics” (Chapters 1 through 8) by J. D. Jackson, John Wiley & Sons, 3rd edition (1999).

Additional ***suggested*** reference material:

“Handbook of Accelerator Physics and Engineering”, edited by A. W. Chao and M. Tigner, World Scientific, 3rd print (2006);

“RF Superconductivity: Science, Technology, and Applications,” by H. Padamsee, Wiley-VCH (2009).

Engineering for Particle Accelerators

Daily Schedule (continuation)

	Monday	Tuesday
9:00-11:30	Vyacheslav (Slava) Yakovlev, The fundamentals of large-scale linear accelerator engineering	Timergali Khabiboulline, SRF cavity EM and mechanical design, RF measurements and tuning
11:30-13:00	Lunch	Lunch
13:00-17:30	Vyacheslav (Slava) Yakovlev, The fundamentals of large-scale linear accelerator engineering (continuation)	Timergali Khabiboulline, SRF cavity EM and mechanical design, RF measurements and tuning (continuation)
19:00-21:00	Study	Study

Engineering for Particle Accelerators

Daily Schedule

	Wednesday	Thursday
9:00-11:30	Thomas Nicol, Mechanical Engineering in Superconducting Magnet and RF Cryomodule Design	Miao Yu, Engineering for Particle Accelerators - Magnets
11:30-13:00	Lunch	Lunch
13:00-17:30	Thomas Nicol, Mechanical Engineering in Superconducting Magnet and RF Cryomodule Design (continuation)	Miao Yu, Engineering for Particle Accelerators – Magnets (continuation)
19:00-21:00	Study	Study

Engineering for Particle Accelerators

Daily Schedule (continuation)

Friday 7/19

9:00-12:00 Wrap-up

USPAS 2024 Students:

1	Angelo, Joseph	LBNL and Indiana University
2	Chen, Jing	SLAC
3	Fletcher, Ethan	Michigan State University
4	Geelhoed, Michael	Fermilab
5	Helsper, Josh	Fermilab
6	Hlavenka, Joshua	Argonne National Lab and Indiana University
7	Intwala, Nishi	Indiana University and LBNL
8	Kim, Kuktae	SLAC
9	Li, Guangjiang	Brookhaven National Lab
10	Loftin, Evan	Los Alamos National Lab
11	Martinic, Kean	Indiana University and Idaho State University
12	McIntyre, Megan	Argonne National Lab and DePaul University
13	Mujica-Schwahn, Natalie	Honeywell International Inc.
14	Olander, Michael	Fermilab and Indiana University
15	Tutt, Patrick	Michigan State University

Vyacheslav (Slava) P. Yakovlev received MS degree in accelerator physics from Novosibirsk State University (NSU), Russia, in 1977, and PhD in accelerator physics from Budker Institute for Nuclear Physics (Budker INP), Novosibirsk, Russia, in 1988, where he worked as a Research scientist and since 1988 as a Senior Scientist. From 1994 to 1996 he was an Associate Professor at Novosibirsk State Technical University. Since 1996 he worked at Yale Beam Lab, Physics Department, Yale University, and Omega-P Inc as a Senior Scientist. Since 2007 he works at Fermilab as a Senior Scientist. Since 2011 to 2021 he was the Head of SRF Development Department at Application Science and Technology Division of Fermilab. Since 2021 to present he is the Head of Quantum Microwave System Department, Superconducting Quantum Materials and Systems Division of Fermilab. From 2017 to present he is an Adjunct Professor of Accelerator Science, Facility for Rare Isotope Beams, Michigan State University, Lansing, USA.

The scope of his professional interest includes physics and techniques of particle accelerators, namely: theory and simulations of the fields and beam dynamics in linear and circular accelerators; physics and technique of RF accelerator structures including room temperature cavities and structures, superconducting cavities and ferrite-tuned cavities; high power RF systems and RF sources for accelerators; tuning systems and cryo-module design, SRF for Quantum Computers. Over 400 publications.



RF accelerating structures

Outline:

1. Introduction;
2. Accelerating, focusing and bunching properties of RF field;
3. RF Cavities for Accelerators

Chapter 1.

Introduction.

Accelerators for scientific applications.

High – Energy Electron accelerators: High Energy Physics, Nuclear Physics, Free-Electron Lasers

High – Energy Proton accelerators: High Energy Physics, Nuclear Physics, source of secondary particles (neutrons, pions, muons, neutrinos), material science, Accelerator-Driven Subcritical reactors (ADS).

Specifics of proton accelerators: protons are non- or weakly relativistic up to high energies: rest mass for protons is 0.938 GeV (compared to 0.511 MeV for electrons).

Types of the accelerators

□ Electrostatic accelerators – acceleration in DC field

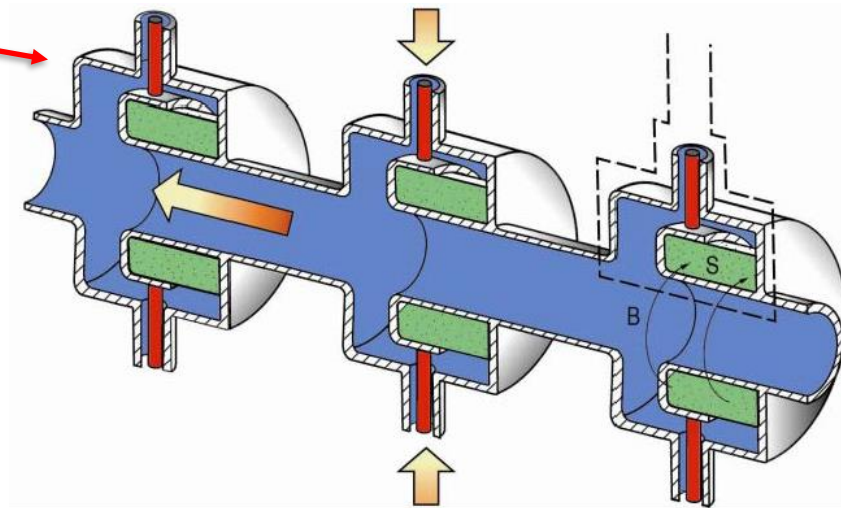
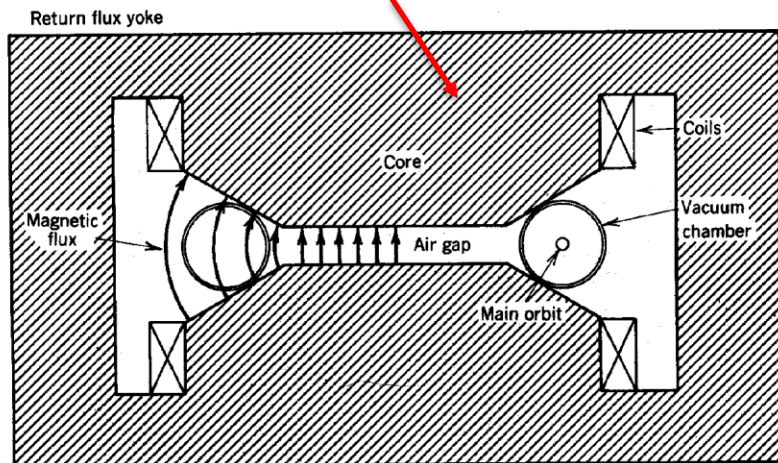
- Van de Graaff (moving belt to charge the high –voltage electrode)
- Cockcroft-Walton (diode-capacitor voltage multiplier).

□ Electrodynamic accelerators – acceleration in changing EM field.

❖ Induction accelerators – acceleration in pulsed eddy electric field

- *Linear induction accelerator*
- *Cyclic induction accelerator*

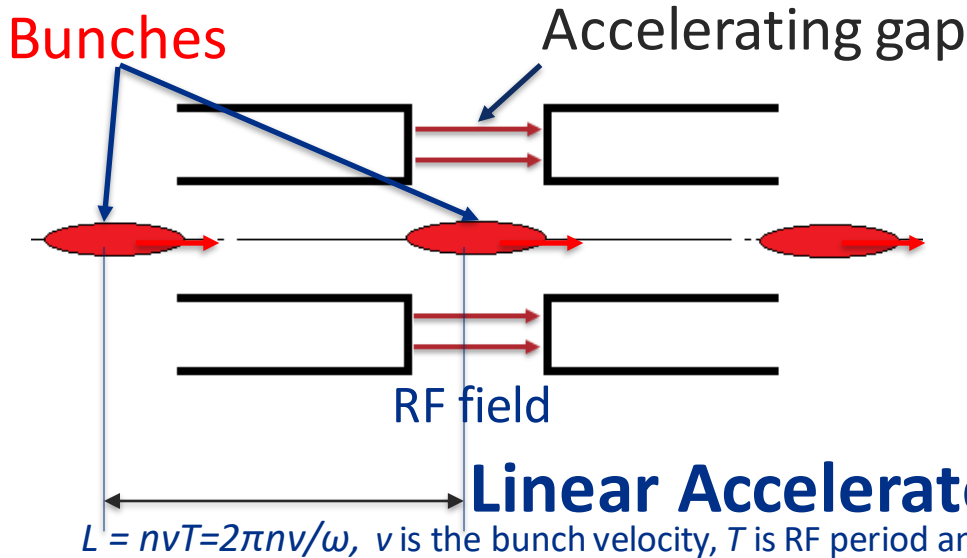
- Betatron



$$e \oint \vec{E} \cdot d\vec{l} = -e \frac{\partial}{\partial t} \int_S \vec{B} \cdot d\vec{S}$$

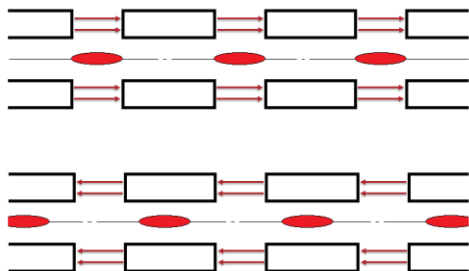
Types of the accelerators

- RF accelerators – acceleration in RF field
- Bunched beam (no particles when the field is decelerating);
- Accelerating RF field is excited in an accelerating gap;



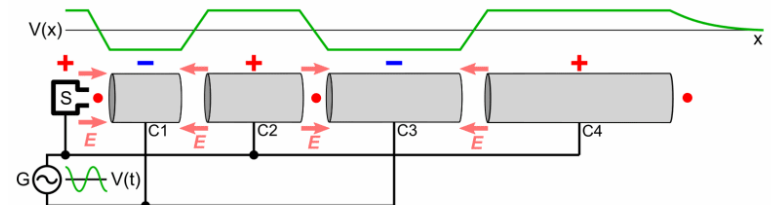
RF field: $E = E_0 \cos(\omega t)$

Particle energy gain $\Delta U \sim E_0$



$\omega t = 2\pi m$, $m=0,1,2,\dots$

$\omega t = (2m+1)\pi$, $m=0,1,2,\dots$

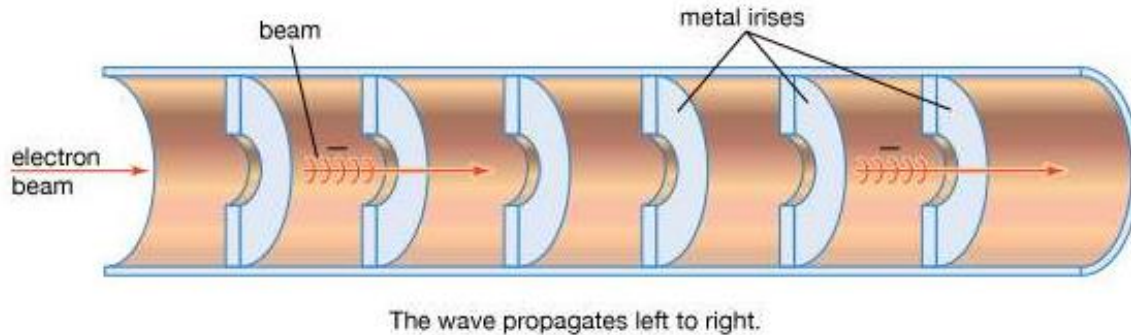


Animation from Wikipedia

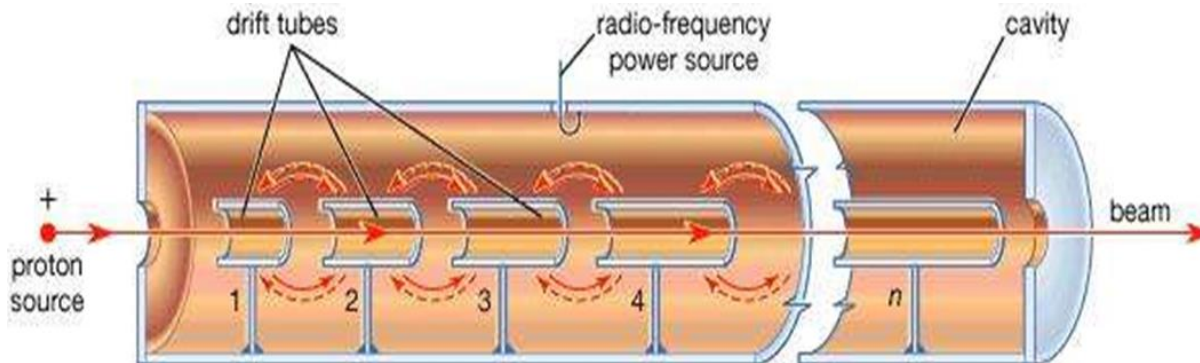
(https://en.wikipedia.org/wiki/Particle_accelerator)

RF linear accelerators

- Travelling wave accelerators.



- Standing wave accelerators.

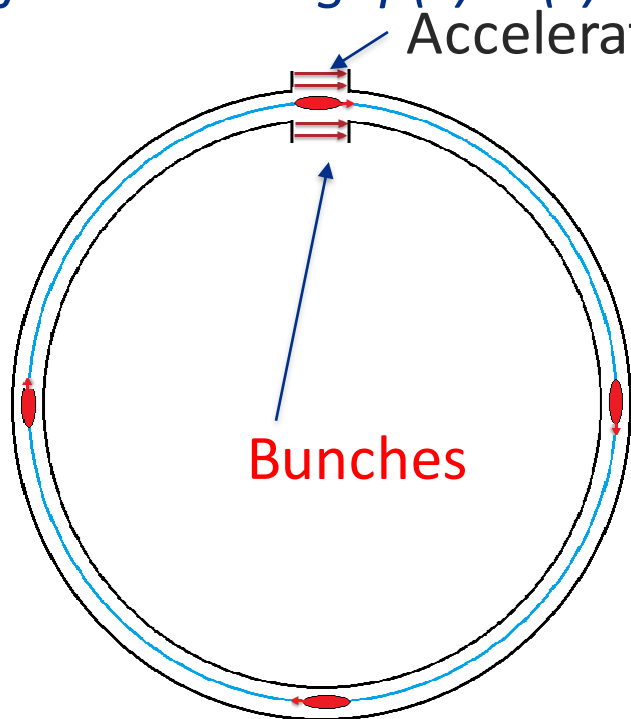


- Room Temperature linear accelerators
- Superconducting linear accelerators

Types of the accelerators

- An accelerated particle passes the same gap many times (cyclic accelerator).

RF fields in the gap(s): $E(t) = E_0 \cos(\omega t)$

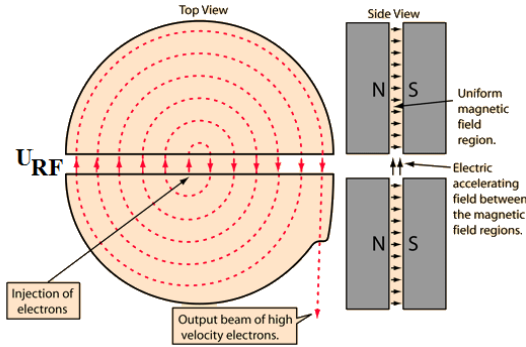


$$\omega = \Omega Nq;$$

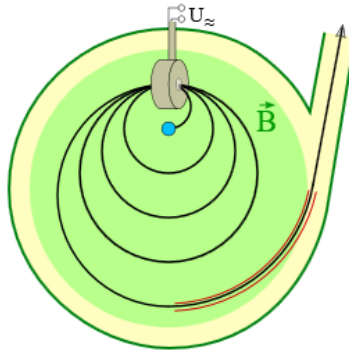
ω is RF frequency,
 Ω is the bunch revolution frequency,
 N is number of bunches
 $q=1,2,3\dots$

$$\omega t = 2\pi m, m=0,1,2\dots$$

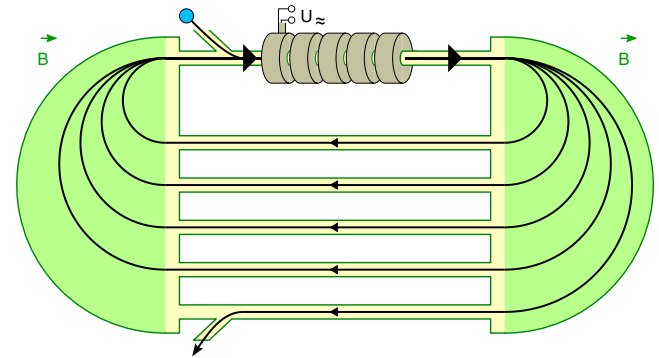
Cyclic accelerators



Cyclotron

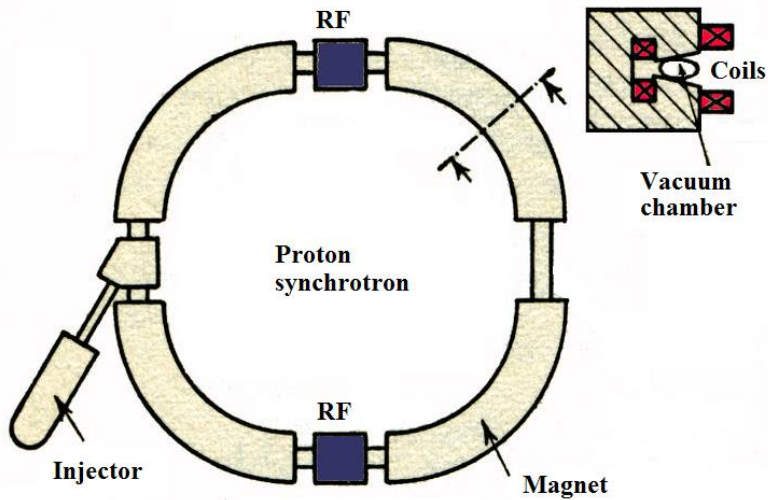


Microtron



Racetrack

$$B = \text{const}, f_{rf} = \text{const}$$

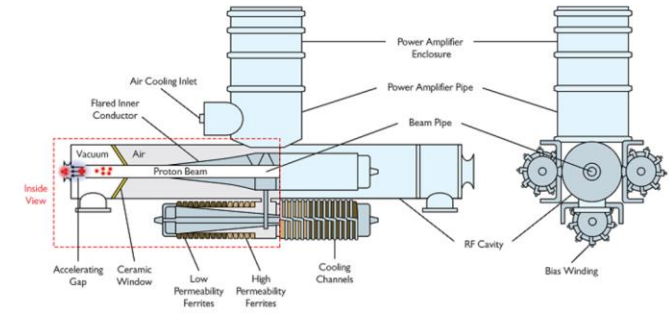


Proton synchrotron:

$$B = B(t), f_{rf} = f_{rf}(t)$$

RF cavities for accelerators

To achieve high accelerating field in the gap resonant RF cavities are used. In all modern RF accelerators, the beam acceleration takes place in a resonance wave (standing or travelling) electromagnetic field excited in an RF cavities.



CW 50.6 MHz cavity of PSI cyclotron. $V = 1.2$ MV

Superconducting 805 MHz multi-cell cavities of SNS linac. $V = 10-15$ MV, $DF = 6\%$.

Tunable cavity for FNAL Booster Synchrotron $F = 37.8-52.8$ MHz. $V = 60$ kV, $DF = 50\%$

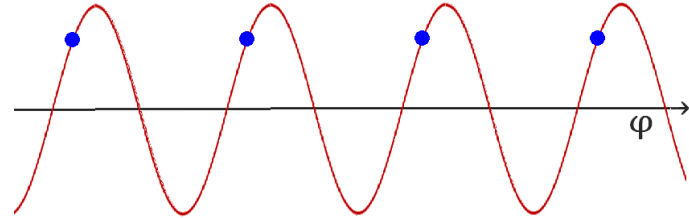


Acceleration principles:

If the charged particle reaches the center of the accelerating gap in arbitrary phase φ , its energy gain is

$$V(\varphi) = V \cos(\varphi)$$

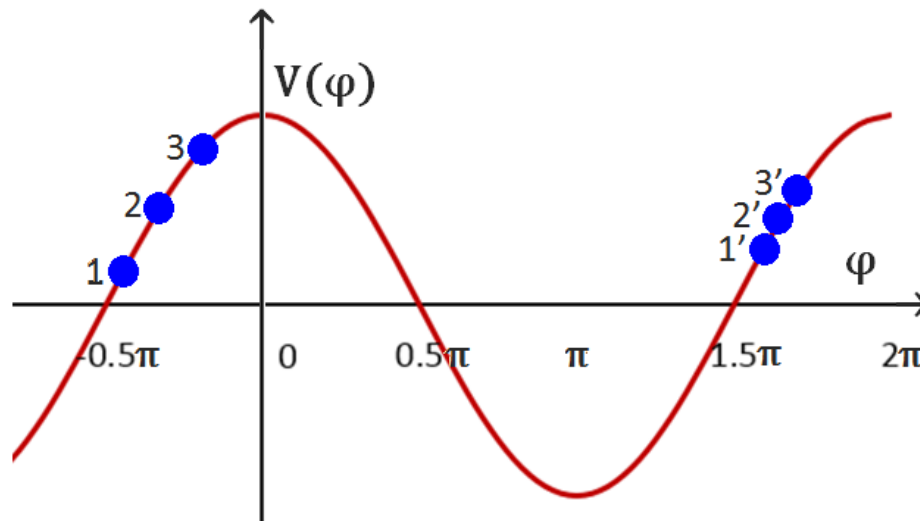
Acceleration: $-\pi/2 < \varphi < \pi/2$



- **Synchronism:** the bunches should reach the center of the acceleration gaps in the same accelerating phase.
- **Autophasing:** longitudinal dynamics should be stable (no bunch lengthening). For linear accelerator $-\pi/2 < \varphi_s < 0$ (φ_s is the phase of the bunch center)



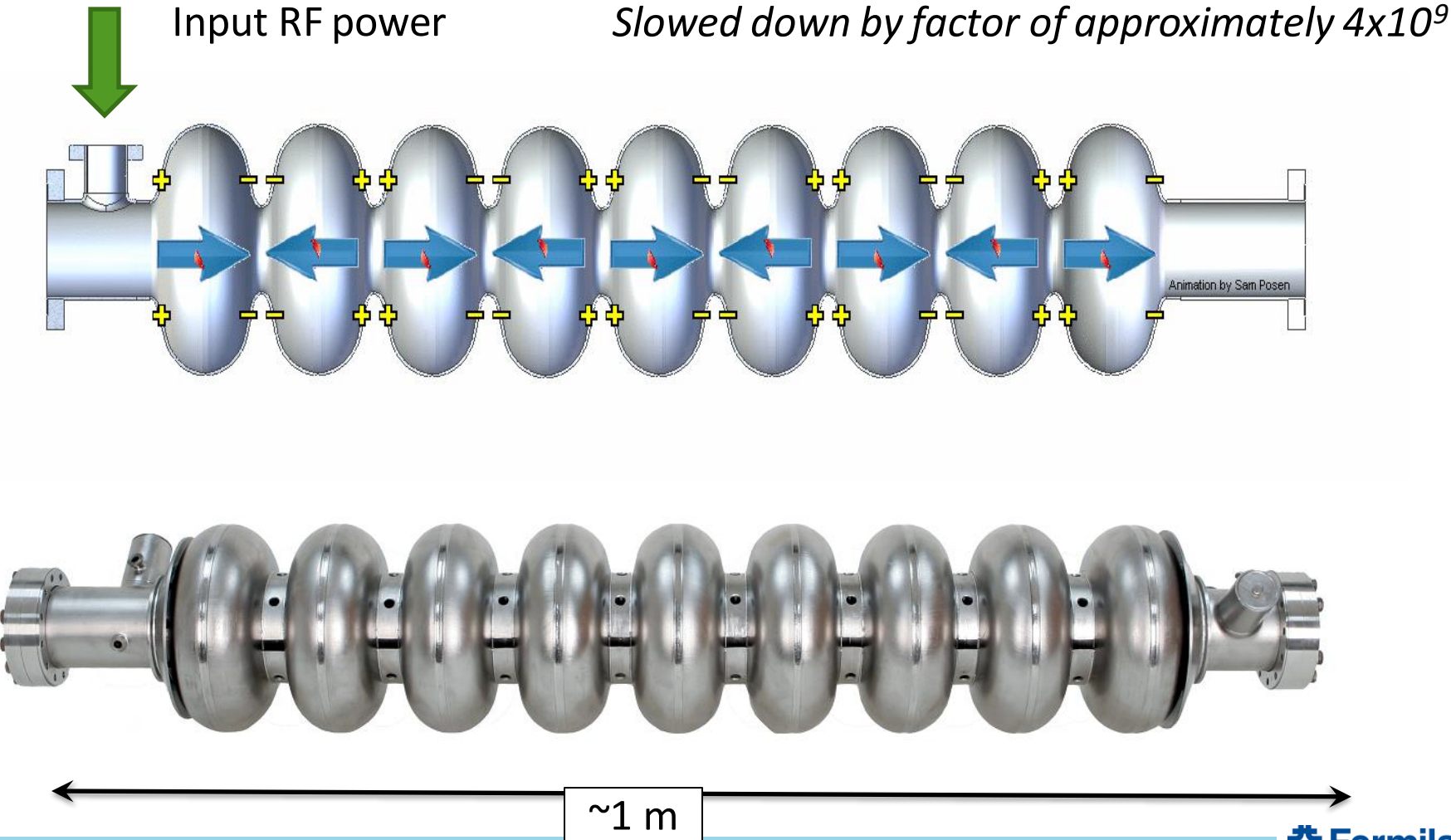
V. Veksler



(linear accelerator)

Illustration of synchronism :

1.3 GHz ILC cavity (animation by Sam Posen, FNAL)



“I do not think that the radio waves I have discovered
will have any practical application.”
– Heinrich Hertz

Chapter 2.

Accelerating and focusing properties of RF field.

- a. Acceleration of charged particles in electromagnetic field;
- b. Focusing properties of RF field;
- c. Bunching properties of RF field;
- d. Summary.

Acceleration and focusing of charged particles in electromagnetic field

Electromagnetic fields in RF cavities are described by Maxwell equations:

$$\text{curl} \vec{E} = -\frac{\partial \vec{B}}{\partial t}, \quad \text{curl} \vec{H} = \frac{\partial \vec{D}}{\partial t} + \vec{J}, \quad \frac{\partial \rho}{\partial t} + \text{div} \vec{J} = 0$$



$$\text{div} \vec{B} = 0, \quad \text{div} \vec{D} = \rho.$$

Linear media:

$$\vec{D} = \epsilon \vec{E}, \quad \vec{B} = \mu \vec{H}, \quad \vec{J} = \sigma \vec{E}.$$

Harmonic oscillations:

$$\vec{E} = \vec{E}(r) \cdot e^{i\omega t}, \quad \text{curl} \vec{E} = -i\omega \mu \vec{H}, \quad \text{curl} \vec{H} = i\omega \epsilon \vec{E}.$$

For vacuum:

$$\mu_0 = 4\pi \cdot 10^{-7} \frac{H}{m}, \quad \epsilon_0 = \frac{10^{-9}}{36\pi} \approx 0.884 \cdot 10^{-11} \frac{F}{m}.$$

Vacuum impedance Z_0 :

$$Z_0 = \sqrt{\frac{\mu_0}{\epsilon_0}} = 120\pi \text{ Ohm}; \quad \frac{1}{\sqrt{\epsilon_0 \mu_0}} = c, \quad c \text{ is speed of light.}$$

$$\nabla \equiv \sum_{i=1}^3 \vec{e}_i \frac{\partial}{\partial x_i}$$

$$\text{grad } f \equiv \nabla f$$

$$\text{div} \vec{A} \equiv \nabla \cdot \vec{A}$$

$$\text{curl} \vec{A} \equiv \text{rot} \vec{A} \equiv \nabla \times \vec{A}$$

\vec{E} - electric field strength, V/m
 \vec{D} - electric field induction, C/m^2
 \vec{B} - magnetic field induction, T
 \vec{H} - magnetic field strength, A/m
 ϵ - permittivity, F/m
 μ - permeability, H/m
 σ - conductivity, S/m
 $\frac{\partial \vec{D}}{\partial t}$ - displacement current density
 \vec{J} - current density, A/m^2
 ρ - charge density, C/m^3

Acceleration and focusing of charged particles in electromagnetic field

From Maxwell equations:

$$-\text{curl curl } \vec{E} = -\omega^2 \epsilon \mu \vec{E} + i\omega \mu \vec{j}$$

For $\vec{j}=0$

$$\text{curl curl } \vec{E} = \omega^2 \epsilon \mu \vec{E} \quad \text{or}$$

$$\Delta \vec{E} + k^2 \vec{E} = 0,$$

Here $k^2 = \omega^2 \epsilon \mu$, $\Delta \equiv \text{grad div} - \text{curl curl}$

Same for magnetic field:

$$\Delta \vec{H} + k^2 \vec{H} = 0$$

$$\Delta = \frac{\partial^2}{\partial x^2} + \frac{\partial^2}{\partial y^2} + \frac{\partial^2}{\partial z^2}$$

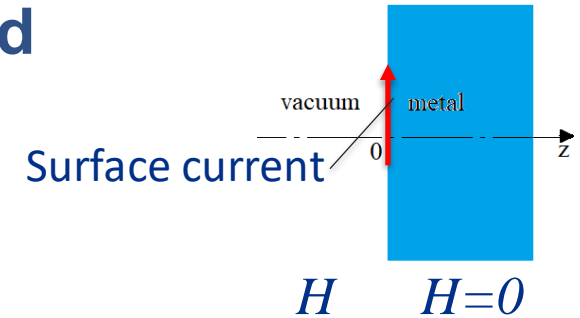
Cartesian (x, y, z)

$$\Delta = \frac{1}{r} \frac{\partial}{\partial r} \left(r \frac{\partial}{\partial r} \right) + \frac{1}{r^2} \frac{\partial^2}{\partial \varphi^2} + \frac{\partial^2}{\partial z^2}$$

Cylindrical (r, φ, z)

Acceleration and focusing of charged particles in electromagnetic field

- Boundary conditions on a conductive wall:



$$\vec{E}_t = Z_s(k) [\vec{H}_t \times \vec{n}],$$

where $Z_s(k)$ is a surface impedance, \vec{n} is directed to the metal.

“Ideal metal”: $Z_s = 0$ or $\vec{E}_t = 0$.

- Wall power loss:

$$P = \frac{1}{2} \text{Re} \int (\vec{E} \times \vec{H}) \cdot \vec{n} dS = \frac{1}{2} \int R_s |H_t|^2 dS,$$

R_s is the surface resistance,

$$R_s = \text{Re}(Z_s(k))$$

Acceleration and focusing of charged particles in electromagnetic field

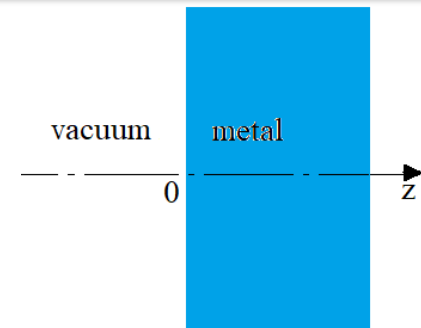
1. Normal-conducting metal, classical skin effect (CSE).

$$\text{curl}\vec{E} = -i\omega\vec{B}, \text{curl}\vec{H} = i\omega\vec{D} + \vec{J} \approx \sigma\vec{E} \quad (\text{in metal } \omega\vec{D} \ll \vec{J} = \sigma\vec{E}),$$

σ is the wall material conductivity.

↓

↑
Ohm's law



$$\text{curl}\text{curl}\vec{H} = -i\omega\mu_0\sigma\vec{H} \rightarrow \underline{\underline{\frac{d^2H_y}{dz^2} = -i\omega\mu_0\sigma H_y = -ikZ_0\sigma H_y}}$$

↓

$$H_y(z) = H_s e^{-(1-i)z/\delta}, \quad \delta = \sqrt{\frac{2}{kZ_0\sigma}}, \quad H_s = H_y(0)$$

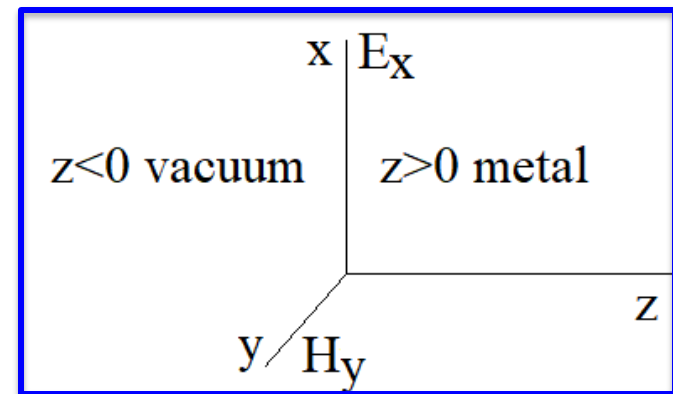
↓

$$E_x(z) = -\frac{1}{\sigma} \frac{dH_y(z)}{dz} = (1-i) \frac{H_s}{\delta\sigma} e^{-(1-i)z/\delta}$$

$$(\text{curl}\vec{H} = -\frac{dH_y(z)}{dz} \approx \sigma\vec{E})$$

↓

$$\frac{E_x(0)}{H_y(0)} = Z_s(k) = (1-i) \frac{1}{\delta\sigma} \quad \longrightarrow \quad Z_s(k) = (1-i) \sqrt{\frac{kZ_0}{2\sigma}}$$



Acceleration and focusing of charged particles in electromagnetic field

- Surface impedance

$$Z_s(k) = \sqrt{\frac{kZ_0}{2\sigma}} (1 - i)$$

where σ is the wall material conductivity.

For copper at room temperature (20°C) $\sigma = 59 \text{ MS/m}$.

- Surface resistivity:

$$R_s = \text{Re}[Z_s(k)] = \sqrt{\frac{kZ_0}{2\sigma}} = \sqrt{\frac{\omega Z_0}{2c\sigma}}$$

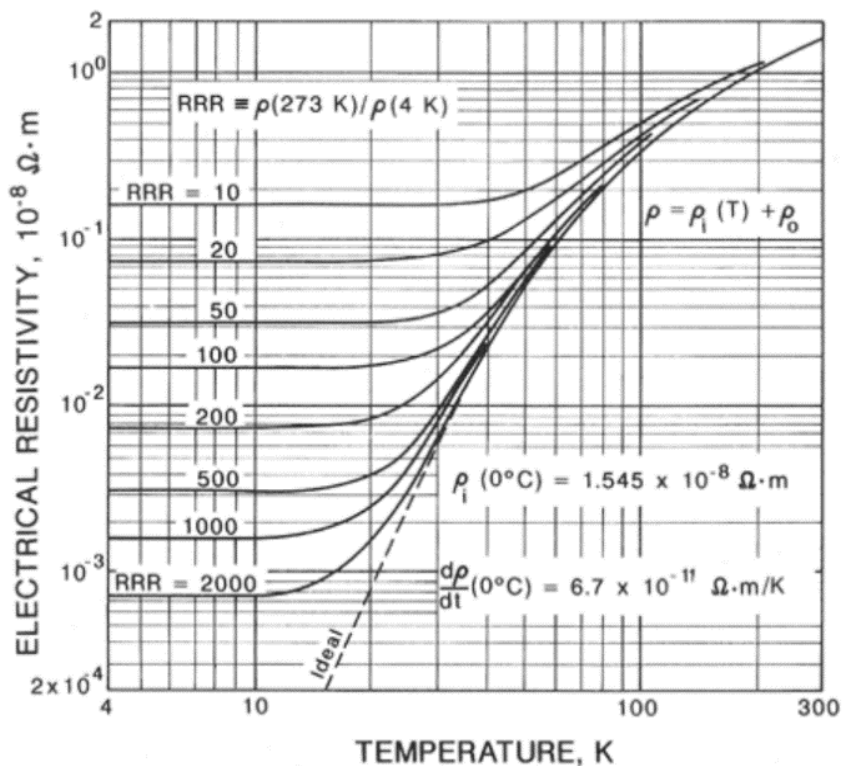
- The RF field $H(z)$ and $E(z)$ decays into the metal exponentially with the distance from the surface z :

$$\frac{H(z)}{H_s} = \frac{E(z)}{E_s} = e^{-(1-i)z/\delta}, \quad \delta = \sqrt{\frac{2}{kZ_0\sigma}} \text{ - classical skin depth.}$$

Acceleration and focusing of charged particles in electromagnetic field

- For pure metals, the conductivity decreases with the temperature.

Copper resistivity $\rho = \sigma^{-1}$ versus temperature for different sample purity:



A commonly used measure of purity is the residual resistivity ratio (RRR), defined as the ratio of the resistivity at 273 K or 0°C over the resistivity at 4K*:

$$RRR = \frac{\rho(273 K)}{\rho(4K)}$$

*In some papers they use $RRR = \frac{\rho(293 K)}{\rho(4K)}$

Acceleration and focusing of charged particles in electromagnetic field

2. Normal-conducting metal, anomalous skin effect (ASE)*:

- At low temperature of metal skin depth δ may be smaller than the mean-free path l of conducting electrons, $l = \frac{\sigma(T)Z_0 cv_F}{\omega_p^2}$ (1) **it is anomalous skin effect.**

Here v_F is the Fermi velocity and ω_p is the plasma frequency of conducting electrons.

- Surface impedance frequency dependence can be estimated using simple consideration, so called “ineffectiveness concept” for extreme ASE, when $\delta/l \ll 1$ (A.B. Pippard, 1947).
 - Solid angle of all the trajectories of electrons started in a thin layer, it is $\sim 2\pi$ in the case when $\delta/l \ll 1$.
 - Solid angle for the effective electrons is $2\pi \times \delta/l$, and the portion of effective electrons, therefore, is δ/l .

- Effective conductance: $\sigma_{eff} \sim \sigma \cdot \frac{\delta}{l}$ (2) $\rightarrow \delta = \sqrt{\frac{2}{kZ_0\sigma_{eff}}}$ (3), $R_s = \sqrt{\frac{kZ_0}{2\sigma_{eff}}}$ (4)

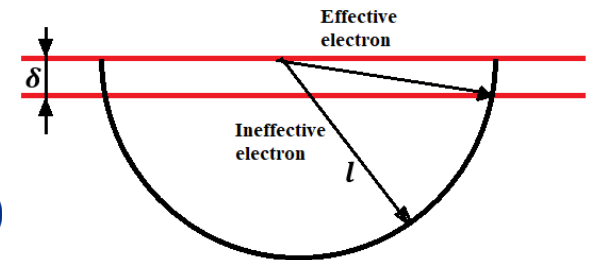
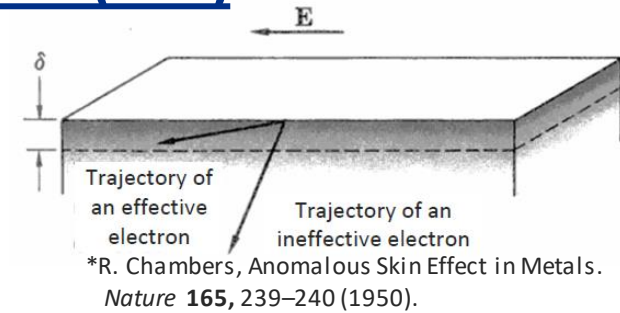


- From (1-4) it follows that $R_s = Z_0 \cdot \left(\frac{k^2 cv_F}{4\omega_p^2}\right)^{1/3}$ (5).

- Exact formula for extreme ASE based on kinetic equations together with Maxwell equations (G.E. Reuter, E.H. Sondheimer, 1948)

$$R_s = Z_0 \cdot \left(\frac{\sqrt{3}k^2 cv_F}{16\pi\omega_p^2}\right)^{1/3}$$

which differs from simple estimation (5) by factor of $\left(\frac{\sqrt{3}}{4\pi}\right)^{-1/3} \approx 2$ only!



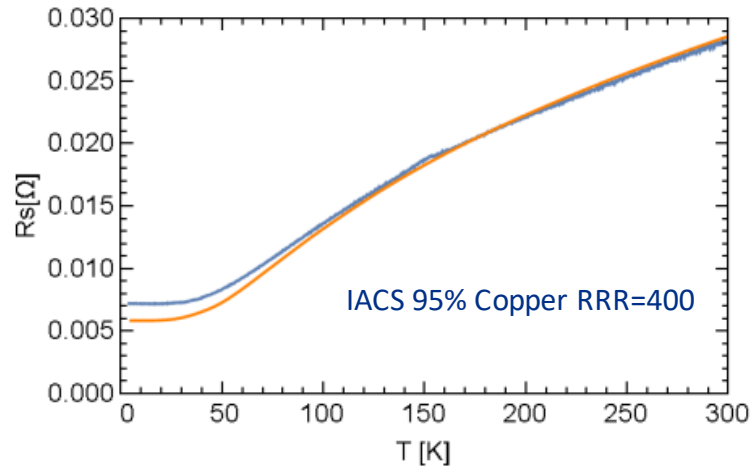
Acceleration and focusing of charged particles in electromagnetic field

- For extreme anomalous skin effect ($l \gg \delta$) the complex surface resistance Z_s may be estimated as

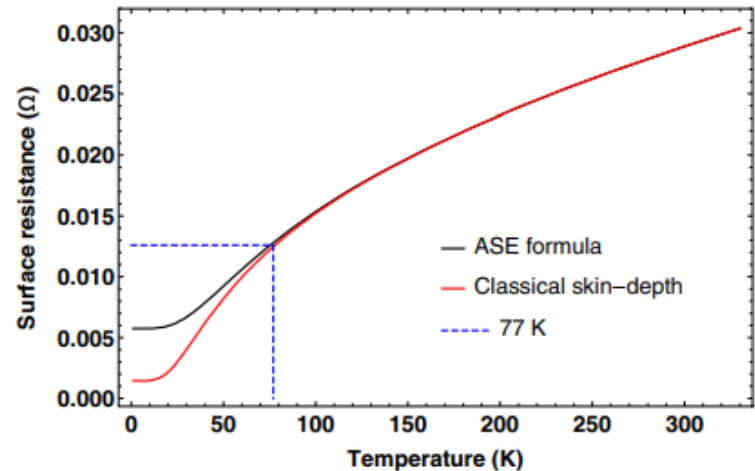
$$Z_s = Z_0 \left(\frac{\sqrt{3} c v_F k^2}{16\pi \omega_p^2} \right)^{1/3} (1 - \sqrt{3}i), \quad R_s = \text{Re}(Z_s) = Z_0 \left(\frac{\sqrt{3} c v_F k^2}{16\pi \omega_p^2} \right)^{1/3}.$$

For copper $v_F = 1.58\text{e}6$ m/sec, $\omega_p = 1.64\text{e}16$ rad/sec; $\frac{3}{2} \left(\frac{l}{\delta} \right)^2 \gg 1$, $\omega \ll \omega_p$. Note that

$$\frac{l}{\delta} \sim \sigma(T)^{3/2}$$



Calculated pure copper surface resistance (orange) versus measured (blue) for the frequency of 11424 MHz.

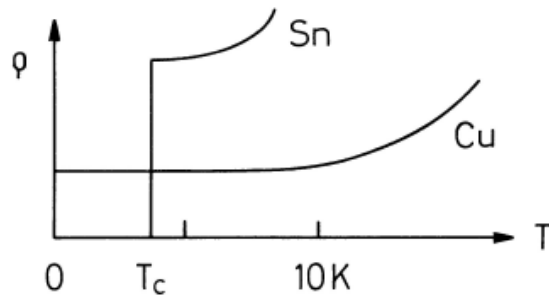


A plot of the surface resistance for copper with RRR = 400 versus temperature at 11424 MHz.

Acceleration and focusing of charged particles in electromagnetic field

2. Superconducting wall:

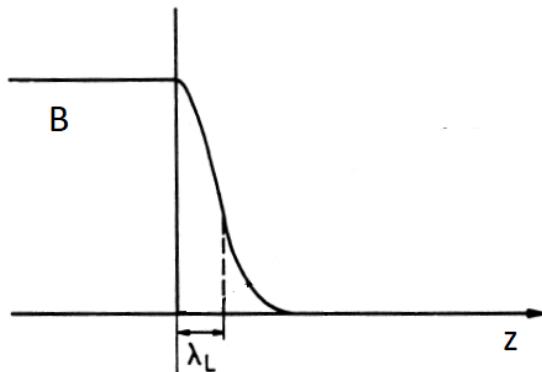
- Superconductivity - the infinitely high conductivity (or zero resistivity) below a 'critical temperature' T_c .



T_c (K):

Al	Hg	Sn	Pb	Nb	Ti	NbTi	Nb ₃ Sn
1.14	4.15	3.72	7.9	9.2	0.4	9.4	18

- Penetration depth $\lambda_L: B(z) \sim \exp(-z/\lambda_L)$



material	In	Pb	Sn	Nb
λ_L [nm]	24	32	≈ 30	32

Acceleration and focusing of charged particles in electromagnetic field

- Two-fluid model: current in a superconductor is carried by
 - the superfluid component (Cooper pairs) - J_s ;
 - the normal component (unpaired electrons) - J_n .

- At DC – no resistance.
- At AC – resistance caused by electron inertia.

For normal component:

$$J_n = \sigma_n E_0 \exp(-i\omega t),$$

For superfluid component:

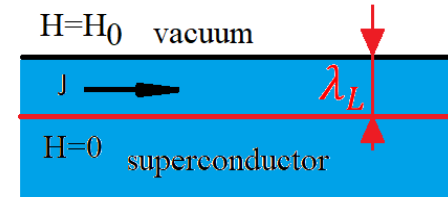
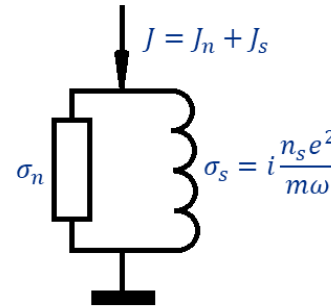
$$m\dot{v} = -eE_0 \exp(-i\omega t) \rightarrow J_s = -en_s v = i \frac{n_s e^2}{m\omega} E_0 \exp(-i\omega t) = \sigma_s E_0 \exp(-i\omega t) \rightarrow \sigma_s = i \frac{n_s e^2}{m\omega}$$

$$R_s = \text{Re} \left(\frac{1}{\lambda_L(\sigma_n + \sigma_s)} \right) \approx \frac{1}{\lambda_L} \cdot \frac{\sigma_n}{|\sigma_s|^2}, \text{ or } R_s \propto \omega^2 \exp\left(-\frac{\Delta}{k_B T}\right) \text{ because}$$

$\sigma_n \propto \exp\left(-\frac{\Delta}{k_B T}\right)$ and $|\sigma_s|^{-2} \propto \omega^2$. Here $\Delta \sim T_c$ is the energy gap and k_B is the Boltzmann constant.

Phenomenological law for Nb:

$$R_{S,BCS} \approx 1.643 \times 10^{-5} \frac{T_c}{T} (f(\text{GHz}))^2 e^{-\frac{1.92T_c}{T}} (\Omega). \quad R_s = R_{S,BCS} + R_{residual}$$



$$Z_s = \frac{1}{\lambda_L(\sigma_n + \sigma_s)}$$

Acceleration and focusing of charged particles in electromagnetic field

Examples:

1. Surface resistance of a copper wall at room temperature for 1.3 GHz.

Mean-free path l is 38 nm compared to classical skin depth δ of 1.9 μm .

$l \ll \delta \rightarrow$ *classical skin effect (CSE)*. Therefore,

$$R_s = \sqrt{\frac{\omega Z_0}{2c\sigma}} = 9.3 \text{ mOhm};$$

$\sigma=59 \text{ MS/m}$; $\omega=2\pi \cdot 1.3\text{e}9 \text{ Hz}$, $Z_0=120\pi \text{ Ohm}$, $c=3\text{e}8 \text{ m/sec}$.

2. Surface resistance of a pure copper (RRR=2500) wall at 2 K for 1.3 GHz.

Mean-free path l is 95 μm compared to classical skin depth of 37 nm.

$l \gg \delta \rightarrow$ *anomalous skin effect (ASE)*. Therefore,

$$R_s = Z_0 \left(\frac{\sqrt{3}}{16\pi} \frac{c v_F k^2}{\omega_p^2} \right)^{1/3} = 1.3 \text{ mOhm}.$$

$v_F = 1.58\text{e}6 \text{ m/sec}$, $\omega_p = 1.64\text{e}16 \text{ rad/sec}$, $k = \omega/c = 2\pi \cdot 1.3\text{e}9/c$.

Classical skin formula gives 0.19 mOhm!

3. BCS resistance of the Nb at 2 K for 1.3 GHz.

$$R_{s,BCS} \approx 1.643 \times 10^{-5} \frac{T_c}{T} (f(\text{GHz}))^2 e^{-\frac{1.92T_c}{T}} = 19 \text{ nOhm}$$

$f=1.3 \text{ GHz}$, $T_c=9.2 \text{ K}$, $T=2\text{K}$.

Acceleration and focusing of charged particles in electromagnetic field

- Dynamics of a charged particle accelerated in a RF field is described by Lorenz equation,

$$\frac{d\vec{p}}{dt} = \vec{F} = e[\vec{E}_0(\vec{r},t) + \vec{v} \times \vec{B}_0(\vec{r},t)], \quad (1)$$

where \vec{v} is the particle velocity, $\vec{E}_0(\vec{r},t)$ and $\vec{B}_0(\vec{r},t)$ are RF electric and magnetic field oscillating at the cavity resonance frequency ω :

$$\begin{aligned} \vec{E}_0(\vec{r},t) &= \vec{E}(\vec{r}) e^{i\omega t} & \vec{p} &= \gamma m \vec{v} \text{ - particle momentum;} \\ \vec{B}_0(\vec{r},t) &= \vec{B}(\vec{r}) e^{i\omega t} & \gamma &= \frac{1}{\sqrt{1 - \frac{v^2}{c^2}}} \text{ - relativistic factor} \end{aligned}$$

- Particle energy W changes is caused by interaction with electric field only. Magnetic field does not change the particle energy:

$$\frac{dW}{dt} = \frac{d(\gamma mc^2)}{dt} = \vec{v} \cdot \frac{d\vec{p}}{dt} = e(\vec{v} \cdot \vec{E}_0 + \vec{v} \cdot [\vec{v} \times \vec{B}_0]) = e\vec{v} \cdot \vec{E}_0 = 0$$

$$(W = \gamma mc^2; \frac{dW}{dt} = \frac{d(\gamma mc^2)}{dt} = \vec{v} \cdot \frac{d(\gamma m \vec{v})}{dt} = \vec{v} \cdot \frac{d\vec{p}}{dt})$$

Acceleration and focusing of charged particles in electromagnetic field

RF electric field has a longitudinal component next to the beam axis. In cylindrical coordinate it may be expanded over azimuthal harmonics, i.e.,

$$E_z(r, \varphi, z) = \sum_{m=-\infty}^{\infty} e^{im\varphi} E_{m,z}(r, z)$$

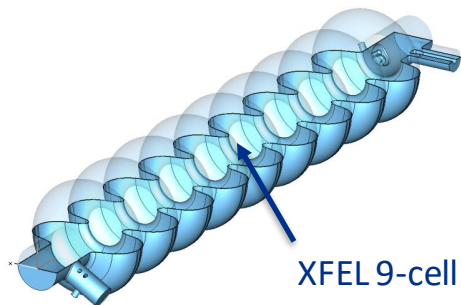
To understand general properties of the acceleration field, the amplitudes may be expanded into Fourier integral for $r < a$, a is the beam aperture :

$$E_{m,z}(r, z) = \frac{1}{2\pi} \int_{-\infty}^{\infty} E_{m,z}(k_z, r) e^{ik_z z} dk_z \quad (1)$$

or over the travelling waves existing from $z=-\infty$ to $z=\infty$.

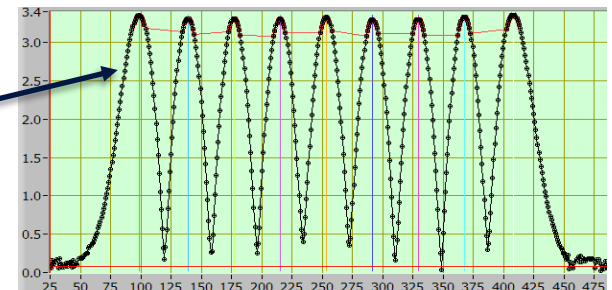
The RF field $\vec{E}_0(\vec{r}, t)$ satisfies the wave equation:

$$\Delta \vec{E}_0(\vec{r}, t) - \frac{\partial^2 \vec{E}_0(\vec{r}, t)}{c^2 \partial t^2} = 0 \quad (2)$$



XFEL 9-cell 1.3 GHz SW cavity

$$|E_{0,z}(0, z)|$$



Acceleration of charged particles in electromagnetic field

Substituting expansion (1) to the wave equation (2), we can find, that $E_{m,z}(k_z, r)$ satisfies Bessel equation, and therefore is proportional to the Bessel function $J_m(x)$,

$$E_{m,z}(k_z, r) = E_{m,z}(k_z)J_m(k_{\perp}r)$$

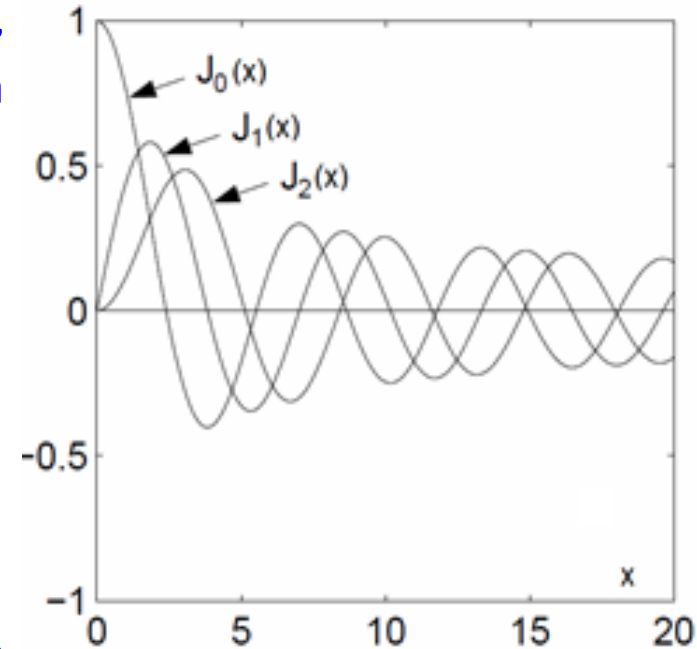
where k_{\perp} is transverse wavenumber, which it turn satisfies dispersion equation:

$$k_{\perp}^2 + k_z^2 = \frac{\omega^2}{c^2} \equiv k^2,$$

here c is speed of light.

If the particle velocity $v = \beta c$ and particle transverse coordinates do not change significantly in the cavity, the energy ΔW particle gains in the cavity is equal to

$$\Delta W(r, \varphi) = e \operatorname{Re} \left[\int_{-\infty}^{\infty} dz E_z(r, \varphi, z) e^{i\omega t} \Big|_{t=\frac{z}{v}} \right]$$



Bessel functions $J_m(x)$.

Acceleration of charged particles in electromagnetic field

Performing integration over z one has:

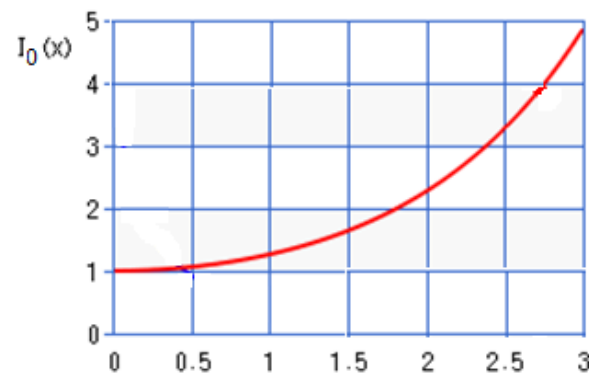
$$\Delta W(r, \varphi) = e \operatorname{Re} \left[\sum_{m=-\infty}^{\infty} E_{m,z} \left(\frac{k}{\beta} \right) I_m \left(kr / \beta \gamma \right) e^{im\varphi} \right], \quad \longrightarrow \quad I_m(x) = i^{-m} J_m(ix)$$

where $I_m(x)$ is modified Bessel function and γ is the particle relativistic factor (note that $k_{\perp} = ik/\beta\gamma$); i.e., the particle gains the energy interacting with synchronous cylindrical wave having the phase velocity equal to the particle velocity (synchronism: $v_{\text{particle}} = \beta c = v_{\text{phase}} = \omega/k_z \rightarrow k_z = k/\beta$ and $k_{\perp} = (k^2 - k_z^2)^{1/2} = ik/\beta\gamma$).

If the cavity and RF field of the operating mode have perfect azimuthal symmetry, one has:

$$\Delta W(r) = e \operatorname{Re} \left[E_{0,z} \left(\frac{k}{\beta} \right) I_0(kr/\beta\gamma) \right] = e |E_{0,z} \left(\frac{k}{\beta} \right)| I_0(kr/\beta\gamma) \cos\phi$$

where ϕ is the RF phase.



$$I_0(x) \approx 1 + \frac{x^2}{4} \quad \text{for } x \ll 1$$

$$I_0(x) \approx \frac{e^x}{\sqrt{2\pi x}} \quad \text{for } x \gg 1$$

Acceleration of charged particles in electromagnetic field

- ❖ For a very slow particle, i.e., when $\beta \ll 1$, if $kr/\beta\gamma \gg 1$ one has*

$$I_0(kr/\beta\gamma) \approx \frac{1}{\sqrt{2\pi kr/\beta\gamma}} e^{kr/\beta\gamma}.$$

It means that for low-beta particle the energy gain increases with the radius r .

- ❖ For the ultra-relativistic particle $k_{\perp} \rightarrow 0$ and one has

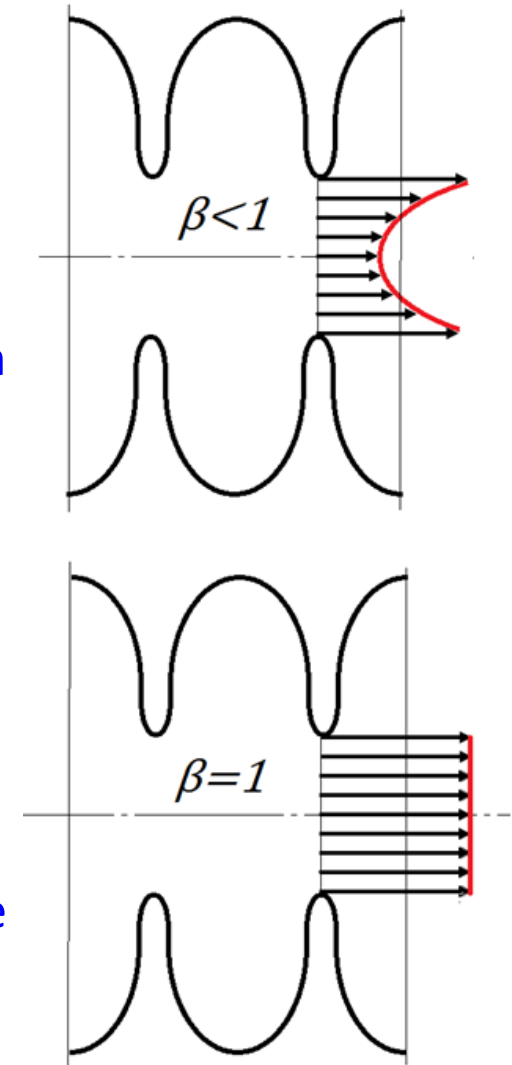
$$V(r, \varphi) = e \operatorname{Re} \left[\sum_{m=-\infty}^{\infty} E_{m,z}(k) r^m e^{im\varphi} \right],$$

For the RF field having perfect azimuthal symmetry

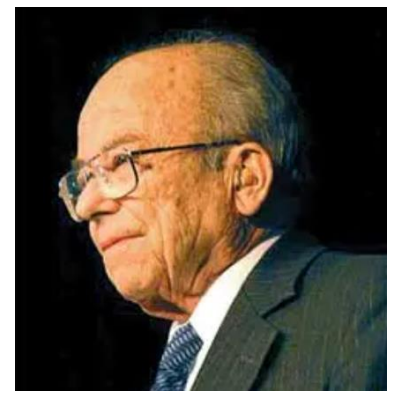
$$V(r) = e |E_{0,z}(k)| \cos\phi$$

and the particle energy gain does not depend on the transverse coordinate.

$$*I_0(x) \approx \frac{e^x}{\sqrt{2\pi x}} \text{ for } x \gg 1$$



Focusing properties of RF field



W. Panofsky

In addition to acceleration, the RF field provides deflection of the beam. Let's consider the particle transverse momentum change caused by the cavity RF field. The particle moves on the trajectory $z=vt$ parallel to the axis but has off-set \vec{r}_\perp .

According to **Panofsky–Wenzel theorem** change of transverse momentum caused by RF field is related to change of the longitudinal momentum:

$$\Delta \vec{p}_\perp = \frac{iv}{\omega} \vec{\nabla}_\perp (\Delta p_\parallel)$$

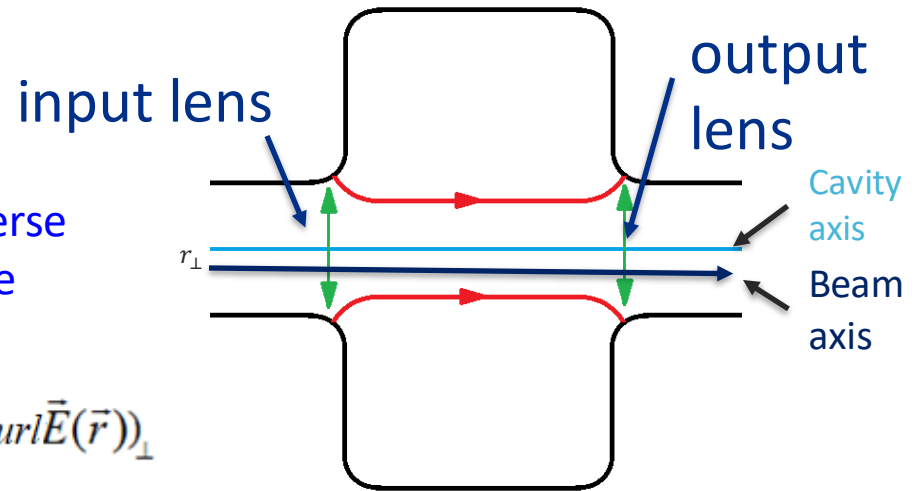
The differential operator $\vec{\nabla}_\perp$ acts on the transverse coordinates \vec{r}_\perp only; longitudinal and transverse momentum changes are (Appendix 2):

$$\vec{F}_\perp(\vec{r}) = \frac{d\vec{p}_\perp}{dt} = \vec{E}_\perp(\vec{r}) + (\vec{v} \times \vec{H}(\vec{r}))_\perp = \vec{E}_\perp(\vec{r}) + (\vec{v} \times \frac{i}{\omega} \text{curl} \vec{E}(\vec{r}))_\perp$$

$$\Delta p_\parallel = e \int_{-\infty}^{\infty} E_z(\vec{r}) e^{i\omega t} dt \Big|_{t=z/v} = \frac{e}{v} \int_{-\infty}^{\infty} E_z(\vec{r}) e^{i\omega z/v} dz;$$

$$\Delta \vec{p}_\perp = e \int_{-\infty}^{\infty} \left[\vec{E}_\perp(\vec{r}) + (\vec{v} \times \frac{i}{\omega} \text{curl} \vec{E}(\vec{r}))_\perp \right] e^{i\omega t} dt \Big|_{t=z/v} = e \int_{-\infty}^{\infty} \left[\cancel{\vec{E}_\perp(\vec{r})} + \frac{iv}{\omega} \vec{\nabla}_\perp E_z(\vec{r}) - \frac{iv}{\omega} \frac{\partial \vec{E}_\perp(\vec{r})}{\partial z} \right] e^{i\omega t} dt \Big|_{t=z/v} = e \int_{-\infty}^{\infty} \frac{iv}{\omega} \vec{\nabla}_\perp E_z(\vec{r}) e^{i\omega t} dt \Big|_{t=z/v} = \frac{iv}{\omega} \vec{\nabla}_\perp (\Delta p_\parallel)$$

No acceleration \rightarrow no deflection!



Focusing properties of RF field

Therefore,

$$Re\Delta p_{\perp} = -\frac{e}{\omega} \sum_{m=-\infty}^{\infty} |E_{m,z} \left(\frac{k}{\beta} \right)| \cdot \vec{\nabla}_{\perp} [I_m(kr/\beta\gamma) \cdot \cos(m(\varphi - \varphi_m))] \cdot \sin \phi$$

where φ_m is polarization of the azimuthal harmonics. The maximum of transverse momentum change is shifted in RF phase versus the maximum the energy gain by -90° : for the particle accelerated on crest of the RF field, transverse momentum change is zero. In order to get longitudinal stability in low-energy accelerator one needs to accelerate the particle at $\phi < 0$. One can see that for the field having perfect azimuthal symmetry

$$Re\Delta p_{\perp} = -\frac{e}{\omega} |E_{0,z} \left(\frac{k}{\beta} \right)| \cdot \vec{\nabla}_{\perp} [I_0(kr/\beta\gamma)] \cdot \sin \phi = -\frac{e}{\beta\gamma c} V_{max}(0) \cdot I_1(kr/\beta\gamma) \cdot \sin \phi$$

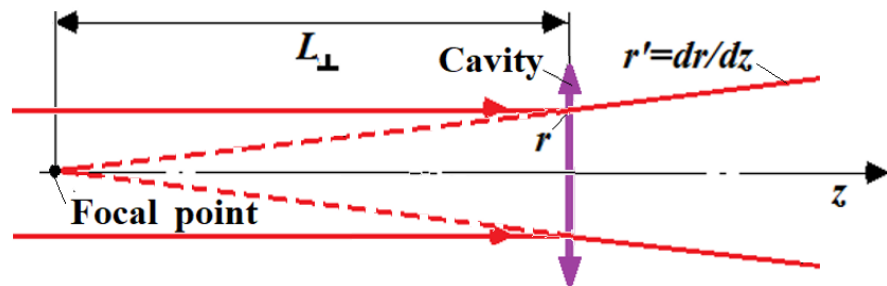
Near the axis, where $kr/\beta\gamma \ll 1$ one has for the trajectory angle r' in the end of acceleration $r' = \frac{\Delta p_{\perp}(r)}{p_{\parallel}} \approx -\frac{kr}{2\beta^3\gamma^3} \frac{V_{max}(0)}{m_0 c^2/e} \cdot \sin \phi$,

where m_0 is the particle rest mass.

Focusing properties of RF field

- ❖ In thin lens approximation the focusing distance L_{\perp} is

$$L_{\perp} = -\frac{r}{r'} = \frac{2\beta^3\gamma^3}{\omega/c} \frac{m_0 c^2/e}{V_{max}(0) \cdot \sin\phi}$$



- Focusing distance L_{\perp} is inversed proportional to the RF frequency and proportional to β^3 . Because of this, at low energies the cavity provides strong defocusing ($\phi < 0!$), and this defocusing should be compensated by external magnetic focusing system.
- To mitigate this defocusing, one should use lower RF frequency ω in low energy parts of the linac ($L_{\perp} \sim 1/\omega$).
- ❖ For an ultra-relativistic particle in this case one has:

$$Re\Delta p_{\perp} = -\frac{e}{\omega} \sum_{m=-\infty}^{\infty} |E_{m,z}(k)| \cdot m r^{m-1} \cdot \sin\phi$$

and in the case of perfect azimuthal symmetry of the field $\Delta p_{\perp} = 0$. However, the RF field provides transfer momentum change for ultra-relativistic particle, i.e., focusing. The reason is that the particle transverse coordinate and energy change during acceleration because of the initial trajectory angle and influence of the RF field.

In this case the transverse momentum change is proportional to the RF amplitude squared.

Focusing properties of RF field

The transport matrix (thick lens) which determines relationship between the input and output transverse coordinates and angles (x and x' respectively) of the relativistic particle is calculated, for example, in [*]. For the RF cavity operating at π -mode (slide) for the particle accelerated on crest, the transport matrix is the following:

$$\begin{bmatrix} x \\ x' \end{bmatrix}_f = \begin{bmatrix} \cos(\alpha) - \sqrt{2} \sin(\alpha) & \sqrt{8} \frac{\gamma_i}{\gamma'} \sin(\alpha) \\ -\frac{3\gamma'}{\sqrt{8}\gamma_f} \sin(\alpha) & \frac{\gamma_i}{\gamma_f} [\cos(\alpha) + \sqrt{2} \sin(\alpha)] \end{bmatrix} \begin{bmatrix} x \\ x' \end{bmatrix}_{in},$$

where $(x, x')_i$ initial coordinate and angle, $(x, x')_f$ are final parameters, γ_i and γ_f are initial and final relativistic factors, γ' is the acceleration gradient over the rest mass in electron-Volts ($\gamma' = \Delta W_{max} / L_c m_0 c^2$ (L_c is the cavity length)) and $\alpha = \frac{1}{\sqrt{8}} \ln \frac{\gamma_f}{\gamma_i}$.

- Note, that the angle x'_f at the cavity output for $x'_i = 0$ is proportional to the gain over the particle energy squared:

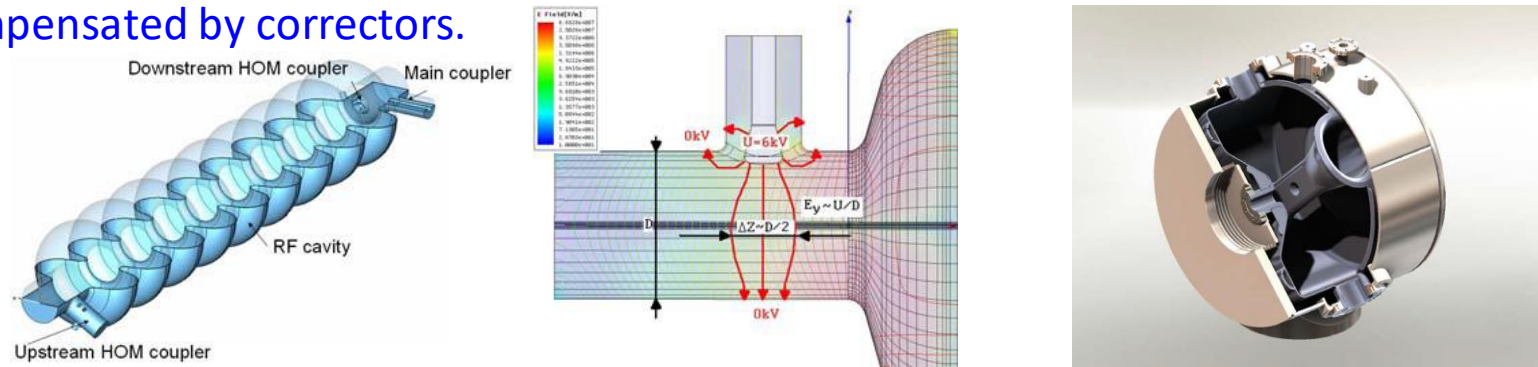
$$x'_f = \frac{\Delta p_{\perp}}{p_{\parallel}} \approx \frac{3}{8} \left(\frac{V_{max}}{\gamma m_0 c^2} \right)^2 \frac{x_i}{L_c} \quad \text{and} \quad L_{\perp} = \frac{x_i}{x'_f} \approx \frac{8}{3} L_c \left(\frac{\gamma m_0 c^2}{V_{max}} \right)^2$$

*J. Rosenzweig and L. Serafini, "Transverse Particle Motion in Radio-Frequency Linear Accelerators," *Phys. Rev. E*, vol. 49, Number 2 (1994).

Focusing properties of RF field

RF acceleration elements (cavities, acceleration structures) typically have no perfect axial symmetry because of design features, coupling elements or manufacturing errors.

- Elliptical SRF cavities have the input couplers, which introduce dipole field components.
- Low-beta cavities like Half-Wave Resonators or Spoke Resonators have quadrupole RF field perturbations cause by spokes, which influence the beam and should be compensated by correctors.



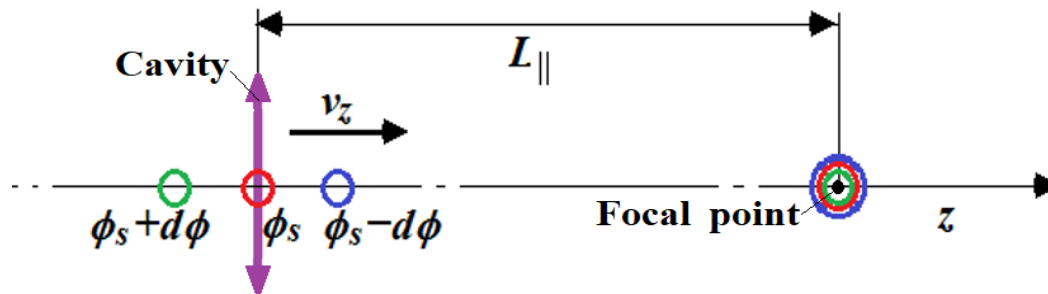
The angle x'_f at the cavity output for $x'_i = 0$ caused by multipole perturbation of m^{th} order ($m > 0$) is linear with respect to the ratio of the gain over the particle energy (ultra-relativistic case):

$$x'_f = \frac{\Delta p_{\perp}}{p_{\parallel}} \approx \frac{m}{ka} \left(\frac{V_{\text{max}}(a)}{\gamma m_0 c^2} \right) \left(\frac{x_i}{a} \right)^{m-1}$$

- It may strongly influence the beam dynamics leading to the beam emittance dilution or result in strong quadrupole beam defocusing .
- On the other hand, the octupole perturbations may be used for the cavity alignment.

Bunching of charged particles in electromagnetic field

Because the particle velocity depends on the energy, the cavity RF field provides the beam bunching (Appendix 2).



In thin lens approximation the longitudinal “focusing” distance $L_{||}$ is:

$$L_{||} = -\frac{\beta^3 \gamma^3}{\omega/c} \frac{m_0 c^2 / e}{V_{max}(0) \cdot \sin \phi_s} = -\frac{1}{2} L_{\perp}$$

For the bunch longitudinal stability $L_{||}$ should be >0 , or $\phi_s < 0$. In this case, one has transverse defocusing.

Note that for small energy (and therefore small β) the bunching may be too strong, and low RF frequency is to be used for acceleration.

Example:

SSR1 cavity (PIP II H⁻ accelerator):

$f=325$ MHz; $V_{\max} = 1$ MV; $\phi_s = -34^\circ$;

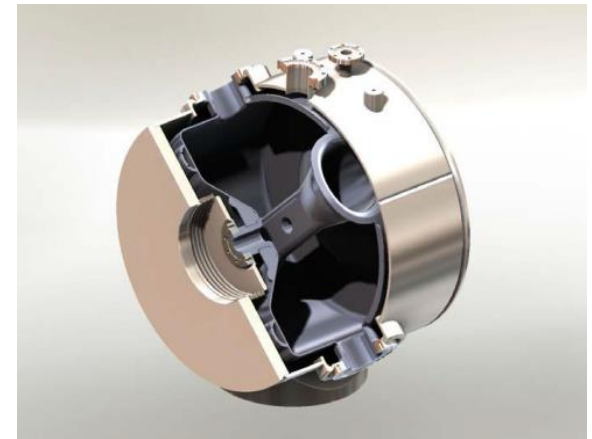
$m_0c^2=E_0=938$ MeV; $E= 10$ MeV $\rightarrow \beta \approx (2E/E_0)^{1/2}=0.146$, $\gamma \approx 1$.

❖ The focusing distance L_\perp is

$$L_\perp = \frac{2\beta^3\gamma^3}{\omega/c} \frac{m_0c^2/e}{V_{\max}(0)\cdot\sin\phi} = \mathbf{-1.55 \text{ m}}$$

❖ Longitudinal “focusing” distance $L_{||}$:

$$L_{||} = -\frac{\beta^3\gamma^3}{\omega/c} \frac{m_0c^2/e}{V_{\max}(0)\cdot\sin\phi_s} = -\frac{1}{2} L_\perp = \mathbf{78 \text{ cm}}$$

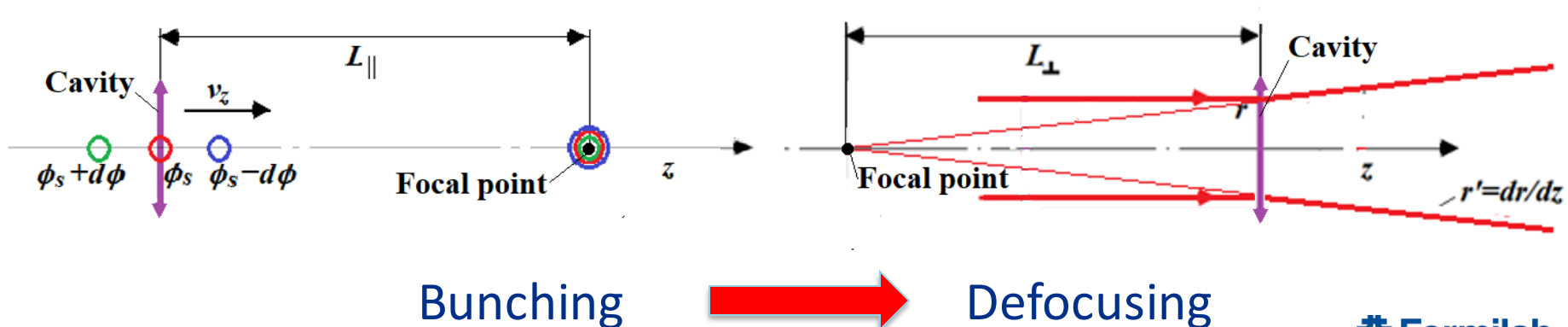


Summary:

- Acceleration of a charged particle moving in axisymmetric RF field parallel to the axis at the radius r is proportional to $I_0(kr/\beta\gamma)$;
 - for non-relativistic particle it increases with the radius → for low-energy particles one should use low frequency;
 - for ultra-relativistic particle it does not depend on the radius.
- Focusing of the accelerating particle is related to acceleration;
 - the maximum of transverse momentum change of the non-relativistic particle is shifted in RF phase versus the maximum the energy gain by -90°
 - The focusing distance of the non-relativistic particle is proportional to $\beta^3\gamma^3/(\omega V_{max})$ → for low-energy particles one should use low frequency.

Summary (continuation):

- The focusing distance for ultra-relativistic particles is quadratic versus the ratio of particle energy over the voltage.
- The focusing distance for ultra-relativistic particles in multipole fields is linear versus the ratio of particle energy over the voltage; **multipole perturbations may strongly affect the beam dynamics.**
- The bunching “focusing” distance of the non-relativistic particle is proportional to $\beta^3 \gamma^3 / (\omega V_{max}) \rightarrow$ **for low-energy particles one should use low frequency.**
- The sign is opposite to the focusing: **if the bunch is stable in longitudinal direction, it is defocused in transverse direction, and vice versa.**
- **In low-energy accelerators external focusing is necessary!**



Chapter 3.

RF Cavities for Accelerators.

- a. Resonance modes – operation mode, High-Order Modes;
- b. Pillbox cavity
- c. Cavity parameters:
 - Acceleration gradient;
 - R/Q;
 - Q_0 and G-factor;
 - Shunt Impedance;
 - Field enhancement factors (electric and magnetic);
- d. Cavity excitation by the input port;
- e. Cavity excitation by the beam;
- f. High-Order Modes (HOMs);
- g. Types of the cavities and their application;
- h. Tools for cavity simulations.

RF cavity:

$$\omega_0 = (LC)^{-1/2}$$

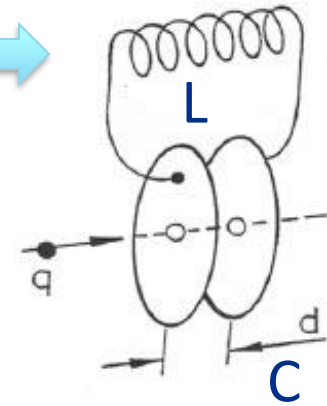
□ An LC circuit, the simplest form of RF resonator:

This circuit and a resonant cavity share common aspects:

- Energy is stored in the electric and magnetic fields
- Energy is periodically exchanged between electric and magnetic field
- Without any external input, the stored energy will turn into heat.

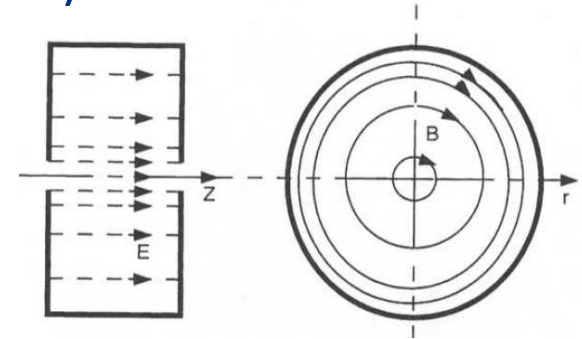
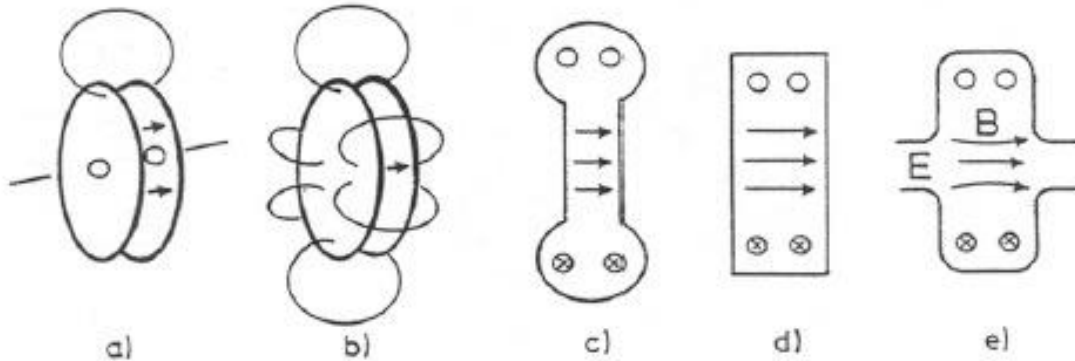
□ To use such a circuit for particle acceleration, it must have opening for beam passage in the area of high electric field (capacitor).

□ As particles are accelerated in vacuum, the structure must provide vacuum space. A ceramic vacuum break (between the two electrode of the capacitor) can be used to separate the beam line vacuum from the rest of the resonator. Or the resonant structure can be enclosed in a vacuum vessel.



From LC circuit to an accelerating cavity:

- Alternatively, we can use “cavity resonators”.
- Metamorphosis of the **LC** circuit into an accelerating cavity:
 1. Increase resonant frequency by lowering **L**, eventually have a solid wall.
 2. Further frequency increase by lowering **C** → arriving at cylindrical, or “pillbox” cavity geometry, which can be solved analytically.
 3. Add beam tubes to let particle pass through.



- Pillbox geometry:
- Electric field used for acceleration is concentrated near the axis
 - Magnetic field is concentrated near the cavity outer wall

Cavity resonators:

A cavity resonator is a closed metal structure that confines electromagnetic fields in the RF or microwave region of the spectrum.

- Such cavities act as resonant circuits with extremely low losses. The RF loss for cavities made of copper is typically 3-4 orders lower than for resonant circuits made with inductors and capacitors at the same frequency.
- Resonant cavities can be made from closed (or short-circuited) sections of a waveguide or coaxial line. Ferrite-loaded cavities are used at low frequencies to make cavities compact and allow very wide frequency tuning range.
- The cavity wall structure can be made stiff to allow its evacuation.
- Electromagnetic energy is stored in the cavity and the only losses are due to finite conductivity of cavity walls and dielectric/ferromagnetic losses of material filling the cavity.

Modes in an RF cavity:

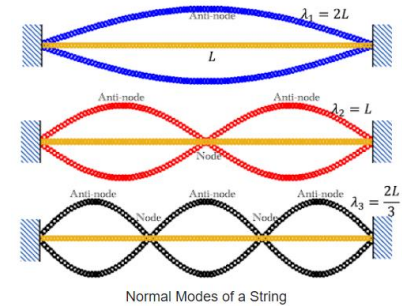
$$\Delta \vec{E} + k^2 \vec{E} = 0, \quad \Delta \vec{H} + k^2 \vec{H} = 0.$$

where $k = \omega \sqrt{\mu \epsilon}$

Boundary conditions

$$\vec{n} \times \vec{E} = 0$$

$$\vec{n} \cdot \vec{H} = 0$$



- There are an infinite number of orthogonal solutions (eigen modes) with different field structure $\vec{H}_m(\vec{r})$ and $\vec{E}_m(\vec{r})$ and resonant frequencies ω_m (eigen frequencies). Here m is the eigenmode number.
- For acceleration in longitudinal direction the lowest frequency mode having longitudinal electric field component is used.

Properties of resonance modes:

- Relation between eigenvalue k_m and eigenfunction \vec{H}_m :

$$k_m^2 = \frac{\int_V |\text{curl} \vec{H}_m|^2 dV}{\int_V |\vec{H}_m|^2 dV}; \quad \omega_m = ck_m = \frac{k_m}{\sqrt{\epsilon\mu}}, \quad \lambda_m = \frac{2\pi}{k_m}.$$

- The eigen functions are orthogonal

$$\int_V \vec{E}_m \cdot \vec{E}_n dV = 0, \quad \int_V \vec{H}_m \cdot \vec{H}_n dV = 0, \quad \text{if } k_m^2 \neq k_n^2$$

- The average energies stored in electric and magnetic fields are equal:

$$\frac{1}{4} \int_V \mu |\vec{H}_m|^2 dV = \frac{1}{4} \int_V \epsilon |\vec{E}_m|^2 dV = \frac{W_0}{2} \rightarrow W_0 = \frac{1}{2} \int_V \mu |\vec{H}_m|^2 dV = \frac{1}{2} \int_V \epsilon |\vec{E}_m|^2 dV$$

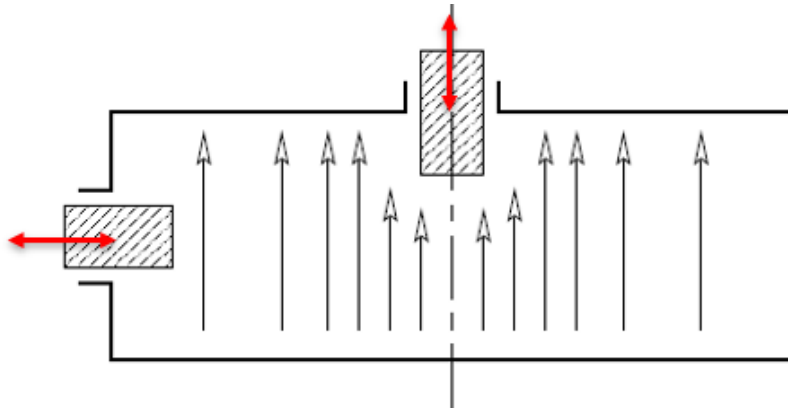
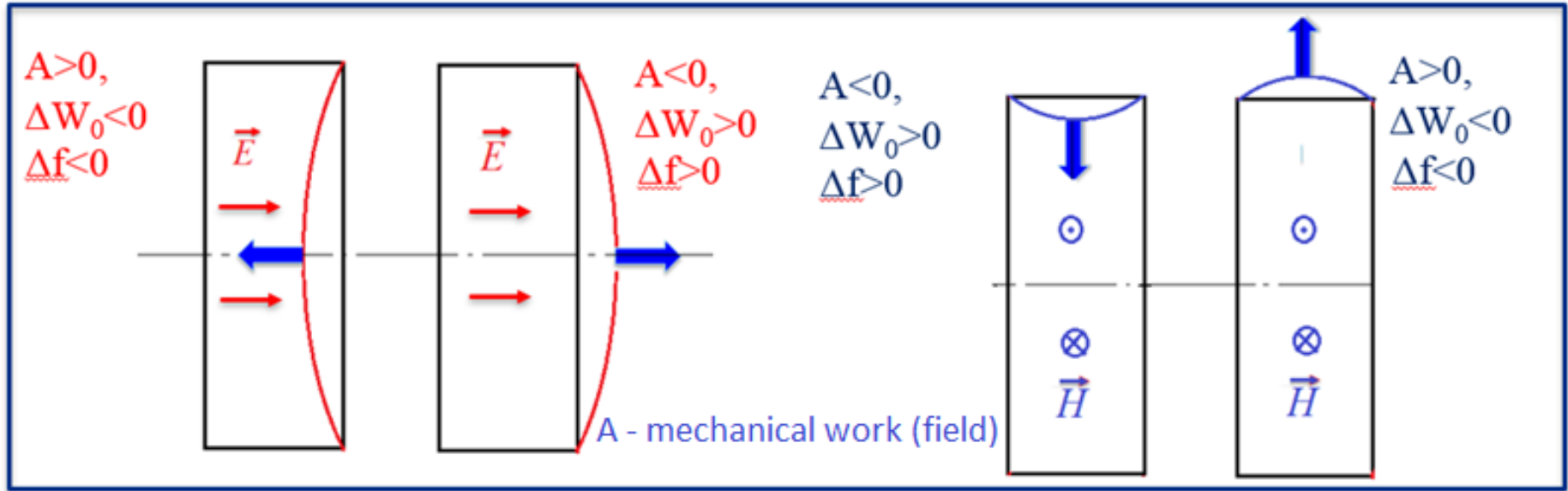
- The eigenmode variation property: for small cavity deformation one has:

$$\frac{W_0}{\omega_0} = \text{const}$$

W_0 is stored energy, ω_0 is the mode circular resonance frequency.

Properties of resonance modes :

Cavity mechanical tuning is based on the eigenmode variation property:

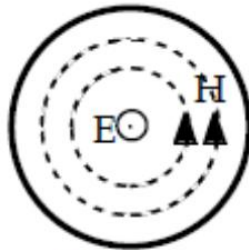


Resonance modes and pillbox cavity:

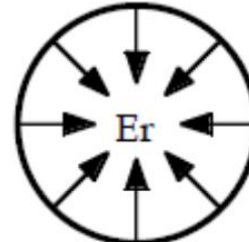
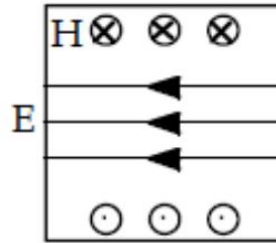
- For pillbox cavities there are two families of the eigen modes:
 - TM -modes, which have no longitudinal magnetic fields;
 - TE-modes, which have no longitudinal electric fields.
- The modes are classified as TM_{mnp} (TE_{mnp}), where integer indices m , n , and p correspond to the number of variations E_z (H_z) has in φ , r , and z directions respectively.
- For “monopole” modes in the axisymmetric cavity of arbitrary shape
 - TM-modes have only azimuthal magnetic field component;
 - TE -modes have only azimuthal electric field component.

For acceleration, lowest TM-mode is used, which has longitudinal electric field on the axis.

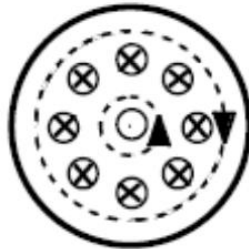
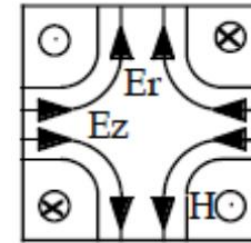
Resonance modes and pillbox cavity:



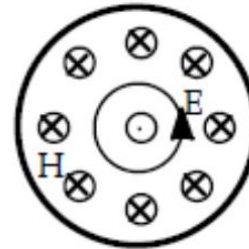
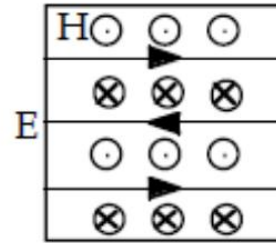
TM₀₁₀



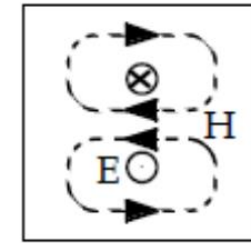
TM₀₁₁



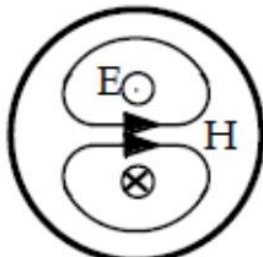
TM₀₂₀



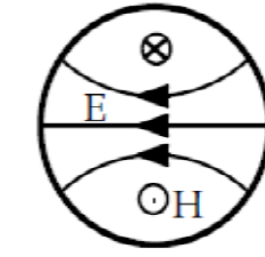
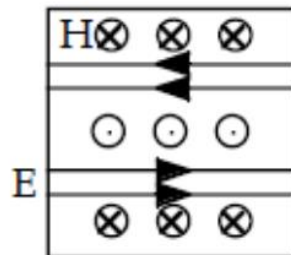
TE₀₁₁



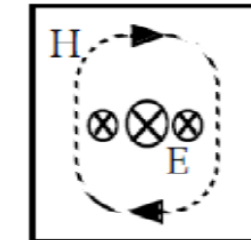
Modes with $m=0$ (“monopole modes”)



TM₁₁₀



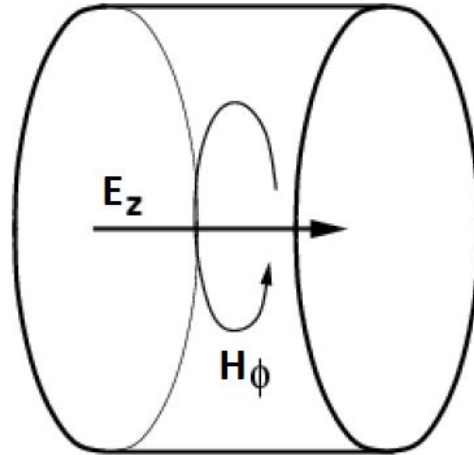
TE₁₁₁



Modes with $m=1$ (dipole modes)

Resonance modes and pillbox cavity:

- ❑ Most of acceleration cavities have axial symmetry (slightly violated by perturbations – coupling units, manufacturing errors, etc).
- ❑ The modes in the axisymmetric cavity of arbitrary shape have azimuthal variations, $\vec{E}, \vec{H} \sim \exp(im\varphi)$:
 - For acceleration TM-modes with $m=0$ (“monopole”) are used;
 - Dipole ($m=1$) TM-modes are used for the beam deflection.
- ❑ The simplest cavity is a pillbox with TM₀₁₀ mode ($m=0, n=1, p=0$):
(m - number of azimuthal variations, n – number of radial variations, p – number of longitudinal variations)



Modes in a pillbox RF cavity:

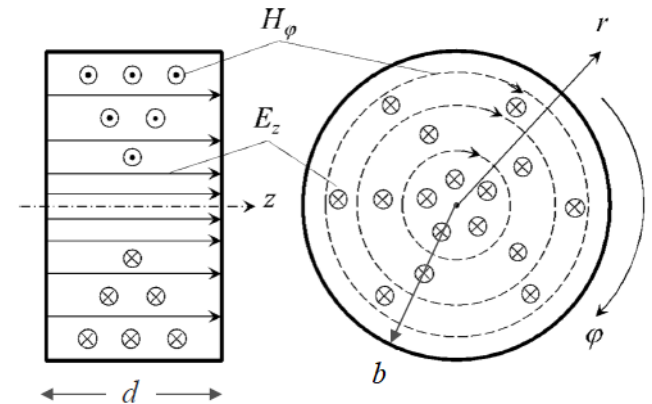
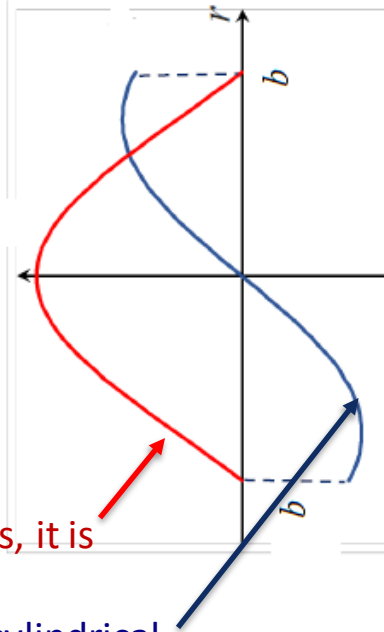
- While TM_{010} mode is used for acceleration and usually is the lowest frequency mode, all other modes are “parasitic” as they may cause various unwanted effects. Those modes are referred to as High-Order Modes (HOMs). Modes with $m=0$ – “monopole”, with $m=1$ – “dipole”, etc.

$$E_z = E_0 J_0 \left(\frac{2.405r}{b} \right) e^{i\omega t}$$

$$H_\phi = -i \frac{E_0}{Z_0} J_1 \left(\frac{2.405r}{b} \right) e^{i\omega t}$$

$$\omega_{010} = \frac{2.405c}{b}, \quad Z_0 = \sqrt{\frac{\mu_0}{\epsilon_0}}$$

$$\lambda_{010} = 2.61 b$$



Next to the cavity axis
 $E_z(r) \sim \text{const}$;
 $H_\phi(r) \sim r$

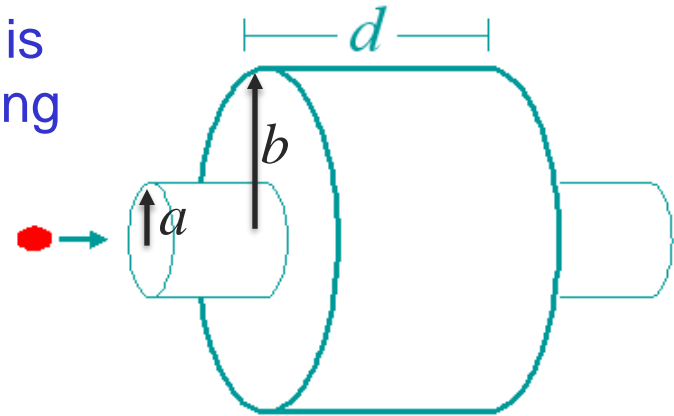
- Electric field is concentrated near the axis, it is responsible for acceleration.
- Magnetic field is concentrated near the cylindrical wall, it is responsible for RF losses.

Note that electric and magnetic fields are shifted in phase by 90 deg.
 For vacuum $Z_0 = 120\pi$ Ohms; b is the pillbox radius, d is its length.

Accelerating voltage and transit time factor:

Assuming charged particles moving along the cavity axis, and the particle velocity change is small, one can calculate *maximal* accelerating voltage V as

$$V = \left| \int_{-\infty}^{\infty} E_z(r=0, z) e^{i\omega_0 z / \beta c} dz \right|$$

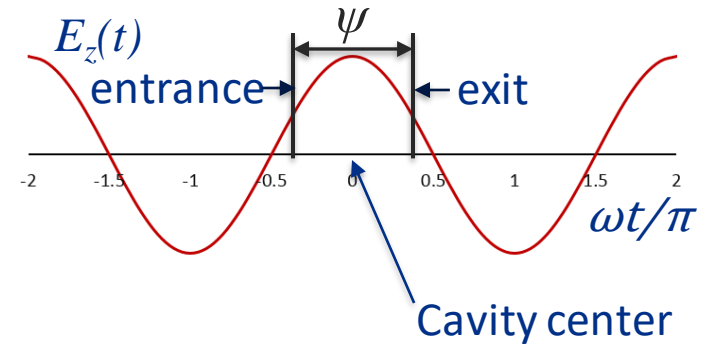
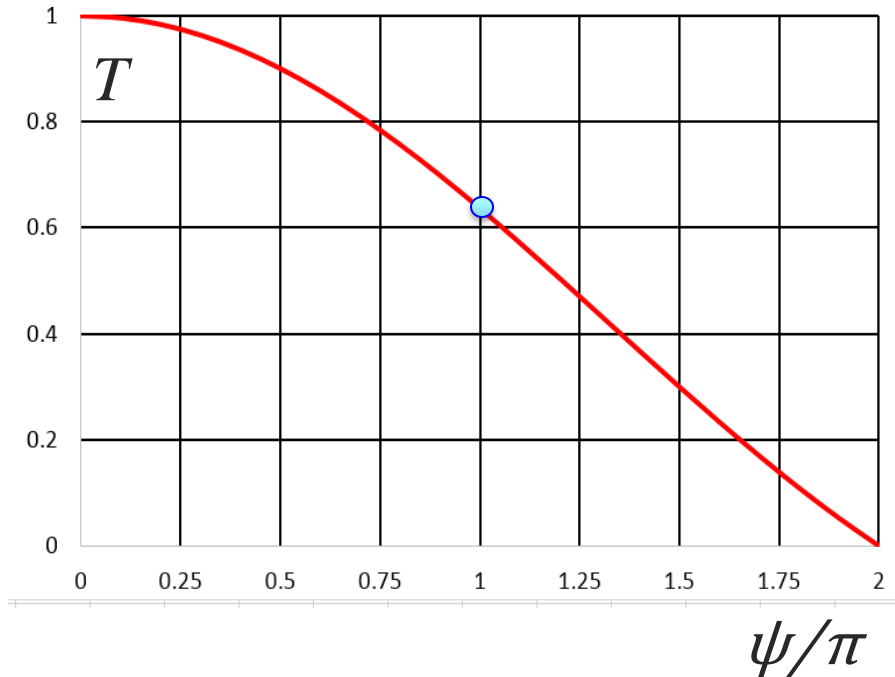


For the pillbox cavity one can integrate this analytically:

$$V = E_0 \left| \int_0^d e^{i\omega_0 z / \beta c} dz \right| = E_0 d \frac{\sin\left(\frac{\omega_0 d}{2\beta c}\right)}{\frac{\omega_0 d}{2\beta c}} = E_0 d \cdot T$$

where T is the transit time factor, $T(\psi) = \frac{\sin(\psi/2)}{\psi/2}$, $\psi = \frac{\omega_0 d}{\beta c}$

Acceleration gradient



Note that maximal acceleration takes place when the RF field reaches maximum when the particle is the cavity center.

In order to “use” all the field for acceleration , $\psi=\pi$ (or $d = \beta\lambda/2$) and $T = 2/\pi$ for the pill box cavity. $\lambda = 2\pi c/\omega_0$ — wavelength.

- **Acceleration gradient E is defined as $E=V/d=E_0T$**

Unfortunately, the cavity length is not easy to specify for shapes other than pillbox so usually it is assumed to be $d = \beta\lambda/2$. This works OK for multi-cell cavities, but poorly for single-cell cavities or cavities for slow particle acceleration.

RF cavity parameters:

- Stored energy U:

$$U = \frac{1}{2} \mu_0 \int_V |\mathbf{H}|^2 dv = \frac{1}{2} \varepsilon_0 \int_V |\mathbf{E}|^2 dv$$

- Losses in the cavity. There are the losses P_c in a cavity caused by finite surface resistance R_s :

$$P_c = \frac{1}{2} R_s \int_S |\mathbf{H}|^2 ds$$

For normal conducting metal at room temperature (no anomalous skin effect)

$$R_s = \frac{1}{\sigma \delta}, \quad \text{where } \sigma \text{ is conductivity and } \delta \text{ is skin depth, } \delta = \frac{1}{\sqrt{\pi f \mu_0 \sigma}}$$

Example:

For copper at room temperature $\sigma=59.6$ MS/m; $R_s= 9.3$ mOhm@1.3 GHz

Simple formula for estimation: $\delta = 0.38 \cdot (30/f(\text{GHz}))^{1/2}$ [μ]

RF cavity parameters:

Unloaded quality factor Q_0 :

$$Q_0 \equiv \frac{\omega_0 \cdot (\text{stored energy})}{\text{average power loss}} = \frac{\omega_0 U}{P_c} = \frac{\omega_0 \mu_0 \int_V |\mathbf{H}|^2 dv}{R_s \int_S |\mathbf{H}|^2 ds}$$

Quality factor Q_0 roughly equals to the number of RF cycles times 2π necessary for the stored energy dissipation.

One can see that

$$Q_0 = \frac{G}{R_s}$$

where G is so-called geometrical factor (**same for geometrically similar cavities**),

$$G = \frac{\omega_0 \mu_0 \int_V |\mathbf{H}|^2 dv}{\int_S |\mathbf{H}|^2 ds}$$

RF cavity parameters:

For a pillbox cavity:

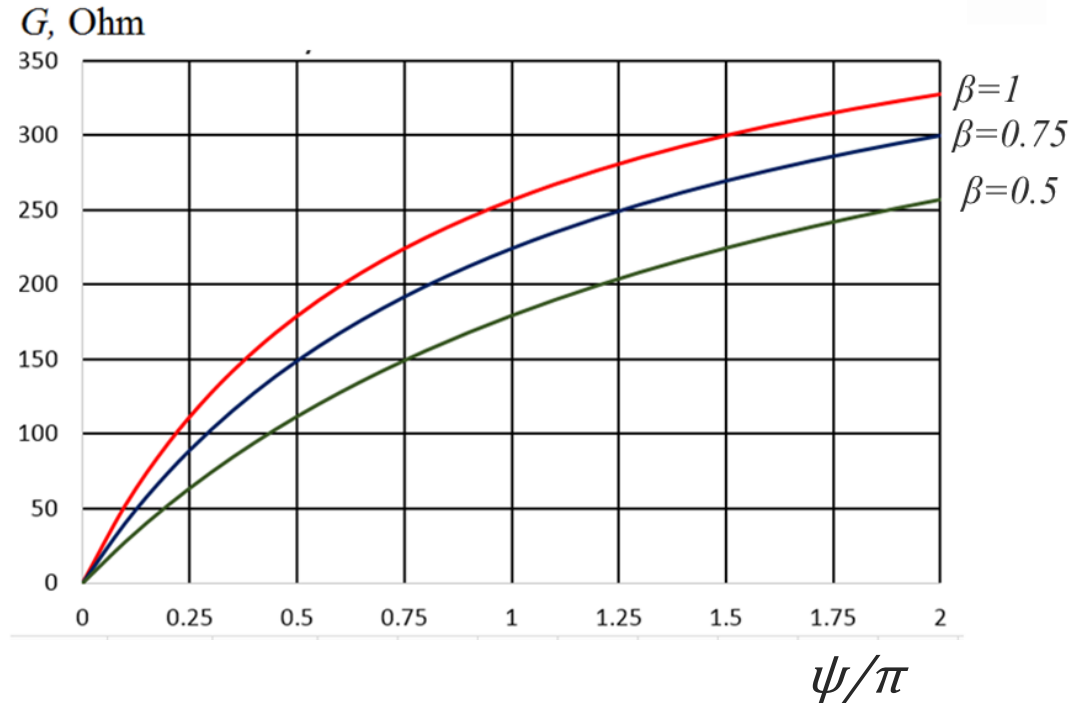
$$H_\varphi = J_1(kr), \quad k = \frac{\omega_{010}}{c} = \frac{2.405}{b}$$

$$\int_V |\vec{H}_m|^2 dV = \pi db^2 J_1^2(kb), \quad \oint_S |\vec{H}_m|^2 dS = 2\pi b(b+d) J_1^2(kb)$$

$$G = \frac{\omega_0 \mu_0 \int_V |\mathbf{H}|^2 dv}{\int_S |\mathbf{H}|^2 ds}$$

and

$$G = 1.2Z_0 \frac{1}{1+b/d}$$



RF cavity parameters:

For a room-temperature pillbox cavity

$$Q_0 = \frac{1}{\delta} \frac{bd}{b+d}$$

$$Q_0 = \frac{\omega_0 \mu_0 \int_V |\mathbf{H}|^2 dv}{R_s \int_S |\mathbf{H}|^2 ds}$$

- For pillbox having $\psi=\pi$ and $\beta=1$ ($d = \lambda/2 = \pi b/2.405$), $G = 257$ Ohms.
- Therefore, 1.3 GHz RT copper pillbox cavity has $Q_0 = 2.6e4$.
- For 1.3 GHz SRF Nb cavity at 2K one has $Q_0 = 3e10$ ($R_s = 8.5$ nOhm).

For geometrically similar RT cavities Q_0 scales as $f^{-1/2}$ or $\lambda^{1/2}$!

RF cavity parameters:

Estimation of the unloaded Q_0 for an arbitrary room-temperature cavity:

$$Q_0 = \frac{\omega_0 \mu_0 \int_V |\vec{H}|^2 dV}{R_s \int_S |\vec{H}|^2 dS}, \quad R_s = \frac{1}{\sigma \delta},$$

Taking into account that $\omega_0 \sigma = \frac{2}{\delta^2 \mu_0}$, one has:

$$Q_0 = \frac{2}{\delta} \frac{\int_V |\vec{H}|^2 dV}{\int_S |\vec{H}|^2 dS}$$

One may introduce the average surface and volume fields:

$$Q_0 = \frac{2}{\delta} \frac{V |H|_V^2}{S |H|_S^2}, \quad 2 |H|_V^2 = A |H|_S^2, \quad \text{for accelerating mode } A \sim l$$

For convex figures $V/S \sim a_{av}/6$ (cube: $V/S = a/6$. sphere: $V/S = 2R/6$) and

$$Q_0 \approx \frac{1}{6} \frac{a_{av}}{\delta} A.$$

Note, that $a_{av} \sim \lambda$, $\delta \sim \sqrt{\lambda}$ and $Q_0 \sim \lambda^{1/2}$,

RF cavity parameters:

- An important parameter is the cavity shunt impedance R , which determines relation between the cavity accelerating voltage V and power dissipation:

$$R = \frac{V^2}{P_c}$$

- Another important parameter is (R/Q) , which determines relation between the cavity voltage V and stored energy U . It is necessary to estimate the mode excitation by the accelerated beam. **It does not depend on the surface resistance and is the same for geometrically similar cavities:**

$$\frac{R}{Q} = \frac{V^2}{\omega_0 U} = 2 \frac{\left| \int_{-\infty}^{\infty} E_z(\rho=0, z) e^{i\omega_0 z / \beta c} dz \right|^2}{\omega_0 \mu_0 \int_V |\mathbf{H}|^2 dv}$$

Note that $R = \frac{R}{Q} \cdot Q_0$ and power dissipation $P_c = \frac{V^2}{\frac{R}{Q} \cdot Q_0} = \frac{V^2 \cdot R_s}{\frac{R}{Q} \cdot G}$

*Sometimes they use a “circuit” definition: $\frac{R}{Q} = \frac{V^2}{2\omega_0 U}$

RF cavity parameters:

For a pillbox cavity:

$$V = E_0 d \cdot T(\psi)$$

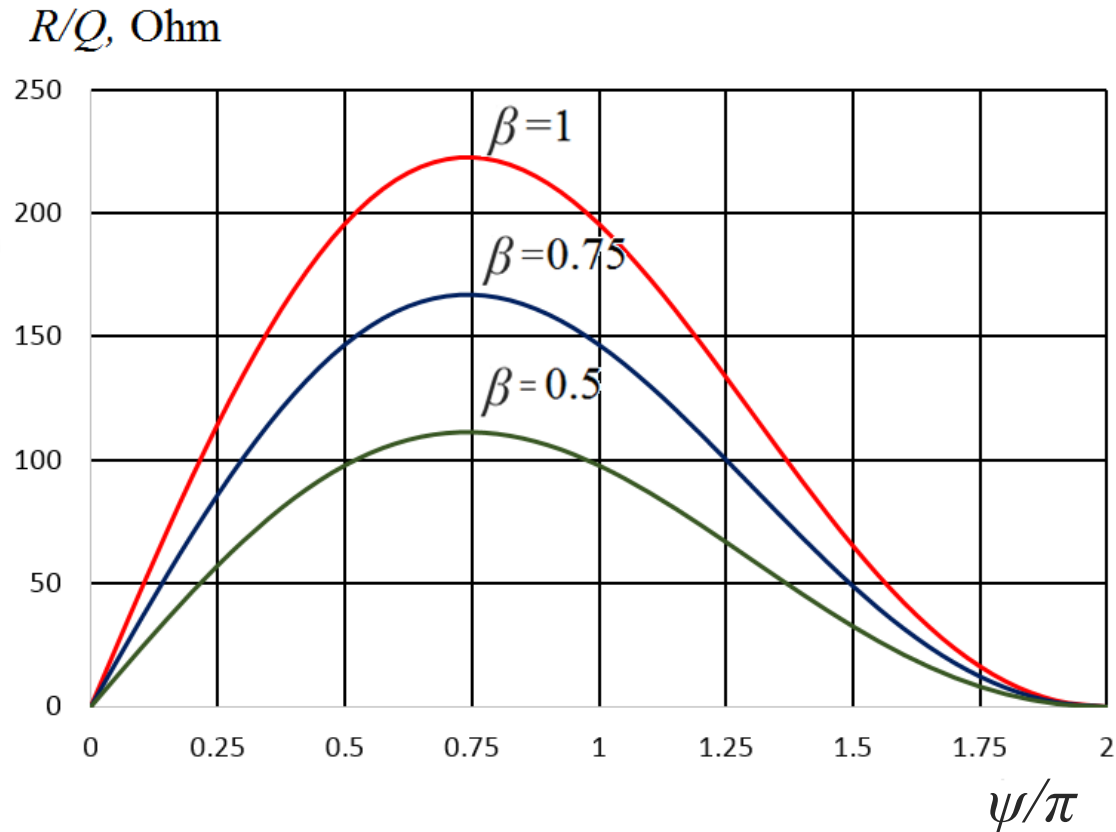
$$\int_V |\vec{H}_m|^2 dV = \frac{E_0^2}{Z_0^2} \pi d b^2 J_1^2(kb),$$

$$J_1(kb) = J_1(2.405) = -0.519$$

$$\omega_0 \mu_0 = Z_0 2.405 / b$$

and

$$\frac{R}{Q} = 0.98 Z_0 d / b \cdot T^2(\psi)$$



- For pillbox having $\psi = \pi$ and $\beta = 1$ ($d = \lambda/2 = \pi b / 2.405$), $R/Q = 196$ Ohms.
- R/Q is maximal for for $\psi \approx 3\pi/4$.

RF cavity parameters:

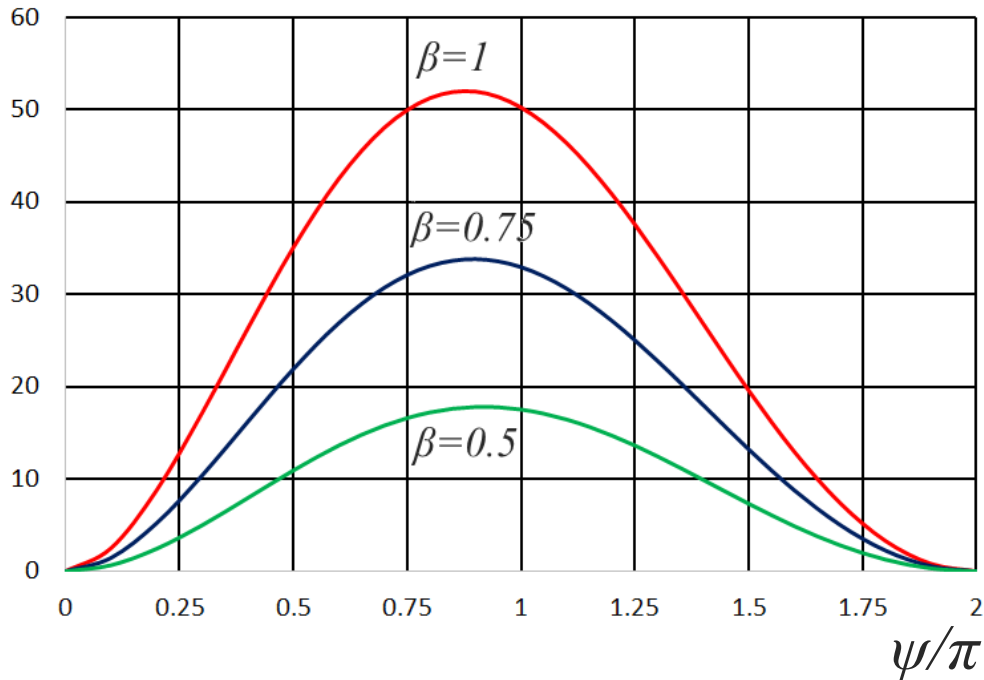
The power loss in the cavity walls is

$$P_c = \frac{V^2 \cdot R_s}{G \cdot (R/Q)}$$

Therefore, the losses are determined by $G \cdot R/Q$.

For pillbox:

$G \cdot R/Q$, kOhm²



$G \cdot R/Q$ is maximal for $\psi \approx 0.9\pi$

RF cavity parameters:

Gradient limitations are determined by surface fields:

❖ RT cavities:

-breakdown (determined mainly by E_{peak})

-metal fatigue caused by pulsed heating (determined by B_{peak})

❖ SRF cavities:

-quench (determined by B_{peak})

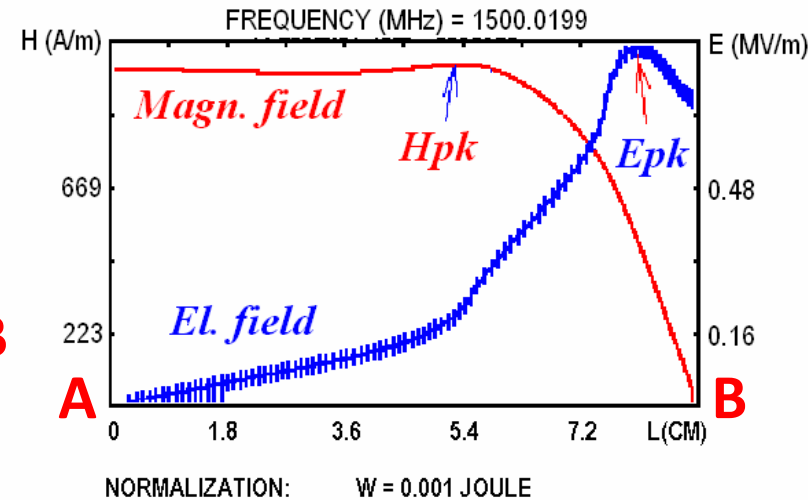
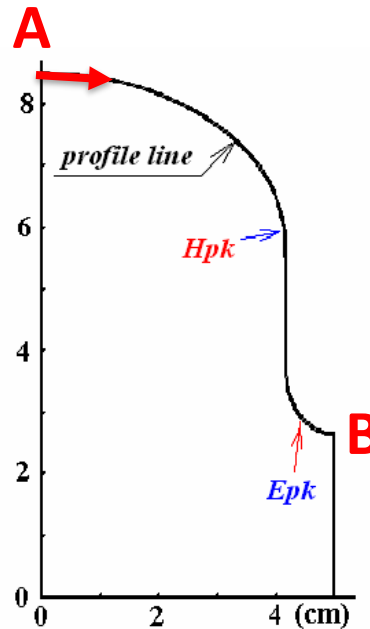
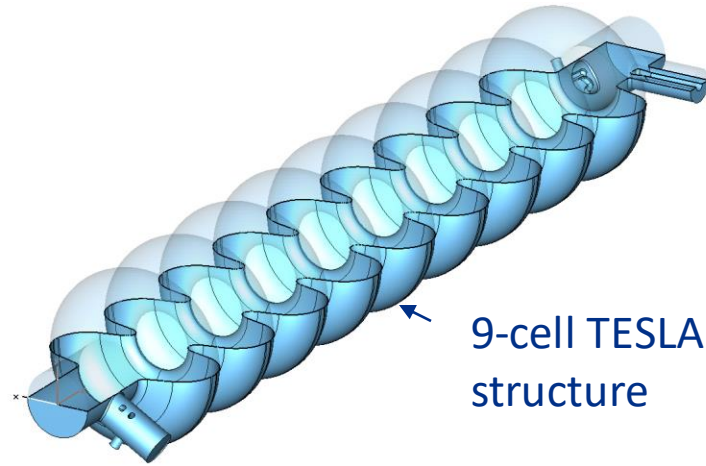
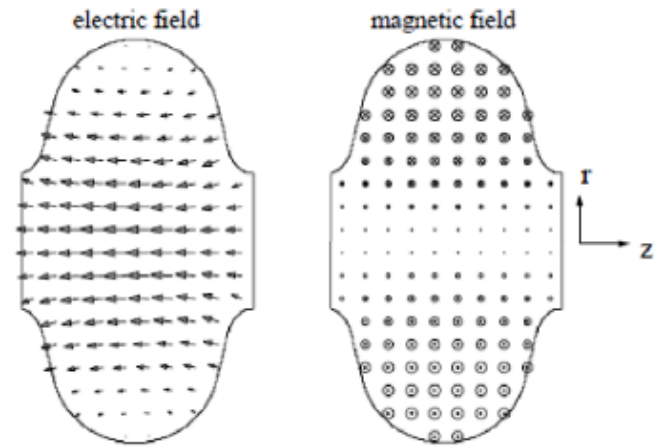
Field enhancement factors:

- Surface electric field enhancement: $K_e = E_{peak}/E$, E_{peak} is maximal surface electric field. K_e is dimensionless parameter.
- Surface magnetic field enhancement: $K_m = B_{peak}/E$, B_{peak} is maximal surface magnetic field. K_m is in mT/(MV/m)

Here E is acceleration gradient.

RF cavity parameters:

Field enhancement factors – example:



$$K_e = E_{peak}/E = 2; \quad K_m = B_{peak}/E = 4.16 \text{ mT/MV/m}$$

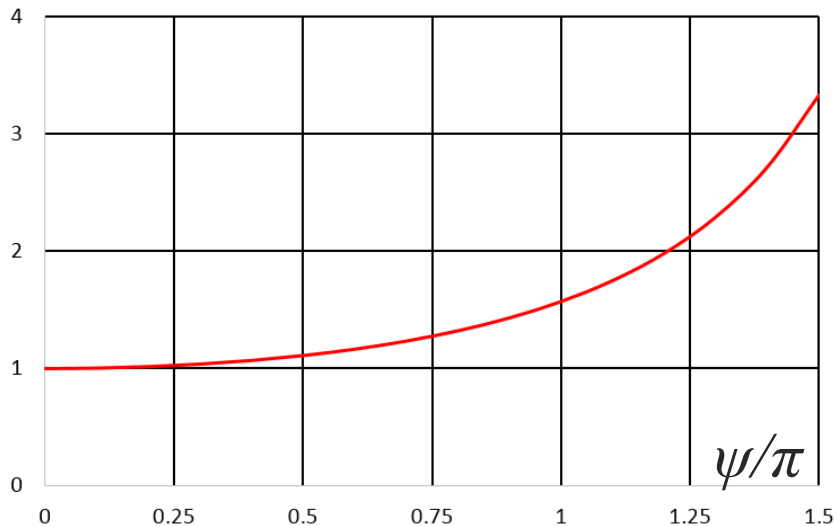
Geometry of an inner half-cell of a multi-cell cavity and field distribution along the profile line.

RF cavity parameters:

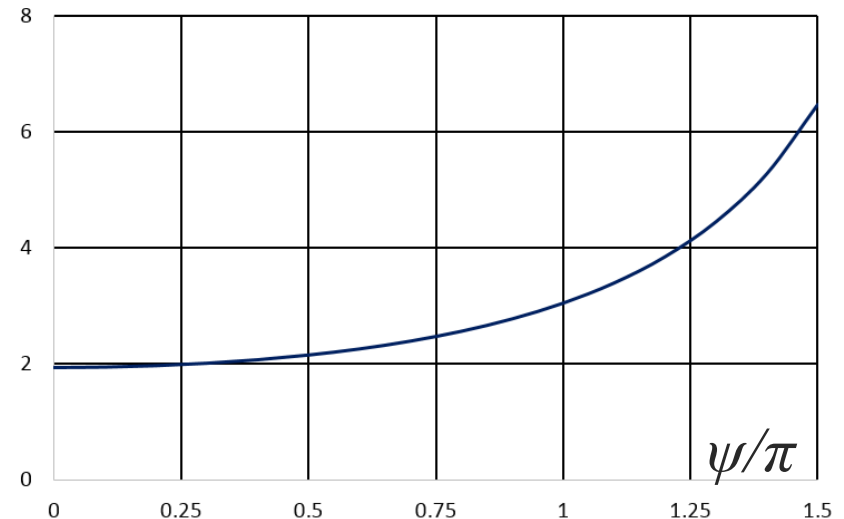
For a pillbox cavity:

- Surface electric field enhancement: $K_e = E_{peak}/E = 1/T(\psi)$
($E_{peak} = E_0$, $E = E_0 T(\psi)$, see slide 47)
- Surface magnetic field enhancement: $K_m = B_{peak}/E =$
 $= 1.94/T(\psi) [mT/(MV/m)]$
($B_{peak} = E_0 \cdot J_1(2.405r/b)_{max}/c = 0.582E_0/c$, see slide 59)

K_e



$K_m, mT/(MV/m)$



Example:

Let's consider a pillbox cavity for high-energy electrons ($\beta \approx 1$), $f=500$ MHz, or wavelength $\lambda=c/f=0.6$ m. The mode is TM_{010} . The cavity voltage V is 3 MV.

1. The cavity radius b (Slide 59):

$$b = 2.405c/(2\pi f) = 230 \text{ mm.}$$

2. The cavity transit time factor for $\psi=\pi$ (Slide 60):

$$T = \sin(\pi/2)/(\pi/2) = 2/\pi = 0.64.$$

3. The cavity length d (Slide 61):

$$d = \beta\lambda/2 = 300 \text{ mm.}$$

4. The cavity G - factor (Slide 64):

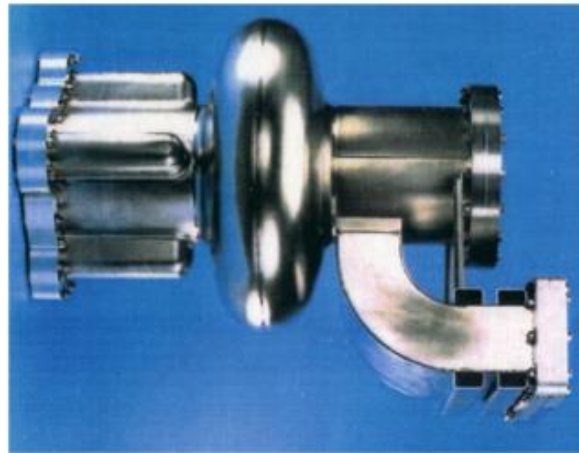
$$G = 1.2Z_0/(1+b/d) = 256 \text{ Ohm}$$

5. The cavity R/Q (Slide 68):

$$R/Q = 0.98Z_0(d/b)T^2 = 196 \text{ Ohm}$$

Pillbox vs. “real life” SC cavity

Quantity	Cornell SC 500 MHz	Pillbox
G	270 Ω	257 Ω
R/Q	88 Ω/cell	196 Ω/cell
$E_{\text{pk}}/E_{\text{acc}}$	2.5	1.6
$B_{\text{pk}}/E_{\text{acc}}$	5.2 $mT/(\text{MV}/\text{m})$	3.05 $mT/(\text{MV}/\text{m})$



Cornell SC 500 MHz

- In “real life” cavities, sometimes it is necessary to damp higher-order modes (HOMs) to avoid beam instabilities.
- The beam pipes are made large to allow HOMs propagation toward microwave absorbers.
- This enhances B_{pk} and E_{pk} and reduces R/Q .

Example:

6. Surface resistance R_s for room-temperature copper (Slide28):

$$R_s = \sqrt{\frac{\omega Z_0}{2c\sigma}} = 5.8 \text{ mOhm}$$

7. Surface resistance R_s for superconducting Nb at 2 K (Slide 33):

$$R_{s,BCS} \approx 1.643 \times 10^{-5} \frac{T_c}{T} (f(\text{GHz}))^2 e^{-\frac{1.92T_c}{T}} = 2.8 \text{ nOhm}$$

8. Copper cavity unloaded quality factor Q_0 (Slide 63):

$$Q_0 = G/R_s = 44e3$$

9. Nb cavity unloaded quality factor Q_0 at 2 K (Slide 63):

$$Q_0 = G/R_s = 9e10 \text{ (compared to } 44e3 \text{ for a copper cavity!)}$$

Example:

10. Copper cavity wall power dissipation (Slide 67):

$$P_{diss} = \frac{V^2}{\frac{R}{Q} \cdot Q_0} = 1 \text{ MW} - \text{unacceptable!}$$

11. Nb cavity wall power dissipation (Slide 67):

$$P_{diss} = \frac{V^2}{\frac{R}{Q} \cdot Q_0} = 0.5 \text{ W!}$$

12. Acceleration gradient (Slide 61):

$$E = V/d = 3 \text{ MeV}/0.3\text{m} = 9 \text{ MV/m}$$

13. Peak surface electric and magnetic fields (Slide 72):

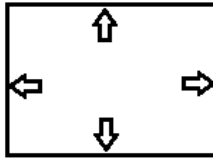
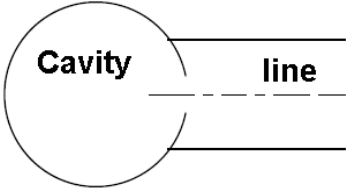
$$E_{peak} = K_e \cdot E = E/T = 14.1 \text{ MV/m} = 141 \text{ kV/cm} - \text{OK for SC}$$

$$B_{peak} = K_m \cdot E = 1.94 \cdot E/T \text{ mT} = 27 \text{ mT} - \text{OK for SC}$$

SC cavities allow much higher acceleration gradient at CW!

The cavity coupling to the line:

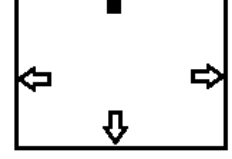
Let's consider the cavity coupled to the feeding line.



Wall loss:
 $Q_0 = \omega_0 U / P_0$



Port radiation:
 $Q_{ext} = \omega_0 U / P_{ext}$



Wall loss and port radiation:
 $Q_L = \omega_0 U / (P_0 + P_{ext})$

↓

$$\frac{1}{Q_L} = \frac{1}{Q_0} + \frac{1}{Q_{ext}}$$

If the incident wave is zero (i.e., if the RF source is off), the loss in the cavity is a sum of the wall P_0 loss and the loss coasted by the radiation to the line P_{ext} :

$$P_{tot} = P_0 + P_{ext}$$

$$P_0 = \frac{V^2}{R/Q \cdot Q_0}, \quad P_{ext} = \frac{V^2}{R/Q \cdot Q_{ext}}$$

where we have defined an external quality factor associated with an input coupler. Such Q factors can be identified with all external ports on the cavity: input coupler, RF probe, HOM couplers, beam pipes, etc. The total power loss can be associated with the loaded Q factor, which is

$$\frac{1}{Q_L} = \frac{1}{Q_0} + \frac{1}{Q_{ext1}} + \frac{1}{Q_{ext2}} + \dots \quad \text{because } P_{tot} = P_0 + P_{ext1} + P_{ext2} \dots = \frac{V^2}{R/Q \cdot Q_L}$$

Coupling parameter:

For each port a coupling parameter β can be defined as

$$\beta \equiv \frac{Q_0}{Q_{ext}} \quad \text{and, therefore,} \quad \frac{1}{Q_L} = \frac{1+\beta}{Q_0}$$

It tells us how strongly the couplers interact with the cavity. Large implies that the power leaking out of the coupler is large compared to the power dissipated in the cavity walls:

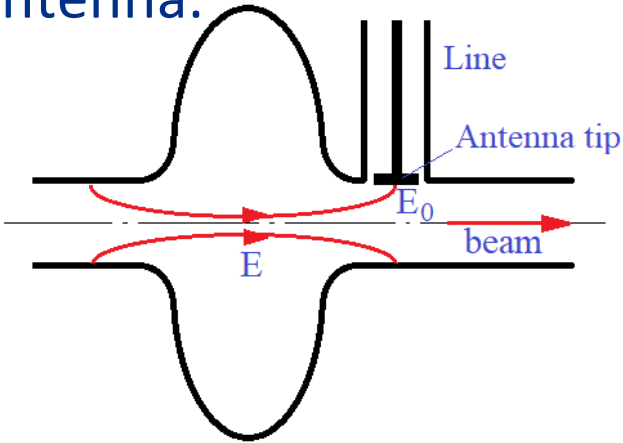
$$P_{ext} = \frac{V^2}{R/Q \cdot Q_{ext}} = \frac{V^2}{R/Q \cdot Q_0} \cdot \beta = \beta P_0$$

In order to maintain the cavity voltage, the RF source should compensate both wall loss and radiation to the line. Therefore, the RF source should deliver the power to the cavity which is

$$P_{tot} = P_{forw} + P_0 = (\beta + 1)P_0$$

The cavity coupling to the line

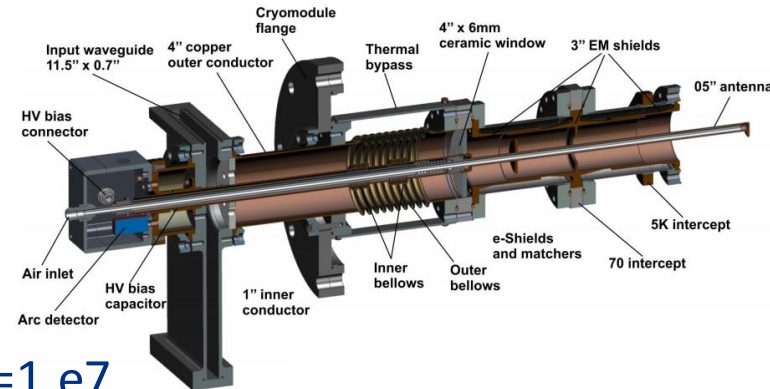
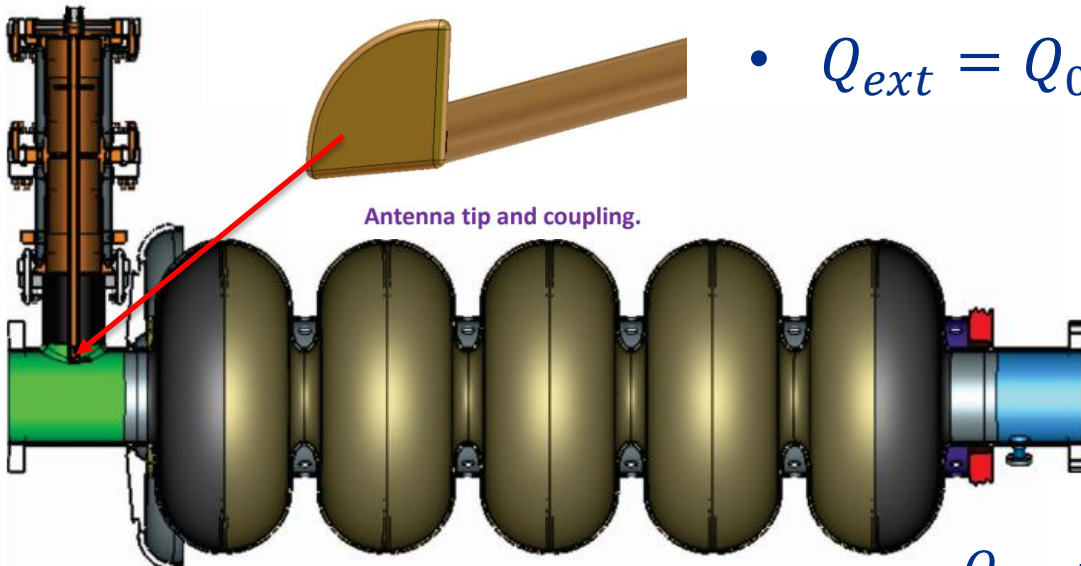
Antenna:



- Antenna tip square is S ;
- The line has impedance Z ;
- Electric field on the tip is E_0
- Antenna tip has a charge q :

$$q = E_0 \epsilon_0 S \rightarrow I = \omega q = \omega E_0 \epsilon_0 S = k S E_0 / Z_0;$$
- Radiated power $P_{ext} = \frac{1}{2} Z I^2$;
- Loss in the cavity $P_0 = \frac{V^2}{R/Q \cdot Q_0}$
- $Q_{ext} = Q_0 \frac{P_0}{P_{ext}} = 2 \frac{Z_0^2}{Z \cdot R/Q} \cdot \left(\frac{V}{k S E_0} \right)^2$

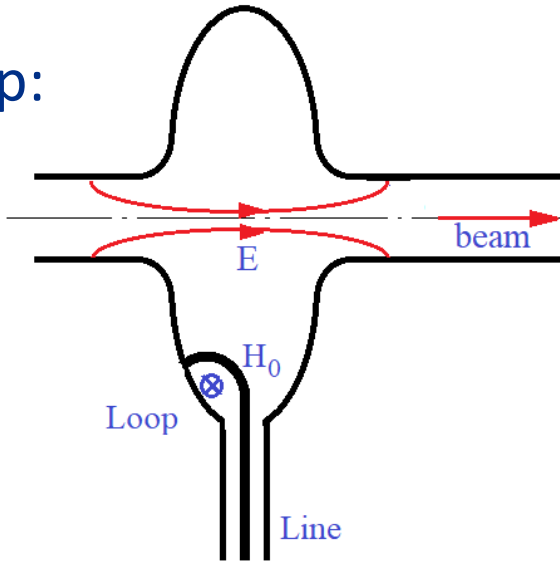
Structure of 650 MHz coupler, new design



$$Q_{ext} = 1.e7$$

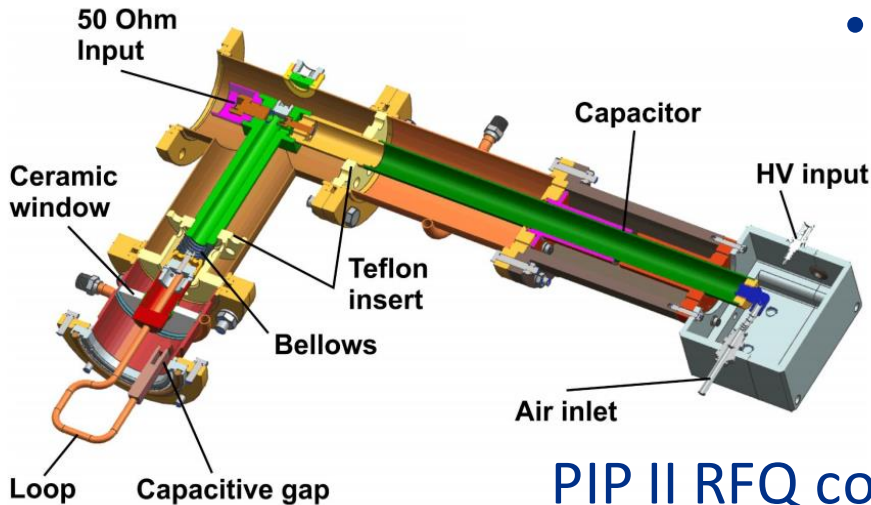
The cavity coupling to the line

Loop:

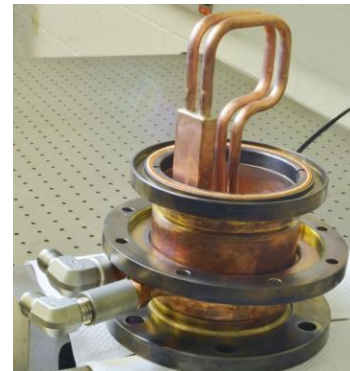


- Loop square is S ;
- The line has impedance Z ;
- Magnetic field on the loop is H_0
- Voltage induced on the loop U :

$$U = \omega H_0 \mu_0 S; \quad \leftarrow \text{curl} \vec{E} = -i\omega \mu_0 \vec{H}$$
- Radiated power $P_{ext} = \frac{U^2}{2Z}$;
- Loss in the cavity $P_0 = \frac{V^2}{R/Q \cdot Q_0}$
- $Q_{ext} = Q_0 \frac{P_0}{P_{ext}} = 2 \frac{Z}{R/Q} \cdot \left(\frac{V}{kSH_0Z_0} \right)^2$

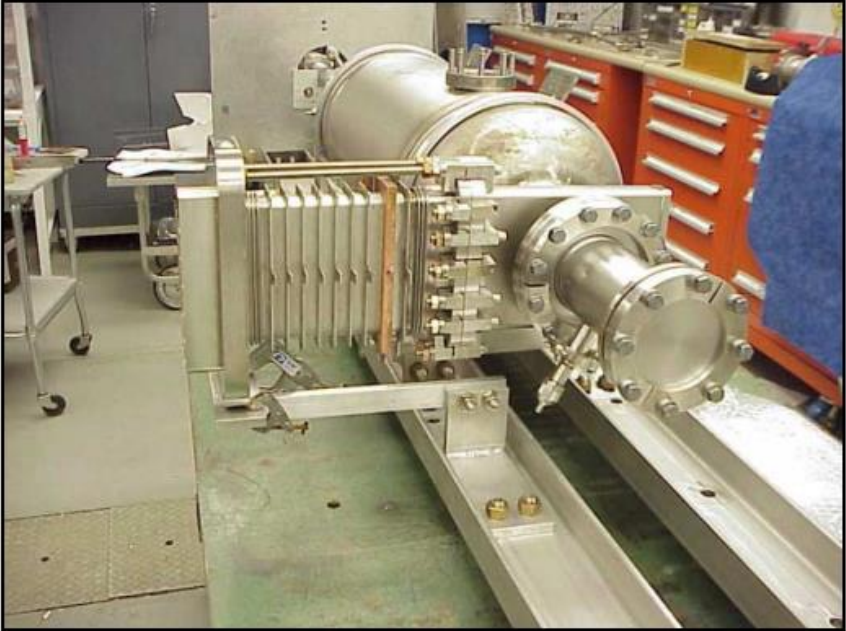
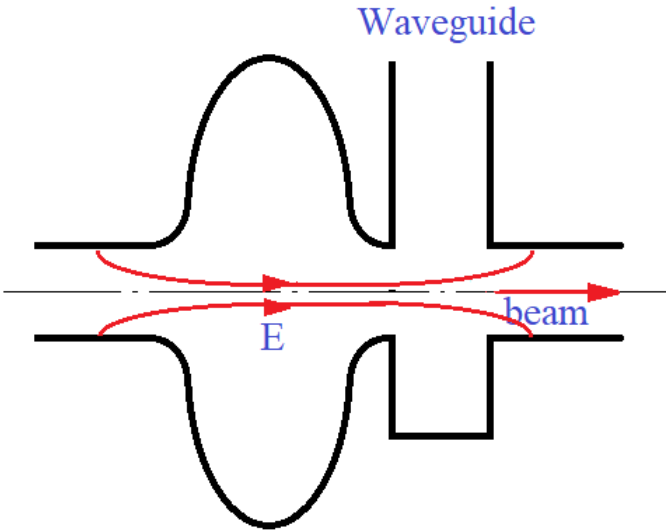


PIP II RFQ coupler



The cavity coupling to the line

Waveguide:



Waveguide on Cavity String



CEBAF couplers

Cavity excited by the beam

- If the cavity is excited by the beam with the *average* current I having the bunches separated by the length equal to integer number of RF periods, i.e., in resonance, the excited cavity voltage provides maximal deceleration. The beam power loss is equal to the cavity loss, i.e., radiation and wall loss:

$$-VI = \frac{V^2}{\left(\frac{R}{Q}\right)Q_L} \quad (1)$$

or

$$V = -I \left(\frac{R}{Q}\right) Q_L = -IR_{sh}$$

$$\frac{1}{Q_L} = \frac{1}{Q_0} + \frac{1}{Q_{ext}} = \frac{1+\beta}{Q_0}$$

$$\beta = \frac{Q_0}{Q_{ext}} \text{ -coupling parameter}$$

(See Slide 78)

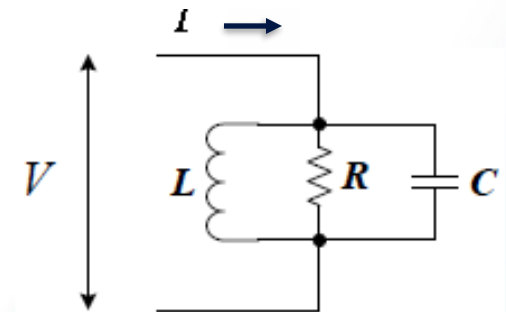
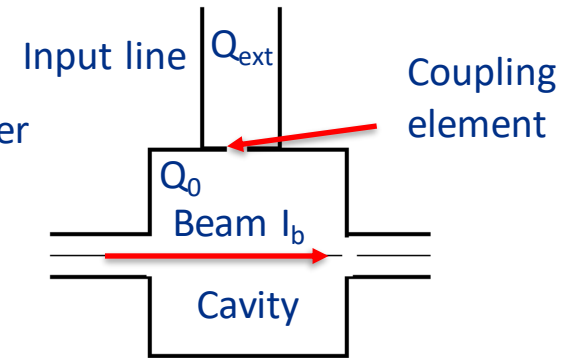
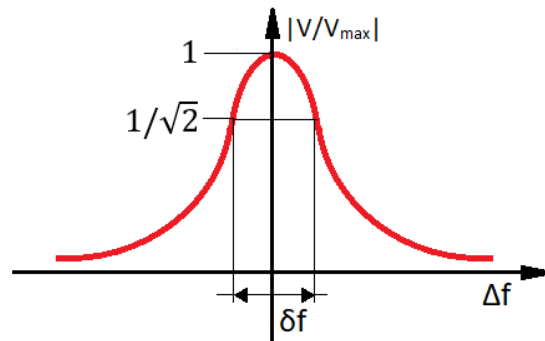
- The cavity excited by the beam off the resonance, the

$$\text{voltage is } V \approx -\frac{I\left(\frac{R}{Q}\right)Q_L}{1+iQ_L\frac{2\Delta f}{f}}$$

where Δf is the distance between the beam spectrum line and the cavity resonance frequency f .

- Cavity bandwidth:

$$\delta f = f/Q_L$$



$$L = (R/Q)/2\omega;$$

$$C = 2/\omega(R/Q);$$

$$R = (R/Q)Q_L/2;$$

$$\omega = 2\pi f$$

Acceleration cavity operating in CW regime:

Energy conservation law:

$$P_0 = P_{backward} + P_{diss} + P_{beam}$$

$$P_0 = E_0^2 / (2Z),$$

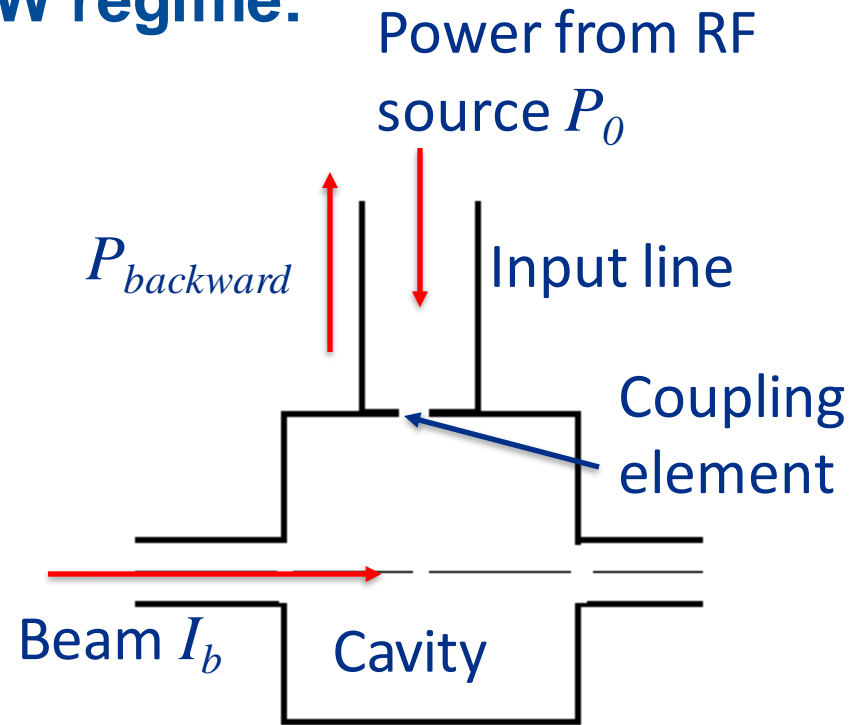
Here Z is the transmission line impedance; E_0 is the incident wave amplitude in the transmission line.

- $P_{backward} = (E_0 - E_{rad})^2 / (2Z)$,
 E_{rad} is the amplitude of wave radiated from the cavity to the transmission line.

$$\beta = P_{rad} / P_{diss}$$

$$P_{rad} = E_{rad}^2 / (2Z) = \beta P_{diss} = \beta V^2 / (Q_0 \cdot R / Q) = V^2 / (Q_{ext} \cdot R / Q);$$

$$P_{beam} = V \cdot I_b$$



Acceleration cavity operating in CW regime:

- If the line is matched to the transmission line,
- coupling is optimal, $\beta = \beta_{opt}$ then

$$P_{backward} = 0, \quad E_0 = E_{rad},$$

and therefore,

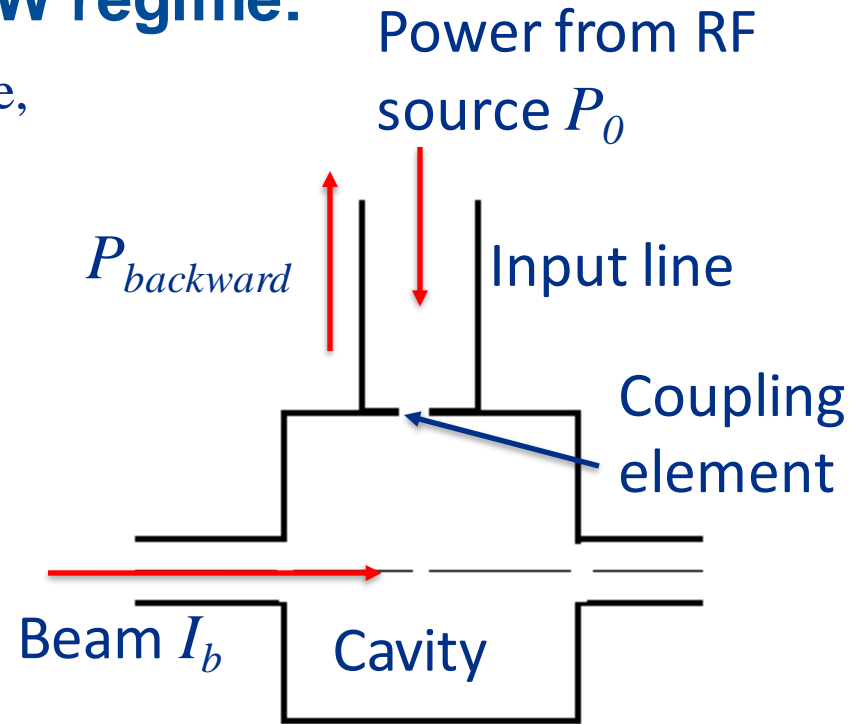
$$P_{rad} = P_0 = P_{diss} + P_{beam}, \text{ or}$$

$$\beta_{opt} V^2 / (Q_0 \cdot R/Q) = V^2 / (Q_0 \cdot R/Q) + VI$$

$$\text{and } \beta_{opt} = I \cdot Q_0 \cdot R/Q / V + 1.$$

$$\text{For } \beta_{opt} \gg 1, \quad \beta_{opt} \approx I \cdot Q_0 \cdot R/Q / V \text{ and}$$

$$Q_L = Q_0 / (1 + \beta_{opt}) \approx V / (R/Q \cdot I)$$



(see Slide 78)

Acceleration cavity operating in pulsed regime:

Energy conservation law:

$$dW/dt = P_0 - P_{backward} - P_{diss} - P_{beam}$$

$$P_0 = E_0^2/2Z; P_{backward} = (E_0 - E_{rad})^2/2Z,$$

$$\beta = P_{rad}/P_{diss}, P_{rad} = E_{rad}^2/2Z = V(t)^2/[(R/Q)Q_{ext}]$$

$$P_{beam} = V(t)I$$

$$W = V(t)^2/(R/Q)\omega;$$

$$\tau = 2Q_L/\omega - \text{time constant.}$$

$$V_0 - \text{operating voltage,}$$

If $\beta \gg 1$, $Q_L \approx V_0/(R/Q \cdot I)$. Here $V_0 = [P_0(R/Q)Q_{ext}]^{1/2}$

Substituting (2) to (1) we have:

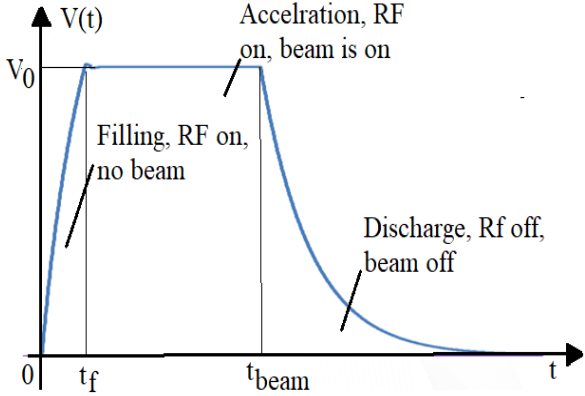
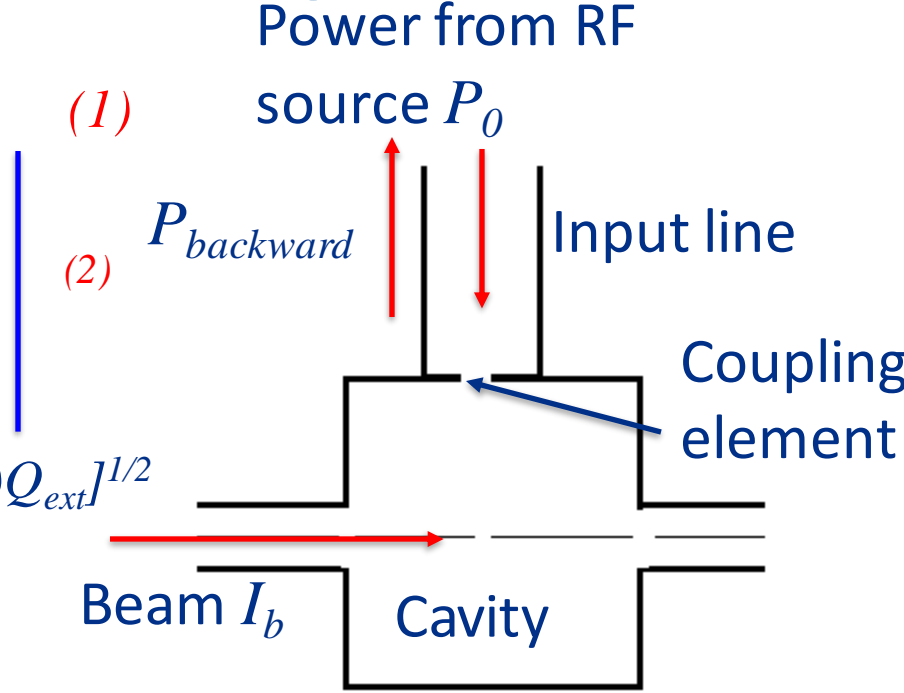
$$dV/dt = (2V_0 - V(t) - I \cdot (R/Q) \cdot Q_L) / \tau$$

RF on:

- Cavity filling, no beam: $I=0$, $V(t) = 2V_0(1 - \exp(-t/\tau))$;
If the filling time $t_f = \tau \ln 2$, $V(t_f) = V_0$,
- Acceleration, the beam is on, $V_0 = I \cdot (R/Q) \cdot Q_L$,
 $dV/dt = (V_0 - V(t))/\tau = 0$ and $V(t) = V_0$;

RF is off:

$dV/dt = -V(t)/\tau$, the cavity discharge, $V(t) = V_0 \cdot \exp(-t/\tau)$.



Example:

Let's consider a SC Nb pillbox cavity for high-energy electrons ($\beta \approx 1$), $f=500$ MHz, or wavelength $\lambda=c/f=0.6$ m. The mode is TM_{010} . The cavity voltage V is 3 MV. The beam current I is 1 A.

1. The cavity R/Q (Slide 68):

$$R/Q = 0.98 Z_0 (d/b) T^2 = 196 \text{ Ohm}$$

2. Nb cavity unloaded quality factor Q_0 at 2 K (Slides 73-76):

$$Q_0 = G/R_s = 9e10$$

3. The cavity loaded quality factor (Slide 84):

$$Q_L \approx V/(R/Q)I = 1.5e3$$

3. The optimal coupling (Slide 84):

$$\beta = Q_0/Q_L - 1 \approx Q_0/Q_L = 6e7$$

4. The power necessary for acceleration (Slide 84):

$$P_0 = P_c + P_{beam} \approx P_{beam} = VI = 3 \text{ MW (compared to } P_c = 0.5 \text{ W!)}$$

High-Order Modes in cavities:

□ Possible issues:

- Trapped modes;
- Resonance excitation of HOMs;
- Collective effects:
 - Transverse (BBU) and longitudinal (klystron-type instability) in linear accelerators;

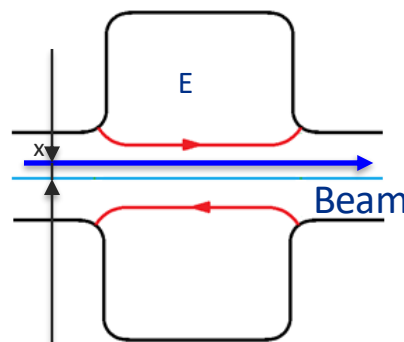


- Additional losses;
- Emittance dilution (longitudinal and transverse)
- Beam current limitation.

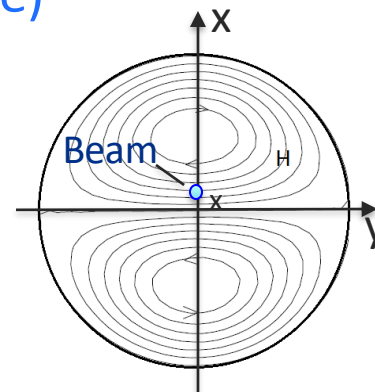
□ Longitudinal modes;

□ Transverse modes.

□ HOM dampers;



Dipole (transverse) mode



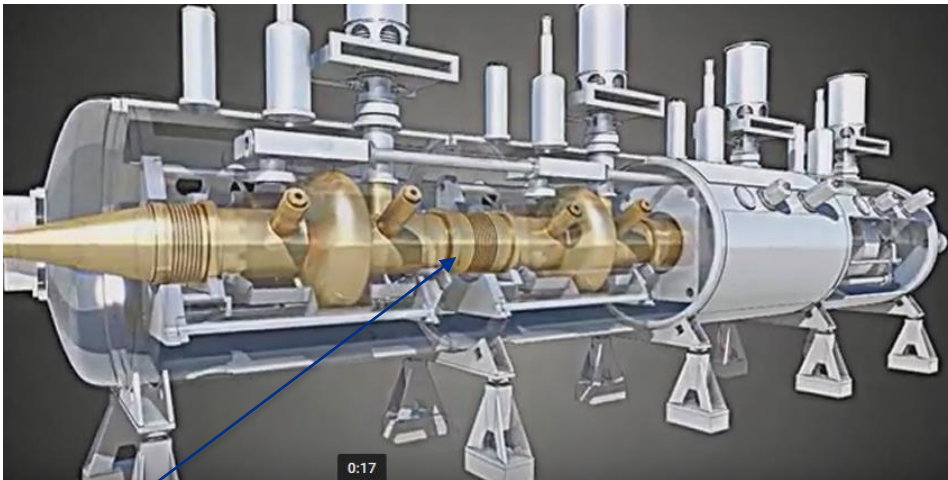
Near axis: $E_z \sim x$, $E_x \sim \text{const}$, $H_y \sim \text{const}$

High-Order Modes in cavities:

□ Longitudinal modes:

$$V_{HOM} = I_{beam} \cdot R_{HOM}, \quad \text{Longitudinal impedance: } R_{HOM} = (R/Q)_{HOM} \cdot Q_{load}$$

- Design of the cavities with small R/Q (poor beam-cavity interaction)
- HOM dampers – special coupling elements connected to the load (low Q_{load}).



LHC main cavity



LHC HOM coupler, $Q_{ext} < 200$
for most “dangerous” modes

- Long wide waveguides between the cavity cells:
- HOMs propagate in the WGs and interact with the beam;
- No synchronism in the WGs (phase velocity $>$ speed of light) \rightarrow reduced R/Q_{HOM} for HOMs

High-Order Modes in cavities

□ Transverse modes:

The beam interacts with the longitudinal component of the HOM electric field and provides transverse kick. For axisymmetric cavity for dipole TM-mode longitudinal field is proportional to the transverse coordinate next to the cavity axis.

Let's consider a cavity excited by a beam current I_0 having offset x_0 . The kick caused by the dipole mode excited by the beam:

$$U_{kick} = ix_0 I_0 Q_{ext} \left(\frac{r_{\perp}}{Q} \right) \quad \text{where}$$

$$\left(\frac{r_{\perp}}{Q} \right) \equiv \frac{\left| \int_{-\infty}^{\infty} \left(\frac{\partial E_z(x, 0, z)}{\partial x} \right)_{x=x_0} e^{ikz} dz \right|^2}{kW \omega_0}$$

is transverse impedance, $k = \omega_0/c$ and $W = \frac{\epsilon_0}{2} \int |\vec{E}|^2 dV$ - stored energy.

Compare to "longitudinal" (R/Q):

$$\left(\frac{R}{Q} \right) \equiv \frac{\left| \int_{-\infty}^{\infty} E_z(0, 0, z) e^{ikz} dz \right|^2}{W \omega_0}$$

$\beta=1$ is considered.

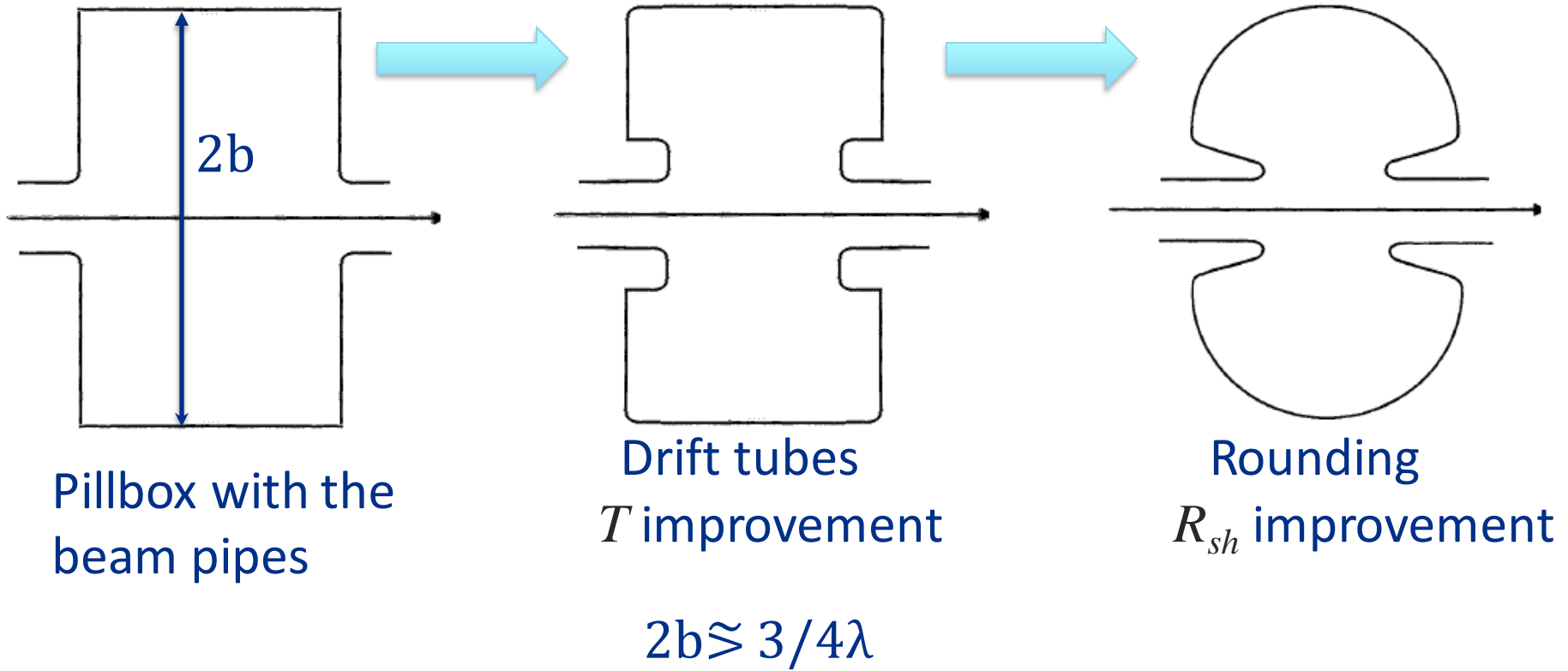
Note that $\left(\frac{r_{\perp}}{Q} \right)$ is measured in Ohm/m.

*Note that sometimes they use other transverse impedance, that is determined as:

$$\left(\frac{r_{\perp}}{Q} \right)_1 = \frac{|U_{kick}|^2}{\omega_0 W_0} = \left(\frac{r_{\perp}}{Q} \right) \times \frac{1}{k}. \quad \text{In this case, } U_{kick} = i(kx_0)I_0 Q_{ext} \left(\frac{r_{\perp}}{Q} \right)_1, \quad \left(\frac{r_{\perp}}{Q} \right)_1 \text{ is measured in Ohm.$$

RF cavity types

Pillbox RT cavities:

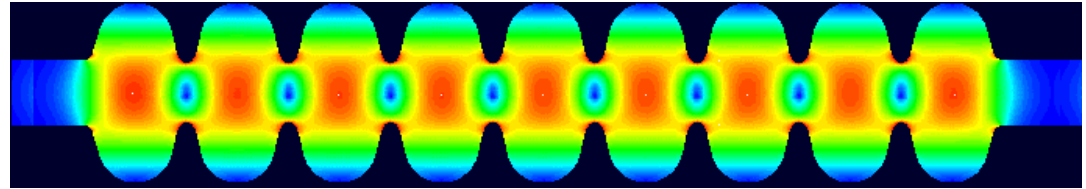


Tools for RF cavity simulations:

I. Field calculations:

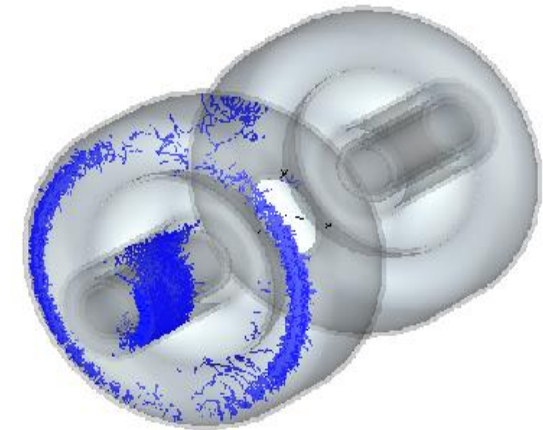
- Spectrum, (r/Q) , G , β (coupling)
- Field enhancement factors

- HFSS (3D);
- CST (3D);
- Comsol (3D)
- Omega-3P (3D);
- Analyst (3D);
- Superfish (2D)
- SLANS (2D, high precision of the field calculation).



II. Multipactoring (2D, 3D)

- Analyst;
- CST (3D);
- Omega-3P

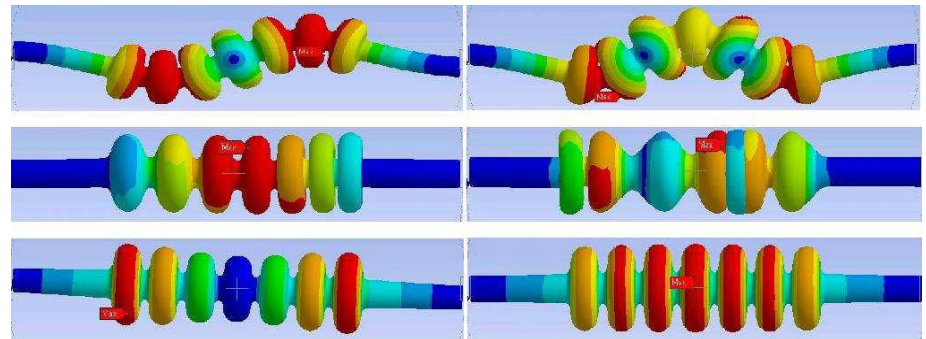


III. Wakefield simulations (2D, 3D):

- GdfidL;
- PBCI;
- ECHO.

IV. Mechanical simulations:

Lorenz force and Lorenz factor,
Vibrations,
Thermal deformations.



a. ANSYS

Summary:

- ❑ To create acceleration RF field, resonance RF cavities are used;
- ❑ The cavities typically have axisymmetric field distribution near the beam axis. Most of cavities have geometry close to axisymmetric.
- ❑ There are infinite number of resonance modes in an RF cavity having different radial, azimuthal and longitudinal variations. The modes are orthogonal;
- ❑ In axisymmetric cavities there are two types of modes, TM and TE;
- ❑ For acceleration, TM_{010} mode is used, which has axial electric field on the axis.
- ❑ Other modes, HOMs, are parasitic, which may caused undesirable effects.

Summary (continuation):

- The cavity mode is characterized by the following parameters:
 - Resonance frequency;
 - Acceleration gradient (energy gain/cavity length);
 - Unloaded Q, Q_0 , which characterize the losses in the cavity;
 - G -factor, which relates Q_0 and surface resistance;
 - (R/Q) , which relates the energy gain and the energy stored in the cavity;
 - Shunt impedance R , which relates the gain and total losses in the cavity;
 - Electric and magnetic field enhanced factors, which relate maximal surface fields and the acceleration gradient;

Summary (continuation):

- ❑ The cavity coupled to the input port is characterized by the following parameters:
 - Coupling to the feeding line, β (do not mix with the relative particle velocity 😊)
 - External Q, Q_{ext}
 - Loaded Q, Q_{load}
- ❑ The beam excites the cavity creating decelerating voltage, which is proportional at resonance to the shunt impedance and the beam current. This voltage should be compensated by the RF source to provide acceleration.
- ❑ High-Order Modes excited by the beam may influence the beam dynamics and lead to additional losses in the cavity.
 - Dipole modes are characterized by transverse impedance, (r_{\perp}/Q) , which relates transverse kick and stored energy.
 - Both monopole and dipole HOMs should be taken into account during the cavity design process, and damped if necessary.

RF accelerating structures

Outline:

4. Periodic acceleration structures;
5. Standing –Wave acceleration structures;
6. Why SRF cavities?

Chapter 4.

Periodic acceleration structures.

- a. Coupled cavities and periodic structure;
- b. Travelling waves in a periodic structure;
- c. Dispersion curve;
- d. Phase and group velocities;
- e. Parameters of the TW structures;
- f. Equivalent circuit for a travelling – wave structure;
- g. Losses in the TW structure;
- h. Types of the TW structures;
- i. Examples of modern TW structures.

Periodic acceleration structures:

- Single – cell cavities are not convenient to achieve high acceleration: a lot of couplers, tuners, etc.
- Especially it is important for electron acceleration:

$R_{sh} = R/Q \cdot Q_0 \sim \omega^{1/2}$, low Ohmic losses at high frequency;
 $v=c$, focusing is quadratic and does not depend on frequency.



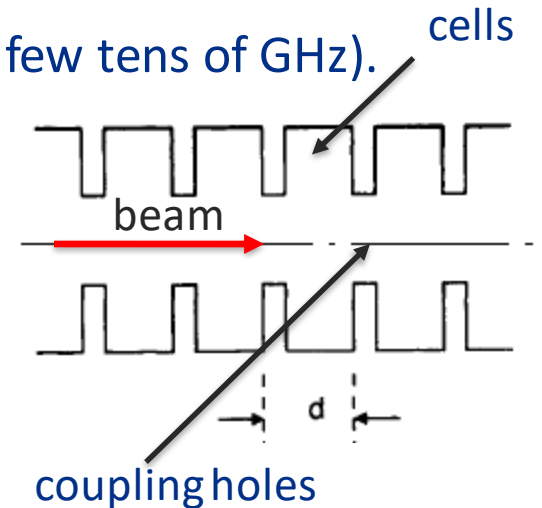
high frequencies are preferable (typically up to few tens of GHz). cells



small cavity size, ~ 1 cm for RT, ~ 20 cm for SRF



periodic structure of coupled cells.



- To provide synchronism with the accelerated particle, the particle velocity $v_p = \beta c = v_{ph} = \omega / k_z$ and the structure period $d = \varphi / k_z = \varphi \lambda / (2\pi \beta)$; φ is phase advance per period, $\varphi = k_z d$.

Periodic acceleration structures:

- Each previous cell excites EM field in a current cell, which in turn excites the field in the next cell.

- Cavity excitation by surface tangential electric field:

$$\vec{E}_j = \sum_{i=0}^{\infty} X_{ij} \vec{E}_i - \text{field in the } j^{\text{th}} \text{ cell;}$$

\vec{E}_i - eigen functions of cells.

- Single-mode approximation:

$$\vec{E}_j = X_j \vec{E}_0 - \text{field in the } j^{\text{th}} \text{ cell. Works everywhere except the hole}$$

\vec{E}_0 - eigen function of the operation TM_{010} mode of a cell.

- Excitation of a cavity by the field of a similar neighboring cavity through a small hole:

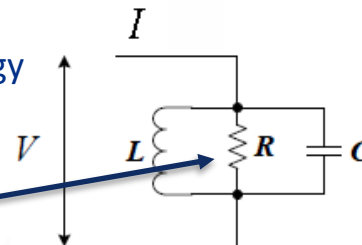
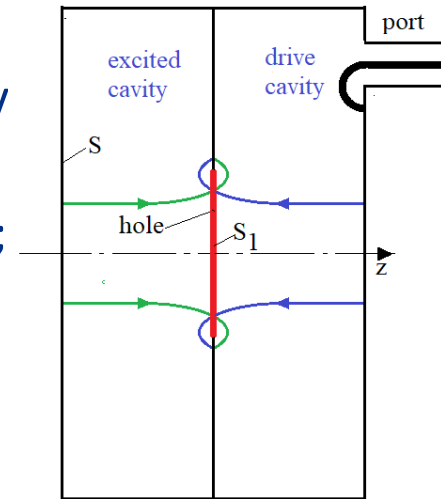
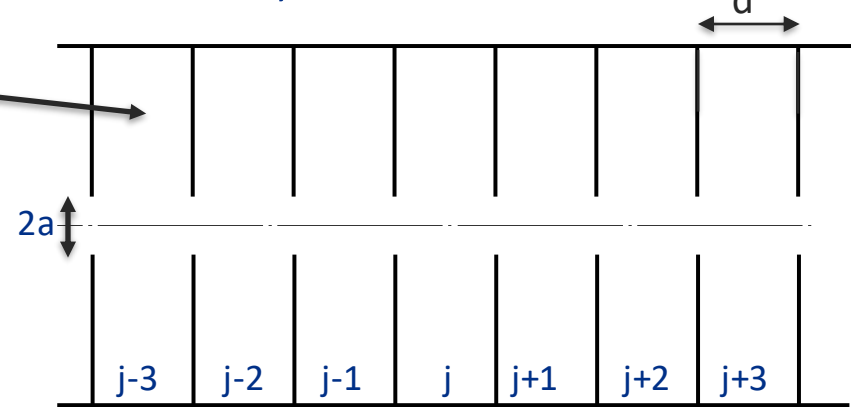
- Boundary conditions for the excited cavity field \vec{E} : $E_t = 0$ on S ; $E_t = \vec{E}_t$ on S_1 (hole). For eigenfunction $E_{0t} = 0$ on $S + S_1$

- From Maxwell equations for eigenfunction and excited field:

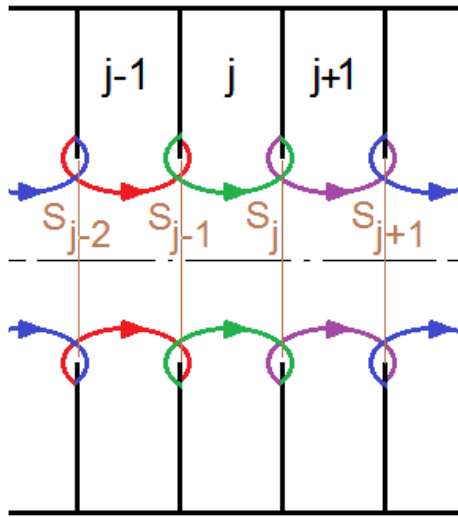
$$X = \frac{\int_{S_1} \vec{E} \times \vec{H}_0 ds}{2\omega W \left(1 - \frac{\omega_0^2}{\omega^2}\right)}, \text{ here } \vec{H}_0 \text{ is eigen magnetic field, } W \text{ - stored energy}$$

ω_0 - eigen frequency, ω - drive frequency.

Amplitude X is the same as for a parallel oscillator



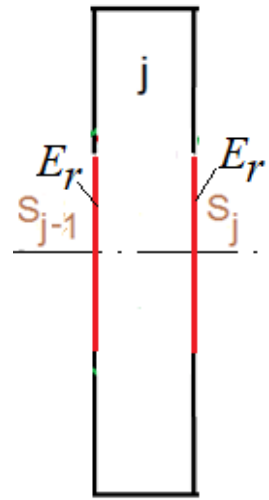
Periodic acceleration structures:



In the j^{th} cell $\vec{E}_j = X_j \vec{E}_0$

Excitation of a cavity by surface electric field:

$$X_j = \frac{\int_{S_{j-1}} \vec{E}_{j-1} \times \vec{H}_0 dS}{2\omega W \left(1 - \frac{\omega_0^2}{\omega^2}\right)} + \frac{\int_{S_j} \vec{E}_j \times \vec{H}_0 dS}{2\omega W \left(1 - \frac{\omega_0^2}{\omega^2}\right)} \quad (1)$$



On the coupling holes tangential electric is superposition of the fields of the current cell and the neighboring cell:

$$\int_{S_{j-1}} \vec{E}_{j-1} \times \vec{H}_0 dS = K\omega_0 W (X_j - X_{j-1}), \quad \int_{S_j} \vec{E}_j \times \vec{H}_0 dS = K\omega_0 W (X_j - X_{j+1}), \quad (2)$$

here $K = \frac{1}{W\omega_0} \int_S \vec{E}_0 \times \vec{H}_0 dS$ - dimensionless constant depending on the cavity shape.

Therefore, from (1) and (2) one has:

$$X_j \left(1 - \frac{\omega_0^2}{\omega^2}\right) - \left(K \frac{\omega_0^2}{\omega^2} X_j - \frac{1}{2} K \frac{\omega_0^2}{\omega^2} X_{j-1} - \frac{1}{2} K \frac{\omega_0^2}{\omega^2} X_{j+1}\right) = 0,$$

or

$$X_j \left(1 - (1 + K) \frac{\omega_0^2}{\omega^2}\right) + \frac{1}{2} K \frac{\omega_0^2}{\omega^2} (X_{j-1} + X_{j+1}) = 0 \quad (3)$$

Periodic acceleration structures:

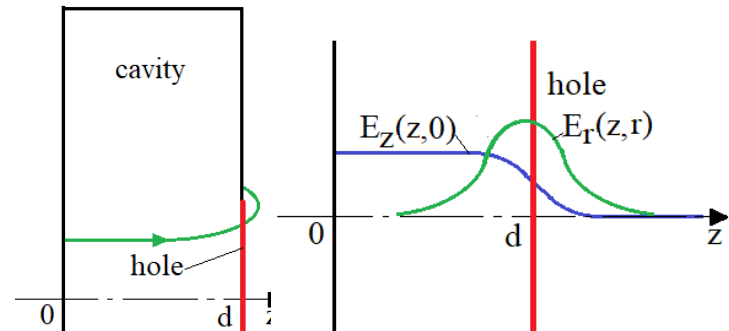
- For a pillbox K depends on the aperture as a^3 :
- In paraxial approximation E_{z0} for TM_{010} modes in a pillbox cavity does not depend on r in cylindrical coordinates $\vec{r}, \vec{\varphi}, \vec{z}$, see Lecture 1, slide 49.
- In presence of a small hole radial electric field $E_{r0} \sim r$ next to the hole.

• On the other hand, $\text{div} \vec{E} = \frac{1}{r} \frac{\partial(rE_r)}{\partial r} + \frac{\partial E_z}{\partial z} = 0 \rightarrow E_{r0}(r) = -\frac{r}{2} \frac{\partial E_z}{\partial z} \approx \frac{rE_{z0}}{4a}$;

$$H_{\varphi 0}(r) = \frac{1}{2i\omega a} \int_0^r E_{z0} r dr \sim r, \text{ and } \int_{S_{j-1}} E_{r0} H_{\varphi 0} dS \sim a^3$$

- For pillbox cells having thin walls and a hole with the radius a one has

$$K = \frac{2E_0^2 a^3}{3Z_0 W_0 c} = \frac{2}{3} \cdot \frac{R/Q}{Z_0} \cdot \frac{k_0 a^3}{d^2 T^2} \quad k_0 = \frac{\omega_0}{c}$$



Axial and radial field distribution along the Axis. Scales for E_z and E_r are different.

Pillbox cavity with a hole



THE

PHYSICAL REVIEW

A journal of experimental and theoretical physics established by E. L. Nichols in 1893

SECOND SERIES, VOL. 66, NOS. 7 AND 8

OCTOBER 1 AND 15, 1944

Theory of Diffraction by Small Holes

H. A. BETHE

Department of Physics, Cornell University, Ithaca, New York

(Received January 26, 1942)

Travelling–Wave acceleration structures:

In the infinite chain of cavities equation $X_j \left(1 - (1 + K) \frac{\omega_0^2}{\omega^2}\right) + \frac{1}{2} K \frac{\omega_0^2}{\omega^2} (X_{j-1} + X_{j+1}) = 0$ (1) has solution (travelling wave):

$$X_j = X e^{ij\varphi} \quad (2)$$

- From (1) and (2) it follows

$$1 = (1 + K) \frac{\omega_0^2}{\omega^2} + \frac{1}{2} K \frac{\omega_0^2}{\omega^2} (e^{i\varphi} + e^{-i\varphi})$$

or

$$\omega(\varphi) = \omega_0 [1 + K(1 - \cos\varphi)]^{1/2}$$

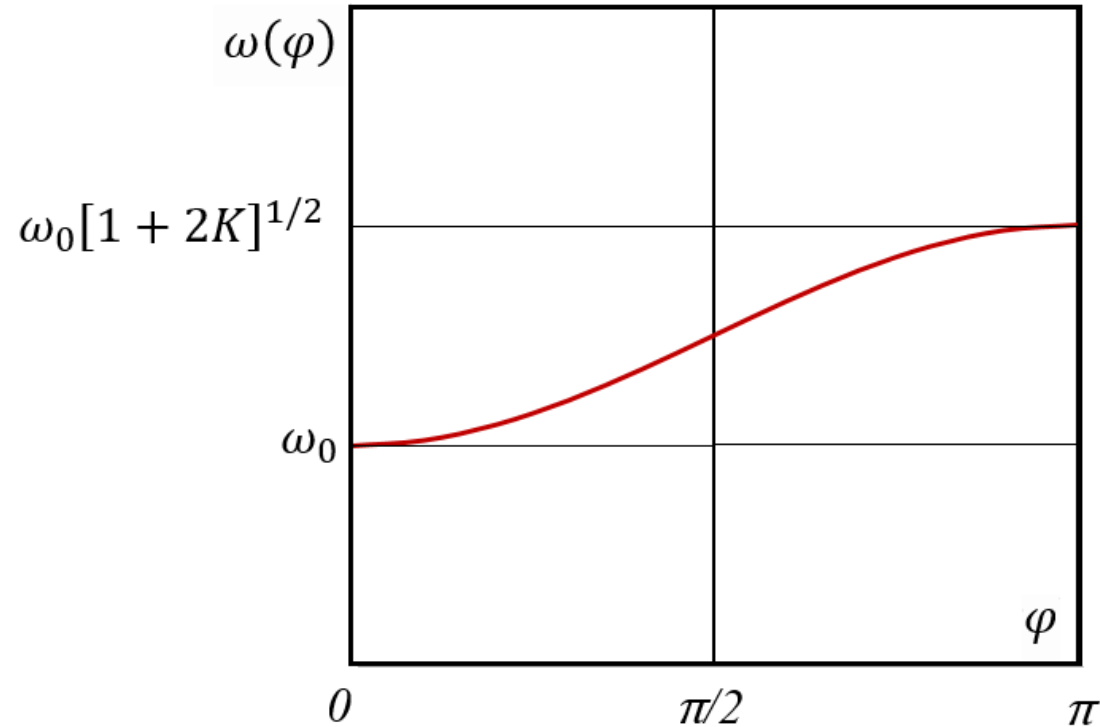
- For small K we have:

$$\omega(\varphi) \approx \omega_0 \left[1 + \frac{1}{2} K(1 - \cos\varphi)\right]$$

- One can see that

$$K = \frac{\omega(\pi) - \omega(0)}{\omega(0)} \quad \text{- a coupling coefficient; here } \omega(\pi) \approx \omega_0(1+K), \omega(0) \approx \omega_0$$

$$\Delta f = f(\pi) - f(0) \quad \text{- a passband width}$$



Travelling–Wave acceleration structures:

- In the arbitrary infinitely long periodic structure, or in the finite structure matched on the ends, there are travelling waves (TW) having arbitrary phase shift per cell φ . Longitudinal wavenumber, therefore, is $k_z = \varphi/d$. Dispersion equation is the same:

$$\omega(k_z) \approx \omega_{\pi/2} \left(1 - \frac{K}{2} \cos(\varphi) \right) = \omega_{\pi/2} \left(1 - \frac{K}{2} \cos(k_z d) \right)$$

Therefore, the phase velocity $v(\varphi)$ is:

$$v_{ph}(\varphi) = \frac{\omega(k_z)}{k_z} = c \frac{2\pi d}{\varphi \lambda}$$

- For acceleration of the particle having velocity $v_p = \beta c$, the cavity cell length d should be equal to

$$d = \frac{\beta \lambda \varphi}{2\pi},$$

because for synchronism we need $v_p = v_{ph}$

For example, for $\varphi = \pi$ the cell should have the length of $\beta \lambda / 2$.

Travelling–Wave acceleration structures:

□ The group velocity* $v_{gr}(\varphi)$ is

$$v_{gr}(\varphi) = \frac{d\omega}{dk_z} \approx c \frac{\pi K d}{\lambda} \sin(\varphi)$$

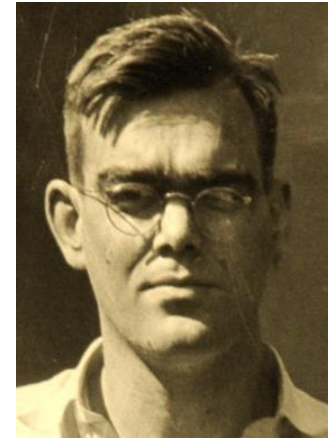
For $\varphi=0$ and $\varphi=\pi$ group velocity is zero!

For $\varphi=\pi/2$ group velocity is maximal:

$$v_{gr}(\pi/2) = c \frac{\pi K d}{\lambda}.$$

- For small K group velocity is small compared to the speed of light.
- In contrast to a waveguide, $v_{ph} \cdot v_{gr} \neq c^2$.

*In homogeneous media $v_{gr} = \frac{P}{w}$, P is power flow density, w is energy density.



W. W. Hansen

Travelling–Wave acceleration structures :



John Stewart Bell

□ For TW in a periodic structure:

- Average stored energy per unit length for electric field w_E is equal to the average stored energy per unit length for magnetic field w_H (the 1st Bell Theorem*):

$$w_E = w_H = w/2$$

- The power P flow is a product of the average stored energy per unit length and the group velocity (the 2^d Bell Theorem*):

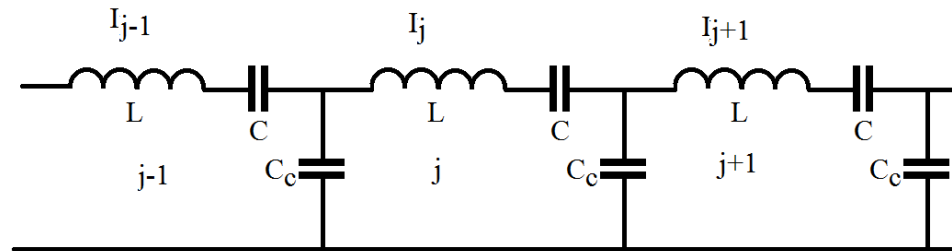
$$P = v_{gr} w.$$

**J.S. Bell, “Group velocity and energy velocity in periodic waveguides,” Harwell, AERE-T-R-858 (1952). See proof in Appendix 11*

Travelling-Wave acceleration structures

Equivalent circuit:

Note that the electrodynamics in the periodic structure is described by the equivalent circuit



For j^{th} cell we have from Kirchhoff theorem:

$$\left(i\omega L + \frac{1}{i\omega C}\right)I_j + \frac{(I_j - I_{j-1})}{i\omega C_c} + \frac{(I_j - I_{j+1})}{i\omega C_c} = 0,$$

For the capacity voltage $X_j = \frac{I_j}{i\omega C}$ we have the same equation as for EM model:

$$X_j \left[1 - (1 + K) \frac{\omega_0^2}{\omega^2}\right] + \frac{1}{2}K \frac{\omega_0^2}{\omega^2} [X_{j-1} + X_{j+1}] = 0$$

Here $\omega_0^2 = \frac{1}{LC}$, $K = \frac{2C}{C_c}$, $C = \frac{2}{\omega_0 R/Q}$, $L = \frac{R/Q}{2\omega_0}$.

Travelling-Wave acceleration structures

Loss in the cells:

Ohmic loss on the metallic surface:

$$\omega_0 \rightarrow \omega_0 \left(1 + \frac{i}{2Q_0}\right)$$



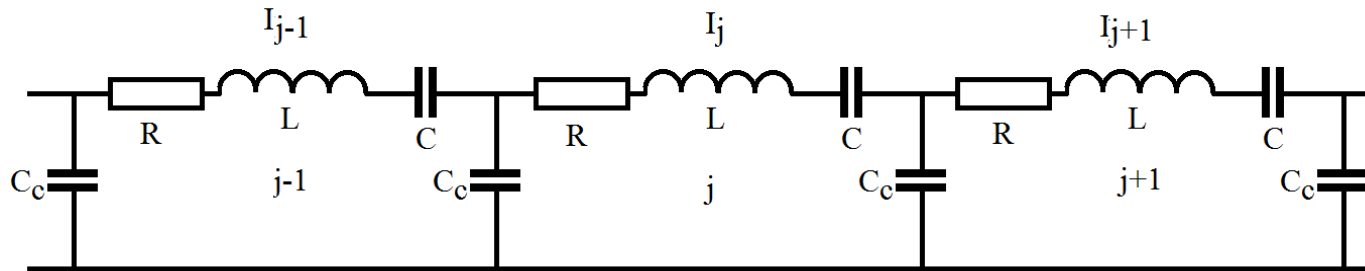
$$\vec{E}, \vec{H} \sim e^{i\omega_0 t - t/\tau} = e^{i\omega_0 t \left(1 + \frac{i}{2Q_0}\right)}$$

$$\tau = \frac{2Q_0}{\omega_0}$$

and

$$X_j \left[1 - (1 + K) \frac{\omega_0^2}{\omega^2} + i \frac{\omega_0^2}{Q_0 \omega^2}\right] + \frac{1}{2} K \frac{\omega_0^2}{\omega^2} [X_{j-1} + X_{j+1}] = 0$$

Equivalent circuit is the following:



where

$$R = \frac{R/Q}{2Q_0} \quad \omega_0^2 = \frac{1}{LC}, \quad K = \frac{2C}{C_c}, \quad C = \frac{2}{\omega_0 R/Q}, \quad L = \frac{R/Q}{2\omega_0}$$

Travelling–Wave acceleration structures

However, in a long periodic TW structure Ohmic losses change acceleration field distribution along the structure.

Energy conservation law in the j^{th} cell:

$$\frac{dW_{0,j}}{dt} = -P_j + P_{j-1} - \frac{\omega_0 W_{0,j}}{Q_0},$$

Taking into account that $w = \frac{W_0}{d}$ and $P = w \cdot v_{gr}$ we have

$$\frac{\partial w}{\partial t} = - \frac{(w \cdot v_{gr}|_j - w \cdot v_{gr}|_{j-1})}{d} - \frac{\omega_0 w}{Q_0} \approx - \frac{\partial(w v_{gr})}{\partial z} - \frac{\omega_0 w}{Q_0}$$

In steady-state case we have $\frac{dw}{dz} = - \frac{w}{v_{gr}} \left(\frac{dv_{gr}}{dz} + \frac{\omega_0}{Q_0} \right)$

- **Constant impedance structure:**

$$v_{gr} = \text{const} \rightarrow w(z) = w(0) e^{-\frac{z \omega_0}{v_{gr} Q_0}} \rightarrow E(z) = E(0) e^{-\frac{z}{v_{gr} \tau}} \quad \tau = \frac{2Q_0}{\omega_0}$$

- **Constant gradient structure:**

$$v_{gr}(z) = v_{gr}(0) - z \frac{\omega_0}{Q_0} \rightarrow w(z) = w(0) \rightarrow E(z) = E(0) = \text{const}$$

Aperture a should decrease with z .

Travelling–Wave acceleration structures

Tolerances:

If the cell frequencies have resonant frequency deviation $\delta\omega_0$, it changes the longitudinal wave number k_z and violates synchronism.

$$\delta k_z = \frac{dk_z}{d\omega_0} \delta\omega_0 = \frac{1}{v_{gr}} \delta\omega_0$$

It means that it is necessary to operate in the middle of dispersion curve, when group velocity is maximal, $\varphi \sim \pi/2 - 2\pi/3$.

If φ close to π , the structure is unstable.

Travelling–Wave acceleration structures

TW structure parameters:

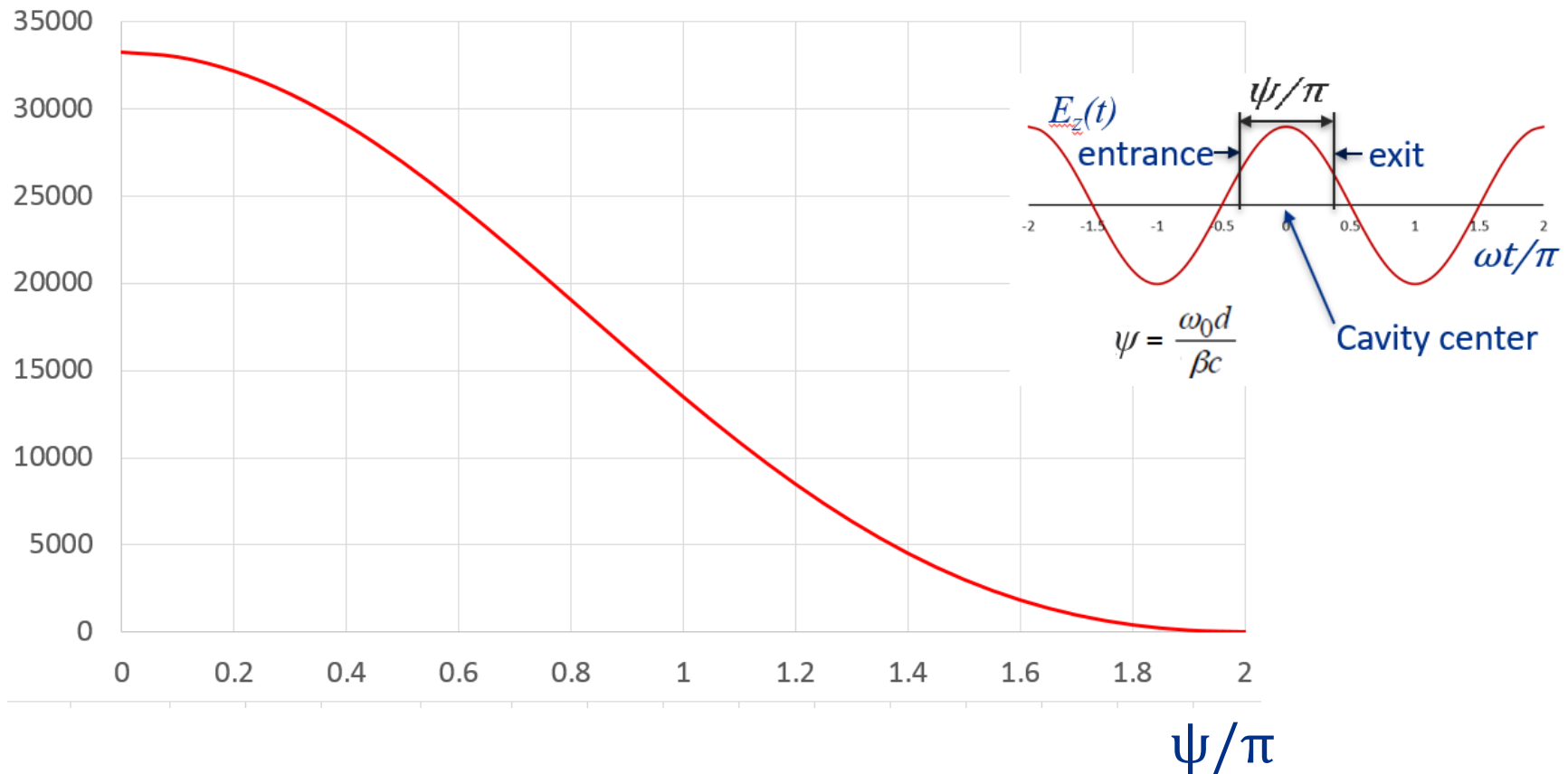
For TW structure R and R/Q are calculated per unit length of the structure.

- ❖ Shunt impedance R is measured in MOhm/m. For geometrically similar cells R scales as $\omega_0^{1/2}$.
- ❖ R/Q is measured in Ohm/m. For geometrically similar cells R/Q scales as ω_0

Travelling-Wave acceleration structures

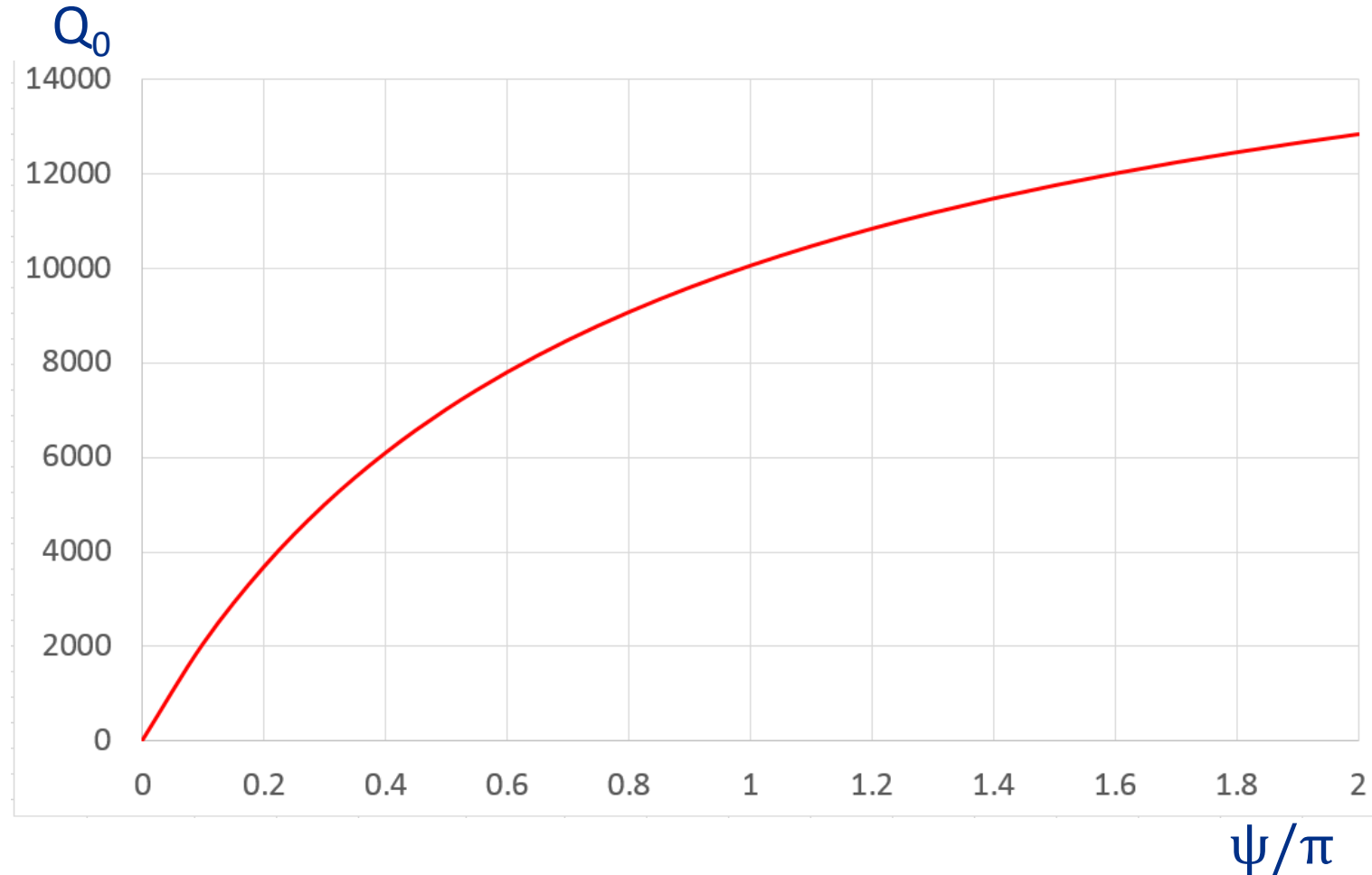
TW structure parameters: (R/Q) for pillbox, $f=10$ GHz (here b is the cavity radius)

$$R/Q, \text{ Ohm/m} \quad \frac{R}{Q} = \frac{0.98Z_0T(\psi)^2}{b}, \quad b = \frac{2.405c}{2\pi f} \quad (\text{See Slide 68})$$



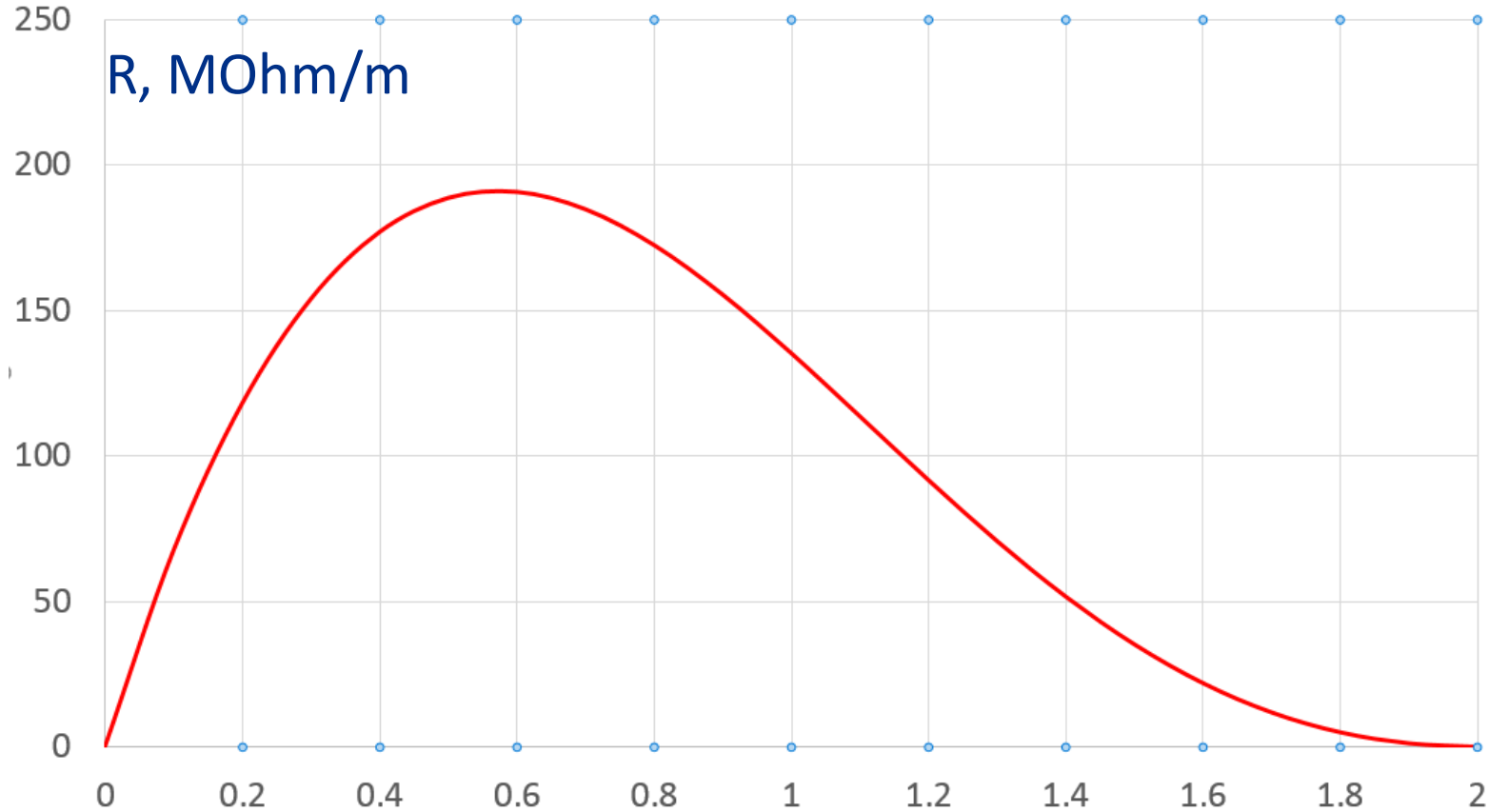
Travelling-Wave acceleration structures

TW structure parameters: Q_0 for pillbox at 10 GHz (see Slide 63)



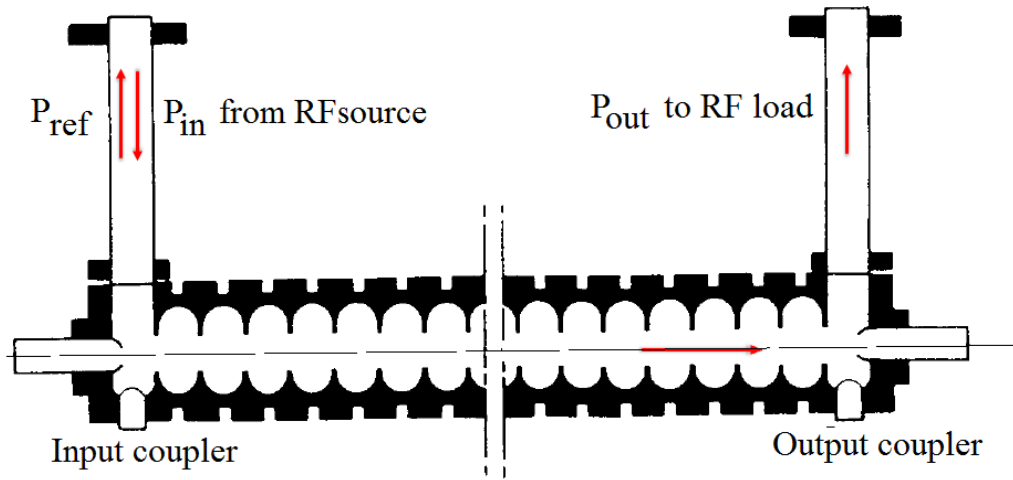
Travelling-Wave acceleration structures

TW structure parameters: Shunt impedance $R=(R/Q)\cdot Q_0$ for pillbox at 10 GHz



R is maximal at $\psi \sim 0.6\pi$. Typically, they use $\psi = 2\pi/3$. ψ/π

Travelling-Wave acceleration structures

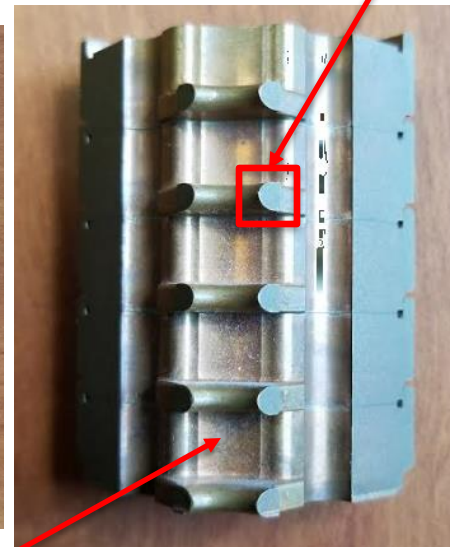
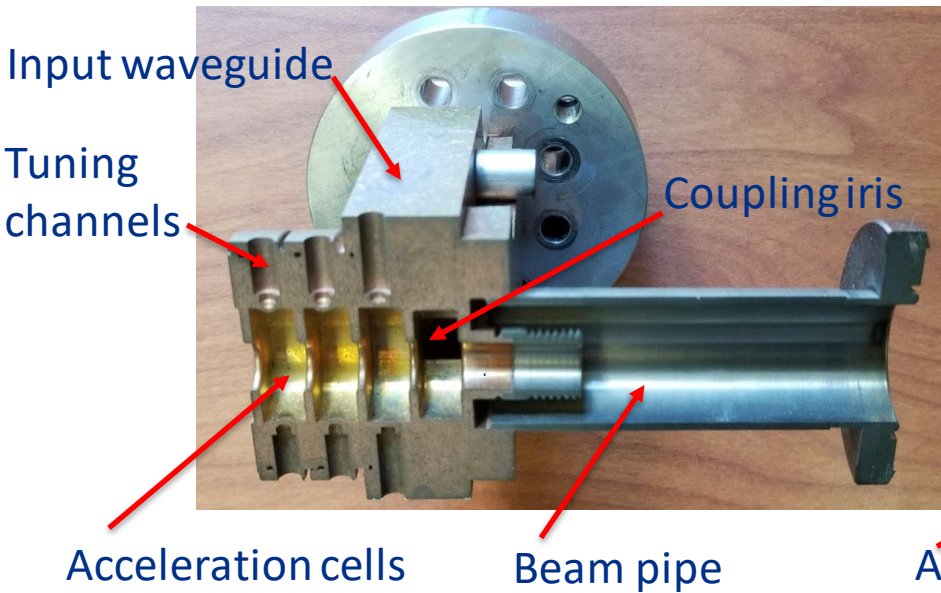


$$P_{in} = P_{ref} + P_{out} + P_{loss} + P_{beam}$$

$$P_{in} \gg P_{out}$$

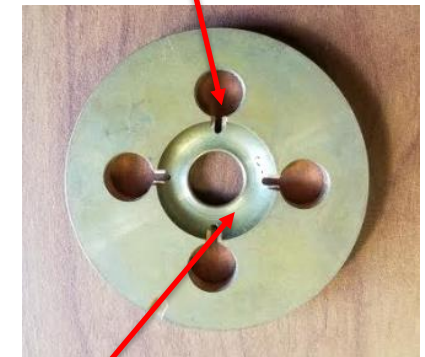


Aperture has elliptical shape to minimize surface electric field



Acceleration cells

HOM dampers



Acceleration cell
NLC structure with
HOM damping



Travelling–Wave acceleration structures

TW structures for acceleration of electrons are widely used in different fields.

❖ High – energy physics:

- SLAC (1968): 3 km, 47 GeV (max), $2\pi/3$ 2.856 GHz (S-band) , 3 m structures.
- SLC (1987) – first e^+e^- linear collider based on the SLAC linac.
- CLIC collider (R&D): up to 50 km, up to 3 TeV c.m., $2\pi/3$ 12 GHz

❖ FELS:

- SwissFEL (PSI) 5.7 GHz linac (2017), 0.74 km, 5.8 GeV, $2\pi/3$ 6 GHz

❖ Industrial and medical accelerators

- Varian S-band (2.856 GHz) and X-band (11.424 GHz) linacs for medical applications
- Industrial linacs

Travelling–Wave acceleration structures

Modern TW structures: 12 GHz CLIC structure*

Accelerating structure parameters

Loaded gradient* [MV/m]	100
Working frequency [GHz]	11.994
Phase advance per cell	$2\pi/3$
Active structure length [mm]	217
Input/output radii [mm]	3.15/2.35
Input/output iris thickness [mm]	1.67/1.00
Q factor [Cu]	7112/7445
Group velocity [%c]	1.99/1.06
Shunt impedance [M Ω /m]	107/137
Peak input power [MW]	60.9
Filling time [ns]	49.5
Maximum E-field [MV/m]	313
Maximum modified Poynting vector [MW/mm ²]	7.09
Maximum pluse heating temperature rise [K]	35

*V. Dolgashev, SLAC, EAAC 2015

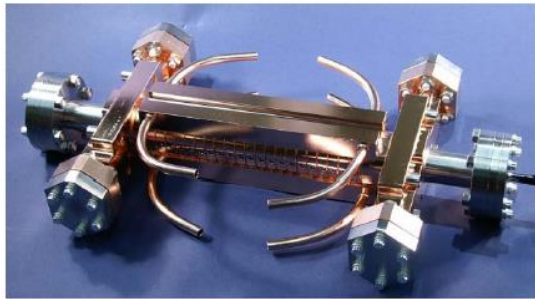
Travelling-Wave acceleration structures

Modern TW structures: 12 GHz CLIC structure*

Traveling Wave accelerator structures, CLIC prototypes

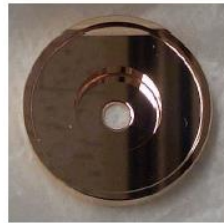
SLAC

T18 → TD18 → T24 → TD24



T18_Disk_#2

2009



undamped



T24_Disk_#3

2011



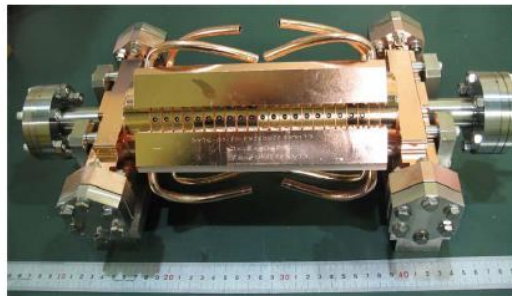
2010



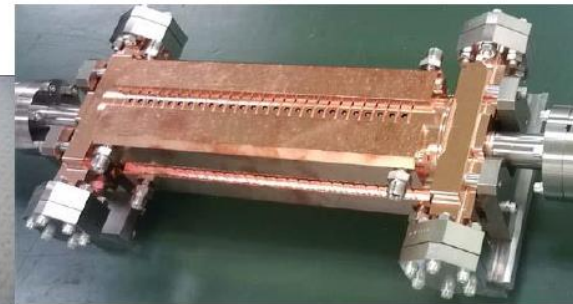
damped



2011~12



TD18_Disk_#2



TD24_Disk_#4

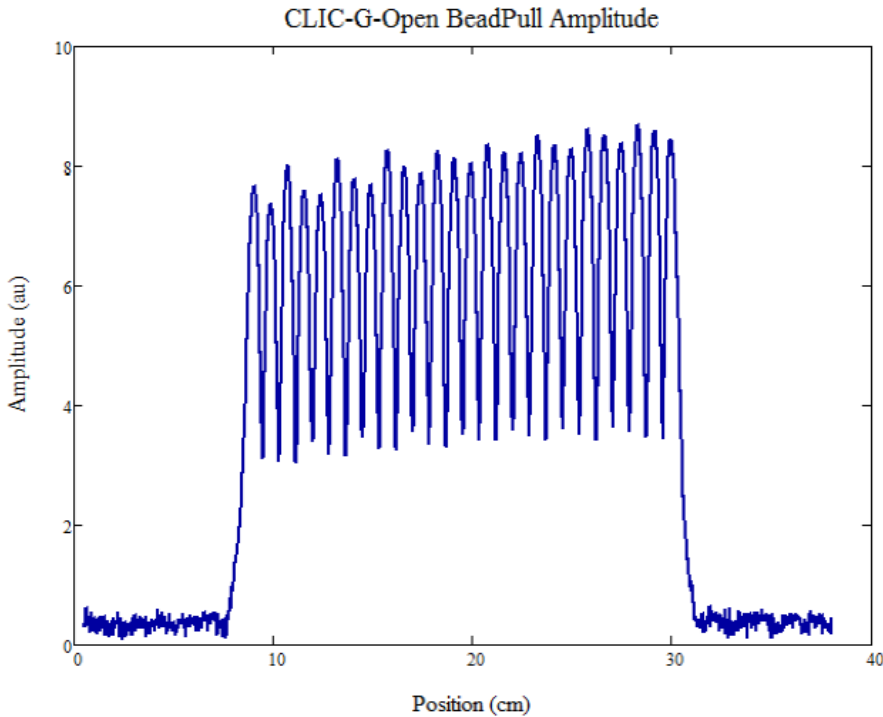
Travelling-Wave acceleration structures

Modern TW structures: 12 GHz CLIC structure*

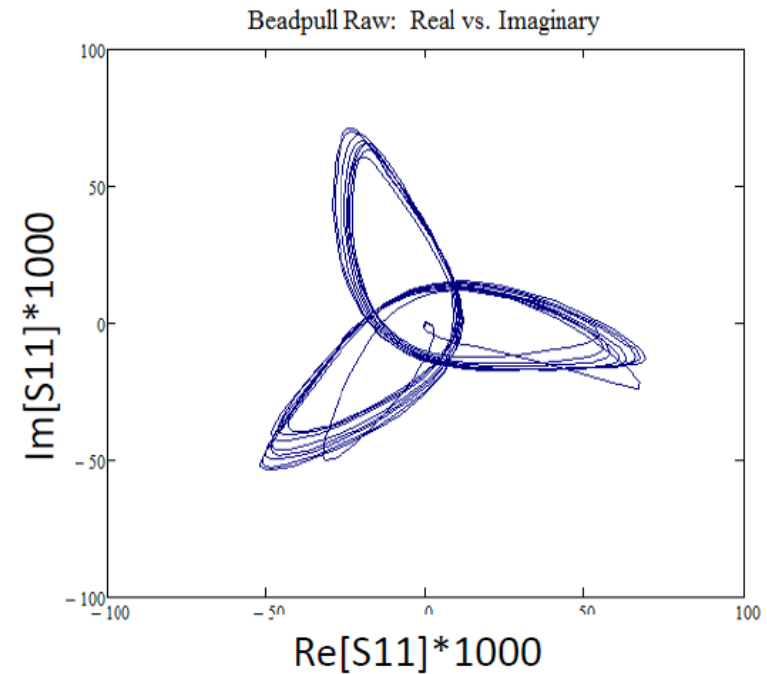


SLAC-CERN  Fermilab

Final beadpull of tuned CLIC-G-OPEN



On-axis field amplitude.

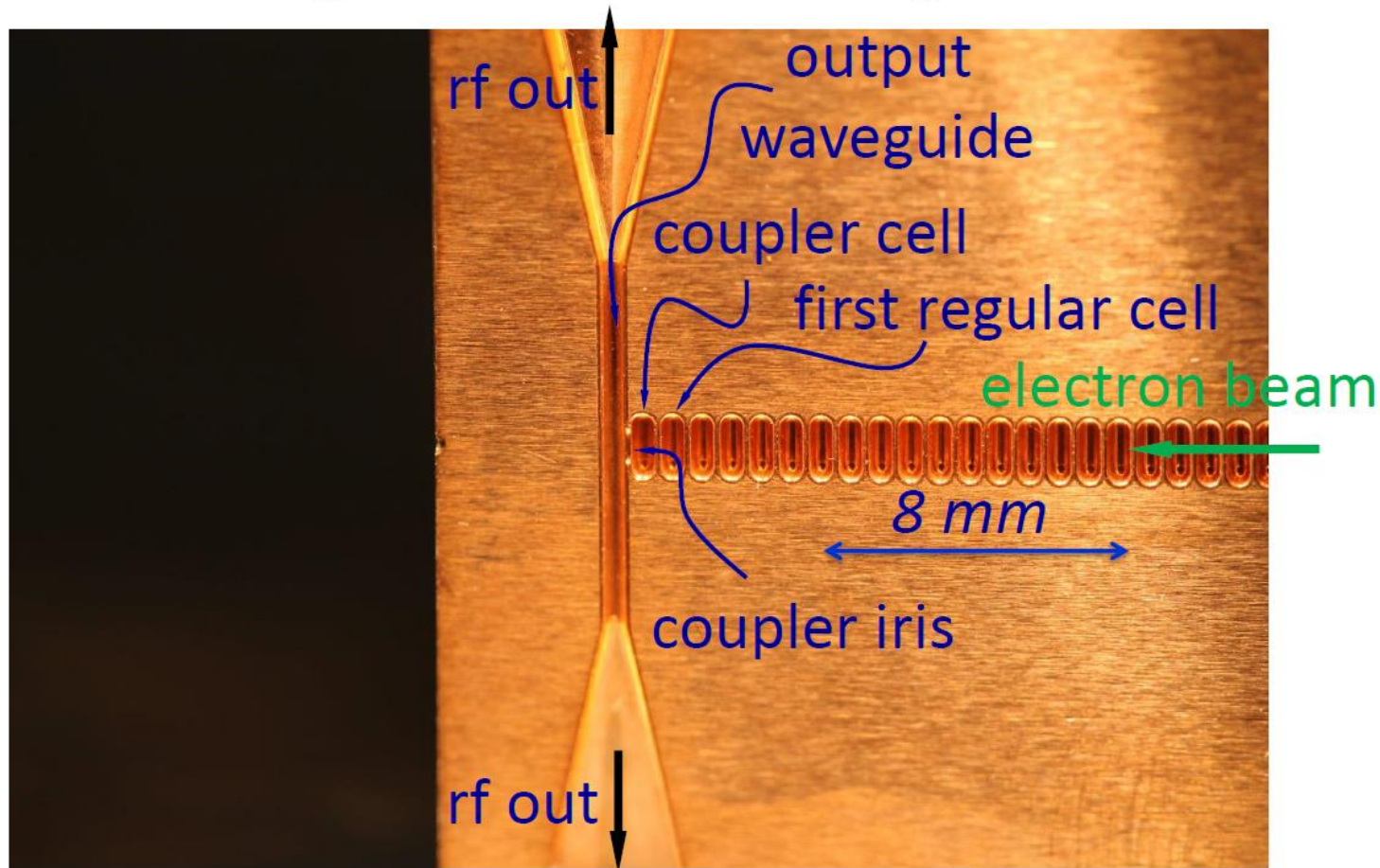


Polar plot of beadpull data.

Travelling-Wave acceleration structures

SLAC

Output Part of the Open 100 GHz Copper Traveling Wave Accelerating Structure



SI AC-INFN

Fermilab

Summary:

- Single – cell cavities are not convenient in order to achieve high acceleration: a lot of couplers, tuners, etc. Especially it is important for acceleration of electrons.
- Periodic structures are used for acceleration, where travelling wave is excited.
- Phase velocity depend on the phase advance per cell. The accelerating wave has the same phase velocity as the accelerated particles (synchronism).
- Average energy of magnetic field is equal to average energy of electric field (the 1st Bell theorem); Power flow is equal to the product of the group velocity to the average stored energy per unit length (the 2^d Bell theorem).
- The passband depends on the value of coupling between the cells K ; it depends on the coupling hole radius a as $\sim a^3 - a^4$; it depends also on the wall thickness.
- Group velocity is maximal if phase advance per cell is $\sim \pi/2$;
- Maximal shunt impedance per unit length is at the phase shift of $\sim 2\pi/3$;
- Loss may change the field distribution. To achieve field flatness along the structure, group velocity (coupling) should decrease from the structure beginning to the end.

Chapter 5.

Standing –Wave acceleration structures.

- a. Standing - wave structures;
- b. Equivalent circuit for a SW structure;
- c. Dispersion curve;
- d. Normal modes;
- e. Perturbation theory for SW structures;
- e. Parameters of SW structures;
- f. Bi-periodic SW structures;
- g. Inductive coupling;
- h. Types of the SW structures;

Standing-Wave acceleration structures

❖ TW structures work very good for RT electron accelerators:

- High frequency \rightarrow lower power ($R \sim f^{1/2}$);
- A lot of cells (many tens) \rightarrow high efficiency (all the power is consumed in the structure, and small fraction is radiated through the output port).

❖ TW structures are not good for RT proton accelerators:

- High frequency is not practical (defocusing is proportional to f)
- Low beam loading \rightarrow large number of cells (impractical from the point of view of focusing and manufacturing, especially if the cell diameter is large because of low frequency);

❖ TW structures are not good for SRF accelerators:

- High frequency is not practical (BCS surface resistance is proportional to f^2)
- Small decay in the cavities
- Very large number of cells + large cell size (impractical from the point of view of manufacturing and processing);
- Feedback waveguide - still under R&D

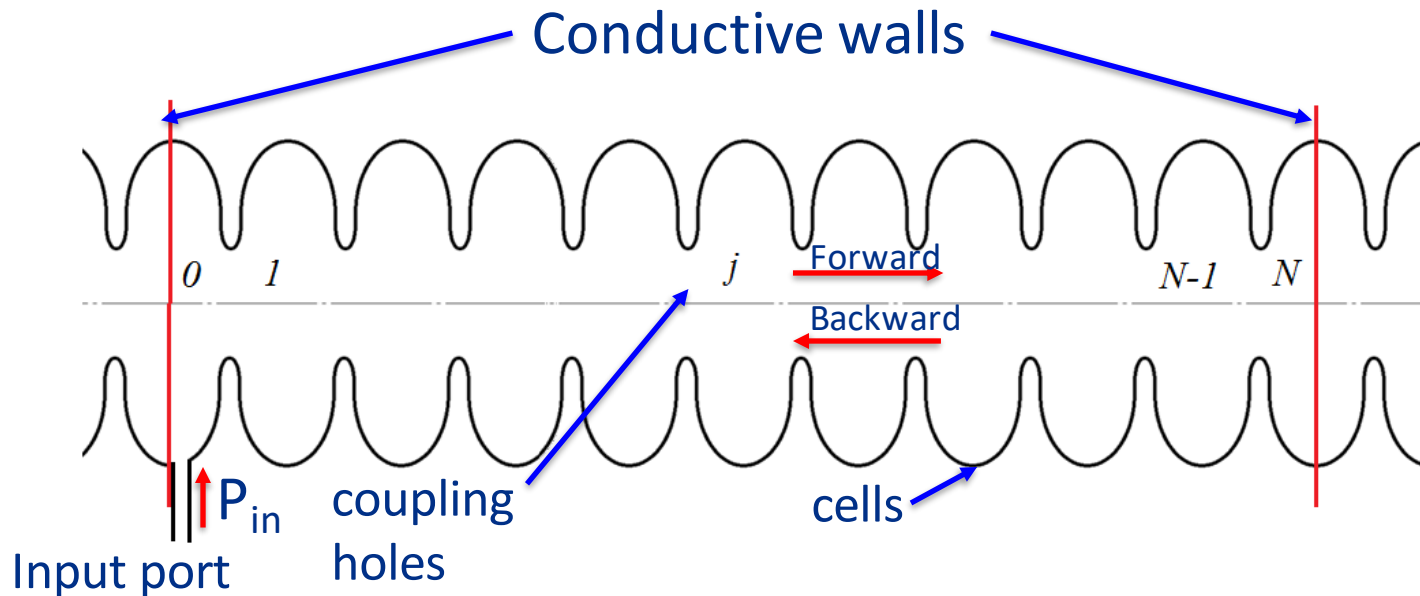
Fermilab & Euclid 3-cell SRF TW structure prototype

Travelling wave is demonstrated in 2023!



Standing-Wave acceleration structures

Standing Wave structures:



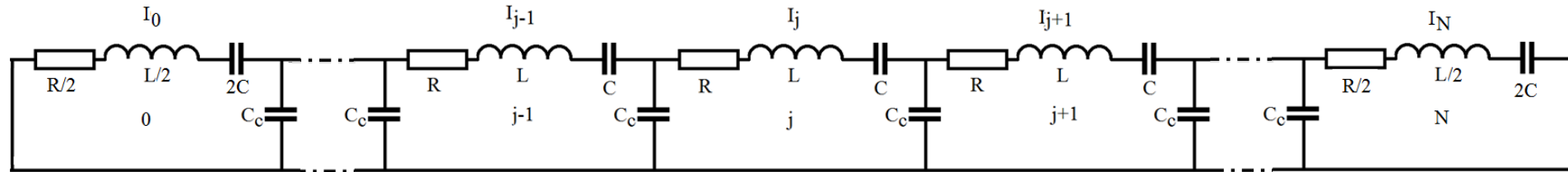
Putting reflective conductive walls in the middle of the end cells, we do not violate boundary conditions for EM field for TM_{010} -like modes.

Forward and backward travelling waves form standing wave.

- N may be small, even $N=2$;
- Frequency may be small, up to hundreds of MHz \rightarrow proton acceleration
- Suitable for SRF
- $P_{in} \ll P_{forward} \approx P_{backward}$

Standing-Wave acceleration structures

Equivalent circuit of the SW structure containing half-cells on the ends:



$$X_0 \left[1 - \frac{\omega_0^2}{\omega^2} + i \frac{\omega_0^2}{Q_0 \omega^2} \right] + K \frac{\omega_0^2}{\omega^2} X_1 = 0$$

$$X_j \left[1 - \frac{\omega_0^2}{\omega^2} + i \frac{\omega_0^2}{Q_0 \omega^2} \right] + \frac{1}{2} K \frac{\omega_0^2}{\omega^2} [X_{j-1} + X_{j+1}] = 0 \quad (1)$$

$$X_N \left[1 - \frac{\omega_0^2}{\omega^2} + i \frac{\omega_0^2}{Q_0 \omega^2} \right] + K \frac{\omega_0^2}{\omega^2} X_{N-1} = 0$$

In matrix form:

$$M \hat{X} - \frac{\omega_0^2}{\omega^2} \hat{X} = 0$$

here $M_{jj} = 1; j = 0, 1, \dots, N;$

$$M_{jj-1} = \frac{K}{2W(j)}; j = 1, 2, \dots, N;$$

$$M_{jj+1} = \frac{K}{2W(j)}; j = 0, 1, \dots, N-1.$$

and $W(j) = 1, j = 1, 2, \dots, N-1$

$$W(j) = \frac{1}{2}, j = 0, N$$

THE REVIEW OF SCIENTIFIC INSTRUMENTS

VOLUME 38, NUMBER 11

NOVEMBER 1967

Coupled Resonator Model for Standing Wave Accelerator Tanks*

D. E. NAGLE, E. A. KNAPP, AND B. C. KNAPP

University of California, Los Alamos Scientific Laboratory, Los Alamos, New Mexico 87544

(Received 22 June 1967; and in final form, 24 July 1967)

Here ω_0 corresponds to the center of dispersion curve.

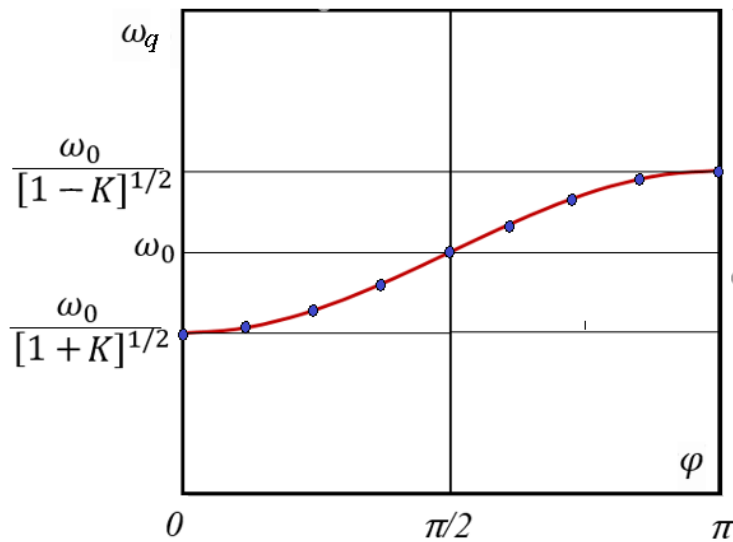


Standing –Wave acceleration structures

Eigenvectors and eigenvalues:

$$\hat{X}_j^q = \cos \frac{\pi q j}{N}; \quad \omega_q^2 = \frac{\omega_0^2}{1 + K \cos \frac{\pi q}{N}}, \quad q = 0, 1, \dots, N$$

Phase advance per cell: $\varphi = \frac{\pi q}{N}, q = 0, 1, \dots, N$



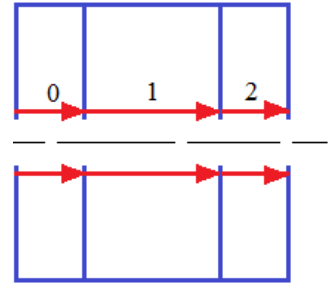
Orthogonality:

$$\hat{X}^q \cdot \hat{X}^r \equiv \sum_{j=0}^N W(j) \hat{X}_j^q \hat{X}_j^r = \frac{N \delta_{qr}}{2W(q)}, \quad \delta_{qq} = 1, \text{ and } \delta_{qr} = 0, \text{ if } q \neq r$$

3-cell cavity (N=2)

0-mode (q=0):

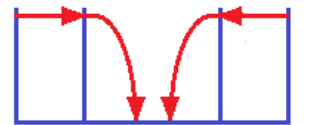
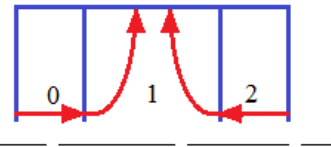
$$\varphi = 0 \quad \omega = \frac{\omega_0}{(1-K)^{1/2}}$$



$\pi/2$ -mode (q=1):

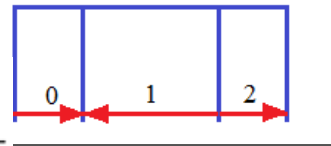
$$\varphi = \pi/2 \quad \omega = \omega_0$$

Even cell is empty!



π -mode (q=2):

$$\varphi = \pi \quad \omega = \frac{\omega_0}{(1+K)^{1/2}}$$



Standing –Wave acceleration structures

- Perturbation of the cell resonance frequencies causes perturbation of the mode resonance frequencies $\delta\omega_q$;
- the field distribution $\delta\hat{X}_q$.

$$\omega_{0j}^{2'} = \omega_0^2 + \delta\omega_{0j}^2 \quad \rightarrow \quad \hat{X}^{q'} = \hat{X}^q + \delta\hat{X}^q, \quad \hat{X}^q \cdot \delta\hat{X}^q$$

Variation of the equation (1) in matrix form $M\hat{X} - \frac{\omega_0^2}{\omega^2}\hat{X} = 0$, see Slide 31

gives
$$M\delta\hat{X}^q = \frac{\omega_0^2}{\omega_q^2} \left[\delta\hat{X}^q + \Omega\hat{X}^q - \frac{\delta\omega_q^2}{\omega_q^2} \hat{X}^q \right],$$



$$\frac{\delta\omega_q^2}{\omega_q^2} = [2W(q)/N] \cdot \hat{X}^q \Omega \hat{X}^q;$$

$$\delta\hat{X}^q = \sum_{q' \neq q} \frac{2W(q') \hat{X}^q \Omega \hat{X}^q}{N \left(\frac{\omega_q^2}{\omega_{q'}^2} - 1 \right)} \hat{X}^{q'}$$

(here $\Omega = \begin{bmatrix} \frac{\delta\omega_{01}^2}{\omega_0^2} & \dots & 0 \\ \vdots & \ddots & \vdots \\ 0 & \dots & \frac{\delta\omega_{0N}^2}{\omega_0^2} \end{bmatrix}$)



$$|\delta\hat{X}^q| \sim \frac{|\delta\omega_{0j}|_{av}}{|\omega_q - \omega_{q\pm 1}|}$$

Standing –Wave acceleration structures

$\pi/2$ -mode ($q=N/2$): N -even, N is the number of cells in the cavity

$$|\delta\hat{X}^{N/2}| \sim \frac{|\delta\omega_{0j}|_{av}}{|\omega_{N/2} - \omega_{N/2-1}|} \sim N \frac{|\delta\omega_{0j}|_{av}/\omega_0}{K}$$

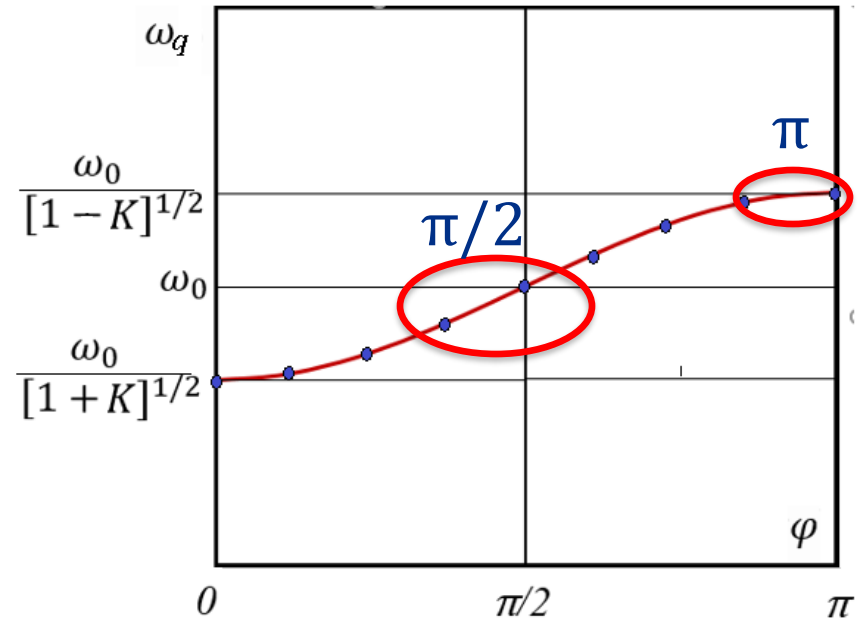
π -mode ($q=N$):

$$|\delta\hat{X}^N| \sim \frac{|\delta\omega_{0j}|_{av}}{|\omega_N - \omega_{N-1}|} \sim N^2 \frac{|\delta\omega_{0j}|_{av}/\omega_0}{K}$$

SW π -mode is much less stable than $\pi/2$ -mode!

For π -mode problems with

- Tuning
- Temperature stability at RT



$$\omega_q^2 = \frac{\omega_0^2}{1 + K \cos \frac{\pi q}{N}}, q = 0, 1, \dots, N$$

Standing –Wave acceleration structures

Solutions:

- ❖ Operate at $\pi/2$ mode;
- ❖ Operate at π mode:
 - Small number of cells N ;
 - Increase K .

1. Operating at $\pi/2$ mode:

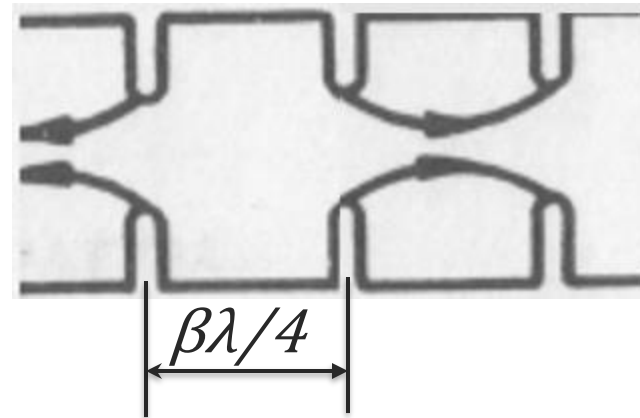
$$\hat{X}_j = \cos \frac{\pi j}{2}$$

Even cells are empty!

Solution – biperiodic structures:

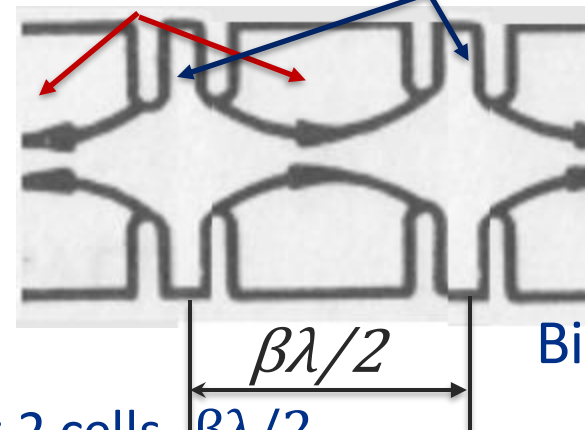
- Narrow even cells (coupling cells)
- Long odd cells (acceleration cells)
- Same length of the period containing 2 cells, $\beta\lambda/2$
- The structure is “ $\pi/2$ for RF” and “ π for the beam”

odd even



Periodic

Accelerating cells (odd) Coupling cells (even)

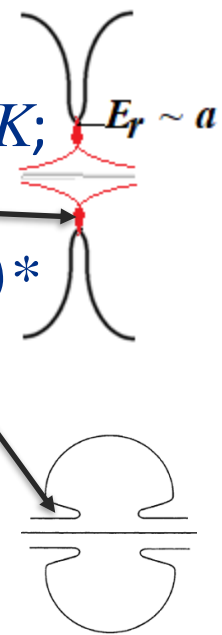


Biperiodic

Standing –Wave acceleration structures

2. Increase K :

- Coupling through the aperture holes does not provide high K ;
 - Aperture is limited by surface electric field
 - At $\beta < c$ acceleration gain on the axis drops as $\sim \exp(ka/\beta)^*$
- In this case, R_{sh} is modest (the drift tubes cannot be used)

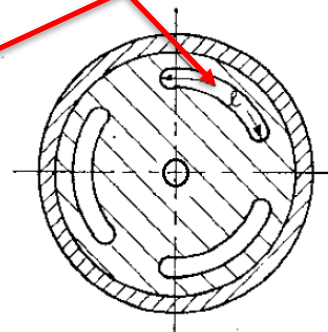
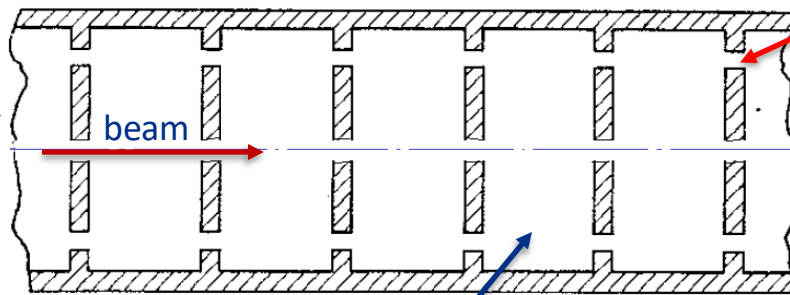


Solution: inductive coupling through the side slots.

Aperture may be small in this case, which provides

- Small field enhancement factors;
- High R/Q and R_{sh} .

Coupling slots



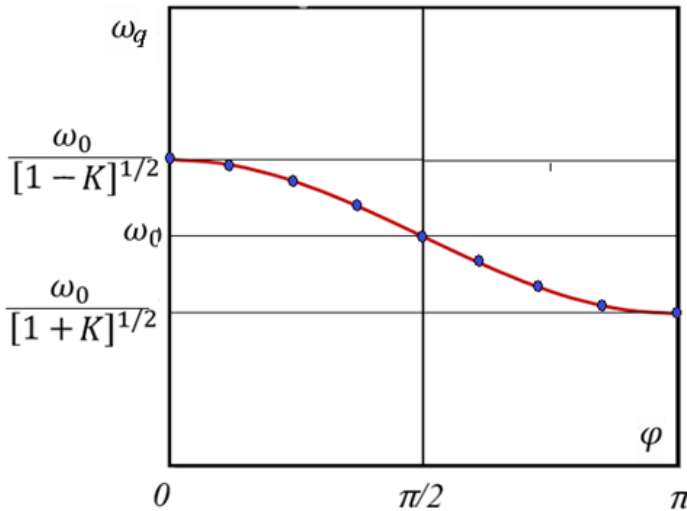
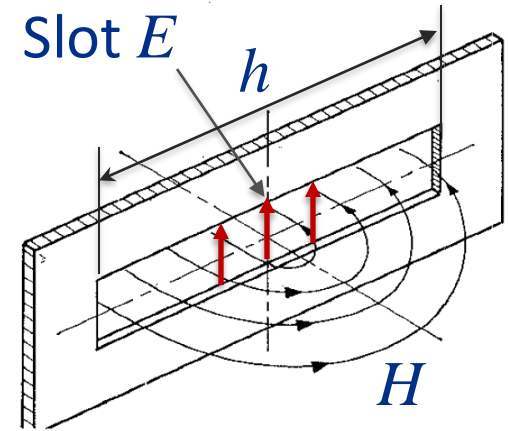
*See slide38

Accelerating cells

Standing-Wave acceleration structures

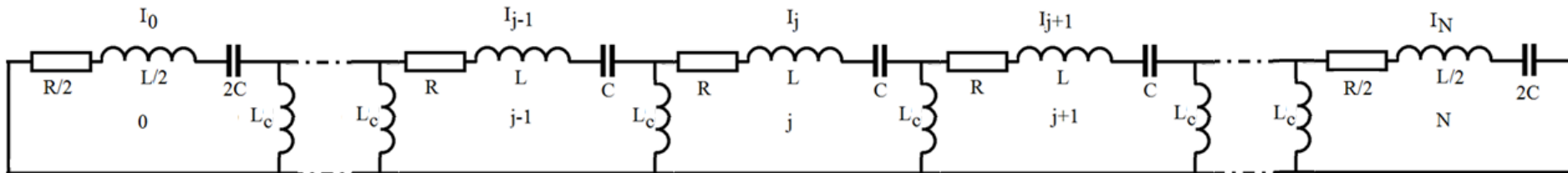
TEM wave in the slot \rightarrow high electric field \rightarrow high coupling

Induction coupling gives negative K



$$K = -\frac{2L_c}{L_c}$$

Slot resonance: $h = \lambda/2$. Typically, $h < \lambda/2$



Equivalent circuit below the slot resonance

Standing-Wave acceleration structures

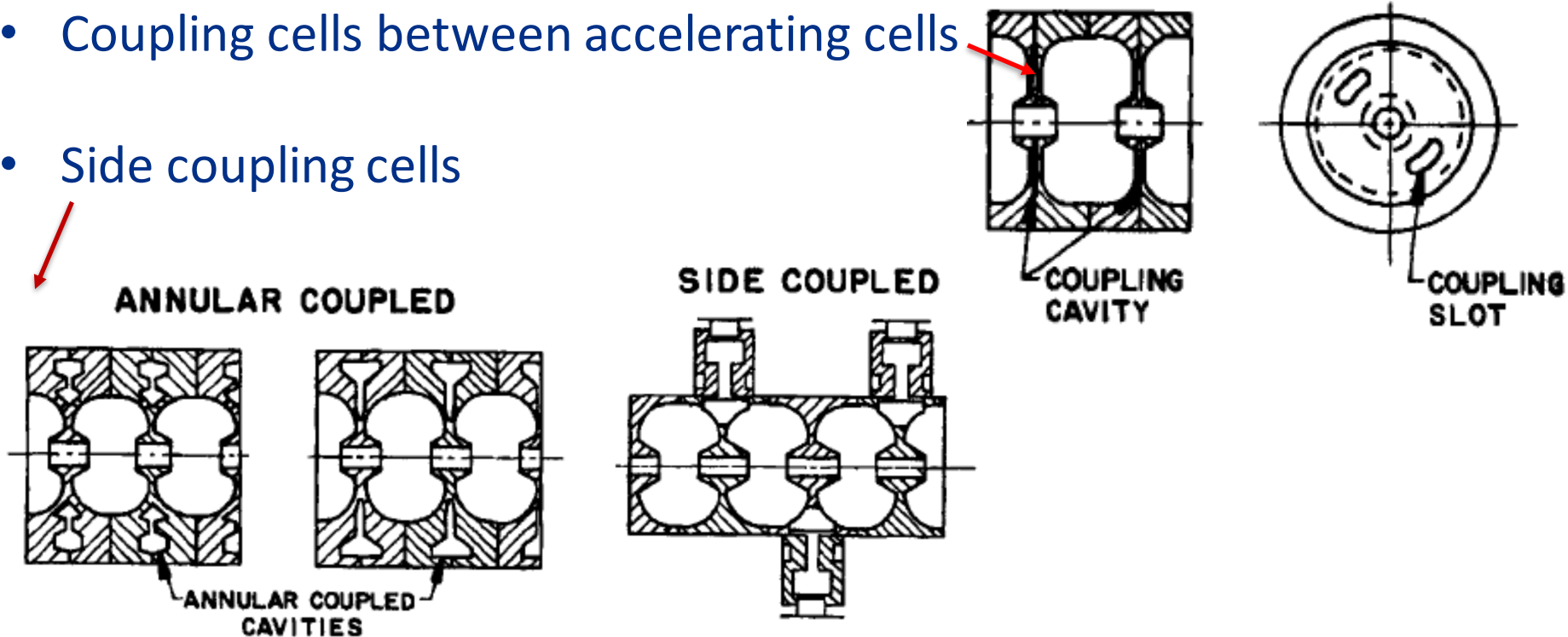
Combination:

- Inductive coupling
- Biperiodic structure



Biperiodic structures with induction coupling

- Coupling cells between accelerating cells
- Side coupling cells



Standing-Wave acceleration structures

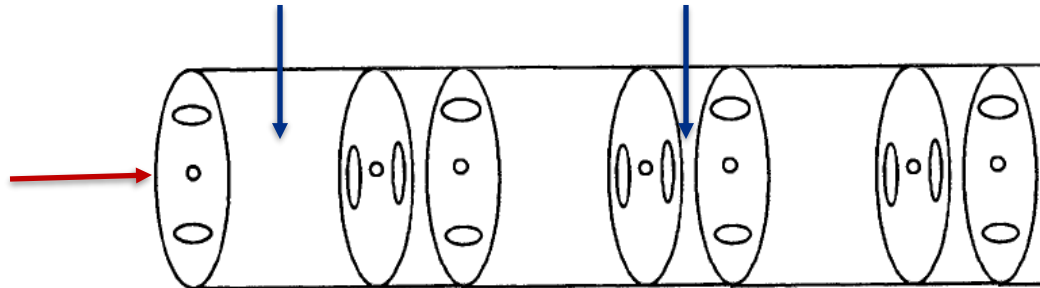
Inductive coupling slots cause multipole perturbation of the acceleration field, which may influence the beam dynamics:

$$x'_f = \frac{\Delta p_{\perp}}{p_{\parallel}} \approx \frac{m}{ka} \left(\frac{V_{max}(a)}{\gamma m_0 c^2} \right) \left(\frac{x_i}{a} \right)^{m-1}$$

Accelerating cell.

Coupling cell.

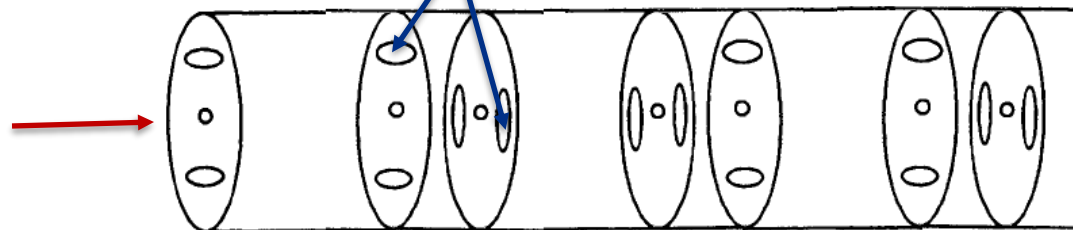
Coupling slot orientation:



Wrong! Strong quadrupole defocusing in one of transverse directions.

beam

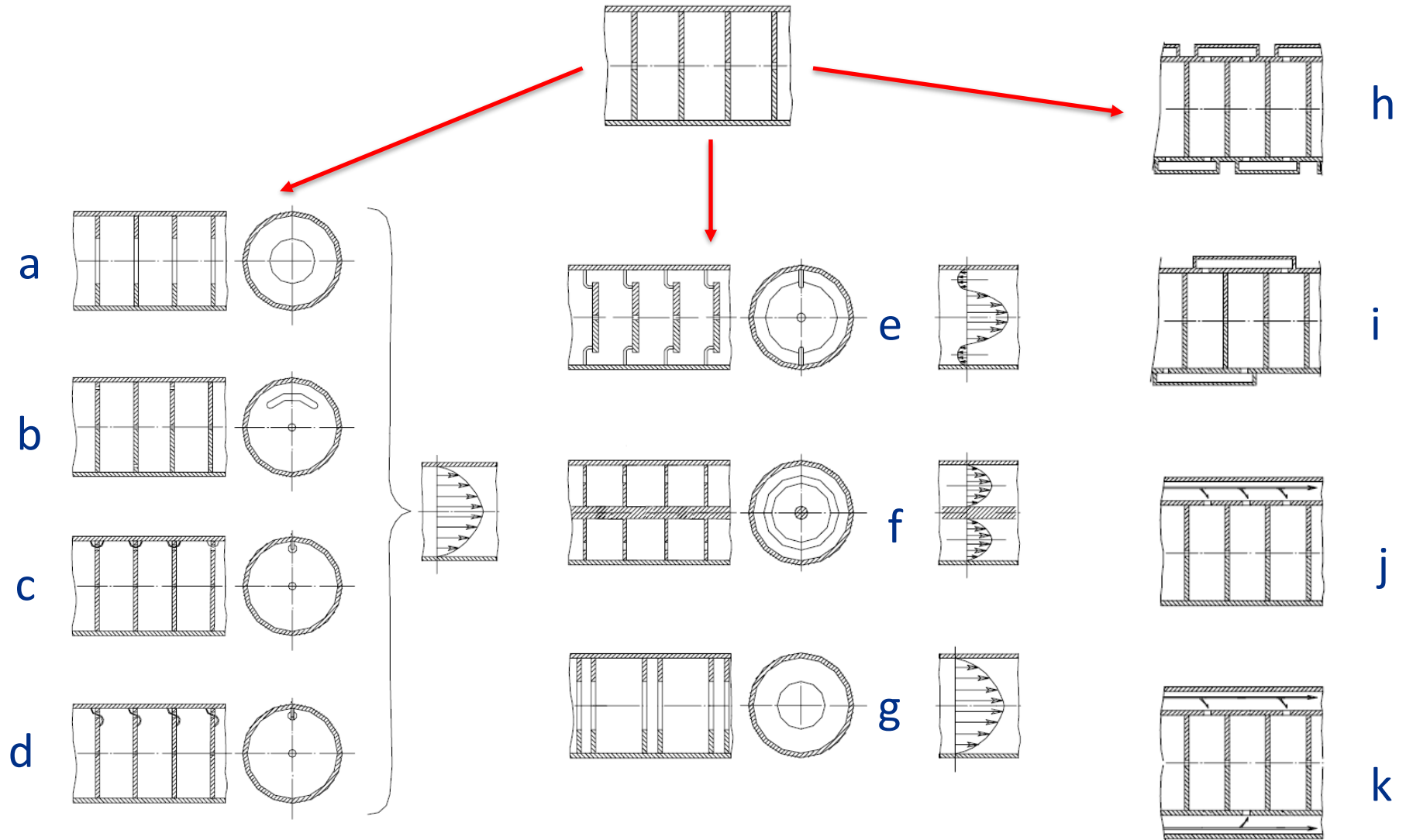
Coupling slots



Right! Strong quadrupole focusing in both directions.

Standing-Wave acceleration structures

Different types of the RT SW acceleration structures:



Summary:

- TW structures are not practical for RT proton accelerators (low beam loading).
- TW structures are not practical for SRF accelerators, proton and electron.
- The cure is a standing – wave structure.
- In the SW structure the operating mode is split, the number of resulting modes is equal to the number of cells.
- $\pi/2$ - mode is the most stable versus cell frequency perturbation, field distribution perturbation is proportional to the number of cells.
- 0- mode and π - mode are less stable versus cell frequency perturbation, field distribution perturbation is proportional to the number of cells squared, which does not allow large number of cells.
- Remedy:
 - biperiodic structures;
 - inductive coupling.

Chapter 6.

Why SRF cavities?

Why SRF?

The surface resistance

The radio-frequency surface resistance can be described in terms of three different contributions:

$$R_S(T, \omega, B, l) = R_{BCS}(T, \omega, l) + R_{fl}(B, l) + R_0$$

Where:

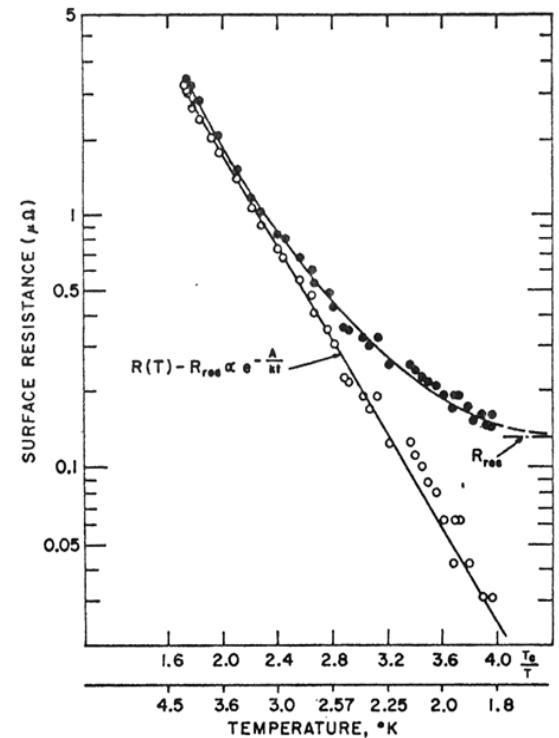
$$R_{BCS}(T, \omega, l) \cong \frac{A(l)\omega^2}{T} e^{-\frac{\Delta}{\kappa_B T}}$$

BCS resistance is caused by electron inertia;

$R_{fl}(B, l) \Rightarrow$ trapped flux surface resistance

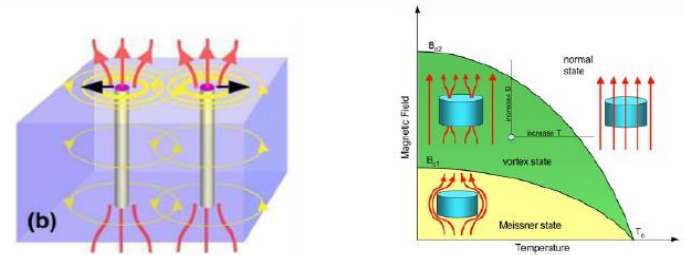
$R_0 \Rightarrow$ intrinsic residual resistance, due to:

- i. Sub-gap states
- ii. Niobium hydrides
- iii. Damaged layer
- iv. ...



J. R. Delayen, SRF1987

Type-II superconductors



Main thermodynamic parameters of type-II superconductors:

1. Critical temperature, T_c
2. Lower critical field H_{c1}
3. Upper critical field H_{c2}

Why SRF?

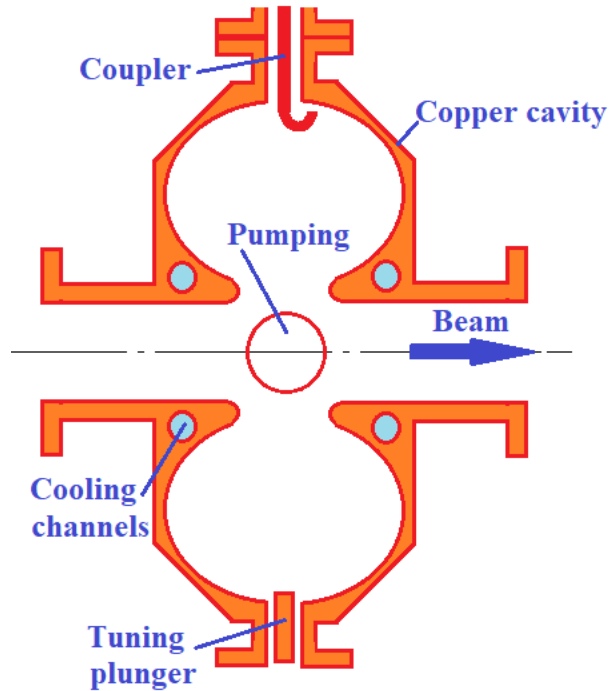
- For copper cavity at RT ($\sigma = 5.96e7$ S/m) for $f=1.3$ GHz one has $R_s = 9.5$ mOhm.
- For SRF Nb cavity at 2K one has $R_s = 8.5$ nOhm (ILC –type cavity, electropolishing),

It is 1.e6 times less!

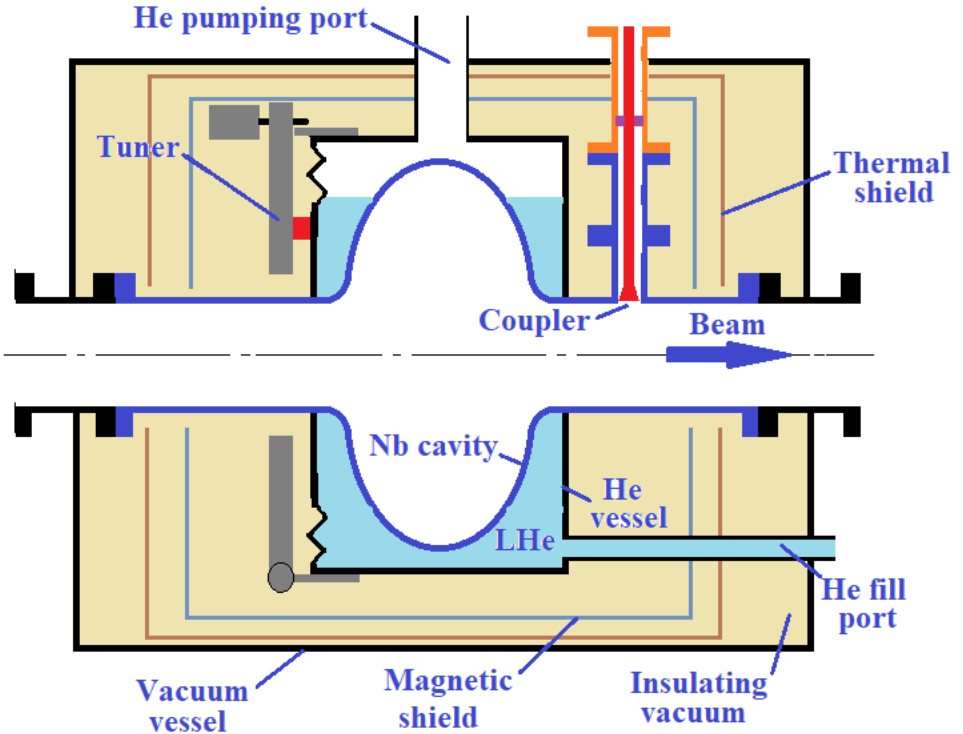
Therefore, CW and high Duty Factor are possible at high gradient, even taking into account “conversion factor” for heat removal at 2K (~1000-1200W/W)

Why SRF?

RT: $Q_0 \sim 1e4$



SRF: $Q_0 \sim 1e10$



SRF cavity needs:

- Liquid He bath (2K);
- Coarse and fine tuners
- Magnetic shield
- Thermal insulation
- Insulating vacuum
- Cryo plant for liquid He supply

Why SRF?

Refrigeration efficiency ($W_{\text{grid}}/W_{\text{cryo}}$):

- Refrigerator's Coefficients of Performance (COP):

$$\text{COP}_{\text{real}} = 1 / (K * \eta_{\text{CARNOT}})$$

$$\eta_{\text{CARNOT}} = T / (300 - T)$$

- Refrigerator's Coefficients of Performance (COP) for different temperatures:

Refrigeration Temperature	Carnot $1/\eta$ IDEAL WORLD	XFEL-Spec REAL WORLD	% Carnot
2 K	149	870	17
5 K	79	220	36
40 K	7	20	33

$$P_{AC} = \sum_T \text{COP}_T \times (P_{\text{dynamic}} + P_{\text{static}})_T$$

In many cases SRF is more efficient than normal conducting RF!

- Low and medium beam loading**
- CW and long-pulse operation**

Why SRF?

Thus, SC provides the following benefits for electron, ion and proton linacs:

1. Power consumption is much less

- operating cost savings, better conversion of AC power to beam power
- less RF power sources

2. CW operation at higher gradient possible

- shorter building, capital cost saving
- need fewer cavities for high DF or CW operation
- less beam disruption

3. Freedom to adapt better design for specific accelerator requirements

- large cavity aperture size
- less beam loss, therefore less activation
- HOMs are removed more easily, therefore better beam quality

Why SRF?

“Practical” gradient limitations for SC cavities:

- Surface magnetic field ~ 200 mT (absolute limit?) – “hard” limit
- Field emission, X-ray, starts at ~ 40 MeV/m surface field – “soft” limit
- Thermal breakdown (limits max surface field for $f > 2$ GHz for typical thickness of material, can be relaxed for thinner niobium) - “hard” limit

SRF allows significantly higher acceleration gradient than RT at high Duty Factor and CW!

Why SRF?

Different mechanisms limiting acceleration gradient:

Room Temperature:

- *Vacuum Breakdown;*
- *Metal fatigue caused by pulse heating;*
- *Cooling problems.*

Breakdown limit:

$$E_a \cdot t_p^{1/6} = \text{const}$$

$E_a \sim 20 \text{ MV/m}$ ($E_{pk} \sim 40 \text{ MV/m}$) @ 1ms or

$E_a \sim 7 \text{ MV/m}$ ($E_{pk} \sim 14 \text{ MV/m}$) @ 1sec (CW)

Superconducting:

- Breakdown usually is not considered for SC cavity;
- Thermal breakdown (quench) – for >2 GHz

Why SRF?

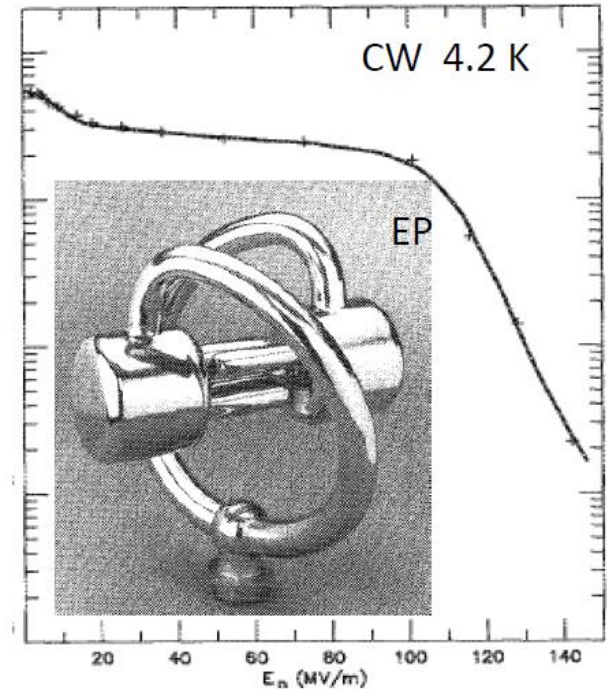
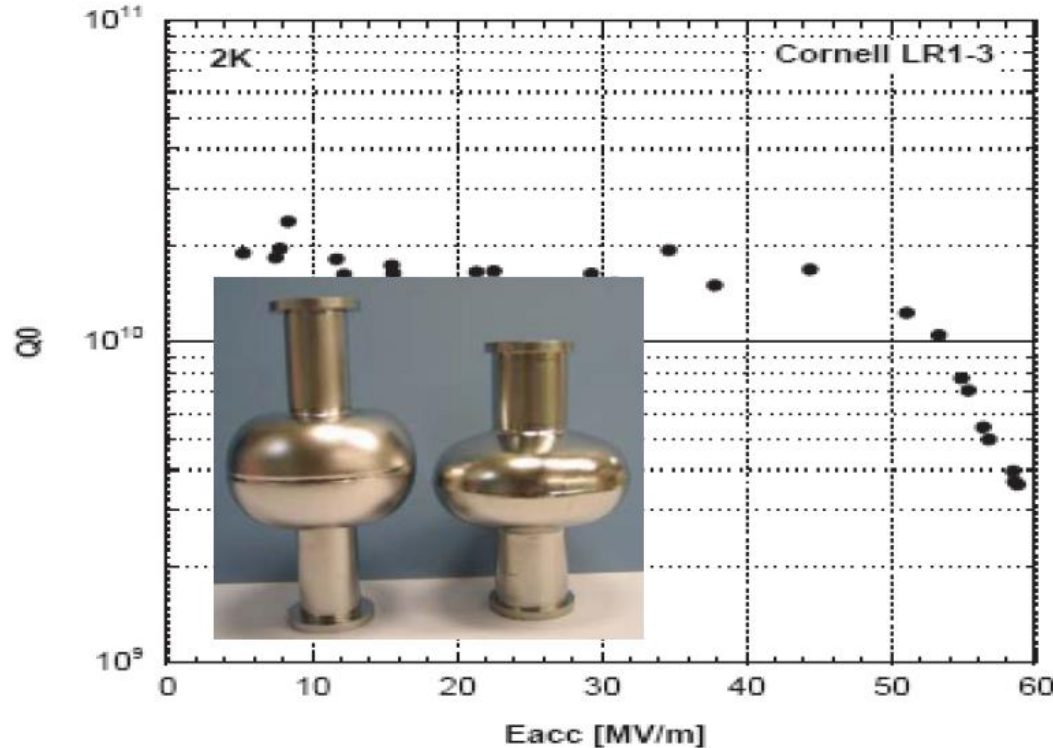
Achieved Limit of SRF electric field

- No known theoretical limit
- 1990: Peak surface field ~ 130 MV/m in CW and 210 MV/m in 1ms pulse.

J. Delayen, K. Shepard, "Test a SC rf quadrupole device", Appl. Phys. Lett, 57 (1990)

- 2007: Re-entrant cavity: $E_{acc} = 59$ MV/m ($E_{pk} = 125$ MV/m, $B_{pk} = 206.5$ mT).

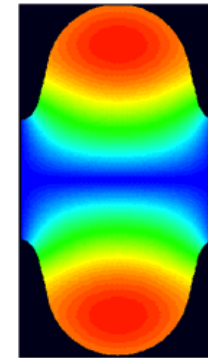
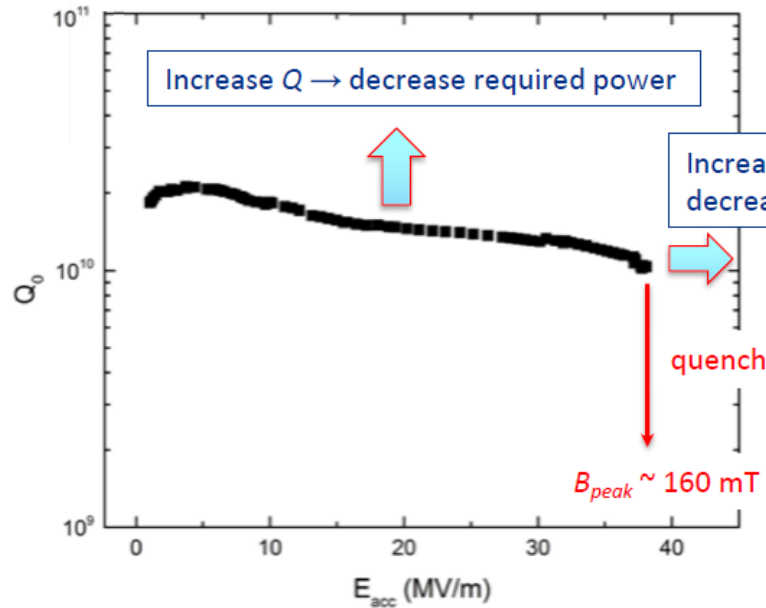
(R.L. Geng et. al., PAC07_WEPMS006) – World record in accelerating gradient



Why SRF?

Introducing Q_0 vs. E_{acc} plot:

Typical ILC-prepared TESLA cavity at $T = 2$ K (state of the art until recent breakthroughs)



Surface magnetic field B

- It is customary to represent performance of an SRF cavity using Q_0 vs. E_{acc} or $Q_0(E_{acc})$ plot.
- Peak surface electric and magnetic fields in the cavity are proportional to E_{acc} . Sometimes Q_0 is plotted vs. peak fields.

Why SRF?

SC cavity performance limitations

▪ Ideal performance: Q_0 is constant until the maximal surface magnetic field is reached:

→ fundamental limitation, limits accelerating gradient to ~ 60 MV/m for typical Nb elliptical cavity shapes.

▪ **Why is $Q_0(E_{acc})$ different in real life?**

Here are some limitations that historically plagued the SRF cavity performance:

- High surface electric field → field emission

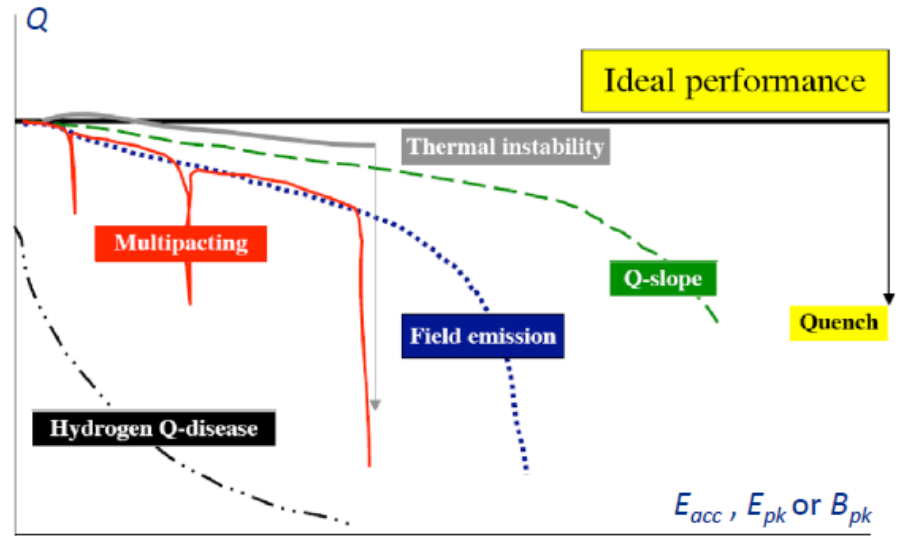
→ can be cured by applying proper preparation techniques: clean room (particulate-free) assembly, high-pressure DI water rinsing (HPR), mechanical polishing of the inner cavity surface.

- Thermal quench → use of high-purity material (RRR) to improve thermal conductivity*, material quality control to avoid mechanically damaged surfaces, particulate free assembly.

- Multipacting → use of elliptical cell shapes.

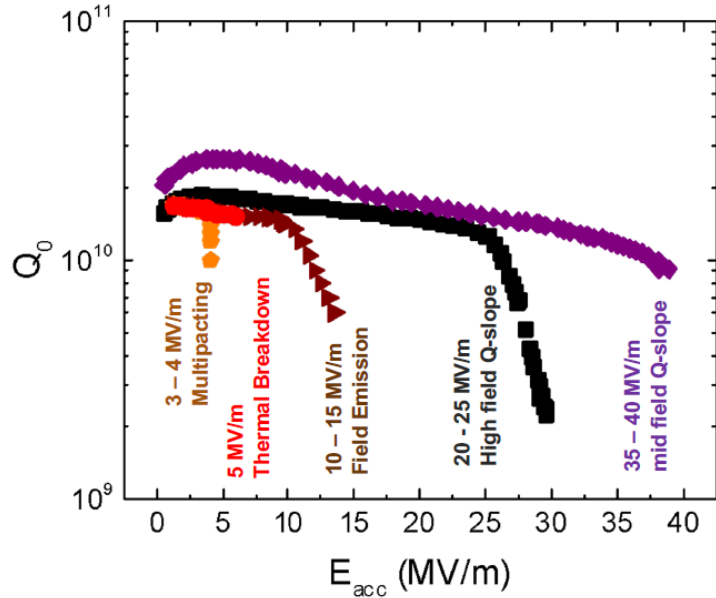
Q-disease due to lossy niobium hydrides → perform acid etch at $T < 15^\circ\text{C}$, rapid cooldown, degassing at $600 - 800^\circ\text{C}$.

***Wiedemann–Franz law** states that the ratio of the electronic contribution of the thermal conductivity (κ) to the electrical conductivity (σ) of a metal is proportional to the temperature (T), or $\kappa = \sigma LT$, L is Lorentz number.

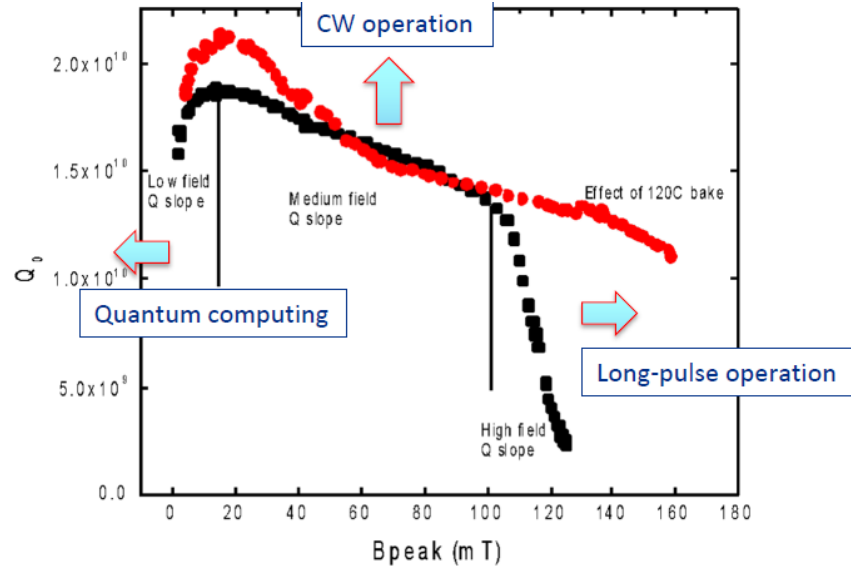


Why SRF?

$Q_0(E_{acc})$ with numbers



Q slopes



Three parts of the curve limiting performance of different applications:

1. Low field Q slope → SRF for quantum computing: need as high Q as possible to increase qubit coherence time;
2. Medium field Q slope → CW operation: cryogenics vs. linac cost optimization determines operating gradient (15-20 MV/m, LCLS-II);
3. High field Q slope → Long-pulse operation tends to favor the highest reliably achievable gradient (23.6 MV/m for XFEL, 31.5 MV/m for ILC)

Why SRF?

Standard SRF cavity surface treatments

Electron-Beam Welding - EBW

Buffered Chemical Polishing –BCP: $\text{HNO}_3 + \text{HF} + \text{H}_3\text{PO}_4$

- H_3PO_4 (phosphoric acid) is necessary to stabilize (buffer) the etching reaction between Nb and HNO_3 (nitric acid) + HF (hydrofluoric acid), which is exothermic and rapid.
- The mixture is used for Nb cavities contains HF(48%), HNO_3 (65%), H_3PO_4 (98%) in proportion 1:1:X, X=1-4.
- Still in use for low-frequency, medium gradient cavities;

Electro-Polishing –EP: $\text{H}_2\text{SO}_4 + \text{HF} + 10\text{-}12\text{V} \rightarrow$ smooth surface, lower surface fields, lower FE, higher E_{acc} and Q_0 .

- A cathode made of pure Al and a Nb cavity as an anode in mixture of sulfuric acid H_2SO_4 (93%) and hydrofluoric acid HF (50%) at 10:1 volume ratio.
- Nb is oxidized by sulfuric acid to niobium-pentoxide, which is dissolved simultaneously by hydrofluoric acid.
- Used for high-gradient cavities in pulsed regime and for medium-gradient cavities in CW.

High-Temperature Treatment

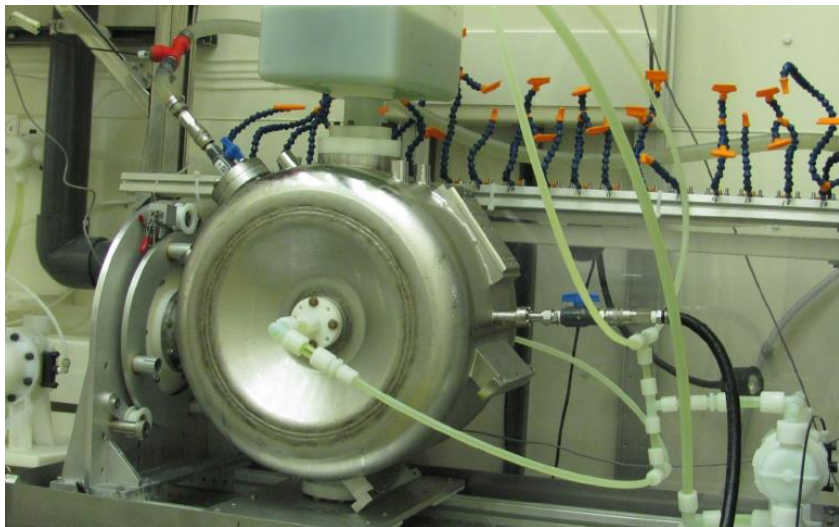
- 800C -900C backing in vacuum is used to relieve the stresses, remove defects and dislocations and degas of hydrogen.

High-Pressure Rinsing (HPR)

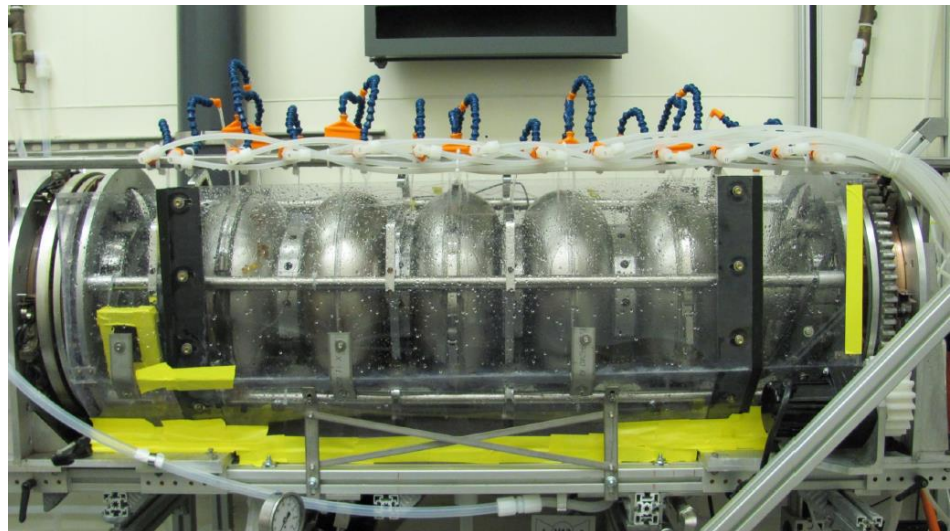
- 100 bar rinsing before assembly in a clean room

Why SRF?

BCP processing for a 325 MHz spoke cavity.



EP processing of 650 MHz elliptical cavity



Why SRF?

- Q_0 Improvement:
 - Improvement of cavity processing recipes;
 - High Q_0 preservation in CM.
- The goal is to achieve $Q_0 > 4e10$ in CM @2 K

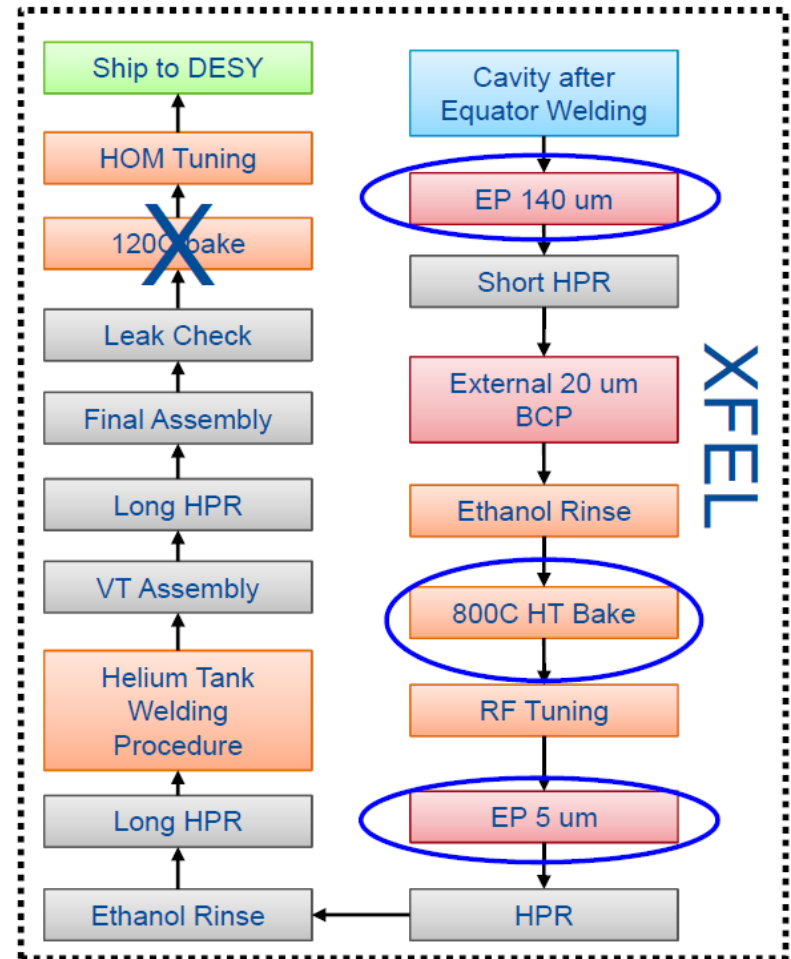
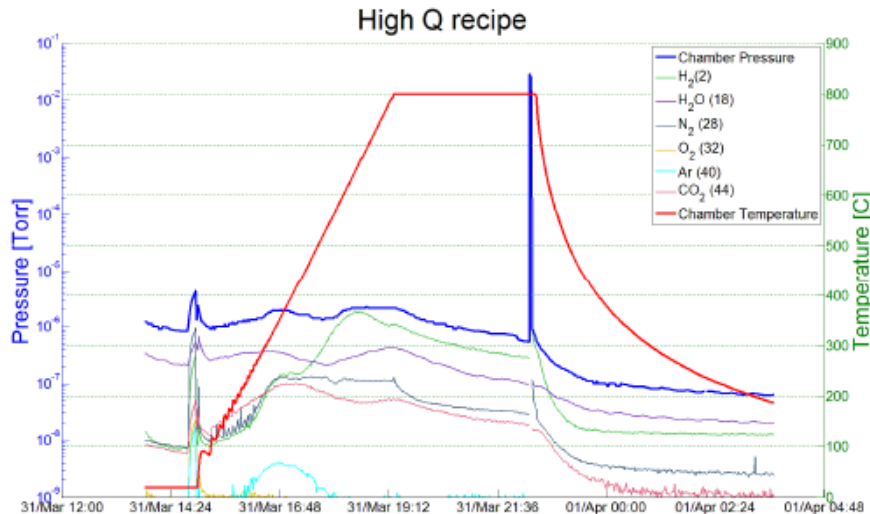


Recent breakthrough in Q_0 increase: N-doping.

- “Standard” XFEL technology provides $\sim 1.4e10 @ 2K$, 20-23 MeV/m (CM);
- N-doping: discovered in the frame of R&D on the Project-X SC CW linac (A. Grassellino).

Cavity Treatment:

- Bulk EP
- 800 C anneal for 3 hours in vacuum
- 2 minutes @ 800C nitrogen diffusion
- 800 C for 6 minutes in vacuum
- Vacuum cooling
- 5 microns EP

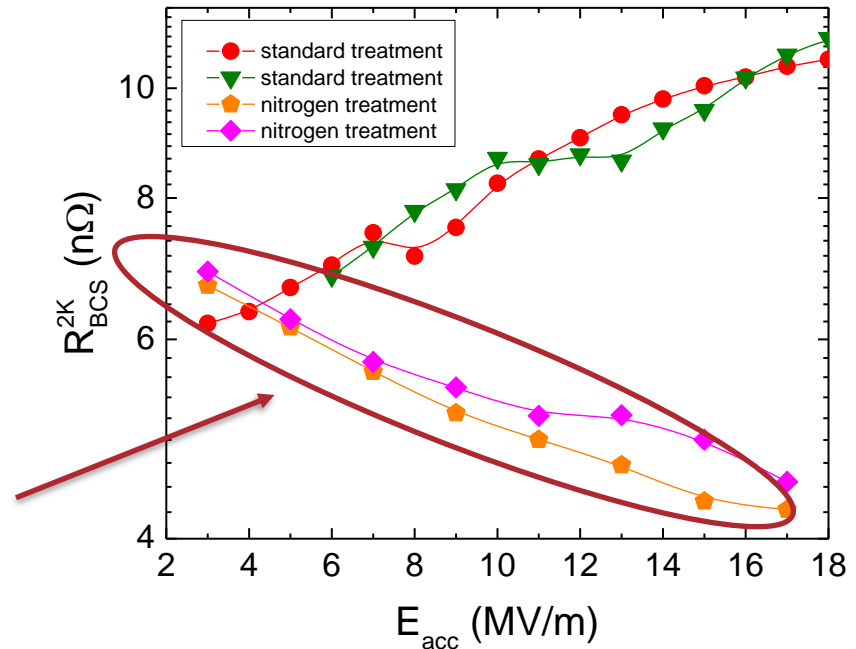
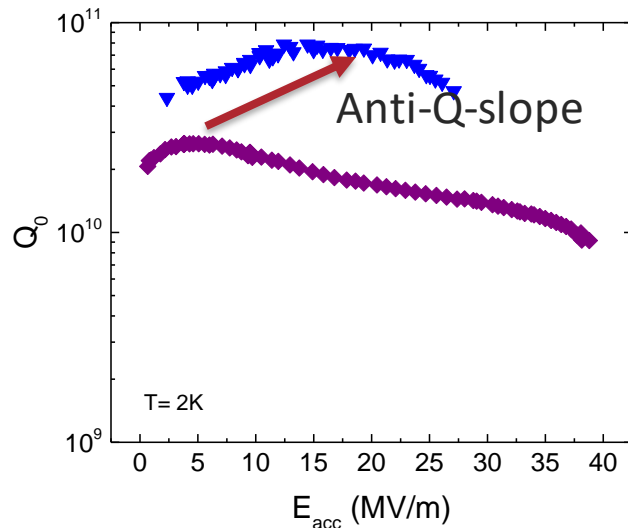


A. Grassellino, N-doping: progress in development and understanding, SRF15

N-doping

Origin of the anti-Q-slope for N-doping

$$R_S(2 K) = R_{BCS}(2 K) + R_0 + R_{fl}$$



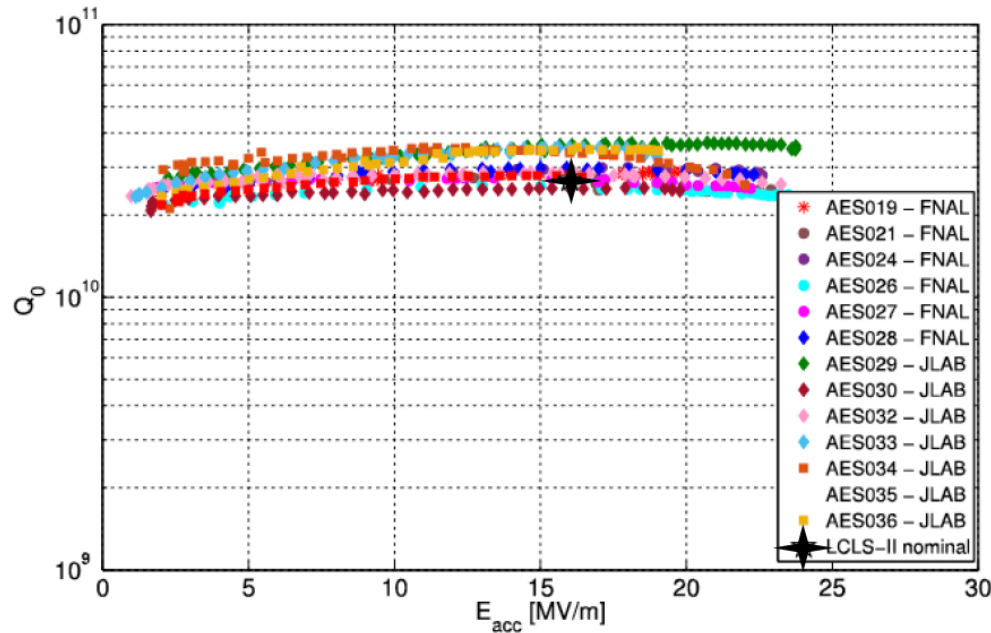
Anti-Q-slope emerges from the BCS surface resistance decreasing with field

A. Grassellino et al, Supercond. Sci. Technol. **26** 102001 (2013) - Rapid Communications
A. Romanenko and A. Grassellino, Appl. Phys. Lett. **102**, 252603 (2013)

M. Martinello, M. Checchin

N-doping:

- Provides Q_0 2.5-3 times higher than “standard” processing.
- Trade-off:
 - Lower acceleration gradient, 20-22 MeV/m – not an issue for ion and proton linacs;
 - Higher sensitivity to the residual magnetic field.
- Remedy:
 - Magnetic hygiene and shielding improvement
 - Fast cooldown

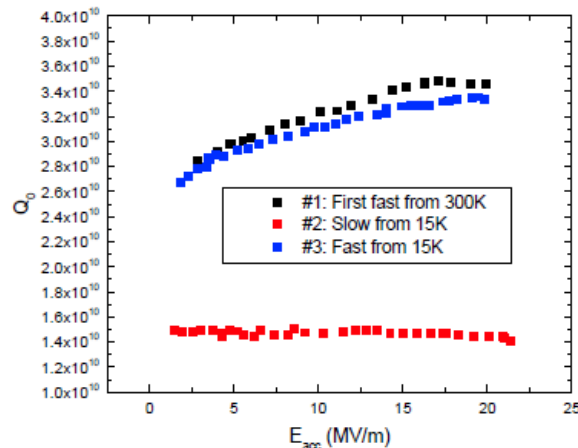


VTS test results of dressed prototype cavities

Fast cooldown

- $Q_0 = G/R_s$; $R_s = 10$ nOhm for $Q_0 = 2.7e10$
 $R_s = R_0 + R_{BCS} + R_{TF}$,
 $R_{TF} = s * \eta * B_{res}$, s is sensitivity to residual magnetic field B_{res} , η is flux expulsion efficiency.
 η is material-dependent!
- For pCM Nb (Wah Chang):
 $R_{BCS} = 4.5$ nOhm, $R_0 = 1-2$ nOhm, $R_{TF} \approx 1$ Ohm for 5mG $\rightarrow Q_0 = 3.5e10$
- For production material:
Change heat treatment temperature from 800 C to 900 C+ deeper EP (S. Posen):
 $R_{BCS} = 4.5$ nOhm, $R_0 \approx 2$ nOhm, $R_{TF} \approx 2$ Ohm for $B_{res} \approx 5$ mG $\rightarrow Q_0 > 3e10$

Dressed N₂ doped 9 cell Sensitivity Test at 2K

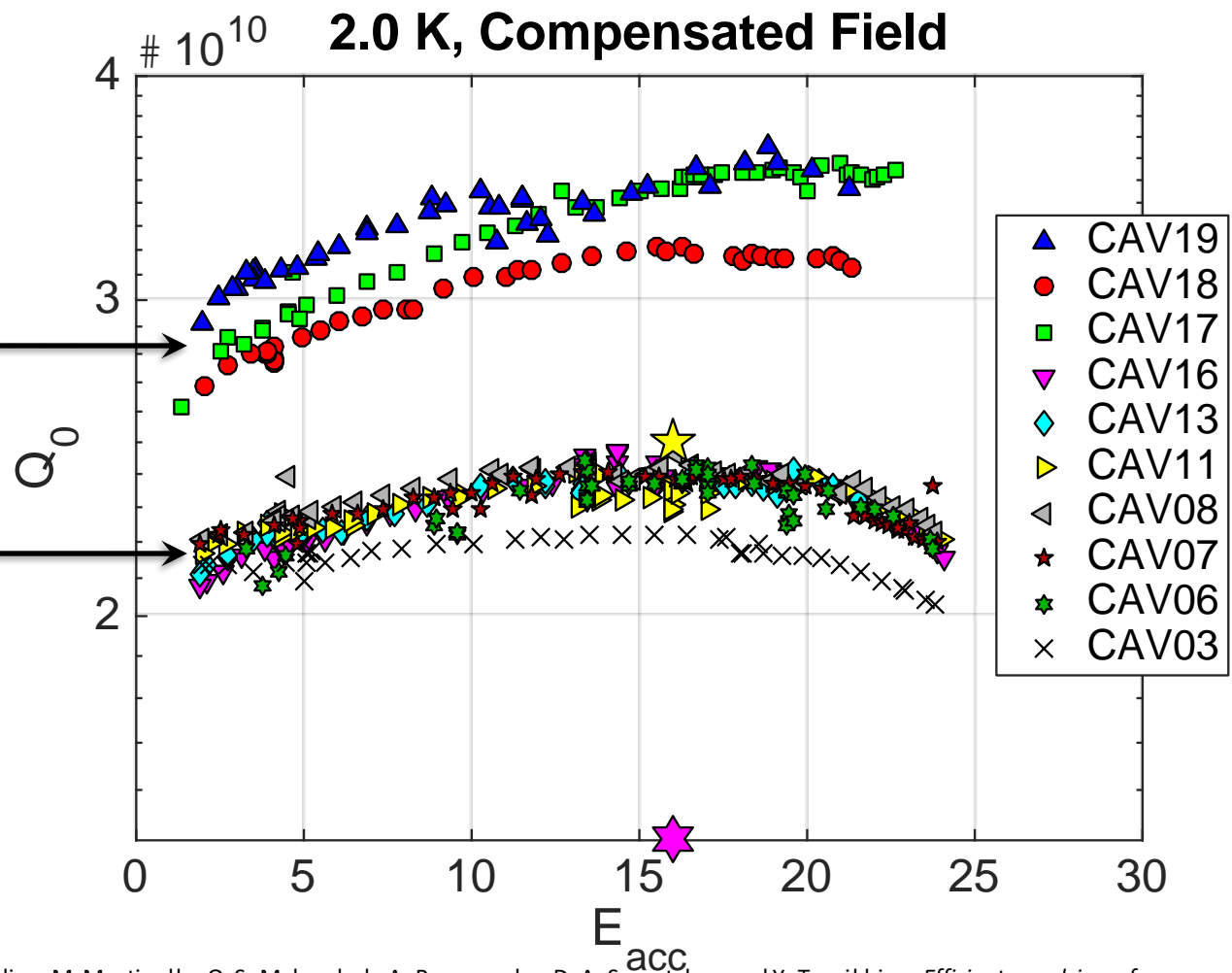


“Fast”: 2 – 3 K/minute, “slow”: < 0.5 K/minute

Impact of Modified LCLS-II Recipe on Q_0

Cavities 17, 18, 19:
modified recipe - 900 C degas, $\sim 200 \mu\text{m}$ EP, 2min/6min N doping at 800 C

Cavities 03...16: First production tests at Fermilab, baseline LCLS-II recipe - 800 C degas, $\sim 130 \mu\text{m}$ EP, 2min/6min N doping at 800 C



Studies leading to modified recipe:

S. Posen, M. Checchin, A. C. Crawford, A. Grassellino, M. Martinello, O.S. Melnychuk, A. Romanenko, D. A. Sergatskov and Y. Trenikhina, *Efficient expulsion of magnetic flux in superconducting radiofrequency cavities for high Q_0 applications*, J. Appl. Phys. **119**, 213903 (2016), [dx.doi.org/10.1063/1.4953087](https://doi.org/10.1063/1.4953087).

A. Romanenko, A. Grassellino, A. C. Crawford, D. A. Sergatskov and O. Melnychuk, *Ultra-high quality factors in superconducting niobium cavities in ambient magnetic fields up to 190 mG*, Appl. Phys. Lett. **105**, 234103 (2014); [http://dx.doi.org/10.1063/1.4903808](https://doi.org/10.1063/1.4903808).

A. Grassellino, A. Romanenko, S Posen, Y. Trenikhina, O. Melnychuk, D.A. Sergatskov, M. Merio, N-doping: progress in development and understanding, Proceedings of SRF15, <http://srf2015proc.triumf.ca/prepress/papers/moba06.pdf>.

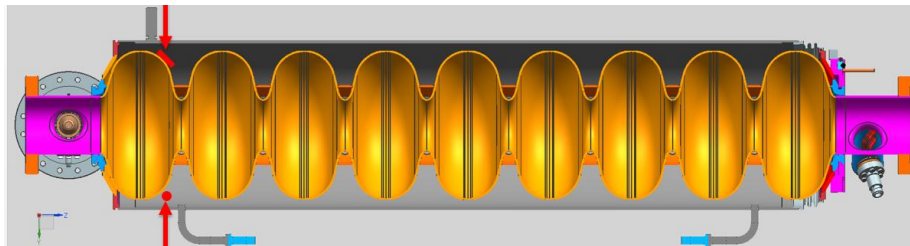


Ambient Magnetic Field Management Methods

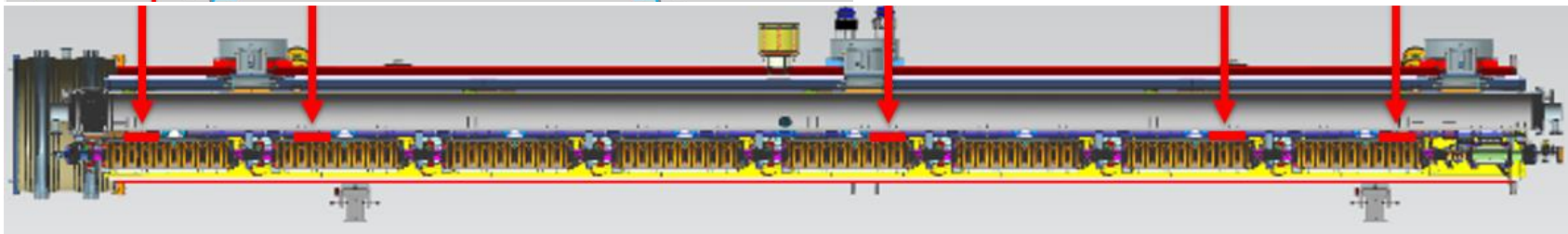
- 2-layer passive magnetic shielding
 - Manufactured from Cryoperm 10
- Strict magnetic hygiene program
 - Material choices
 - Inspection & demagnetization of components near cavities
 - Demagnetization of vacuum vessel
 - Demagnetization of assembled cryomodule / vessel
- Active longitudinal magnetic field cancellation

Magnetic field diagnostics:

- 4 cavities instrumented with fluxgates inside helium vessel (2 fluxgates/cavity)
- 5 fluxgates outside the cavities mounted between the two layers of magnetic shields



Fluxgates monitored during cryomodule assembly

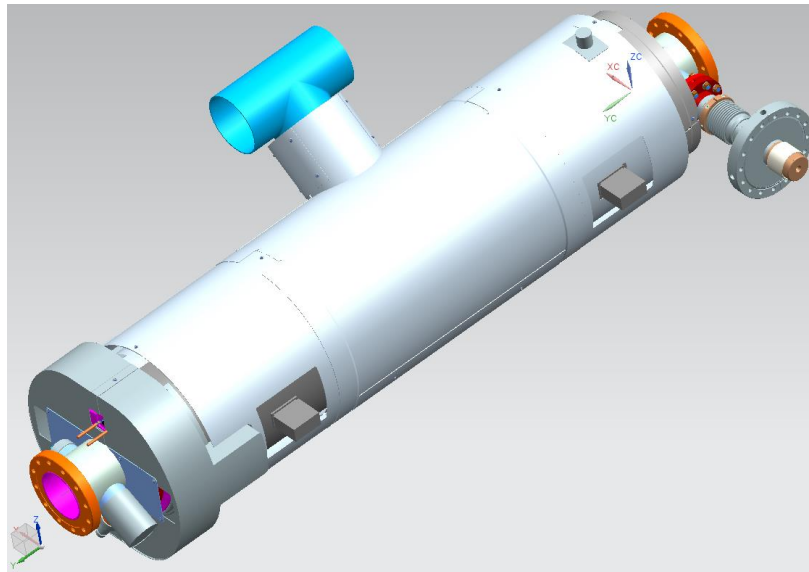


A. Crawford, arXiv:1507.06582v1, July 2015; S. Chandrasekaran, TTC Meeting, Saclay 2016

Ambient Magnetic Field Management Methods

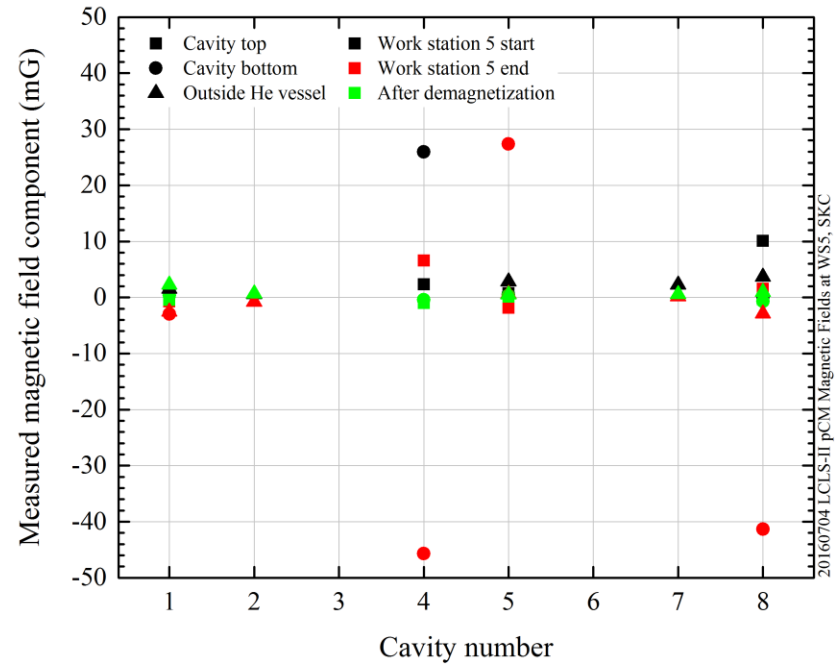


Helmholtz coils wound onto vessel directly



2-layer magnetic shields
manufactured from Cryoperm 10

S. Chandrasekaran, Linac 2016, TUPLR027



Prototype Cryomodule Latest Preliminary Results

- Cryomodule remnant field ≈ 1 mG
- Fast cool down in a cryomodule demonstrated
- $Q_0 \approx 2.7e10$ in a CW cryomodule

Cavity	VTS		pCM after RF_Conditioning			
	Max Gradient [MV/m]	Q0 @16MV/m	Max Gradient*** [MV/m]	Usable Gradient* [MV/m]	FE onset [MV/m]	Q0 @16MV/m 2K** extrapolated
TB9AES021	23	3.1E+10	19.6	18.2	14.6	2.6E+10
TB9AES019	19.5	2.8E+10	19	18.8	15.6	2.6E+10
TB9AES026	21.4	2.6E+10	17.3	17.2	17.4	2.7E+10
TB9AES024	22.4	3.0E+10	21	20.5	21	2.5E+10
TB9AES028	28.4	2.8E+10	14.9	14.2	13.9	2.4E+10
TB9AES016	18	2.8E+10	17.1	16.9	14.5	2.9E+10
TB9AES022	21.2	2.8E+10	20	19.4	12.7	3.2E+10
TB9AES027	22.5	2.8E+10	20	17.5	20	2.5E+10
Average	22.1	2.8E+10	18.6	17.8	16.2	2.7E+10
Total Voltage	183.1 MV		154.6	148.1		

*Usable Gradient: demonstrated to stably run CW, FE < 50 mR/h, no dark current

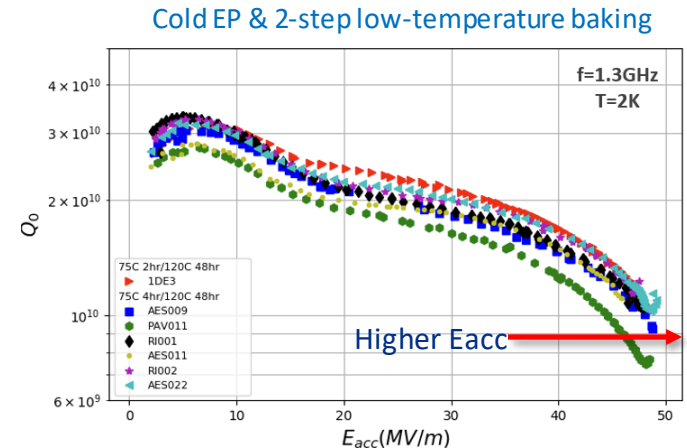
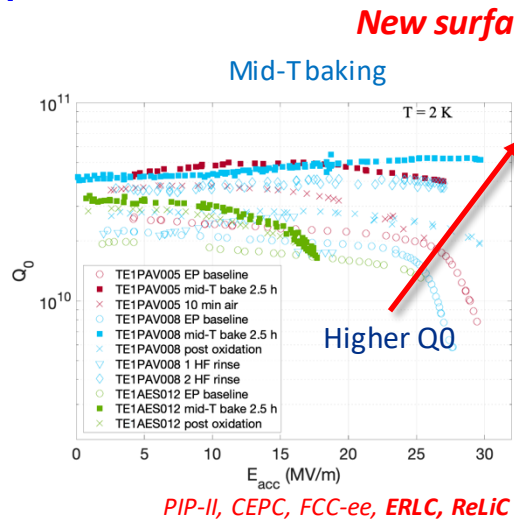
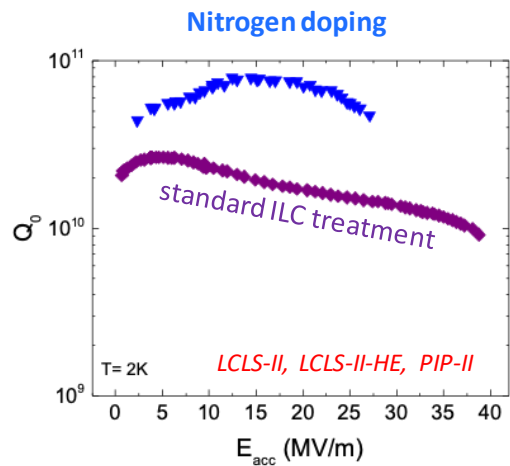
**Fast cooldown from 45K, >40 g/sec, extrapolated from 2.11K

G. Wu, FNAL SRF Department meeting, 24 October 2016, <https://indico.fnal.gov/conferenceDisplay.py?confId=13185>



Further Improving cavity performance via surface treatment

- Breakthrough caused by invention of **nitrogen doping** (N-doping) triggered investigations of other surface treatment methods:
 - Mid-T backing and
 - Cold EP & 2-step baking.

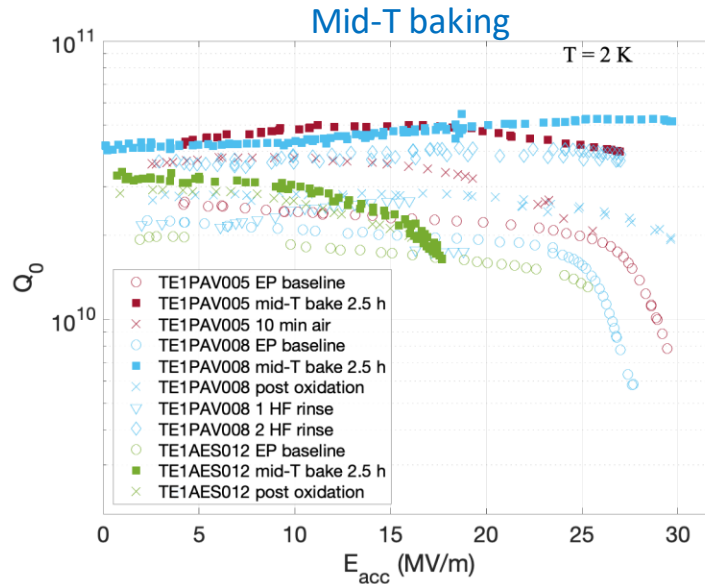


- There are active studies to push performance of bulk niobium cavities, improve our understanding of SRF losses and ultimate quench fields via experimental and theoretical investigations
- The ultimate goal is on developing methods for nano-engineering the niobium surface layer and tailoring SRF cavity performance to a specific application

Mid-T baking: Initial results

- Medium temperature baking in vacuum (Mid-T, 300°C to 400°C) was developed to improve cryogenic performance of SRF cavities at medium accelerating gradients ($E_{acc} = 20 - 30$ MV/m), extending beyond N-doping in E_{acc} while maintaining high Q_0

This is a new, simpler alternative to nitrogen doping



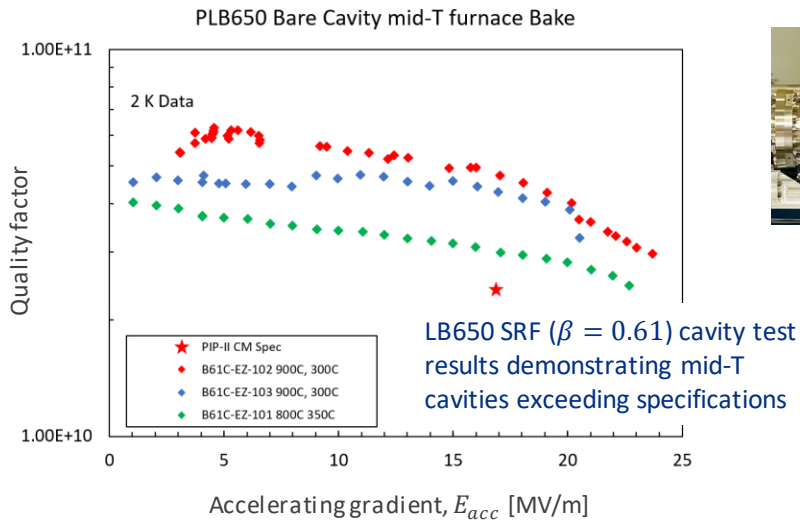
S. Posen et al. *Phys. Rev. Applied* **13**, 014024 (2020)



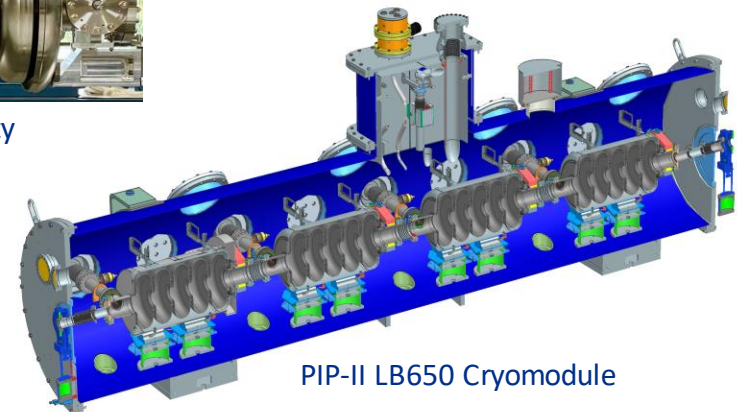
Note: Our standard “vehicle” for R&D is a single-cell 1.3 GHz elliptical TESLA shape cavity

Mid-T baking at 650 MHz (5-cell cavities)

- After initial R&D efforts at 1.3 GHz, this recipe was successfully tested on the low-beta 650 MHz (LB650) PIP-II cavities and was accepted as a baseline treatment



PIP-II LB650 SRF cavity



PIP-II LB650 Cryomodule

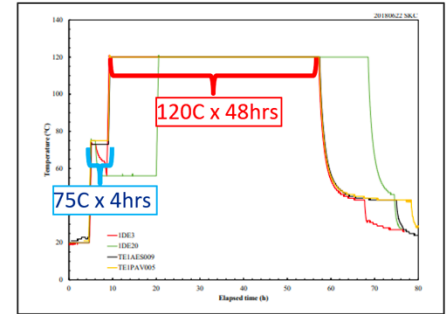
Courtesy of Genfa Wu (FNAL)

Note: Need to multiply Q by a factor of 1.4 to compare with TESLA shape cavities

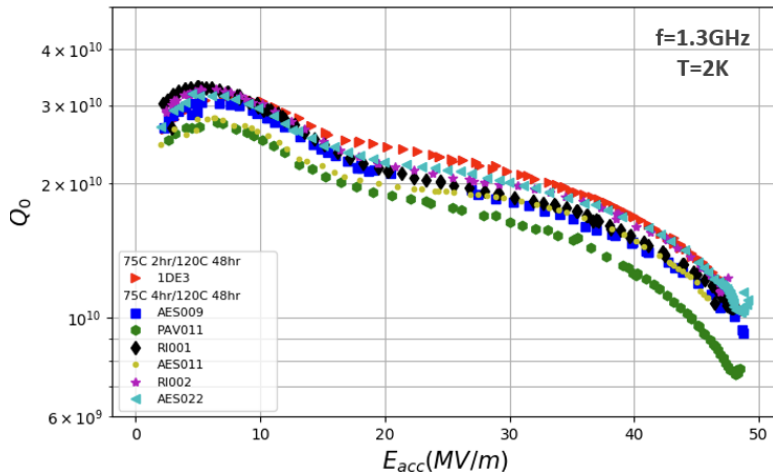
- Mid-T baking is relevant to ERL-based liner colliders (as well as circular colliders)

Pushing toward 50 MV/m

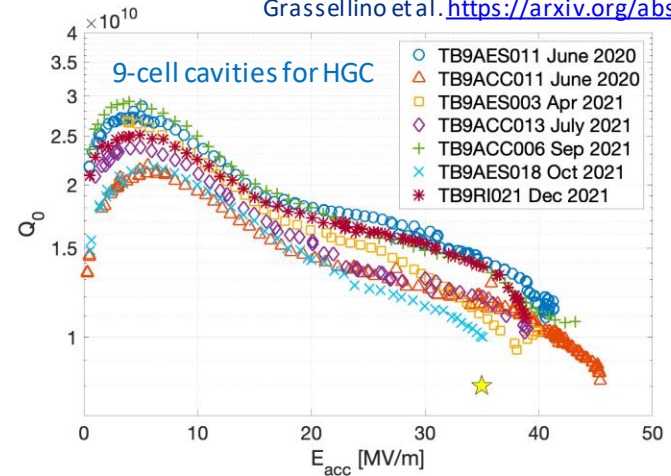
- Application of a combination of cold electropolishing (EP) and 2-step low-temperature baking to single-cell TESLA cavities demonstrated accelerating gradients ~ 50 MV/m
- The recipe is transferred to 9-cell cavities: average 40.4 MV/m!
- A High-Gradient Cryomodule (HGC) is being prepared at Fermilab for testing



2-step low-temperature baking (single-cell cavities)

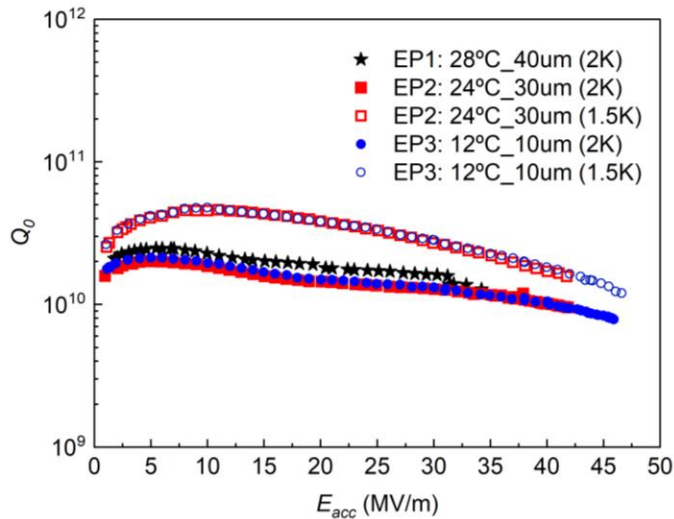


Grassellino et al. <https://arxiv.org/abs/1806.09824>

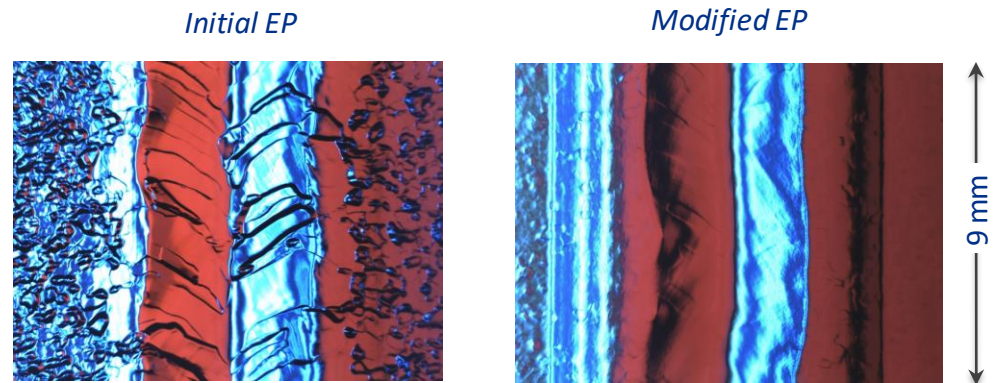


Cold EP or 2-step baking?

- It is not clear yet, whether cold EP, 2-step baking (as opposed to standard low-temperature baking) or a combination of both is responsible for improving accelerating gradient
- Cold EP provides much smoother surface than EP at higher temperatures
- Recently, a 9-cell cavity subjected to cold EP and 120°C baking reached 46 MV/m
- Systematic studies are under way



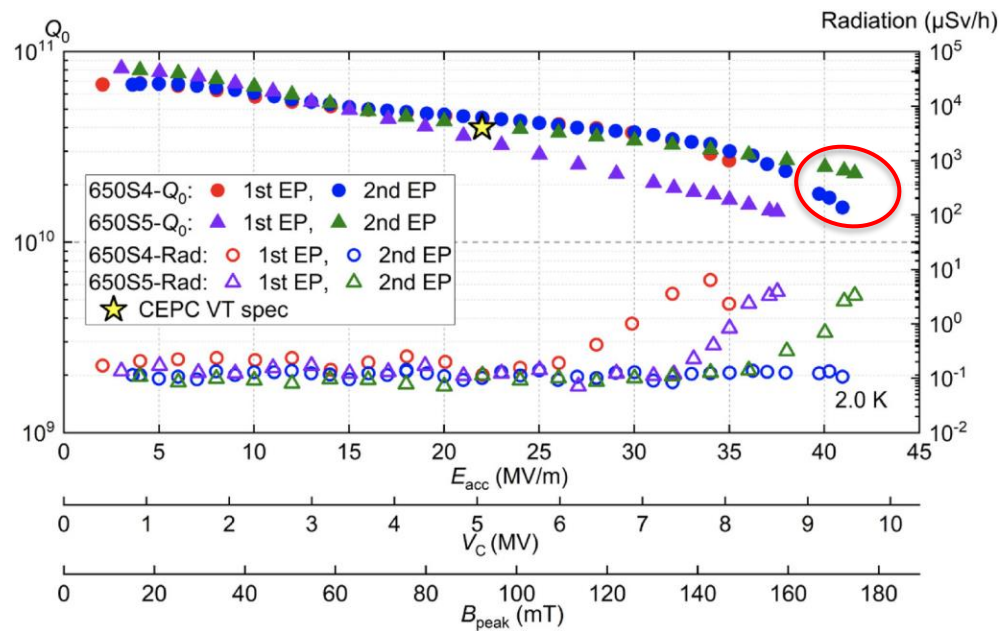
Courtesy of V. Chouhan (FNAL)



V. Chouhan *et al.*, *Nucl. Instrum. Methods Phys. Res. A* **1051** (2023) 168234

Recent results on single-cell 650 MHz cavities

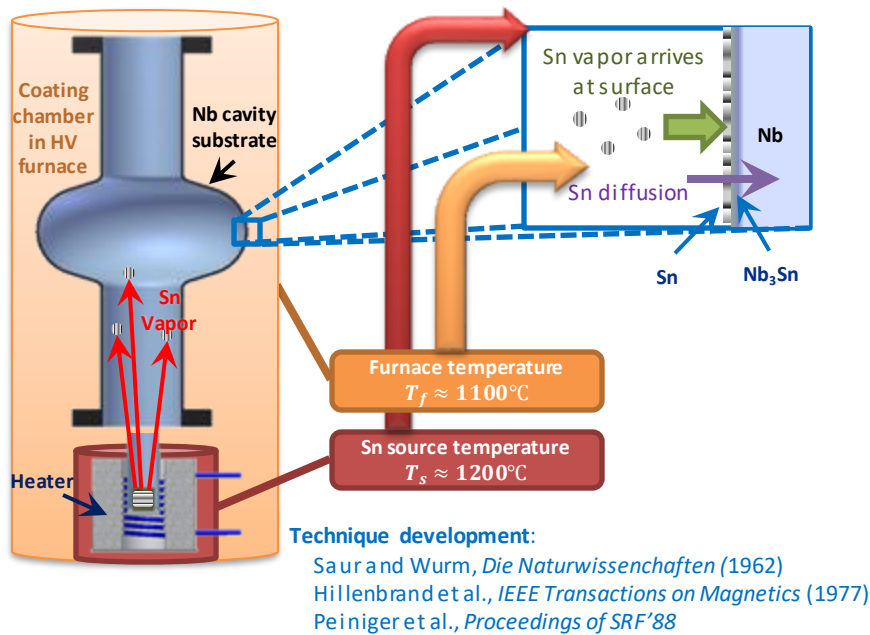
- Recently, cold EP and 120°C backing applied to single-cell 650 MHz cavities produced excellent results at IHEP (China)
- Similar performance was demonstrated at Fermilab



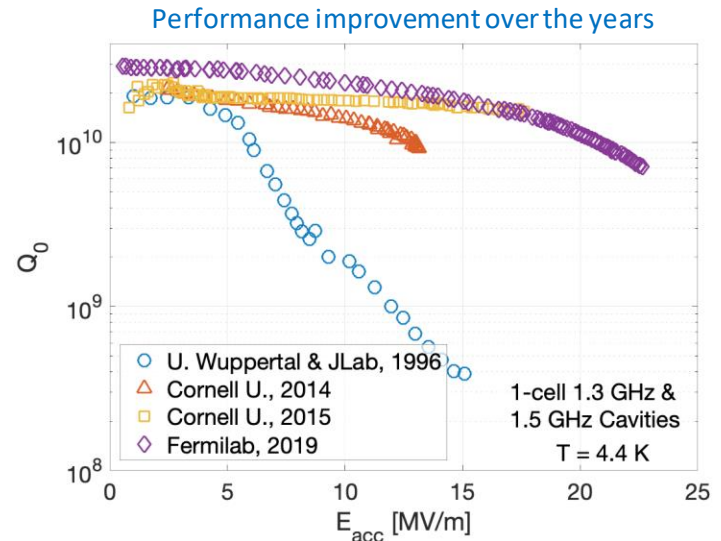
P. Sha et al. *Nucl. Sci. Tech.* (2022) **33**:125

New materials: Nb₃Sn

- High T_c material → low losses at 4 K, a candidate for cryocooler-based applications
- Potential for high gradients, ~ 90 MV/m**
- So far, the best progress with **vapor diffusion technique**

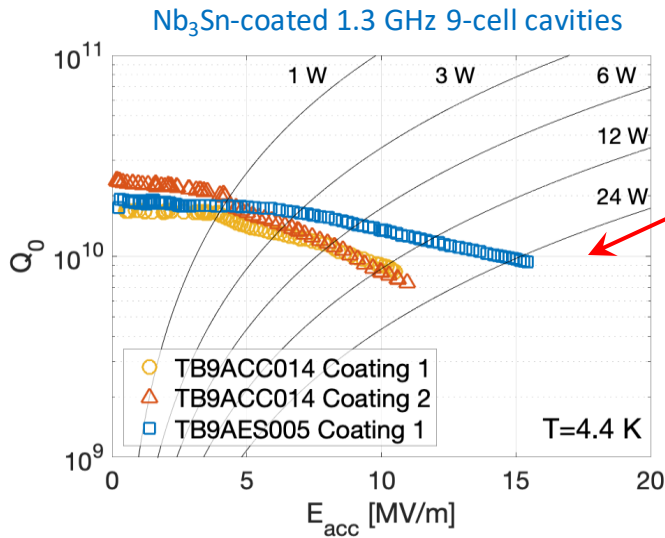


- Best performance of a single-cell Nb₃Sn cavity so far is only ~ 24 MV/m

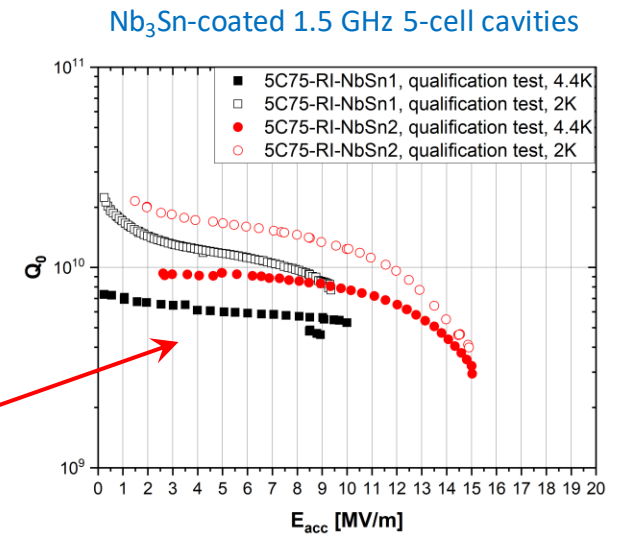
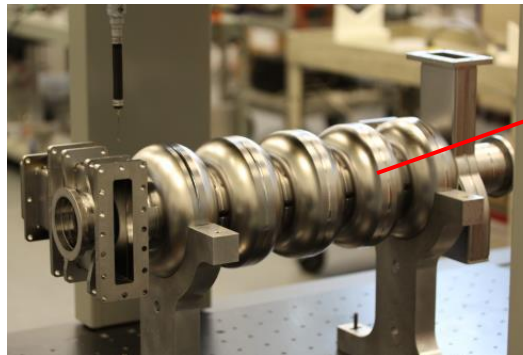
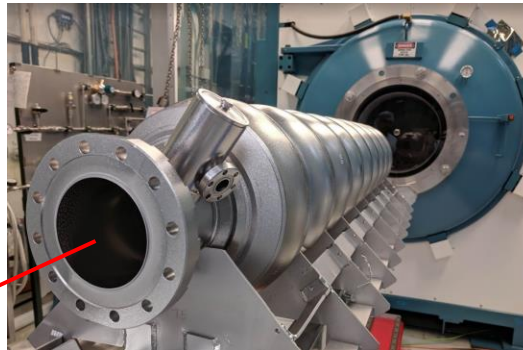


Multi-cell Nb₃Sn cavities

- The best multi-cell cavities reached 15 MV/m



Courtesy of S. Posen (FNAL)

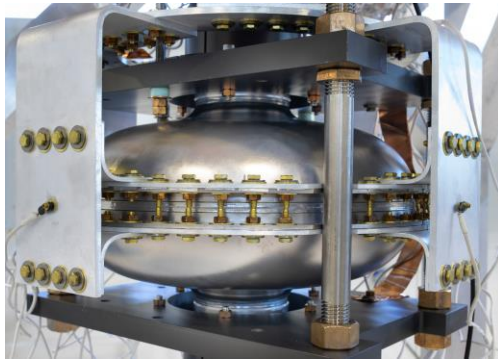


G. Ereemeev and U. Pudasaini, presentation at the TTC meeting, October 2022

Conduction-cooled cavities

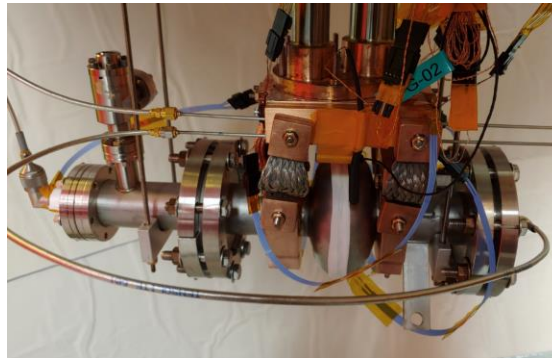
- Conduction cooling of Nb₃Sn SRF cavities via a cryocooler was demonstrated recently
- This is promising for **new compact accelerator applications for industry**

Fermilab



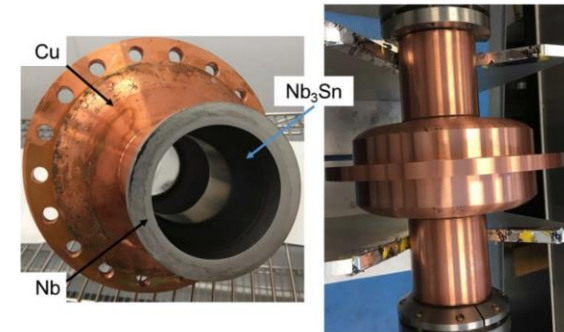
R.C. Dhuley et al, *Supercond. Sci. Technol.* **33**, 06LT01 (2020)

Cornell University



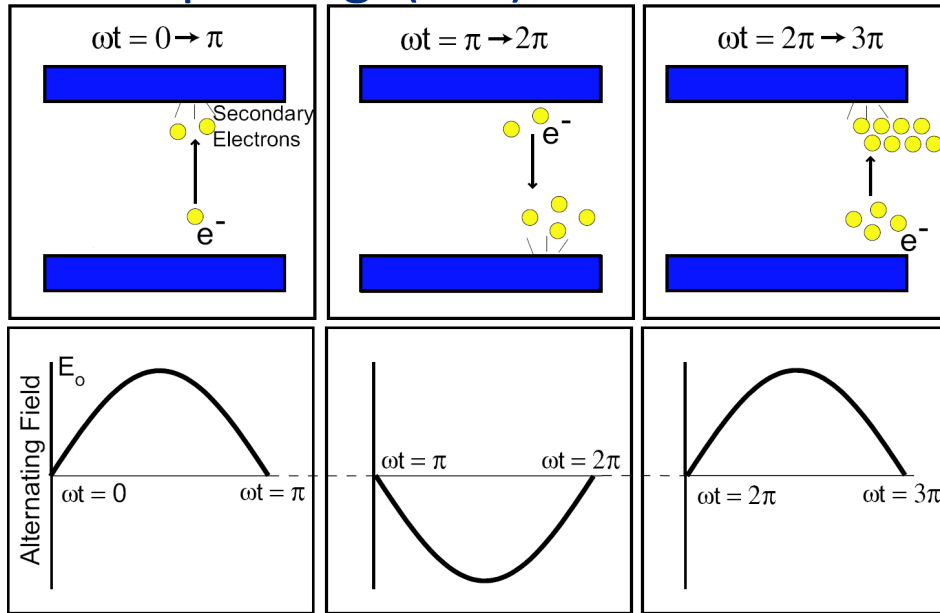
N. Stilin et al, arXiv:2002.11755v1 (2020)

Jefferson Lab

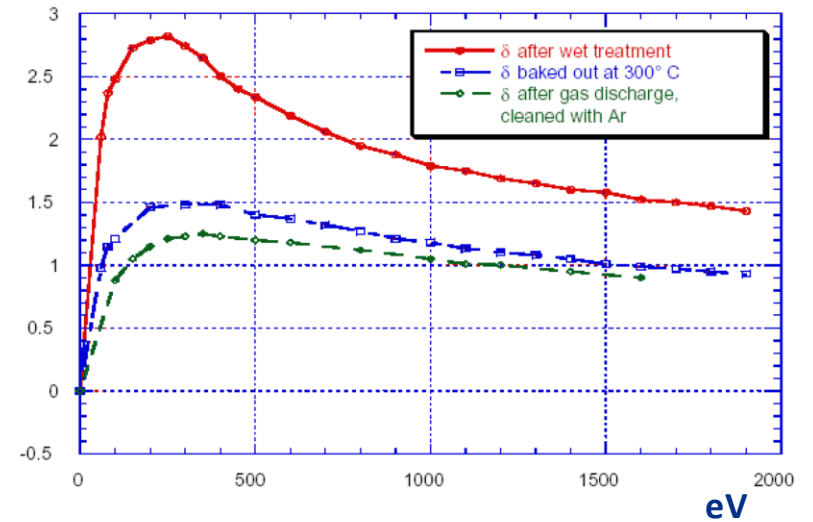


G. Ciovati et al, *Supercond. Sci. Technol.* **33**, 07LT01 (2020)

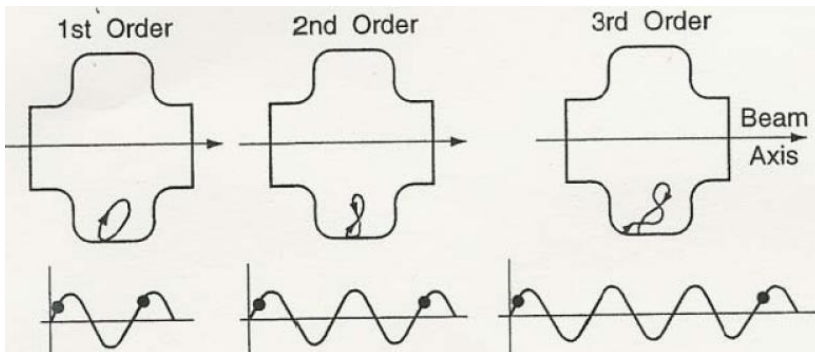
Multipacting (MP) in SRF cavities



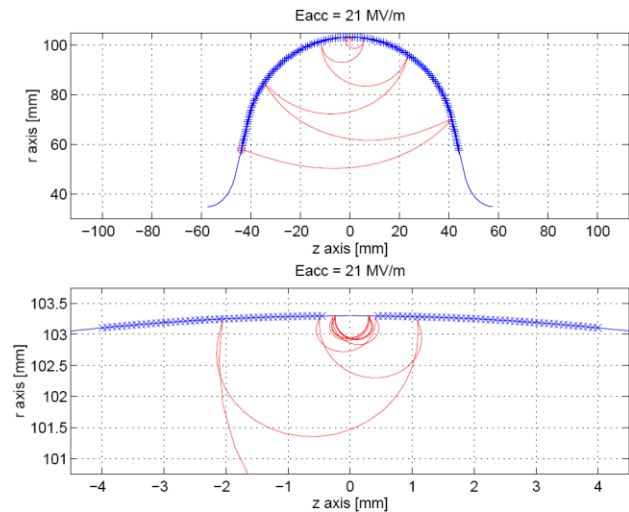
Secondary emission coefficient for Nb



Multipactor discharge with an electric field oscillating between two metal electrodes.

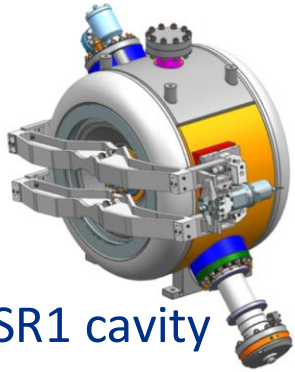


Typical one-point multipactor trajectories for orders 1, 2 and 3.

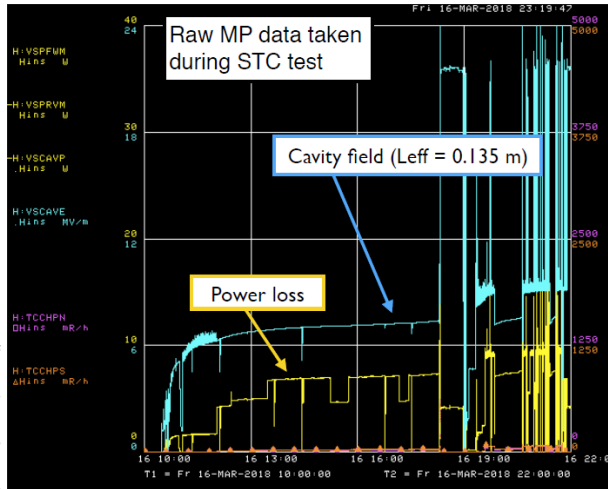


Two point MP in 1.3GHz TESLA cavity. 2D simulations

Multipacting in SRF cavities



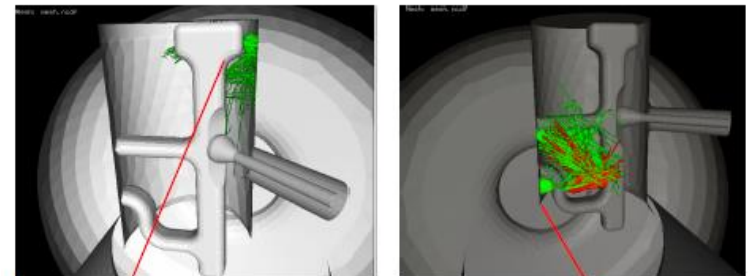
Strong MP in SSR1 at 5, 6.5 and 7 MV/m. 120 C bake for 48 h helps to reduce MP conditioning time



3.9 GHz HOM coupler failure due to overheating caused by MP: redesigned to shift MP barriers above operating gradients



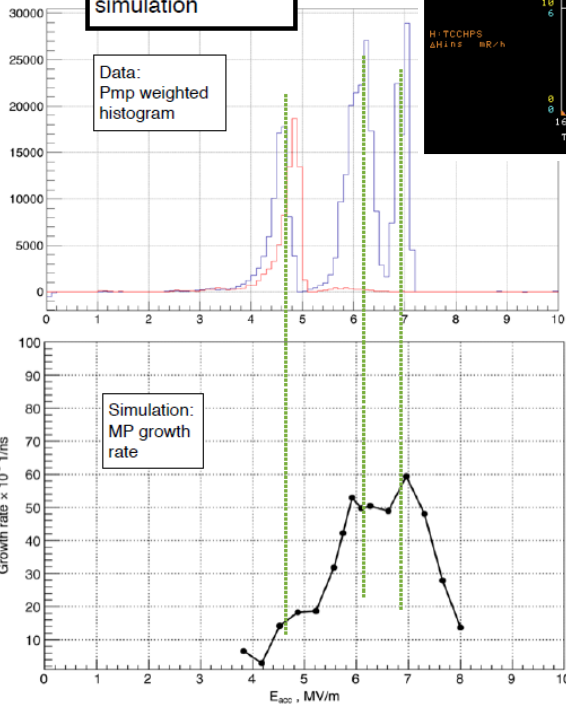
Multipacting in HOM2 at SNS



Comparison to MP simulation

Data: Pmp weighted histogram

Simulation: MP growth rate



- QWR, HWR and SSR are prone to MP, need up to 10 -15 hours to process;
- Elliptical cavities have much better performance.

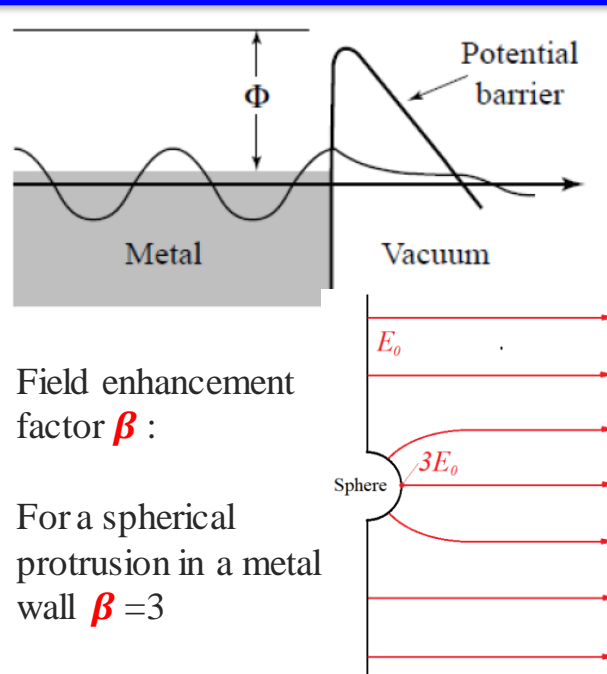
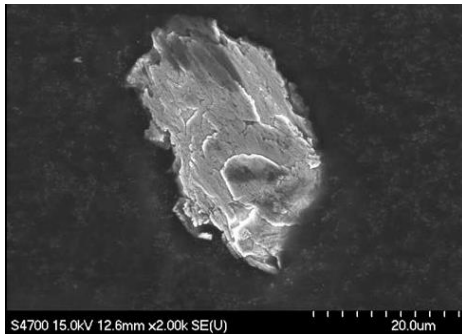
Good agreement between MP conditioning data (Pmp weighted histogram) and MP simulation (growth rate)

Field emission (FE) and dark currents in SRF cavities

- ❖ FE in SRF cavities is originated from *localized sites* on the inner cavity surface.
- ❖ The predominant source emitters are microscopic particulates adhering to the inner cavity surface, chemical residuals, and geometrical flaws.
 - Field emitters introduced by the necessary chemical surface processing → post chemistry ultrasonic cleaning and high pressure water rising.
 - Field emitters introduced through the cavity opening ports onto the cavity surface, at a time beyond the completion of final cleaning, from external sources → SRF cavities are assembled in large-sized high-quality Class 10 cleanliness clean rooms into cavity strings; critical assembly steps are done with the opening port facing down; cavity strings are evacuated slowly etc.

❖ Diagnostics:

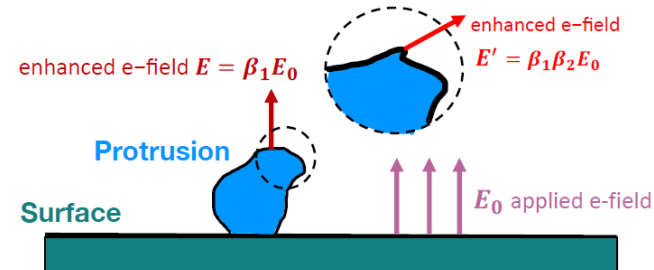
- X-ray monitoring/mapping
- Temperature monitoring/mapping
- Electron detecting
- Optical imaging:



The tunneling current density, $j(E)$

$$J(E) = k \frac{1.54 \times 10^{-6} (\beta E)^{5/2}}{\Phi} \exp\left(-\frac{6.83 \times 10^9 \Phi^{3/2}}{\beta E}\right)$$

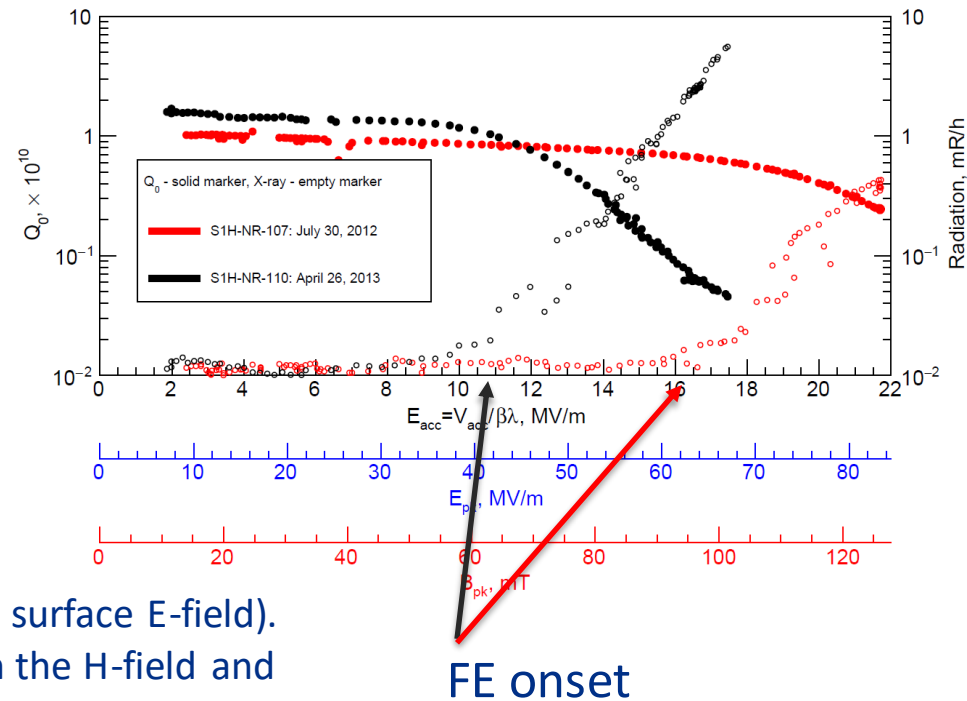
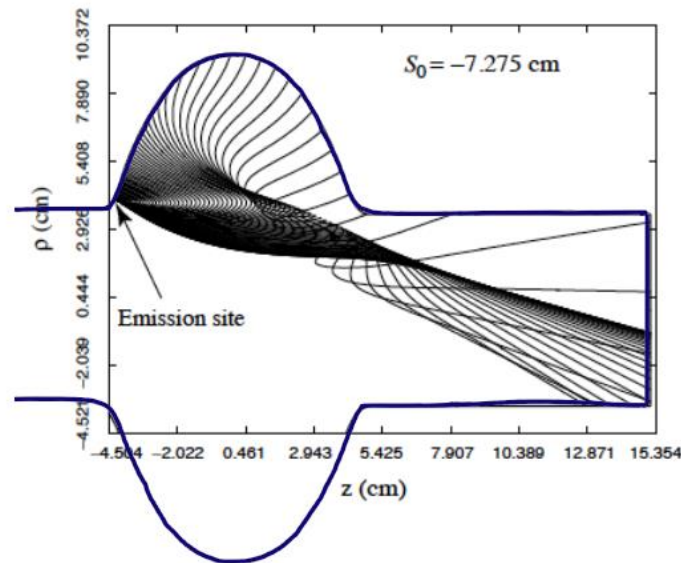
- j – current density in A/m²,
- E – surface electric field in MV/m,
- Φ – work function in eV,
- β – field enhancement factor (10-100)
- k – effective emitting surface area.



Field emission (FE) and dark currents in SRF cavities

Effect of dark current

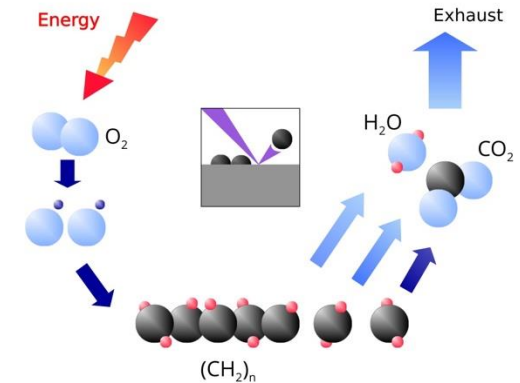
- heat and RF loading of the cavity
- production of avalanches of secondary electrons
- accelerating to hundreds of MeV before being kicked out by down stream quadrupoles
- originating electromagnetic cascade showers in the surrounding materials



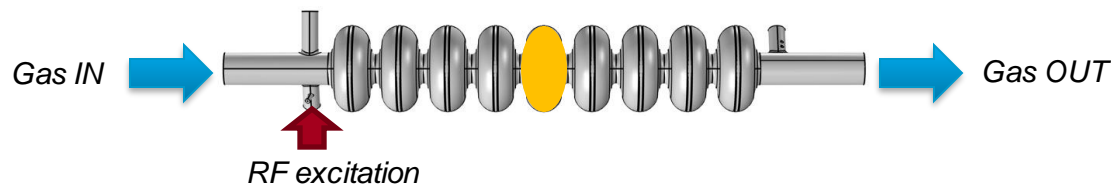
- The emitter is located at the cell entrance (high surface E-field).
- Significant number of FE electrons bend back in the H-field and strike the wall

In situ field emission mitigation via plasma processing

- While procedures of the cryomodule cavity string assembly are being improved continuously (e.g., R&D on using robotic manipulators), field emission (FE) remains a problem
- Plasma processing was first developed at Oak Ridge National Laboratory
- Gas flow of Ne-O mixture (mostly Ne with a few % of O₂) at pressure ~ 75-150 mTorr. Argon is used
- Once plasma is ignited, oxygen reacts with hydrocarbons
- Reaction products (mostly CO, CO₂, H₂O) are pumped out
- Work function increases, reducing FE
- This method was adapted to LCLS-II and LCLS-II-HE and being investigated for other applications including International Linear Collider
- Recently it was demonstrated that plasma processing helps mitigating multipacting as well



M. Doleans, et al., *Nucl. Instrum. Methods Phys. Res. A* **812**, 50-59 (2016)



P. Berrutti, et al., *J. Appl. Phys.* **126**, 023302 (2019); B. Giaccone et al., *Phys. Rev. Accel. Beams* **24**, 022002 (2021)

Microphonics and Lorentz Force Detune:

Narrow bandwidth of the cavities caused by low beam loading:

- $Q_{load} = U / (R/Q) / I_{beam}$ - very high for small beam current of few mA, $Q_{load} \sim 1e7-1e8$;
- Cavity bandwidth: $f / Q_{load} \sim$ tens of Hz.



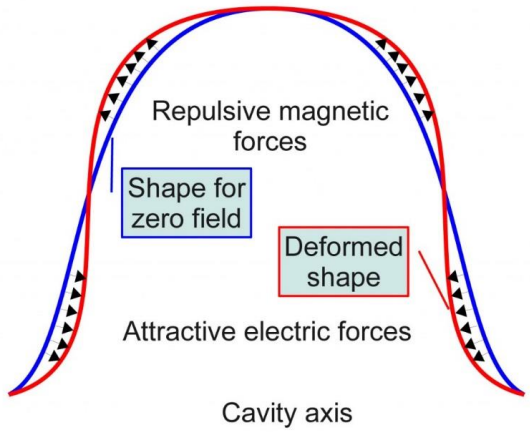
• Pressure variation in the surrounding He bath:

$\Delta f_{He} = df/dP \times \Delta P$, $\Delta P \sim 0.05-0.1$ mbar at 2 K.
 $df/dP = 30-130$ Hz/mbar (ILC)

• Internal and external vibration sources (microphonics);

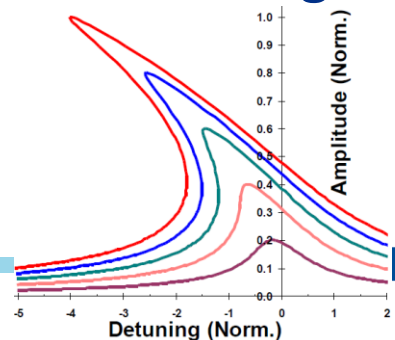
• Radiation pressure from the RF field, Lorentz Force Detuning:

$\Delta f_{LFD} = k_L E^2$, k_L - Lorentz coefficient,
 For typical elliptical cavities $k_L \sim -1$ Hz/(MeV/m)².



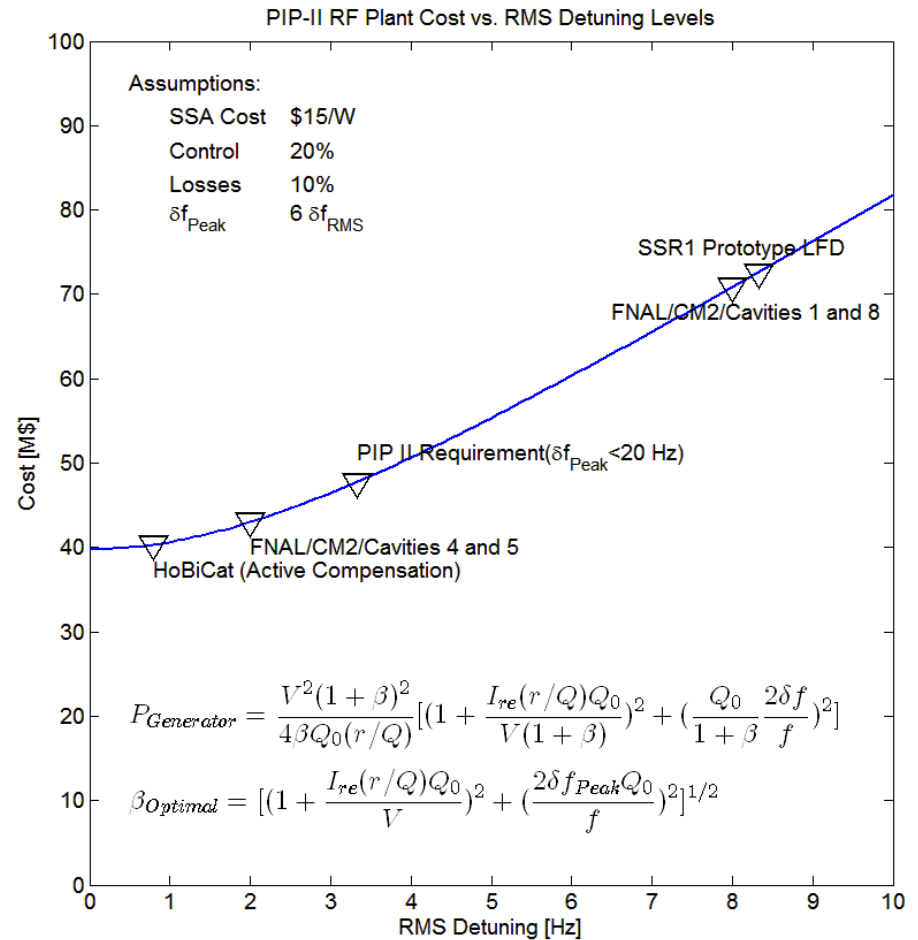
$$P_s = \frac{1}{4} (\mu |\vec{H}|^2 - \epsilon_0 |\vec{E}|^2)$$

$$\Delta f_0 = (f_0)_2 - (f_0)_1 = -K E_{acc}^2$$



Microphonics:

- Detuned cavities require more RF power to maintain constant gradient
- Providing sufficient reserve increases both the capital cost of the RF plant and the operating cost of the machine
- **PEAK** detuning drives the RF costs
- Beam will be lost if RF reserve is insufficient to overcome PEAK detuning

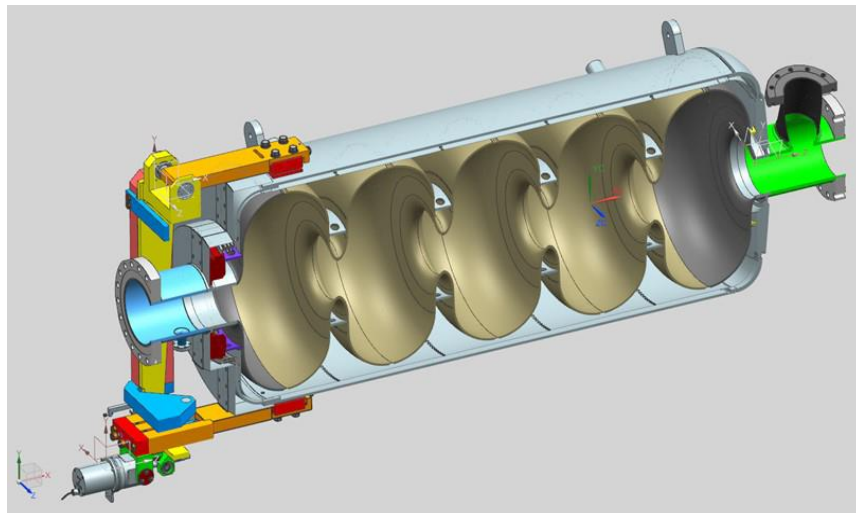


Microphonics Control Strategies

Microphonics can be mitigated by taking some combination of any or all of the following measures:

- Providing sufficient reserve RF power to compensate for the expected peak detuning levels.
- Improving the regulation of the bath pressure to minimize the magnitude of cyclic variations and transients.
- Reducing the sensitivity of the cavity resonant frequency to variations in the helium bath pressure (df/dP).
- Minimizing the acoustic energy transmitted to the cavity by external vibration sources.
- Actively damping cavity vibrations using a fast mechanical or electromagnetic tuner driven by feedback from measurements of the cavity resonant frequency.

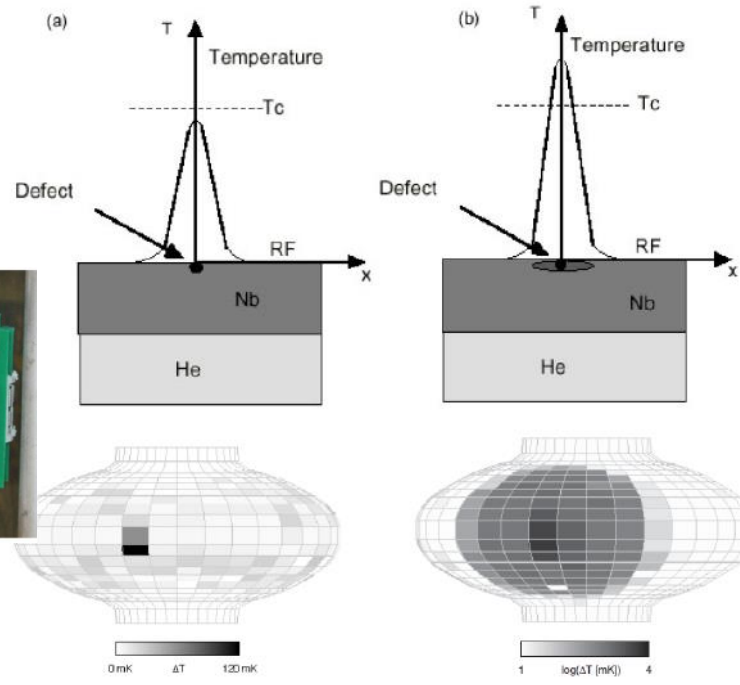
The optimal combination of measures may differ for different cavity types.



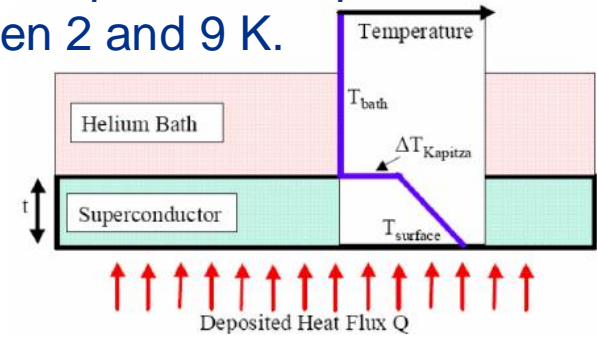
Thermal breakdown

- If there is a localized heating, the hot area will grow with field. At a certain field there is a thermal runaway and the field collapses (loss of superconductivity or quench).
- Thermal breakdown occurs when the heat generated at the hot spot is larger than that can be evacuated via Nb wall to the helium bath.

Temperature mapping



- Both the thermal conductivity and the surface resistivity of Nb are highly temperature dependent between 2 and 9 K.



$$H_b^2 = \frac{T_0^3}{2 \cdot R_s(T_0) \cdot (\Delta \cdot T_c - T_0)} \cdot \left(\frac{k \cdot h}{k + h \cdot d} \right)$$

T_0 - He bath temperature,
 T_c - critical temperature,
 Δ - energy gap,

$h(T_0)$ - Kapitza resistance,
 $k(T_0)$ - thermal conductivity,

$$R_s(T) = R_0 \cdot \left[\frac{f(\text{GHz})}{1.3} \right]^2 \cdot \left(\frac{T_c}{T} \right) \cdot e^{-\Delta \cdot \frac{T_c}{T}}$$

$$R_0 = 10^{-5} [\Omega]; \quad \Delta = 1.8; \quad T_c = 9.2^\circ\text{K}$$



Summary:

- SRF technology allows 10^6 less surface losses than RT technology and consequently, much high acceleration gradient at high duty cycle or in CW regime;
- Losses at SRF are determined mainly by BCS resistance (inertia), flux trapping and intrinsic residual resistance;
- The acceleration gradient is limited mainly by thermal breakdown, field emission, etc., but not by breakdown.
- Modern cavity processing techniques (N-doping, etc.) allow very high Q_0 .
- To achieve high Q_0 small residual magnetic field may be required, and therefore, good shielding and degaussing. The cryo-system should allow fast cooling for flux expulsion.
- Resonance discharge (multipacting) may be an issue; cavity processing is required; the cavity shape should be optimized.
- Field emission may limit the gradient; large-scale clean rooms are necessary among other means.

RF accelerating structures

Outline:

7. Multi-cell SRF cavities;
8. SRF Cavities for Low β Accelerators;
9. Beam-cavity Interaction

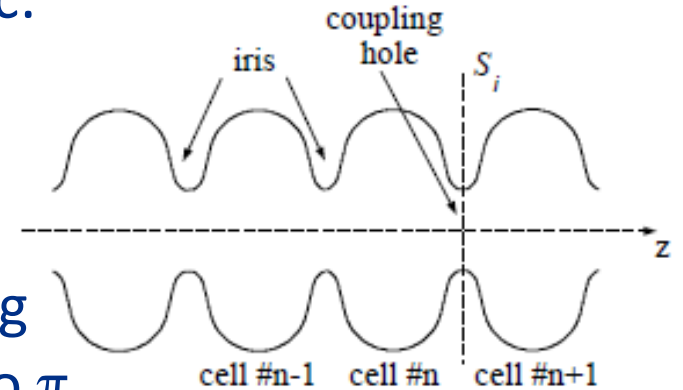
Chapter 7.

Multi-cell SRF cavities.

- a. Multi-cell SRF cavities;
- b. Why π -mode?
- c. Equivalent circuit and normal modes;
- d. Parameters of the SRF SW cavity;
- c. Cavity efficiency at different particle velocity versus the number of cells;
- d. Why elliptical multi-cell cavity does not work at low particle velocity.

Multi-cell SRF cavity:

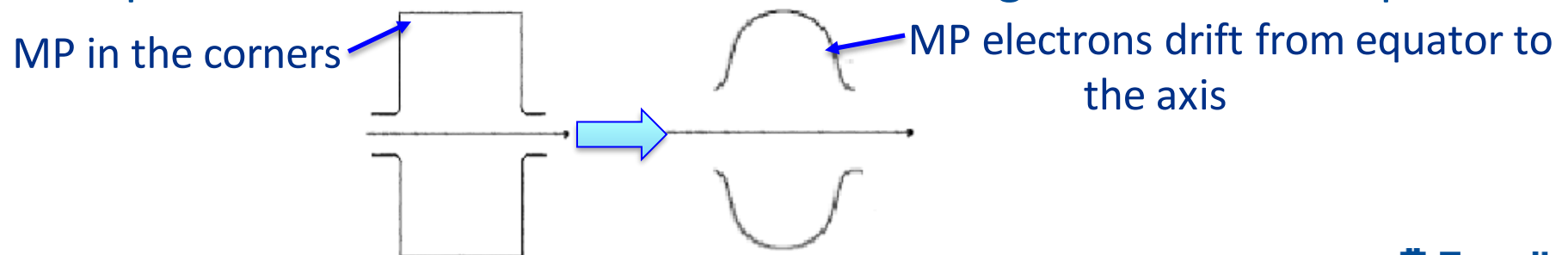
- Single – cell cavities are not convenient to achieve high acceleration: a lot of couplers, tuners, etc.
- Multi-cell cavities are used in both RT and SRF accelerators.
- Multi-cell SRF cavity is a standing–wave periodic acceleration structure, operating at the phase advance per period equal to π (i.e, the fields in neighboring cells have the same distribution, but opposite sign).
- To provide synchronism with the accelerated particle, period is $\beta\lambda/2$ (in general case it is $\varphi\beta\lambda/2\pi$; φ is phase advance per period).
- The end cells have special design (full length, not half) to provide field flatness along the structure for operation mode with the phase advance π .



Why SW π - mode?

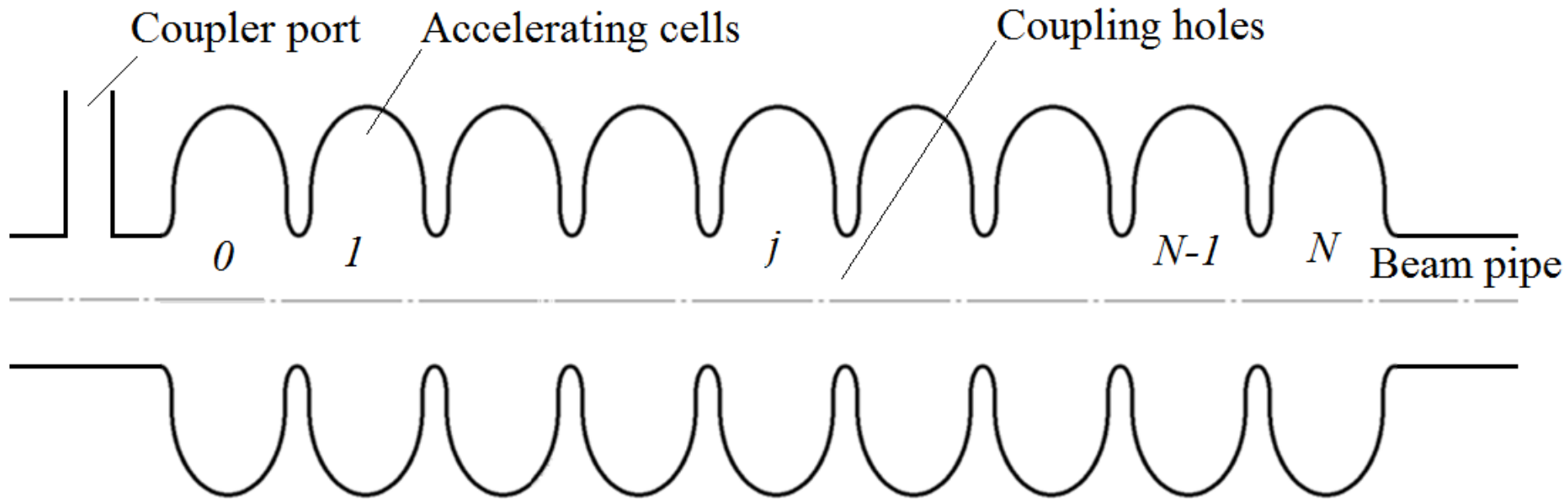
- The SW modes except π have small acceleration efficiency because most of the cavities have small field (in ideal case $X_{ni} \sim \cos(\pi qj/N)$, q - mode number, j - cell number).
- Bi-periodic structure $\pi/2$ -mode does not work because it is prone to multipacting in the empty coupling cells and difficult for manufacturing (different cells) and processing (narrow coupling cells).
- π -mode structure is simple, easy for manufacturing and processing.
- Drawback:
 - Big aperture to provide big coupling;
 - Considerably small number of cells N (5-9).

□ Elliptical cavity is not prone to multipacting in contrast to a pillbox.



Why SW π – mode?

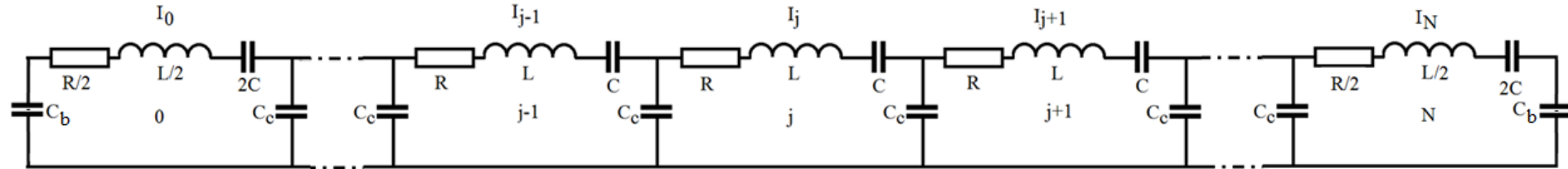
Schematic of the SRF multi-cell cavity



- The cells have elliptical shape to get rid of multipacting;
- The end cells have full length, but the shape is different;
- The coupler is placed in the beam pipe.

Why SW π – mode?

Equivalent circuit of the SRF multi-cell cavity



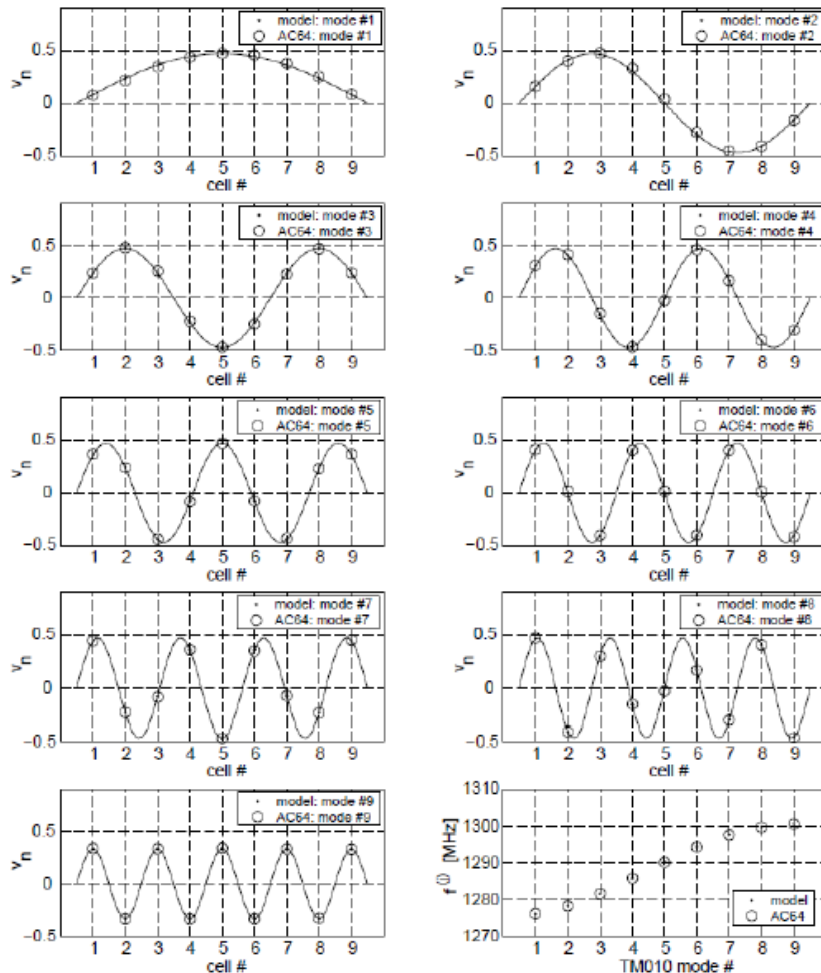
- C_b represents the fringing fields in the beam pipe.
- The shape of the 0^{th} and N^{th} cell are selected to achieve flat field distribution for π -mode only.

$$X_0 \left[1 - \frac{\omega_0^2}{\omega^2} + i \frac{\omega_0^2}{Q_0 \omega^2} \right] + K \frac{\omega_0^2}{\omega^2} X_1 + K_1 \frac{\omega_0^2}{\omega^2} X_0 = 0$$

$$X_j \left[1 - \frac{\omega_0^2}{\omega^2} + i \frac{\omega_0^2}{Q_0 \omega^2} \right] + \frac{1}{2} K \frac{\omega_0^2}{\omega^2} [X_{j-1} + X_{j+1}] = 0$$

$$X_N \left[1 - \frac{\omega_0^2}{\omega^2} + i \frac{\omega_0^2}{Q_0 \omega^2} \right] + K \frac{\omega_0^2}{\omega^2} X_{N-1} + K_1 \frac{\omega_0^2}{\omega^2} X_N = 0$$

Multi-cell RF cavity:

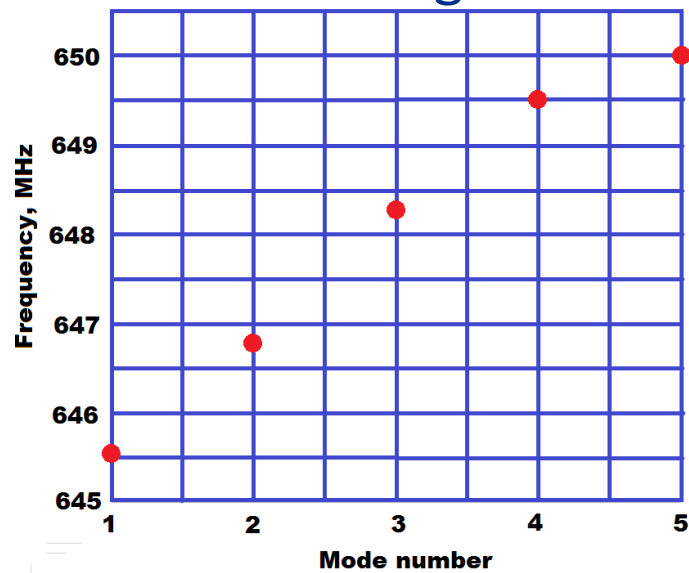


An example of calculated eigen modes amplitudes in a 9-cell TESLA cavity compared to the measured amplitude profiles. Also shown are the calculated and measured eigen frequencies. The cavity has full size end cells especially tuned to get field flatness for the operating mode.

Normal modes in a standing-wave elliptical cavity:

PIP II 650 MHz cavity

“Brillouin diagram”:

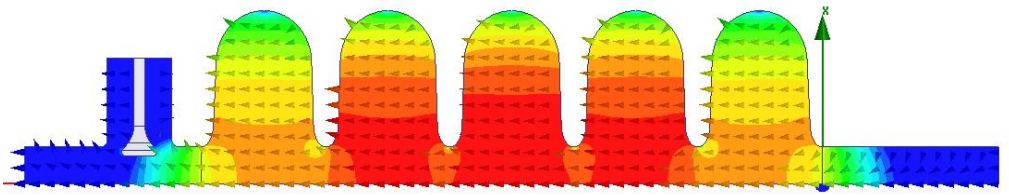


$$f(q) \approx f_0 \left(1 - \frac{k}{2} \cos \frac{\pi(q-1)}{(N-1)} \right)$$

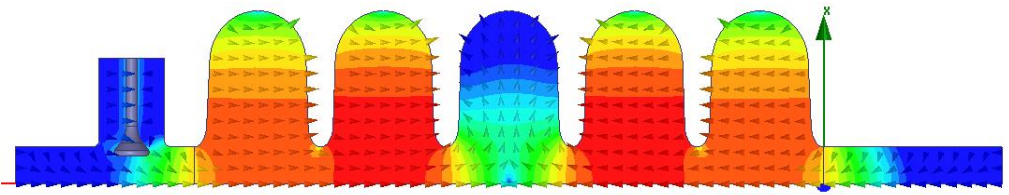
q —the mode number;
 N — the number of cells;
 k — coupling: $k=0.7\%$

Operation mode “ π ”

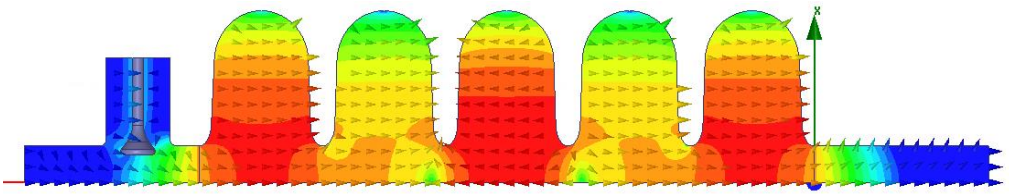
Mode 1
“0”



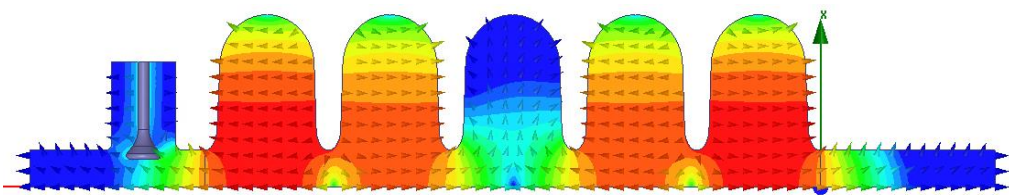
Mode 2
“ $\pi/4$ ”



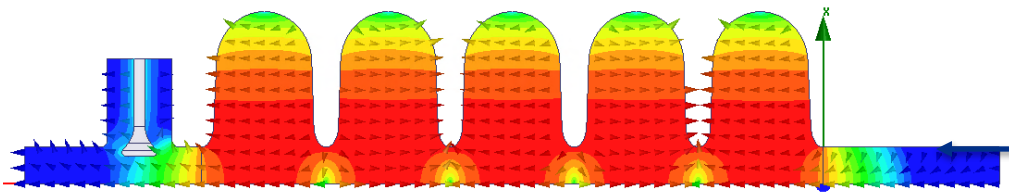
Mode 3
“ $\pi/2$ ”



Mode 4
“ $3\pi/4$ ”



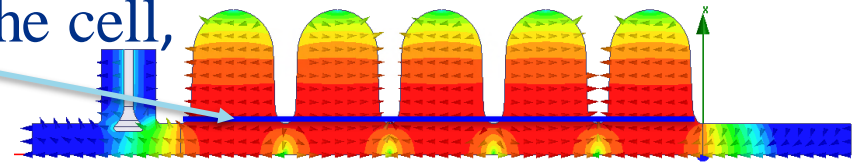
Mode 5
“ π ”



Axial acceleration field distribution

At the aperture, $E_z(a, z) \sim \text{const}$ over the cell,

$$E_z(a, z) \sim \sum A_{2n} \cos(2nk_0 z / \beta);$$



$$E_z(0, z) \sim \sum A_{2n} \cos(2nk_0 z / \beta) / I_0 [ak_0 a (4n^2 / \beta^2 - 1)^{1/2}] = \sum B_{2n} \cos(2nk_0 z / \beta)$$

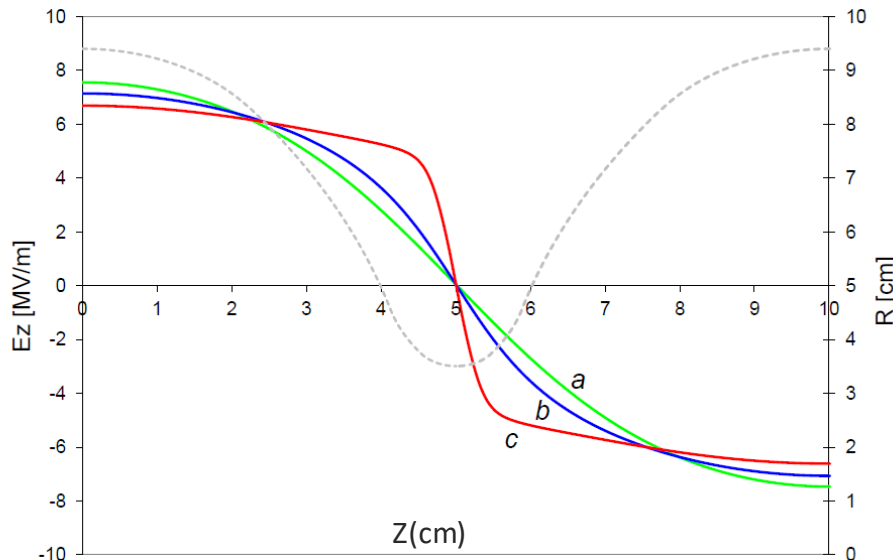


$$B_{2n} = A_{2n} I_0 [ak_0 a (4n^2 / \beta^2 - 1)^{1/2}];$$

for example for $\beta = 1$ $B_0 = A_0$ and $B_{2n} \approx A_{2n} \exp(-2nk_0 a) \ll B_0$



$E_z(0, z) \sim A_0 \cos(k_0 z)$ – sinusoidal distribution on the axis! Valid for $\beta < 1$.

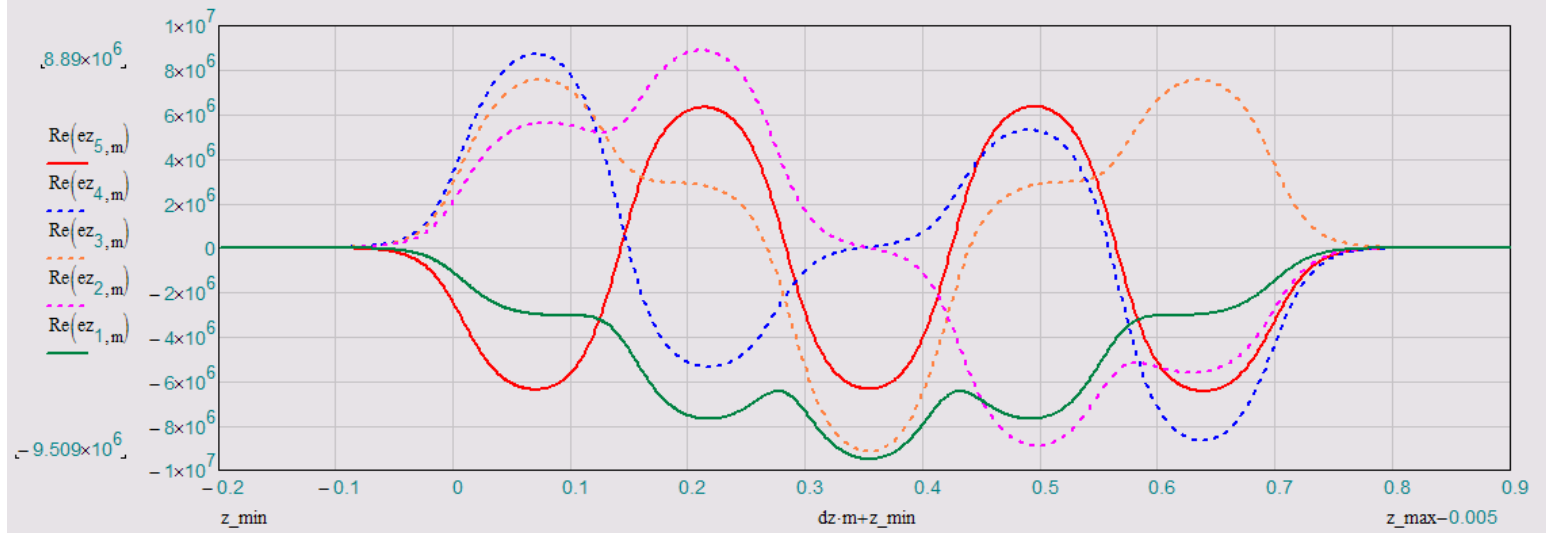
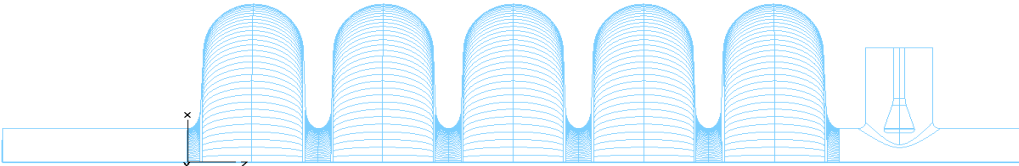
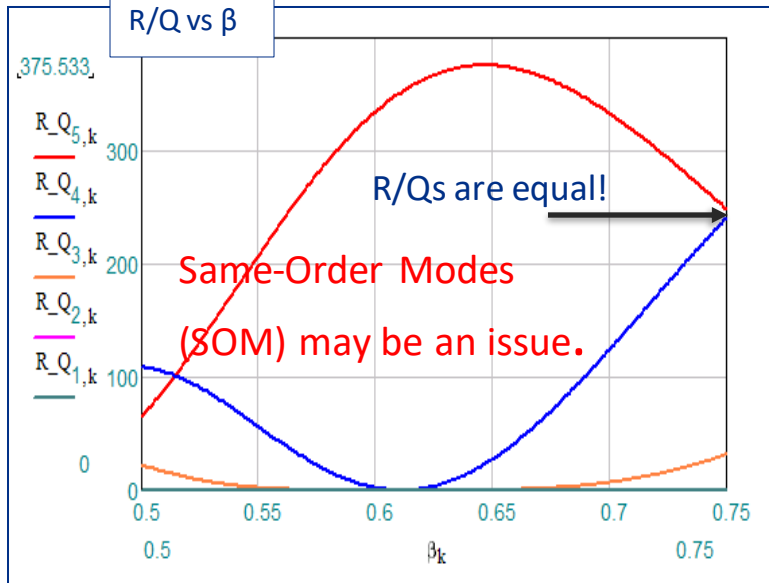


Geometry of an iris of a CEBAF multi-cell cavity (gray line). Longitudinal electric field at a different radial position: $r = 0$ cm (green line), $r = 2.5$ cm (blue line), $r = 3.45$ cm (red line). Fields are normalized to 4 MeV/m accelerating gradient.

- Field at the aperture close to rectangular
- Field on the axis is close to sinusoidal

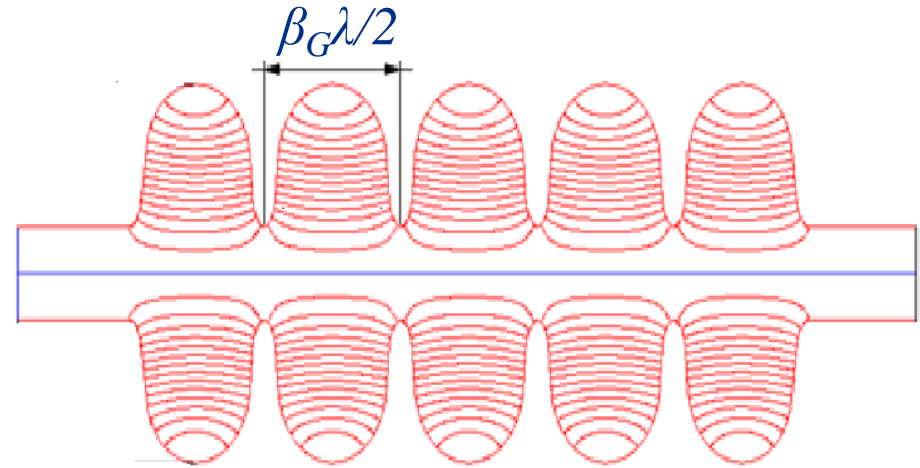
PIP II $\beta_G=0.61$, 650 MHz elliptical cavity:

Mode	Freq [GHz]	(R/Q) _{opt} [Ω]	β_{opt}
0	0.6456	0.5	>0.75
$\frac{1}{4} \pi$	0.6468	0.4	0.69
$\frac{1}{2} \pi$	0.6483	32.1	>0.75
$\frac{3}{4} \pi$	0.6495	241.0	>0.75
π	0.6500	375.5	0.65



Parameters of a multi-cell cavity:

- “Geometrical beta”: $\beta_G = 2l/\lambda$,
 l is the length of a regular cell,
 λ is wavelength.



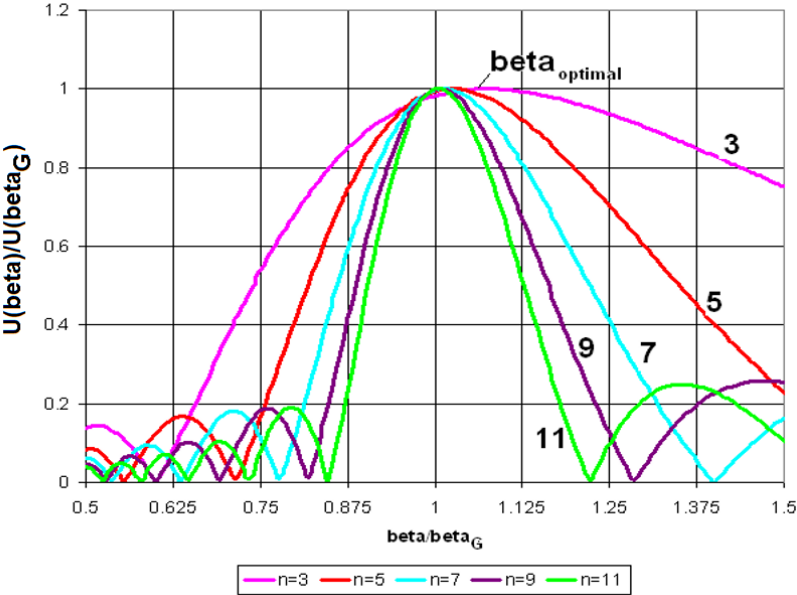
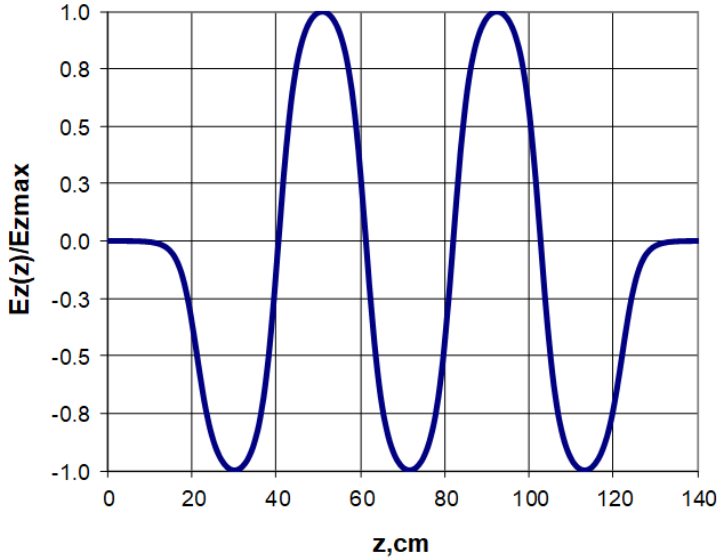
- $R/Q = V^2/\omega U$, V is the energy gain per cavity (in optimal acceleration phase), $V = V(\beta)$; ω – cyclic operation frequency; U is EM energy stored in a cavity; R/Q is a function of β , as well as V . R/Q is the same for geometrically similar cavities. Decreases when the cavity aperture a increases.
- “Optimal β ”: value of β , where V (and R/Q) is maximal.
- Acceleration gradient: $E = V/L_{eff}$, $L_{eff} = n\beta_G \lambda / 2$ – effective length, n is the number of cells.

Parameters of a multi-cell cavity (cont)

- Surface electric field enhancement: $K_e = E_{peak}/E$, E_{peak} is maximal surface electric field.
- Surface magnetic field enhancement: $K_m = B_{peak}/E$, B_{peak} is maximal surface magnetic field.
- Unloaded quality factor: $Q_0 = \omega W/P_{loss}$, P_{loss} – surface power dissipation.
- G -factor: $G = Q_0 * R_s$, R_s is the surface resistance. G is the same for geometrically similar cavities. At fixed gain the losses are proportional to $G*(R/Q)$.
- Loaded quality factor: $Q_{load} = \omega W/P$, $P = P_{loss} + P_{load}$; P_{load} – power radiated through the coupling port.
- **Coupling:** $K = 2(f_\pi - f_0)/(f_\pi + f_0)$,

Multi-cell cavity

A multi-cell SRF elliptical cavity is designed for particular $\beta = \beta_G$, but accelerates in a wide range of particle velocities; the range depends on the number of cells in the cavity N . Field distribution for the tuned cavity has equal amplitudes for each cell; longitudinal field distribution for considerably large aperture is close to sinusoidal (see slide 10):



$$\frac{V(\beta)}{V(\beta_{optimal})} = \frac{2\beta}{\pi N} \left(\frac{\sin\left(\frac{\pi N(\beta - \beta_G)}{2\beta}\right)}{\beta - \beta_G} - (-1)^n \frac{\sin\left(\frac{\pi N(\beta + \beta_G)}{2\beta}\right)}{\beta + \beta_G} \right)$$

$$\beta_{optimal} \approx \beta_G \left(1 + \frac{6}{\pi^2 N^2} \right)$$

V is the energy gain per cavity.

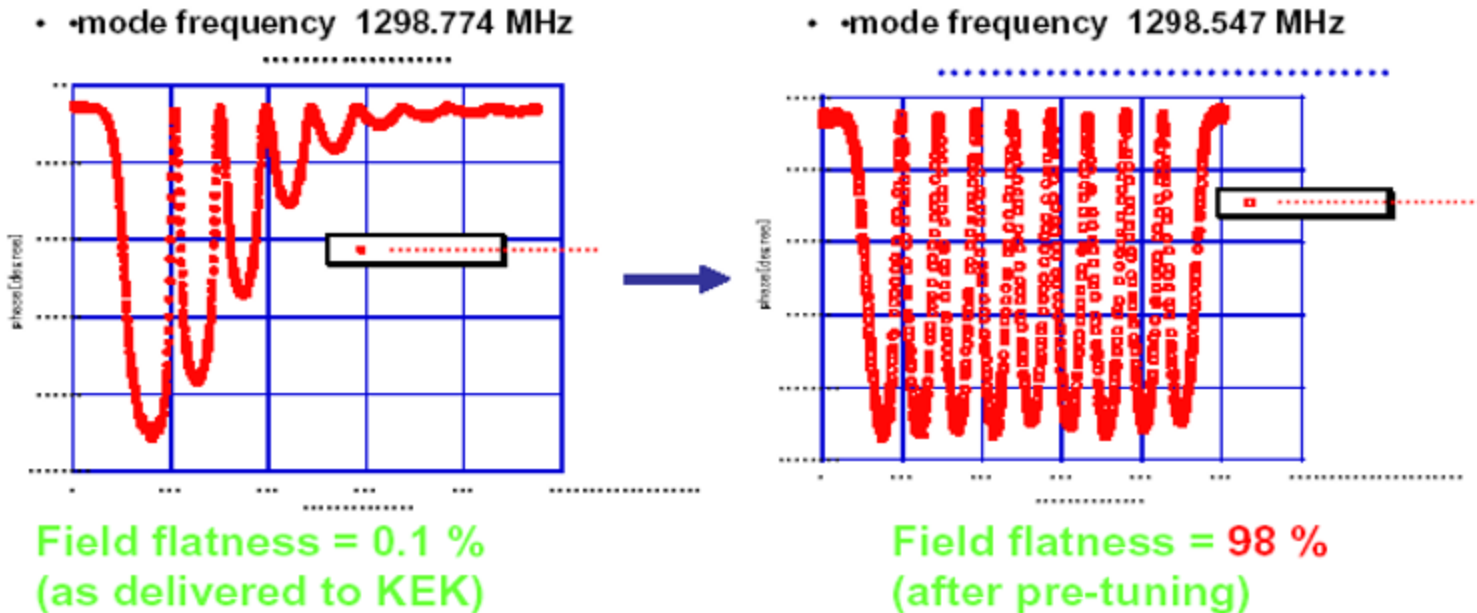
The cavity containing more cells provides effective acceleration in more narrow particle velocity range!



Why SW π – mode?

Cavity tuning:

- Compensation of the errors caused by manufacturing
- Compensation of the errors caused by cool-down.
- Field flatness
- Tuning the operating mode frequency to resonance.



Field flatness in ILC – type cavity before and after pre-tuning.

Elliptical cavities:

INFN Milano, 700 MHz, $\beta_G = 0.5$



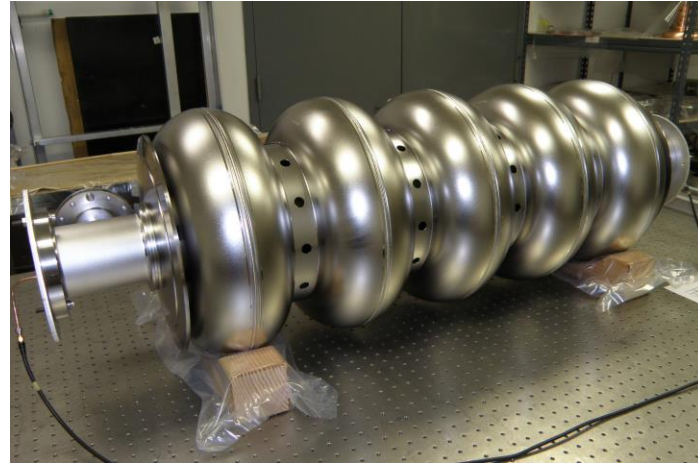
SNS, 805 MHz, $\beta_G = 0.61$



SNS, 805 MHz, $\beta_G = 0.81$



PIP II, 650 MHz, $\beta_G = 0.9$



XFEL, 1300 MHz, $\beta_G = 1$



XFEL, 3900 MHz, $\beta_G = 1$



Multi-cell cavity is not effective for low β :

□ For small β

$$I_0(kr/\beta\gamma) \approx \frac{1}{\sqrt{2\pi kr/\beta\gamma}} e^{kr/\beta\gamma}$$

Synchronous EM is concentrated on the cavity periphery, not on the axis! Consequences:

- Small (R/Q) :

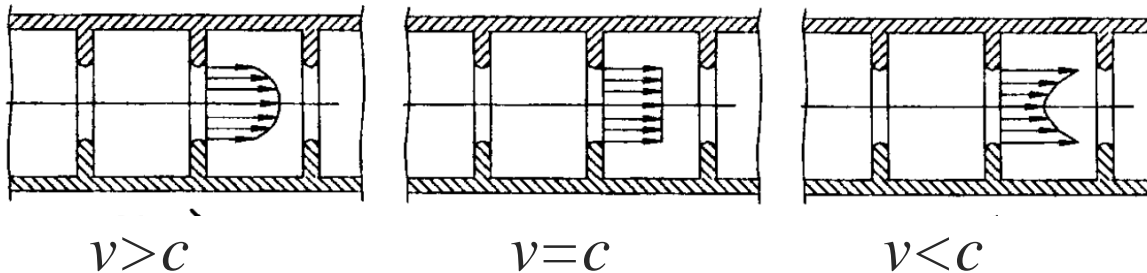
$(R/Q) \sim \exp(-4\pi a/\lambda\beta)$, a is the cavity aperture radius;

- High K_e

$K_e \sim \exp(2\pi a/\lambda\beta)$;

- High K_m .

$K_m \sim \exp(2\pi a/\lambda\beta)$.



Multi-cell cavity is not effective for low β :

□ RF cavity provides the beam focusing,

$$\frac{1}{F} \sim \frac{\pi}{\beta^3 \gamma^3} \frac{V}{U_0} \frac{1}{\lambda} \sin(\varphi_s)$$

- For $\varphi_s < 0$ (necessary for longitudinal stability) the cavity provides defocusing!

- Defocusing:

$$\sim 1/\beta^3;$$

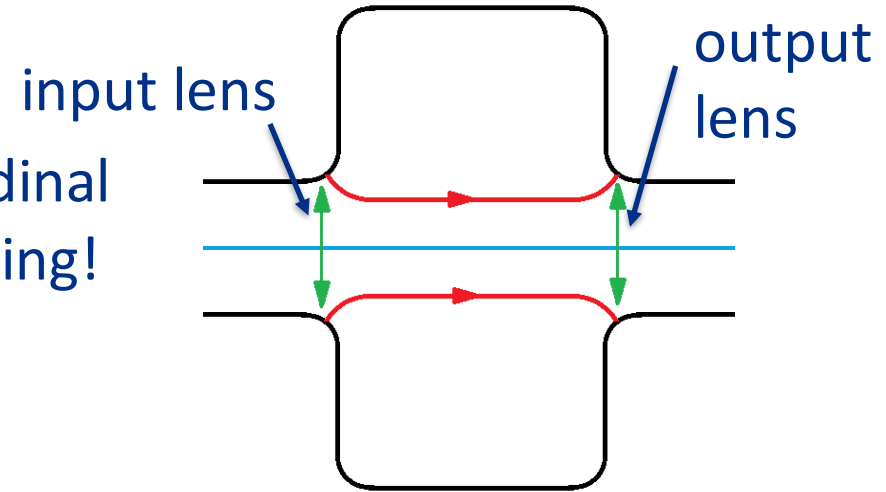
$$\sim 1/\lambda.$$

Defocusing should be compensated by external focusing elements,
-solenoids (low energy);
-quads (high energy).

For small β longer RF wavelength (lower frequency) should be used.

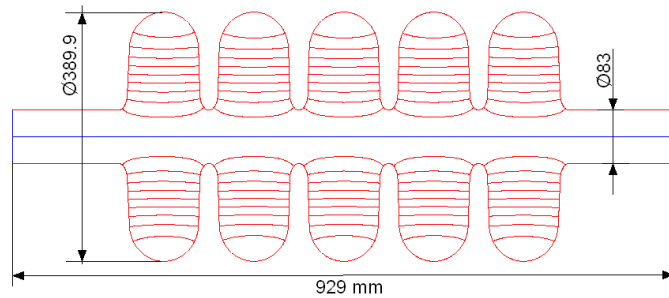
But axisymmetric cavity has very big size, $D \sim 3/4 \lambda$

For small β other types of cavities should be used!

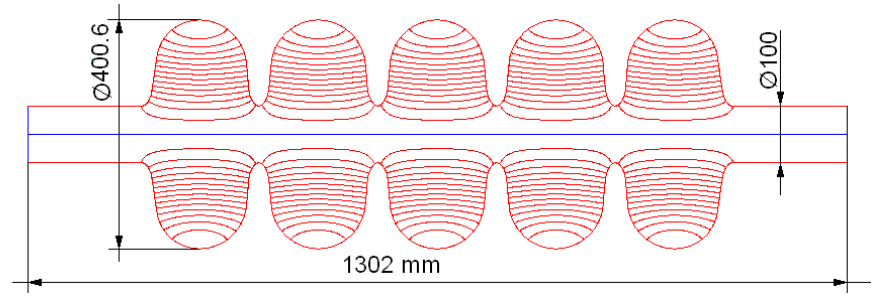


Parameters of an elliptical cavity (cont)

Example for the 650 MHz cavities for PIP II



LB650 ($\beta_G=0.61$)



HB650 ($\beta_G=0.9$)

Parameter		LH650	HB650
β_G		0.61	0.9
β_{optimal}		0.65	0.94
Cavity Length = $n_{\text{cell}} \cdot \beta_{\text{geom}} \lambda / 2$	mm	703	1038
R/Q	Ohm	378	638
G-factor	Ohm	191	255
K_e		2.26	2.0
K_m	mT/(MeV/m)	4.22	3.6
Max. Gain/cavity (on crest)	MeV	11.7	17.7
Acc. Gradient	MV/m	16.6	17
Max surf. electric field	MV/m	37.5	34
Max surf. magnetic field,	mT	70	61.5
Q_0 @ 2K	$\times 10^{10}$	2	3
P_{2K} max	[W]	24	24

Summary:

- ❑ Single – cell cavities are not convenient in order to achieve high acceleration: a lot of couplers, tuners, etc; multi-cell π -mode elliptical cavities are used in SRF accelerators;
- ❑ Why π -mode?
 - The SW modes except π have small acceleration efficiency because most of cavities have small field;
 - Bi-periodic structure $\pi/2$ -mode does not work because it is prone to multipacting in the empty coupling cells and difficult for manufacturing (different cells) and processing (narrow coupling cells).
 - π -mode structure is simple, easy for manufacturing and processing.
- ❑ Elliptical cavities are used to mitigate multipacting;
- ❑ End cells have the same length as regular ones, but a bit different shape to keep field flatness for operation π -mode.
- ❑ Range of acceleration efficiency strongly depends on the number of cells: cavities with smaller number of cells operate in wider β range.
- ❑ Elliptical cavities are not effective for low particle velocity.

Chapter 8.

SRF Cavities for Low β Accelerators.

- a. Why TEM-type cavities work at low particle velocities;
- b. Types of TEM cavities;
- c. Velocity range of TEM-type cavities.

RF cavity types

Quarter-wave resonator (QWR)

concept:

Resonance:

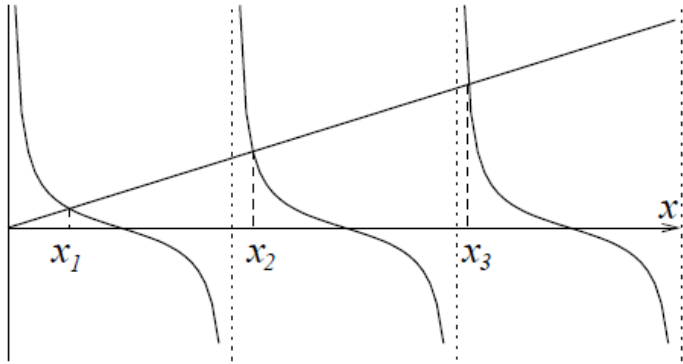
$$\frac{1}{i\omega C} + iZ_c \tan\left(\frac{\omega l}{c}\right) = 0$$

$$\text{or } \cot\left(\frac{\omega l}{c}\right) = \omega C Z_c.$$

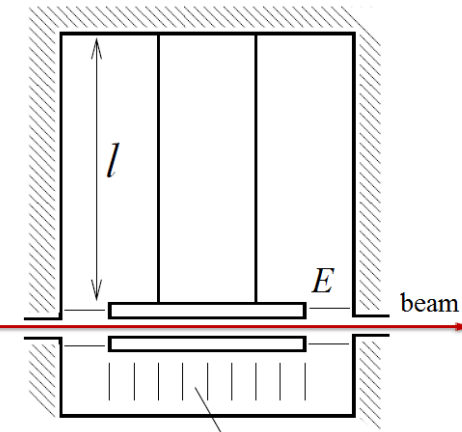
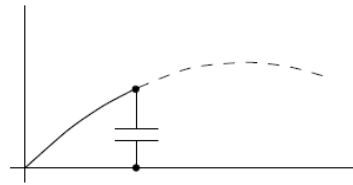
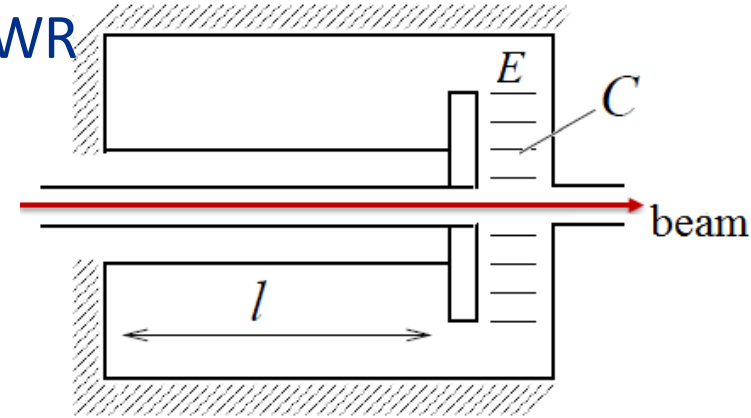
Z_c here is the coaxial impedance

Compact ($L \approx \lambda/4$) compared to pillbox ($D \approx 3/4\lambda$).

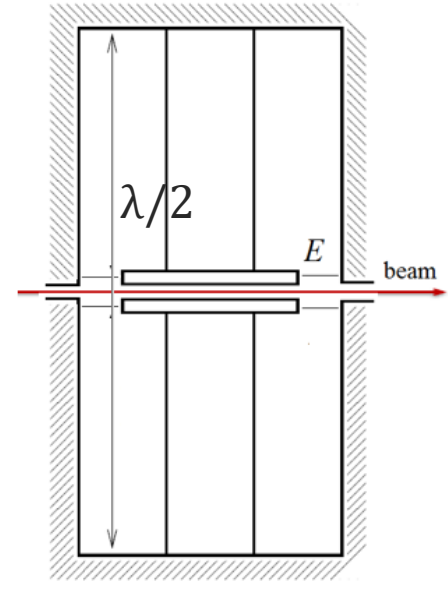
$$\frac{\omega l}{c} = x, \frac{C Z_c c}{l} = A \rightarrow \cot(x) = Ax.$$



One-gap QWR



Two-gap QWR



Half-wave resonator (HWR)

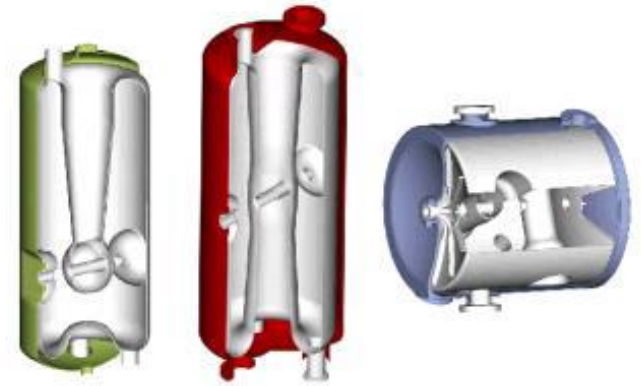
RF cavities for low β :

TEM-like cavities:

- Split-ring resonator;
- Quarter-wave resonator;
- Half-wave resonator;
- Spoke resonator.



Split-ring



QWR

HWR

SSR

(single-spoke)

- Narrow acceleration gap ($\sim\beta\lambda$) allows concentrate electric field near the axis;
- Aperture $\sim 0.02-0.03\lambda$ allows acceptable field enhancement;
- Number of gaps in modern cavities is 2 for small beta which allows operation in acceptably wide beta domain. For $\beta > 0.4$ multi-gap cavities are used –double- and triple-spoke resonators;
- Focusing elements (typically, solenoids) are placed between the cavities.

RF cavities for low β :

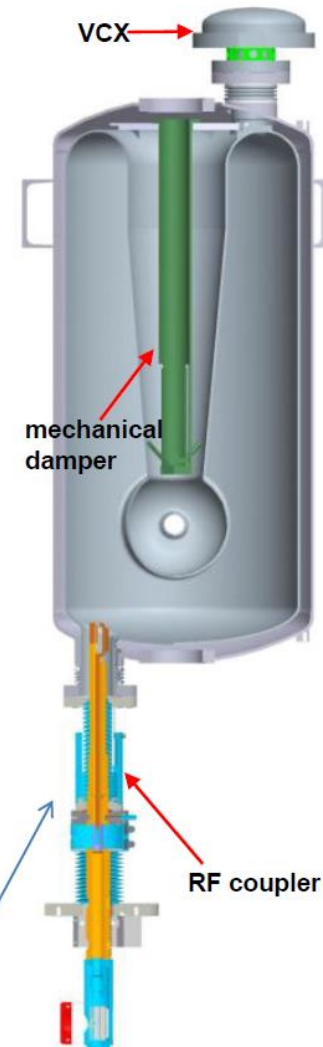
Quarter-wave resonator:

- Allows operate at very low frequency ~ 50 MHz, (and thus, low beta) having acceptable size;
- Has a good (R/Q);
- Low cost and easy access.

But:

- Special means needed to get rid of dipole and quadrupole steering, and
- Provide mechanical stability

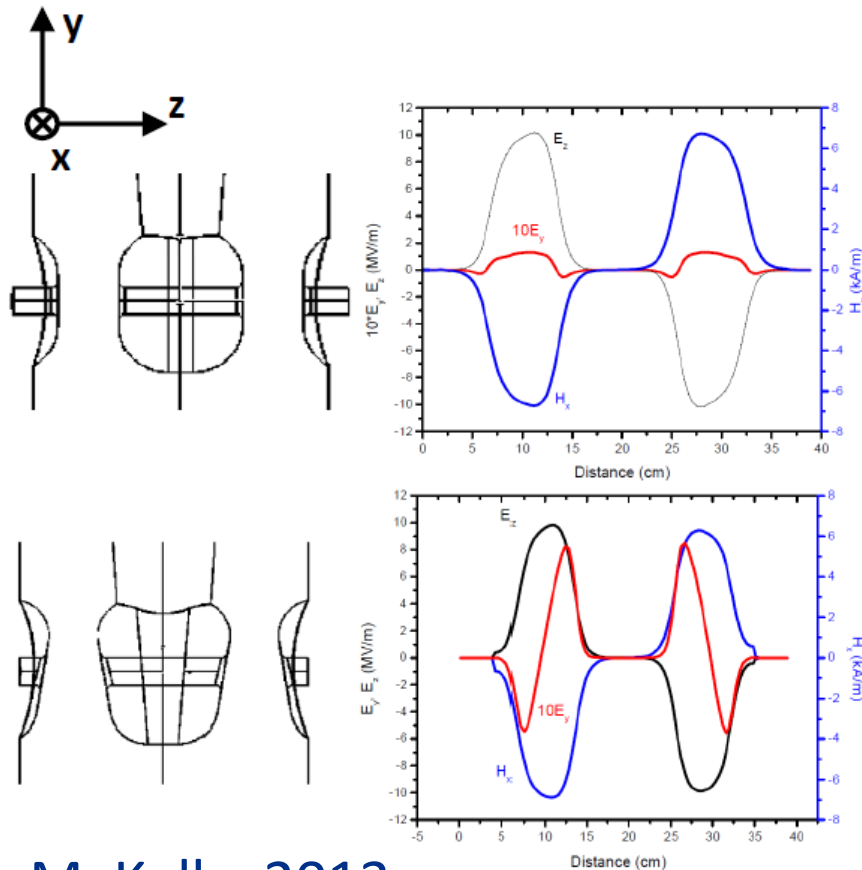
beta=0.14, 109.125 MHz QWR(**Peter N. Ostroumov**)



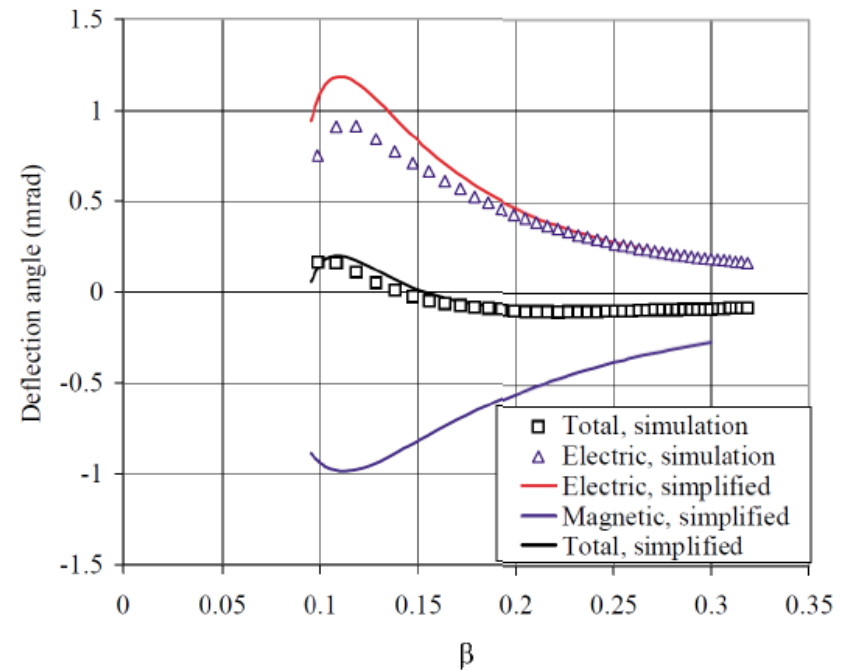
RF cavities for low β

Beam Steering in Quarter-wave Cavities*

- Beam steering due to unavoidable magnetic field on the beam axis.
- One remedy: The vertical field E_y , normally small, may be modified by the cavity geometry to cancel magnetic steering due to H_x .



$$\Delta p_y \sim \frac{1}{\beta^2} \int_{L/2}^{-L/2} E_y \cos(kz + \varphi) + \beta c \cdot B_x \sin(kz + \varphi) dz$$



M. Kelly, 2013

RF cavities for low β :

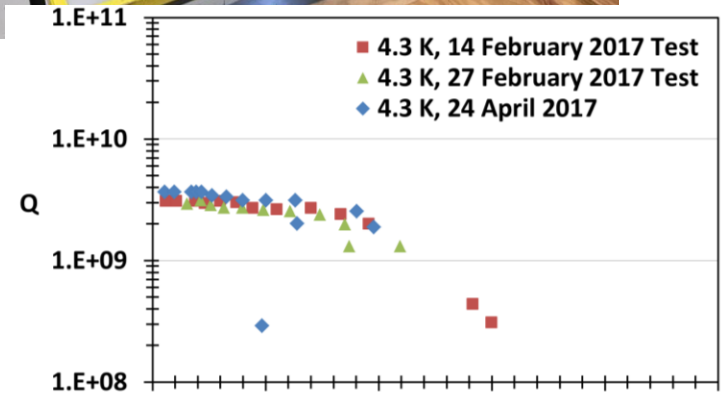
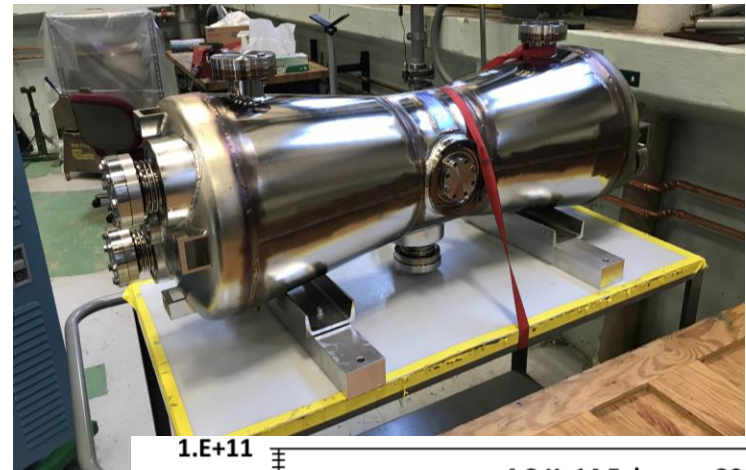
Half-wave resonator (HWR):

- No dipole steering;
- Lower electric field enhancement;
- High performance;
- Low cost;
- Best at ~ 200 MHz.

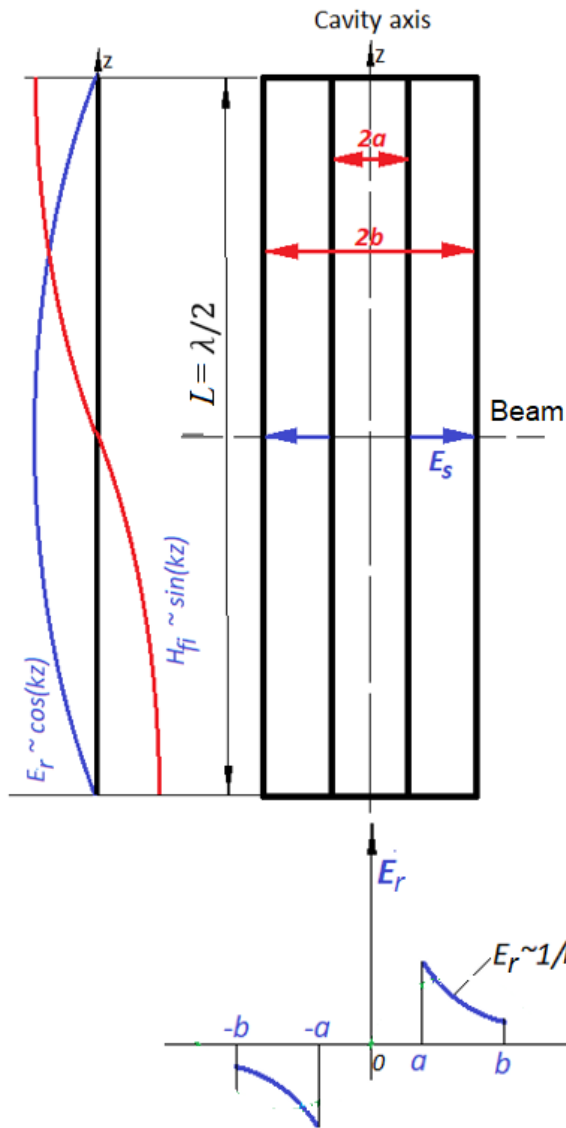
But:

- Special means needed in some cases to get rid of quadrupole effects;
- Two times lower R/Q

PIP II HWR cavity, 162.5 MHz
(M.Kelli, Z. Conway, P. Ostroumov)



Ideal HWR



- The cavity is a TEM coaxial line shortened at $z = \pm L/2$
- Electric field in a coaxial line:

$$E_r(r, z) = \frac{C}{r} \cos(kz), \quad a \leq r \leq b;$$

$$E_r(r, z) = 0, \quad r < a;$$

$$E_r(r, z) = 0, \quad r > b, \quad k = \frac{\omega}{c}$$

$$E_r(r, z) = \frac{C}{r} \cos(kz),$$

$$U = \int_a^b E_r(r, 0) dr = C \cdot \ln\left(\frac{b}{a}\right)$$

$$\rightarrow C = \frac{U}{\ln\left(\frac{b}{a}\right)}$$

$$E_r(r, z) = \frac{U}{\ln\left(\frac{b}{a}\right)} \cdot \frac{1}{r} \cos(kz),$$

- Magnetic field:

From Maxwell equations:

$$H_\phi(r, z) = \frac{i}{\omega\mu_0} \cdot \frac{\partial E_r}{\partial z} = \frac{iC}{Z_0 r} \sin(kz) =$$

$$= \frac{iU}{2\pi Z_c r} \sin(kz); \quad Z_c = \frac{1}{2\pi} Z_0 \ln\left(\frac{b}{a}\right) - \text{the line impedance}; \quad Z_0 = \sqrt{\frac{\mu_0}{\epsilon_0}} = 120\pi \text{ Ohm}$$

- Resonance frequency:

$$kL = \pi \rightarrow k = \frac{\pi}{L} \rightarrow \omega = \frac{\pi c}{L} \rightarrow f = \frac{c}{2L}, \quad c \text{ is speed of light.}$$

- Stored energy:

$$W = \frac{\mu_0}{2} \int |H|^2 dV = \frac{\pi}{4} \frac{U^2}{\omega Z_c}$$

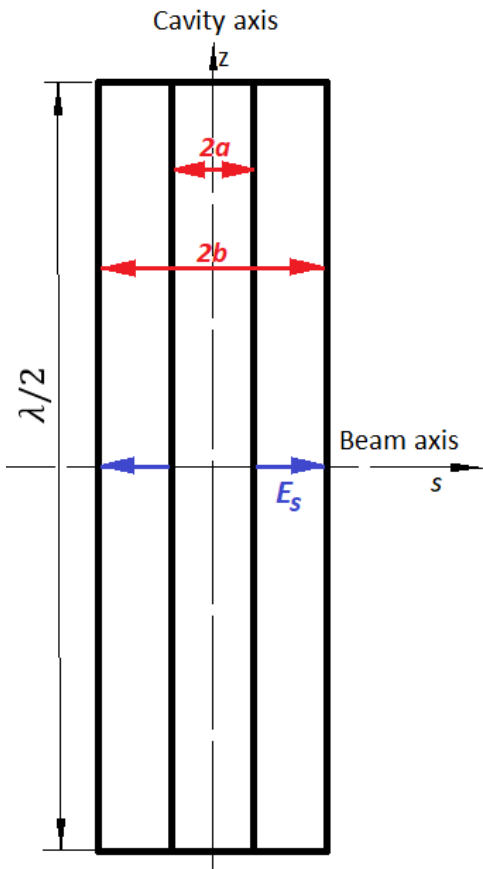
- Ohmic loss:

$$P = \frac{1}{2} \oint R_s H^2 dS = \frac{R_s U^2}{8\pi Z_c^2} \left[L \left(\frac{1}{b} + \frac{1}{a} \right) + 4 \ln\left(\frac{b}{a}\right) \right]$$

- Unloaded quality factor:

$$Q_0 = \frac{\omega W}{P}.$$

Ideal HWR



- Acceleration field on the beam axis: $E_s(s) = \frac{U}{\ln\left(\frac{b}{a}\right)} \cdot \frac{1}{s}$

- Acceleration voltage:

$$V = \frac{2U}{\ln\left(\frac{b}{a}\right)} \int_a^b \frac{\sin\left(\frac{ks}{\beta}\right)}{s} ds = \frac{2U}{\ln\left(\frac{b}{a}\right)} \left[Si\left(\frac{kb}{\beta}\right) - Si\left(\frac{ka}{\beta}\right) \right]$$

where $Si(x) = \int_0^x \frac{\sin(x)}{x} dx$. We have two gaps \rightarrow factor "2" in the nominator.

Optimal acceleration:

$$\frac{dV}{d\beta} = 0 \rightarrow \sin\left(\frac{kb}{\beta}\right) - \sin\left(\frac{ka}{\beta}\right) = 2\sin\left(\frac{k(b-a)}{2\beta}\right) \cos\left(\frac{k(a+b)}{2\beta}\right) = 0$$

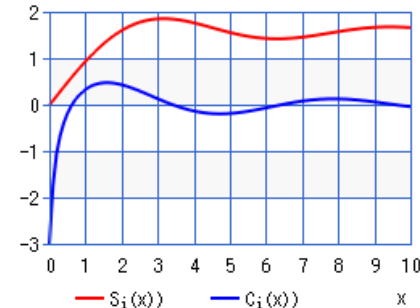
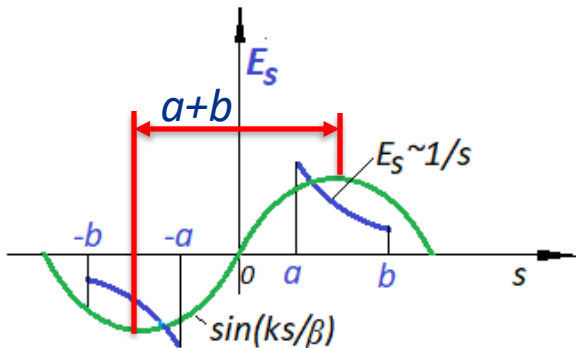
$$\rightarrow \frac{k(a+b)}{2\beta} = \frac{\pi}{2} \rightarrow \frac{a+b}{2} = \frac{\beta\lambda}{4}$$

- "Effective cavity length": $L_{eff} = \beta\lambda$

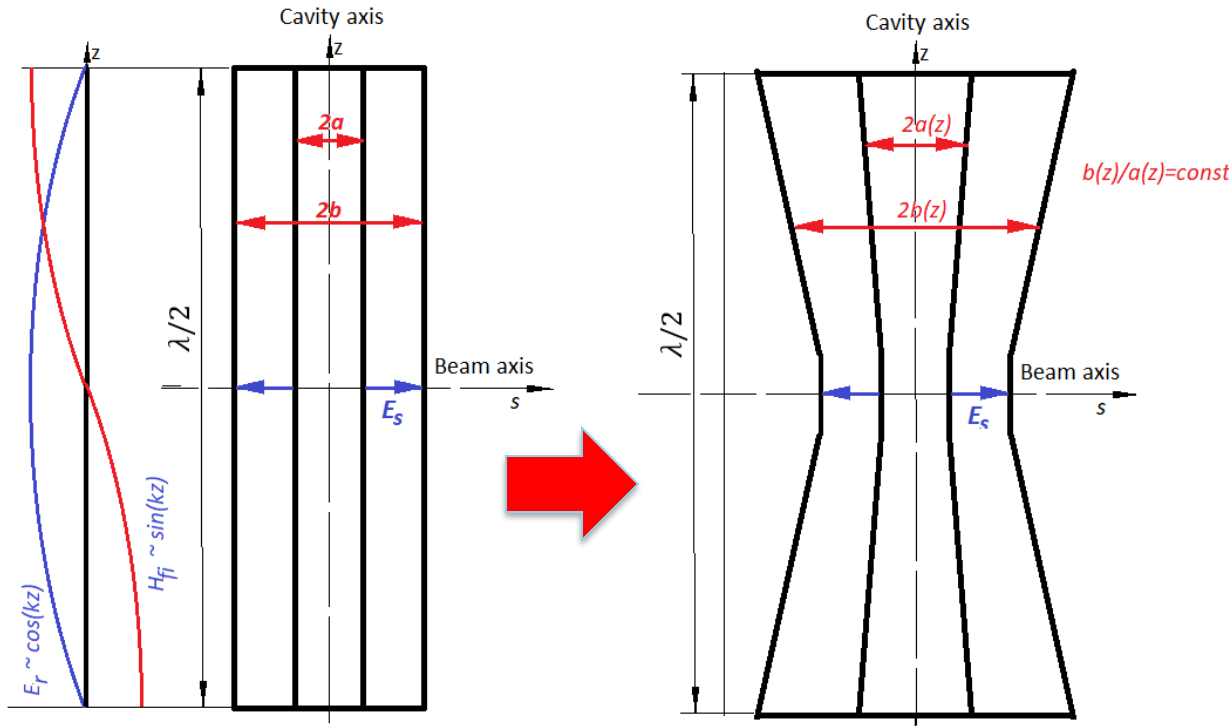
(compare to multi-cell elliptical cavity: $L_{eff} = \frac{\beta\lambda}{2} n$, n is number of gaps)

$Si(x)$ calculator:

<https://keisan.casio.com/exec/system/1180573420>



Loss reduction in HWR: conical HWR*



Increase the cavity transverse size at the ends keeping about the same ratio $b(z)/a(z)$ helps to decrease loss without change of the R/Q , which is determined in high degree by Z_c

$$H_\varphi(r, z) = \frac{I}{2\pi r} \sin(kz) = \frac{U}{2\pi Z_c r} \sin(kz);$$

$$Z_c = \frac{Z_0}{2\pi} \ln\left(\frac{b(z)}{a(z)}\right) = \text{const. } b(z) = b(0) + \frac{b(L/2) - b(0)}{L/2} z; a(z) = a(0) + \frac{a(L/2) - a(0)}{L/2} z$$

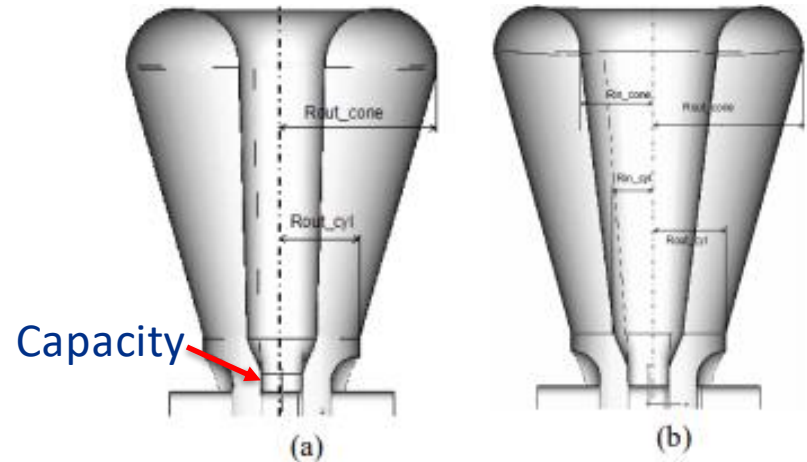
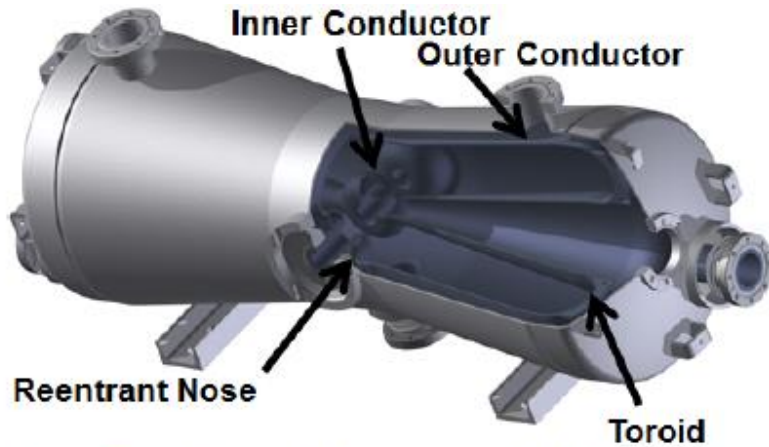
$$P = \frac{1}{2} \oint R_s H^2 dS = \frac{R_s U^2}{8\pi Z_c^2} \left[4 \int_0^{L/2} \sin^2(kz) \left(\frac{1}{b(z)} + \frac{1}{a(z)} \right) dz + 4 \ln\left(\frac{b(L/2)}{a(L/2)}\right) \right] \sim \frac{R_s U^2}{8\pi Z_c^2} \left[L \left(\frac{1}{b(L/2)} + \frac{1}{a(L/2)} \right) + 4 \ln\left(\frac{b(L/2)}{a(L/2)}\right) \right]$$

$$\frac{P_{ideal}}{P_{con}} = \frac{G_{con}}{G_{ideal}} \lesssim \frac{a(L/2)}{a(0)}, \frac{K_{Mcon}}{K_{Mideal}} \lesssim \frac{a(0)}{a(L/2)}, \frac{K_{Econ}}{K_{Eideal}} \sim 1$$

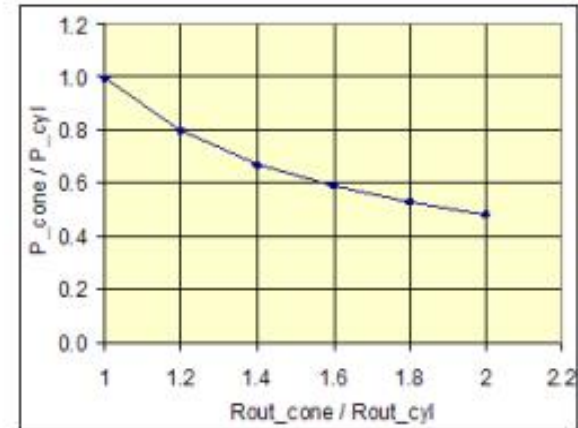
If $\frac{a(L/2)}{a(0)} \sim 3$, one may expect reduce loss and surface magnetic field 2 – 3 times.

*P. Ostroumov, E. Zaplatin

Loss reduction in HWR: conical HWR*



HWR with enlarged outer (a) and central conductor (b) dome diameters.

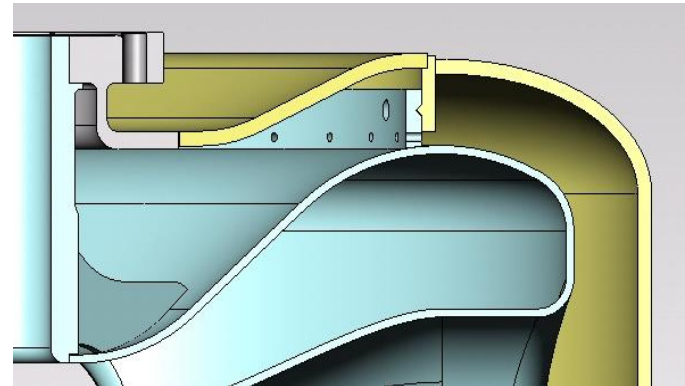


Power dissipation in conical HWR relative to cylindrical shape.

PIP II HWR
(P. Ostroumov)

RF cavities for low β :

Spoke resonator

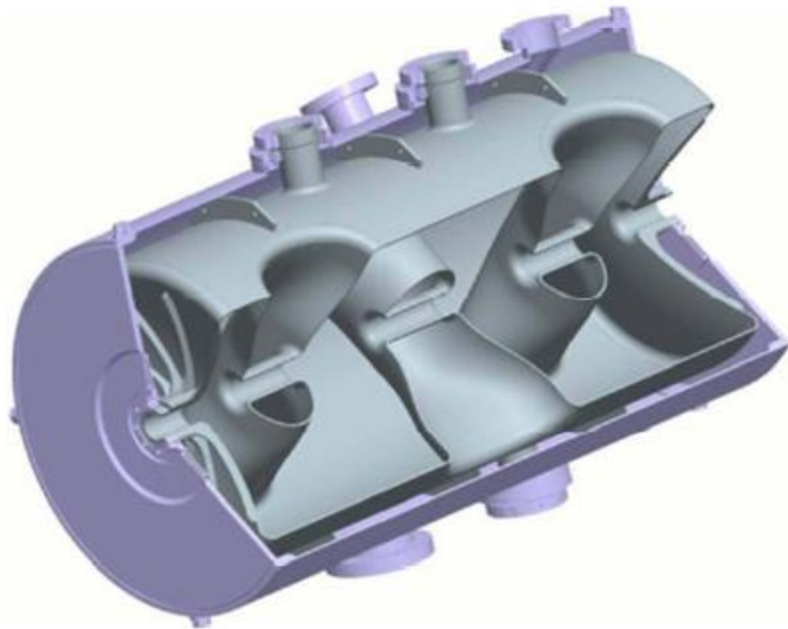


Mechanical coupling of the cavity to the He vessel in order to improve mechanical stability.

FNAL 325 MHz SSR1 cavity layout and photo. $\beta=0.22$

RF cavities for low β :

Multi-spoke resonators



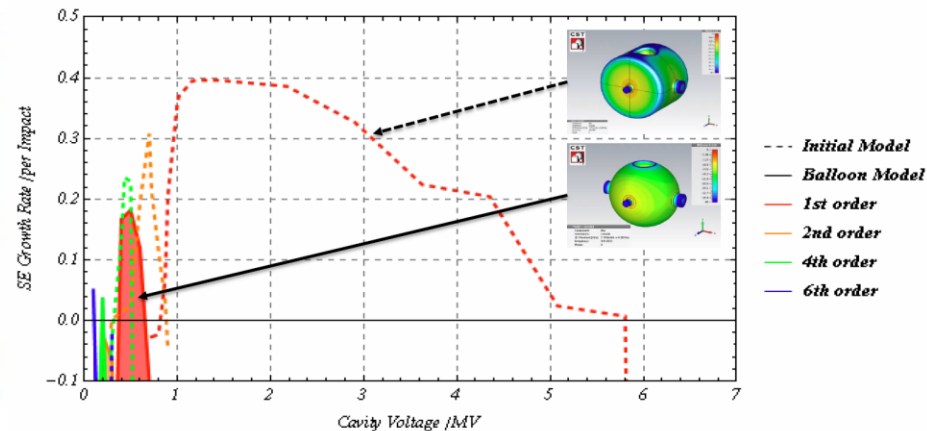
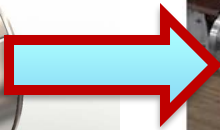
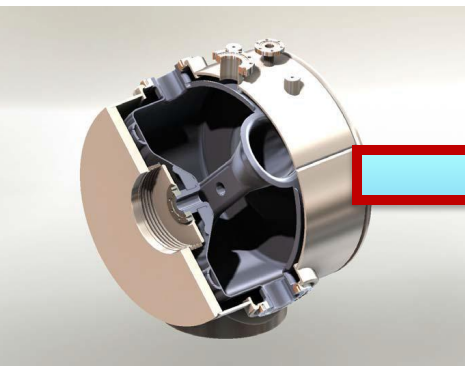
Triple-spoke cavity



345 MHz, $\beta=0.4$,
3-gap spoke cavity
for ion beam acceleration
ANL

RF cavities for low β :

- TEM-type cavities are prone to multipacting;
- Elliptical cavities have much better performance (MP electrons drift towards the axis)
- Idea (R. Laxdal): combine SR and elliptical cavity \rightarrow balloon cavity.

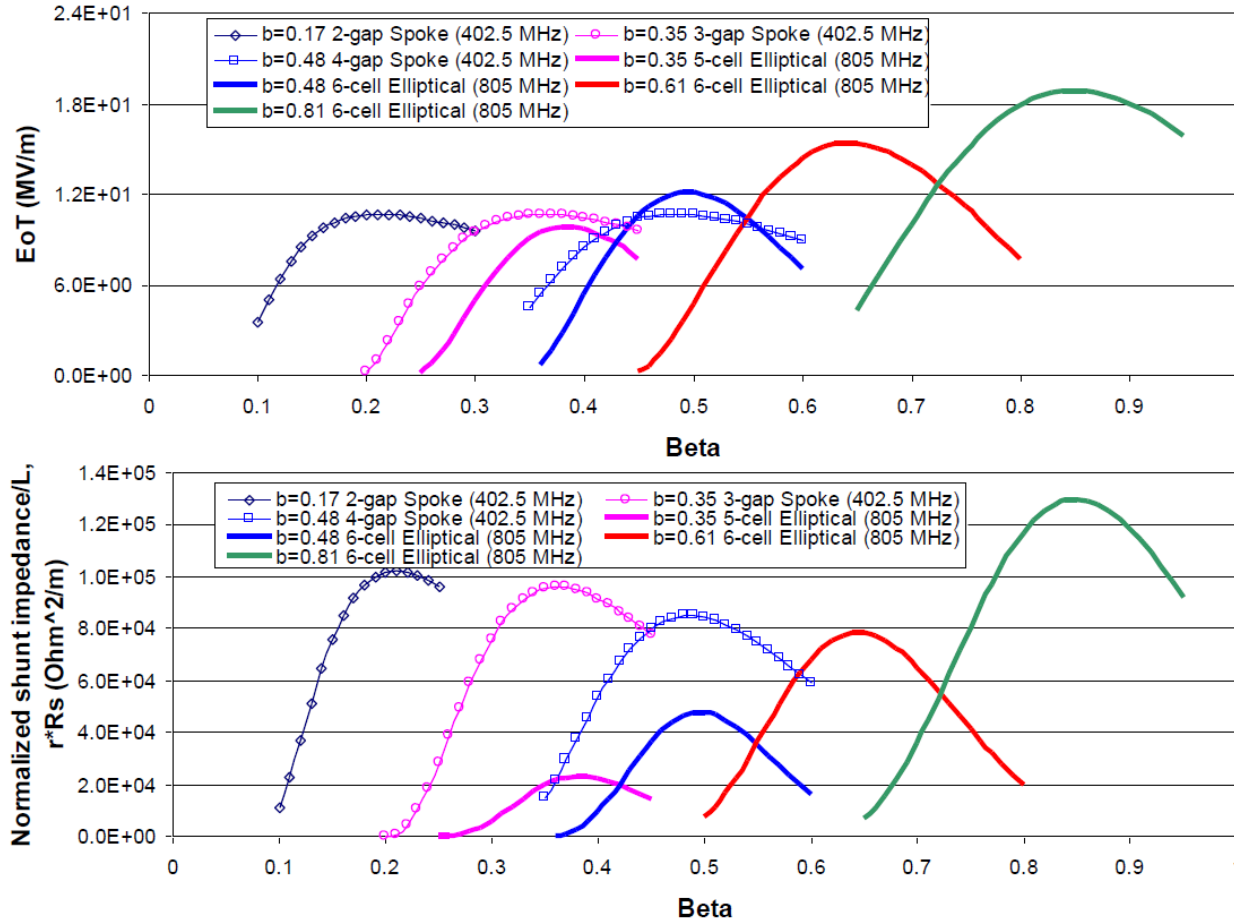


- Balloon cavity is successfully tested (R. Laxdal and colleagues): condition time reduced from ~ 10 hours to ~ 30 mins!

Why not multi-spoke for $\beta > 0.5$?

Comparison of RF properties (elliptical cavity versus spoke cavity)*

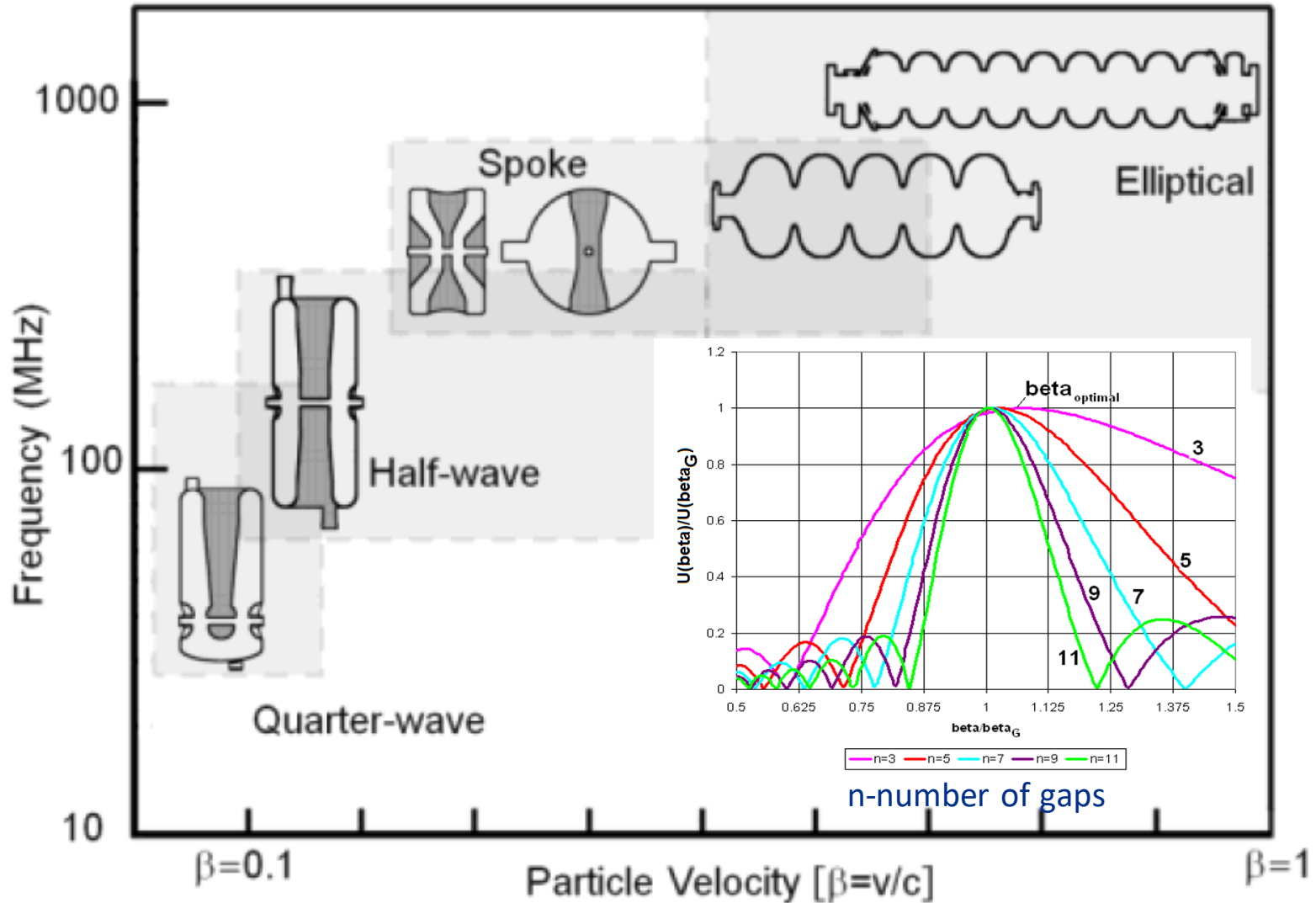
Spoke cavities (402.5 MHz) and elliptical cavities (805 MHz) are optimally designed under the same criteria: $E_{\text{peak}} \approx 40 \text{ MV/m}$ and $B_{\text{peak}} \approx 85 \text{ mT}$. Here EoT is gradient, and r^*R_s is $R/Q \cdot G$ per unit length.



For $\beta > 0.5-0.6$ elliptical cavity is preferable!

*Sang-Ho Kim, Mark Doleans, USPAS, January 2013, Duke University

SRF Cavity types depending on particle velocity



Summary:

- ❑ For acceleration of the particles having low velocity, QWR, HWR and spoke cavities are used in modern RT and SRF accelerators, which have high R/Q at low β .
- ❑ Double and triple-spoke resonators are also used up to $\beta = 0.5$.
- ❑ QWR, HWR and SR are prone to MP; Balloon cavity has no MP.
- ❑ TEM-type cavities are used up to $\beta = 0.5$. For higher β elliptical cavities are used in SRF accelerators.

Chapter 9.

Beam-cavity Interaction

- a. Beam loading;
- b. Optimal coupling;
- c. Wake potential;
- d. HOM excitation effects.

Beam Loading

Wilson's Theorems:

1. The bunch exiting the empty cavity, decelerates by $V_i/2$, where V_i is the voltage left in the cavity.

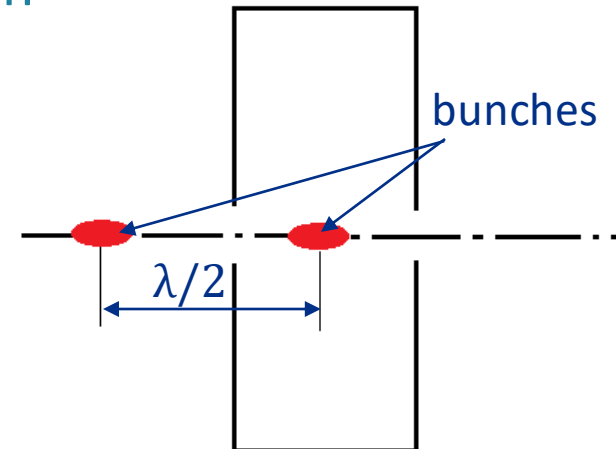
Two bunches with the distance between them of $\lambda/2$ excite total zero voltage.

If one bunch "sees" fraction α of V , one has:

$$q_b (V_i - \alpha V_i) = q_b \alpha V_i \rightarrow \alpha = 1/2.$$



Perry B. Wilson
1927-2013



Beam Loading

Wilson's theorems:

2. The voltage V exited by the bunch with the charge q_b is

$$V_i = 1/2 \cdot R/Q \cdot \omega \cdot q_b$$

Energy conservation law:

$$1/2 \cdot V_i \cdot q_b = V_i^2 / (R/Q \cdot \omega) \rightarrow V_i = 1/2 \cdot R/Q \cdot \omega \cdot q_b$$

The energy loss of the bunch is equal to

$$U = 1/2 \cdot V_i \cdot q_b = 1/4 \cdot R/Q \cdot \omega \cdot q_b^2 = k \cdot q_b^2$$

here k is loss factor,

$$k = 1/4 \cdot R/Q \cdot \omega.$$

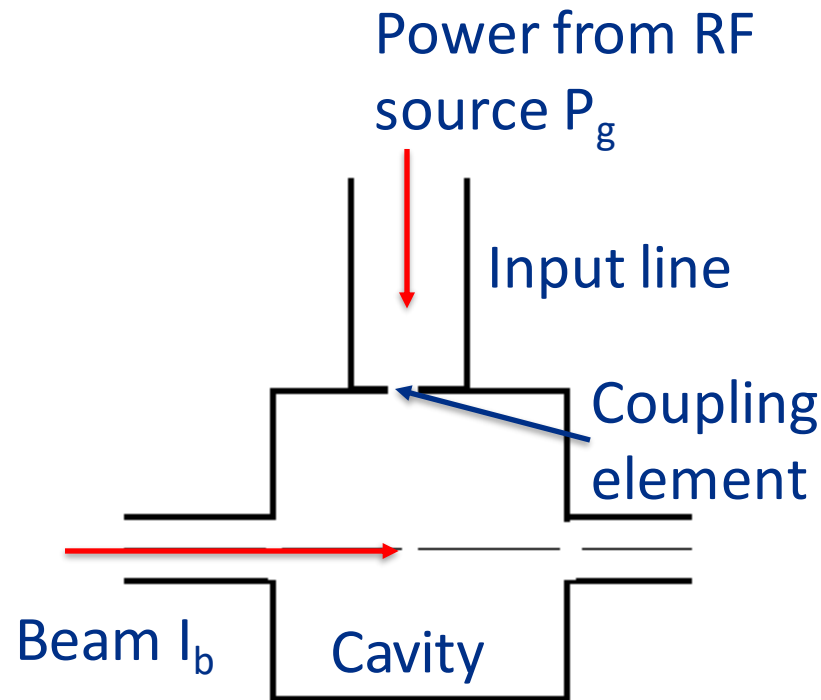
If the beam pulse is short compared to time constant τ (field decay time),

$$V_I = 1/2 \cdot R/Q \cdot \omega \cdot q$$

is a total voltage induced by the beam pulse in the cavity,

q is a total charge, $q = \sum q_b = I \cdot t_{beam}$.

Beam Loading

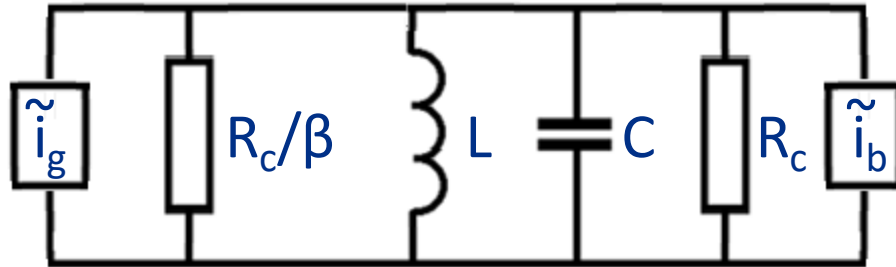


- RF source and beam $\omega_g = \omega_b = \omega$;
- Cavity: ω_0
- Cavity voltage : V_c
- Shunt impedance: R_{sh}
- Losses: $P_c = V_c^2 / R_{sh} = V_c^2 / (Q_0 \cdot R / Q)$
- Radiation to the line: $V_c^2 / (Q_{ext} \cdot R / Q)$
- Coupling: $\beta = Q_0 / Q_{ext}$
- Loaded Q: $Q_L = Q_0 / (1 + \beta)$
- Average beam current: I_b
- Synchronous phase: φ
- Power consumed by the beam: $P_b = I_b V_c \cos \varphi$
- Input power P_g
- Reflected power: $P_r = P_g - P_c - P_b$

Details are in Appendix 8

Beam Loading

Equivalent circuit for the beam-loaded cavity transformed to the resonance circuit:



$$L = R/Q / (2\omega_0)$$

$$C = 2 / (R/Q \cdot \omega_0)$$

$$R_c = R/Q \cdot Q_0 / 2$$

$$\tilde{i}_b = -2I_b$$

From this equivalent circuit we have:

$$P_g = \frac{V_c^2 (1 + \beta)^2}{4\beta Q_0 (R/Q)} \left[\left(1 + \frac{I_{Re} (R/Q) Q_0}{V_c (1 + \beta)} \right)^2 + \left(\frac{Q_0}{1 + \beta} \frac{(\omega^2 - \omega_0^2)}{\omega_0^2} + \frac{I_{Im} (R/Q) Q_0}{V (1 + \beta)} \right)^2 \right]$$

where $I_{Re} = I_b \cos\varphi$ and $I_{Im} = I_b \sin\varphi$

Beam Loading

If the cavity is detuned by Δf versus the RF source frequency and r.m.s. microphonics amplitude is δf , the required power is the following :

$$P_g = \frac{V_c^2(1+\beta)^2}{4\beta Q_0(R/Q)} \left[\left(1 + \frac{I_{\text{Re}}(R/Q)Q_0}{V_c(1+\beta)} \right)^2 + \left(\frac{Q_0}{1+\beta} \frac{2\delta f}{f} + \left| \frac{Q_0}{1+\beta} \frac{2\Delta f}{f} + \frac{I_{\text{Im}}(r/Q)Q_0}{V_c(1+\beta)} \right| \right)^2 \right]$$

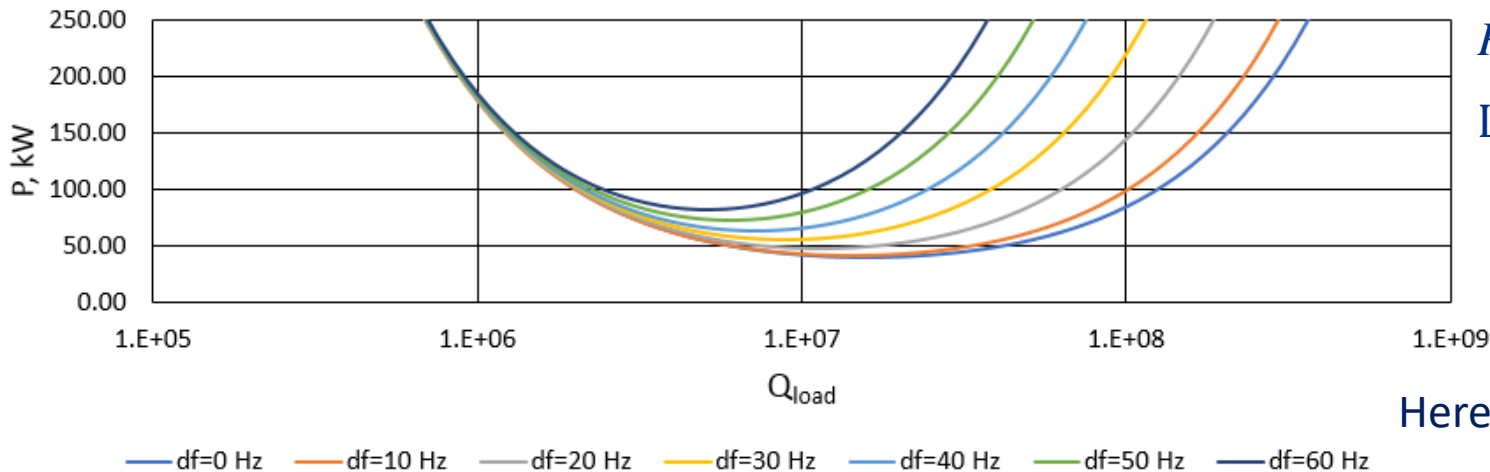
Typically, the cavity has “static detune”:

$$\Delta f = -f \frac{I_{\text{Im}}(R/Q)}{2V_c}$$

In this case.

$$P_g = \frac{V_c^2(1+\beta)^2}{4\beta Q_0(R/Q)} \left[\left(1 + \frac{I_{\text{Re}}(R/Q)Q_0}{V_c(1+\beta)} \right)^2 + \left(\frac{Q_0}{1+\beta} \frac{2\delta f}{f} \right)^2 \right]$$

The optimal coupling providing minimal power: $\beta_{opt} = \left[\left(1 + \frac{I_{\text{Re}}(R/Q)Q_0}{V_c} \right)^2 + \left(\frac{2\delta f Q_0}{f} \right)^2 \right]^{1/2}$



$P_g(\delta f)$ for
LB 650 (PIP II)

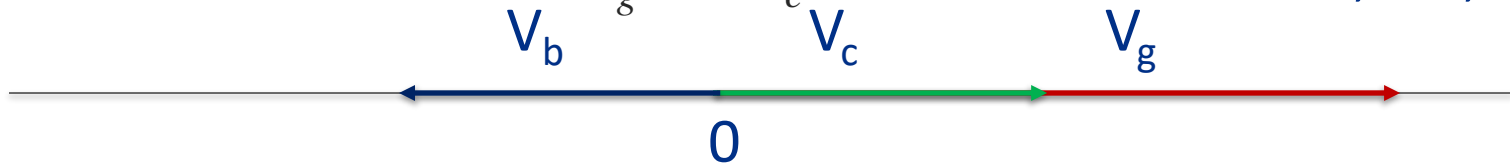
$$Q_{load} = \frac{Q_0}{1+\beta}$$

$$df = \frac{f}{Q_{load}}$$

Here df -cavity bandwidth

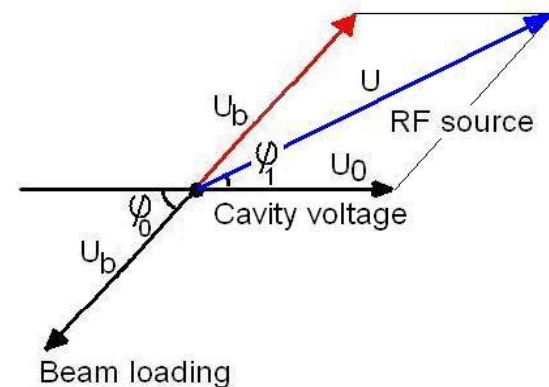
Beam Loading

- In resonance for a SRF cavity $\beta_{opt} \gg 1$ and $\beta_{opt} = I_b \cdot R/Q \cdot Q_0/V_c$ and $Q_L = V_c / (I_b \cdot R/Q)$. The cavity bandwidth $\Delta f = f/Q_L = f \cdot I_b \cdot (R/Q)/V_c$.
- for optimal coupling for the SRF cavity $V_b = -V_c$ and $P_g = |V_c \cdot I_b|$. Note that in this case $V_g = 2V_c$ and reflection is zero, i.e., $P_r = 0$.



- Without the beam in order to maintain the same voltage in the SRF cavity at the same coupling $P_{g0} = 1/4 \cdot P_g$. For SRF cavity reflection in this case is $\sim 100\%$.

- Phase shift between the bunch and the cavity voltage

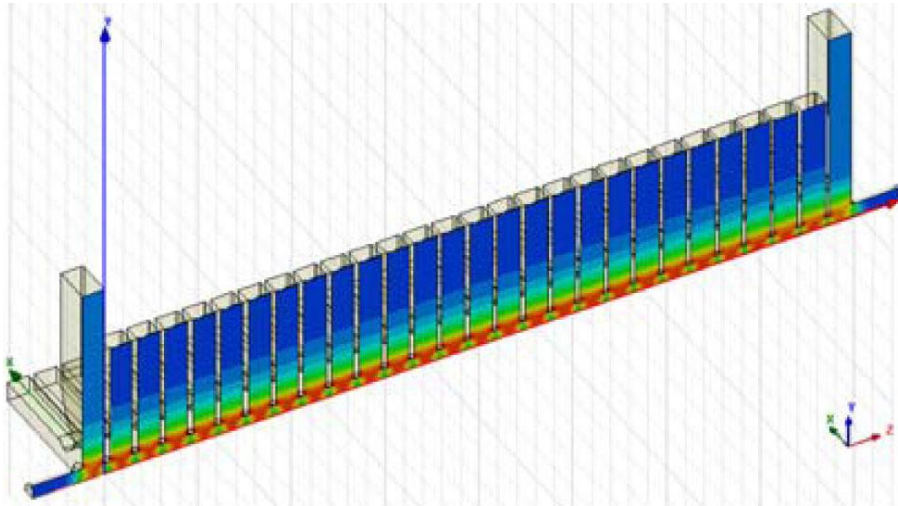


Beam Loading, Travelling Wave

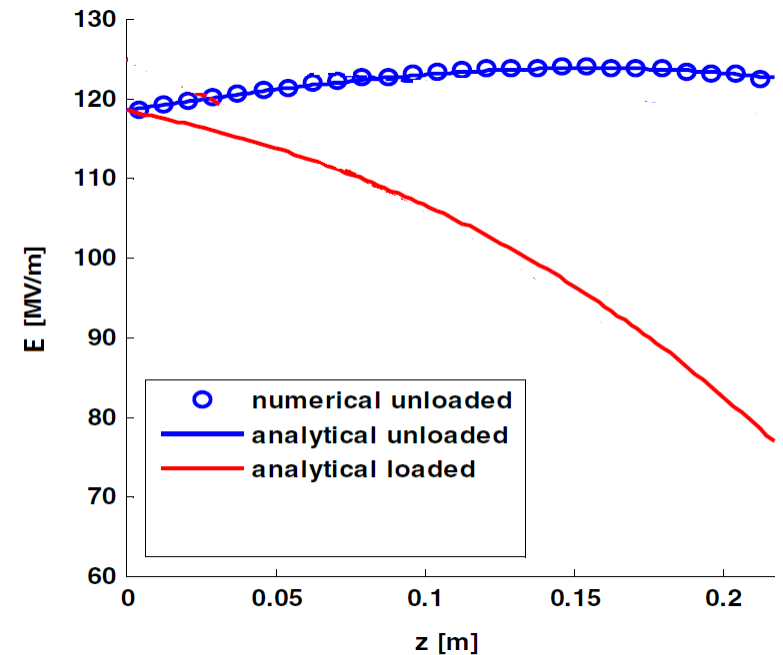
In presence of a beam (see Lecture 8, slide 14):

$$\frac{dW_{0,j}}{dt} = -P_j + P_{j-1} - \frac{\omega_0 W_{0,j}}{Q_0} - V_c I_b \quad (1)$$

Beam loading changes the field distribution along the structure.



CLIC 12 GHz structure



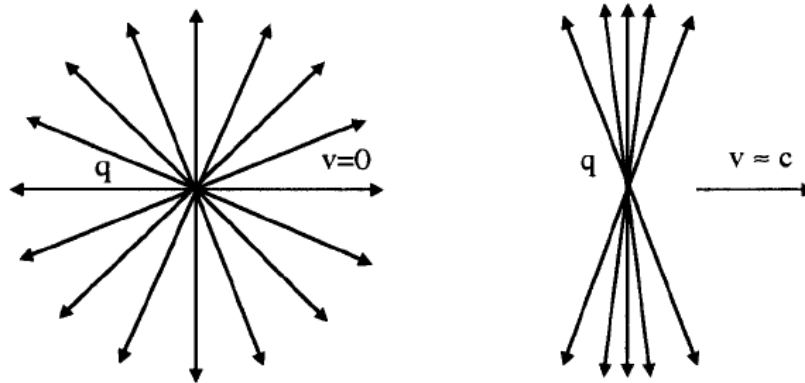
Wake potentials

1. Fields of a moving charge in free space:

$$\mathbf{E} = \frac{q\hat{r}}{4\pi\epsilon_0 r^2 \gamma^2 (1 - \beta^2 \sin^2\psi)^{3/2}}$$

For $\gamma \rightarrow \infty$

$$E_r = \frac{q\delta(z - ct)}{2\pi\epsilon_0 r} \quad B_\theta = \frac{\mu_0 c q \delta(z - ct)}{2\pi r}$$



$$F_r = q'(E_r - cB_\theta) = \frac{q'q\delta(z - ct)}{2\pi\epsilon_0 r} - \frac{q'q\mu_0 c^2 \delta(z - ct)}{2\pi r} = 0$$

Wake potentials

1. Fields in the smooth waveguide with ideally conducting walls:

No radiation (lack of synchronism: $v_{ph} > c$)

Coulomb forces (including image):

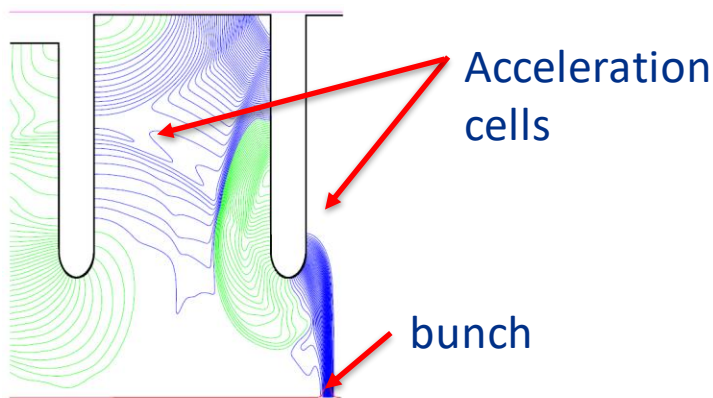
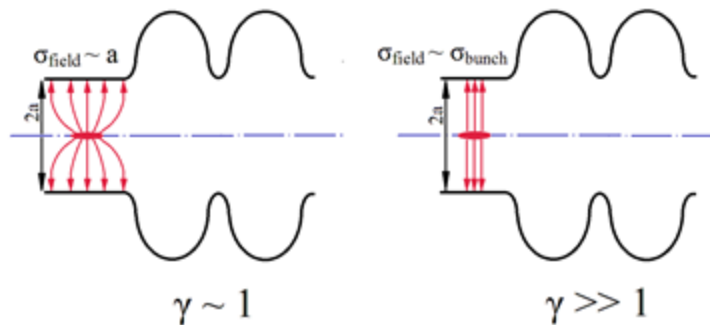
$$F_r = q(E_r - vB_\phi) \sim 1/\gamma^2$$

$F_z \sim 1/\gamma^2$ (static field is compensated by eddy field).

2. In presence of obstacle radiation takes place

- change of cross section,
- finite conductivity
- dielectric wall

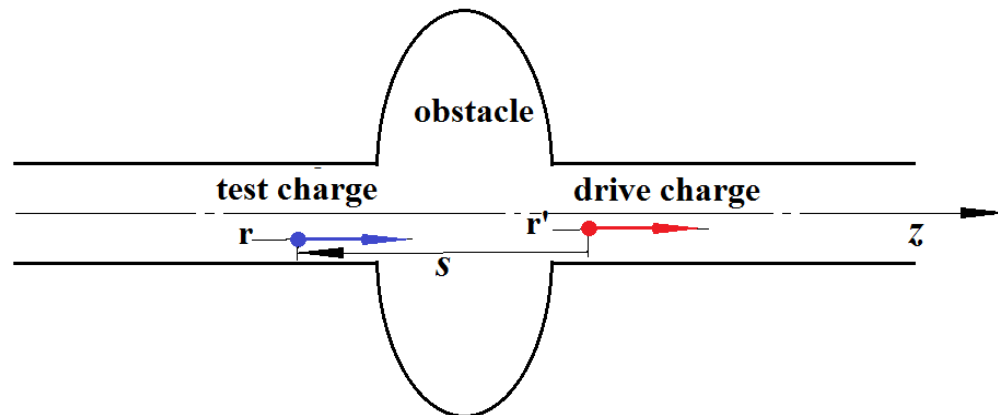
Wake potentials



Blue – deceleration, green – acceleration

- Energy lost by the bunch:
 $W = kq^2$
 k is the loss factor.
- Transverse momentum kick:
 $\Delta p_{\perp} c = r q^2 k_{\perp}$
 k_{\perp} is a kick factor

Radiation fields in the TW acceleration structure



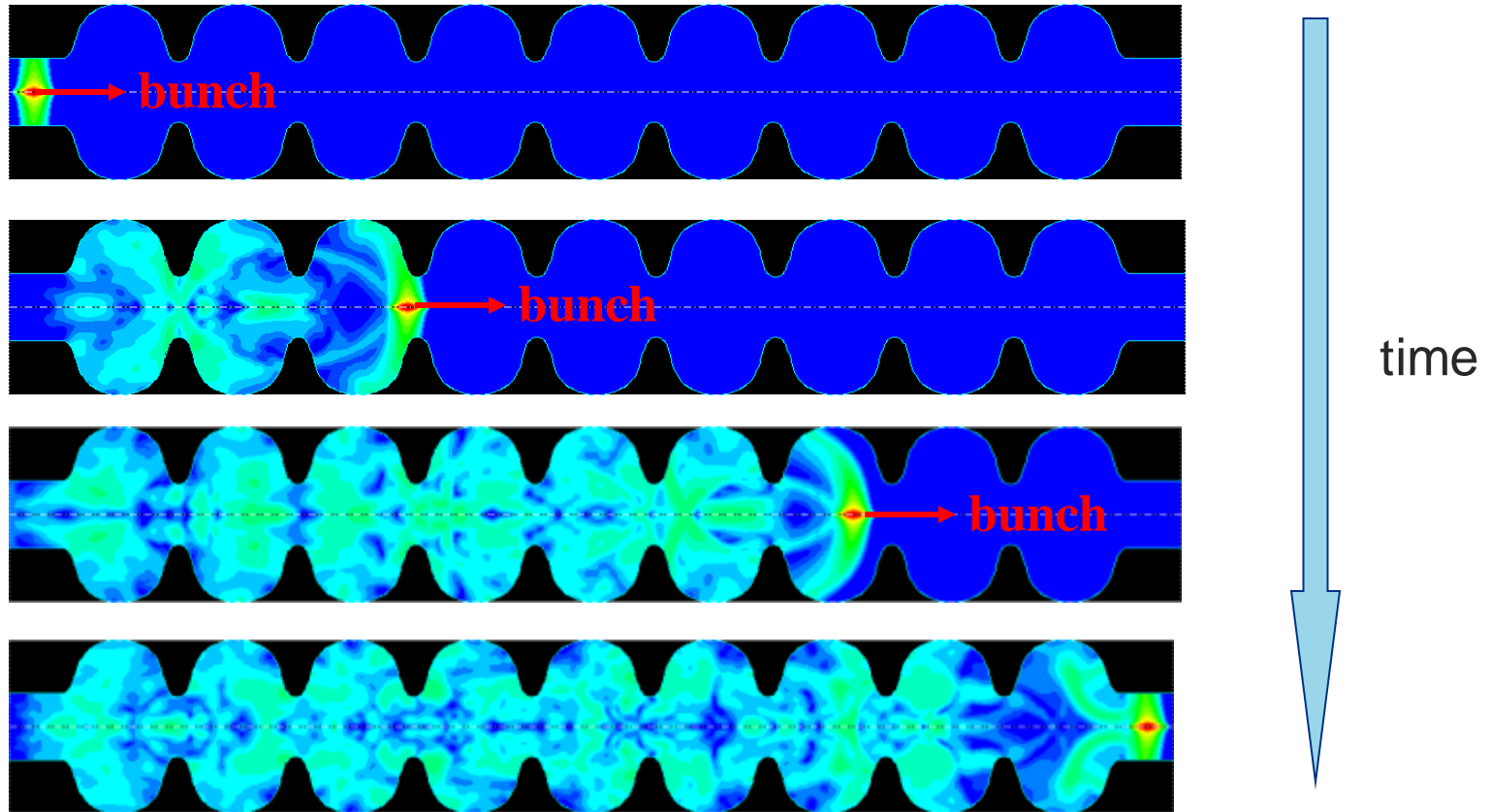
$$W_z(\vec{r}, \vec{r}', s) = -\frac{1}{q} \int_{z_1}^{z_2} dz [E_z(\vec{r}, z, t)]_{t=(z+s)/c}$$

$$\vec{W}_{\perp}(\vec{r}, \vec{r}', s) = \frac{1}{q} \int_{z_1}^{z_2} dz [\vec{E}_{\perp} + c(\hat{z} \times \vec{B})]_{t=(z+s)/c}$$

$$W_z=0, W_{\perp}=0 \text{ for } s < 0$$

More details: Appendix 13

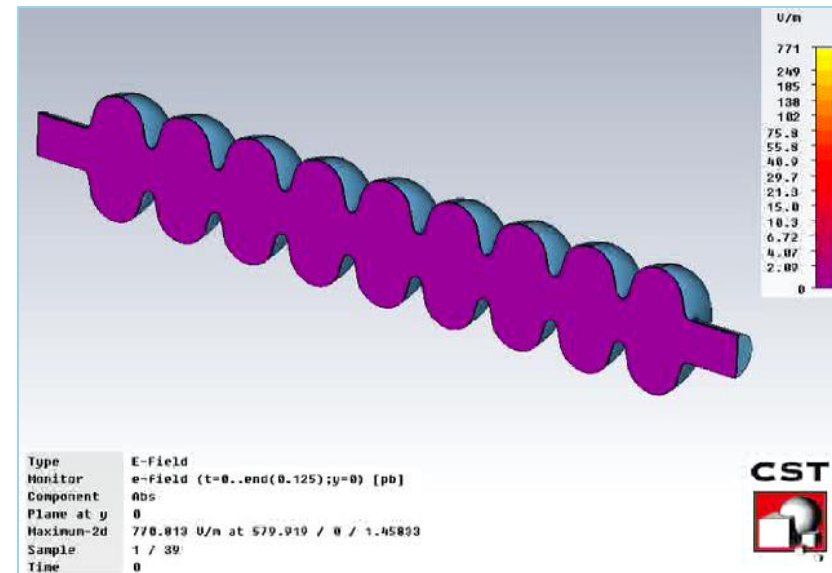
Electromagnetic field excited by bunch



The bunched beam excites electromagnetic field inside an originally empty cavity.

Short- and long-range wakefields

- Short range wake-field → Fields along the bunch and just behind it:
 - Cause bunch energy loss and energy spread along the bunch
 - Single bunch break up instability
 - Cooper pair breaking in the case of extremely short bunches
- Long range wakes (HOMs):
 - Monopole modes: Longitudinal coupled bunch instabilities; RF heating; Longitudinal emittance dilution ...
 - Dipole modes: Transverse transverse coupled bunch instabilities; Emittance dilution; beam break-up instabilities ...

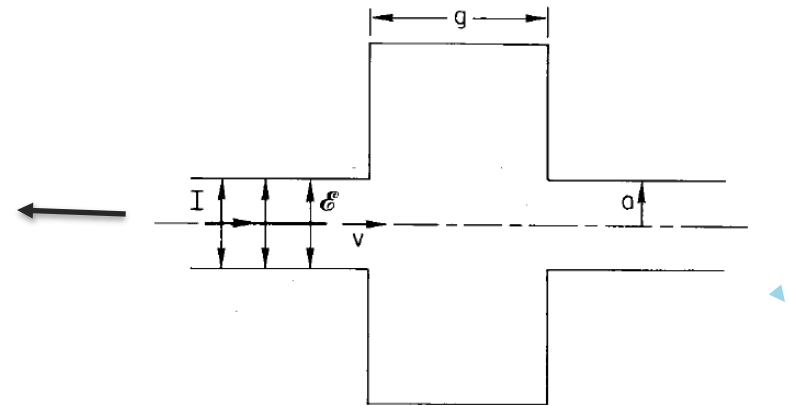


Wake potentials

Pillbox with the holes:

$$k_{\parallel}(\sigma) = \frac{Z_0 c}{\pi^{5/2} a} \sqrt{\frac{g}{\sigma}} \left[\Gamma(1/4)/4 - \left(\frac{\omega_c \sigma}{c} \right)^{1/2} \right]$$

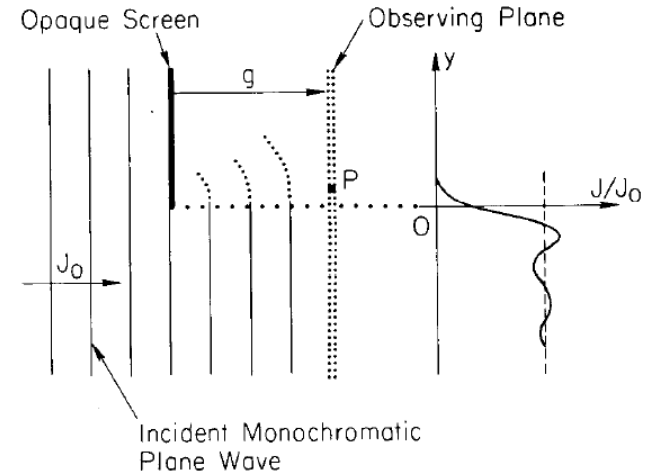
$$k_{\perp}(\sigma) = (4.36..) \frac{Z_0 c}{\pi^3 a^3} \sqrt{g \sigma}$$



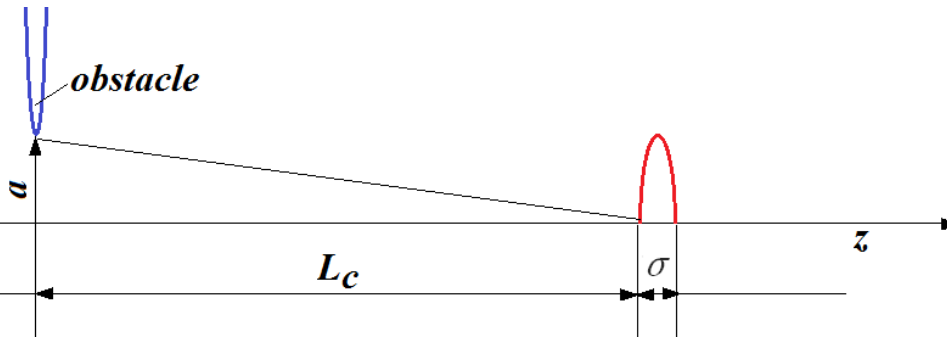
Loss and kick factors depend on the cavity geometry and the bunch Length.

For Gaussian bunch, $\Gamma(1/4)/4 = 0.908..$

Catch-up problem:



Diffraction model:



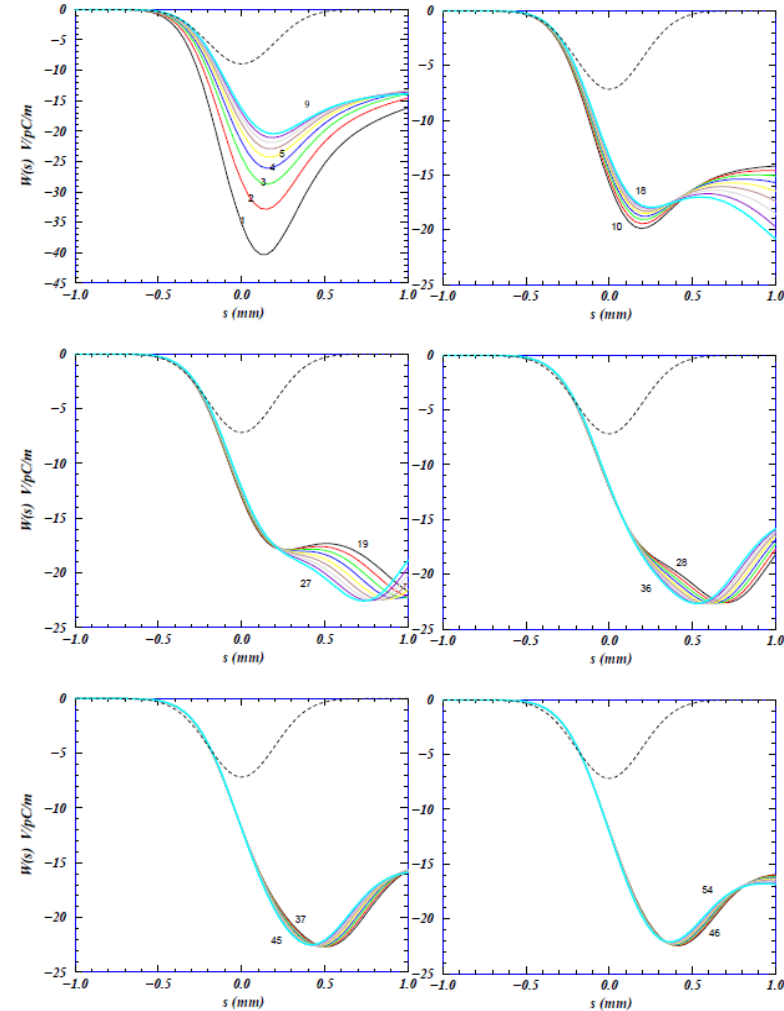
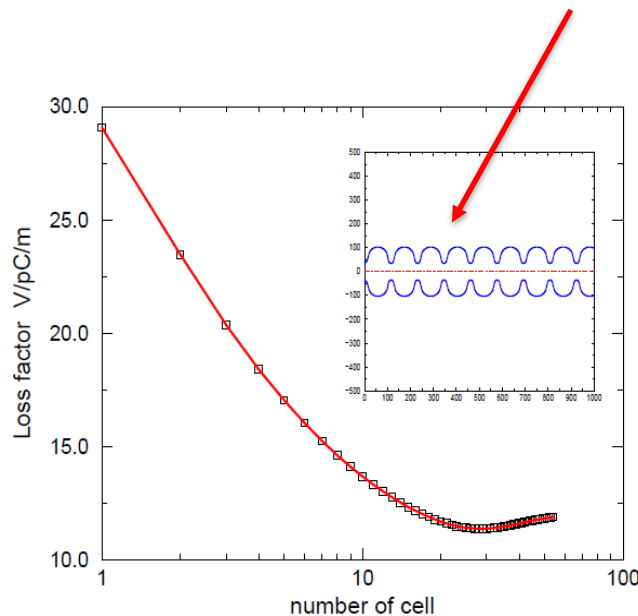
$$(L_c^2 + a^2)^{1/2} = L_c + \sigma \quad L_c \approx a^2 / 2\sigma$$

Wake potentials

Transition of the wakefield in semi-infinite periodic structure:

- Calculations of the loss distribution for a chain of TESLA cells. The loss factor and wake amplitude decrease with the cell number. The shape of the wake does not change significantly after the bunch exceeds the catch-up distance, which is ~ 3 m (27 TESLA cells) for this case ($\sigma = 0.2$ mm, $a = 35$ mm)

$$L = \frac{a^2}{2\sigma_z}$$

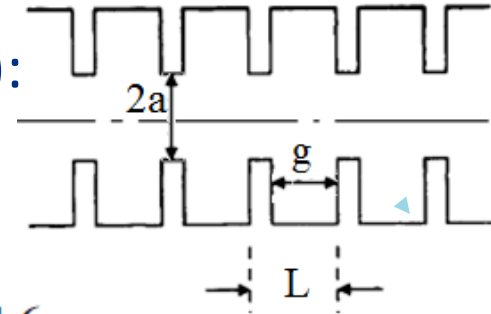


Wake potentials

Semi-Infinite periodic structure (steady-state wake):

→ wakes per unit length.

- Karl Bane model (KB) :



$$W_L(s, s_0) = \frac{Z_0 c}{\pi a^2} \exp\left(-\sqrt{s/s_0}\right); \quad \text{where} \quad s_0 = 0.41 \frac{a^{1.8} g^{1.6}}{L^{2.4}},$$

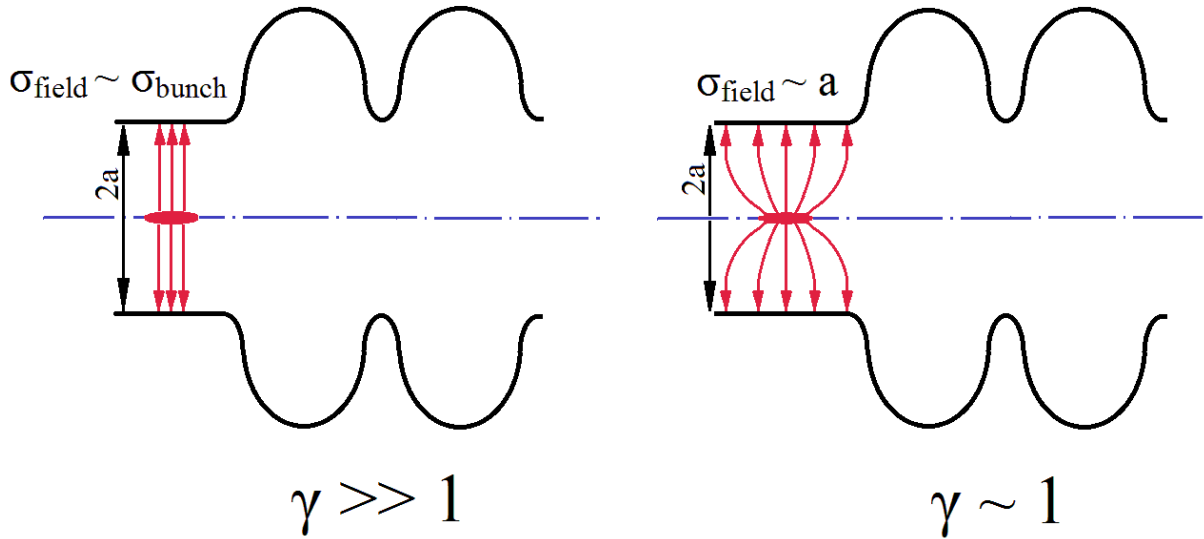
$$\text{when } \sigma \rightarrow 0, \quad k_l = \frac{Z_0 c}{\pi a^2}$$

Steady-state wake – when the structure length > catch-up distance.

- ❖ Wake potentials limit the cavity aperture and therefore, determine the cavity design, especially for SRF electron linacs for FELs, where the bunch length is small.

Wake potentials

Wakefiled for non-relativistic bunch:



HE electron linac
(ILC, XFEL or LCLS II)

$$f_{\text{max}} \sim c/\sigma_{\text{bunch}}$$

Proton linac

$$f_{\text{max}} \sim c/a$$

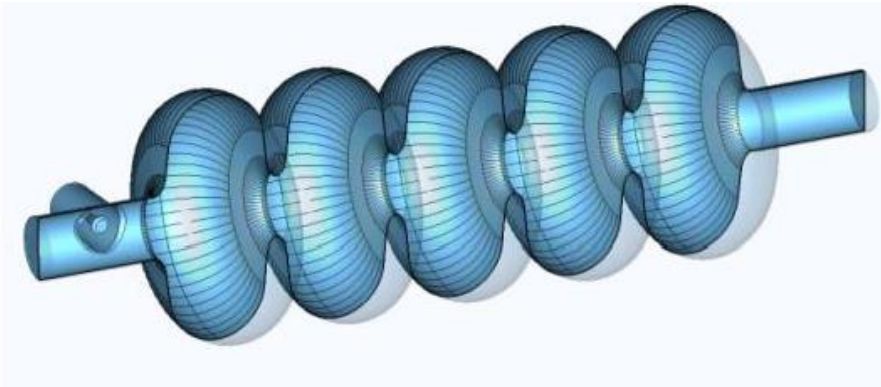
for $\sigma_{\text{bunch}} = 50\mu$, $f_{\text{max}} < 6 \text{ THz}$ for $a = 50\text{mm}$, $f_{\text{max}} < 6 \text{ GHz}$

Diffraction losses are determined by σ_{field} , $P \sim (\sigma_{\text{field}})^{-1/2}$

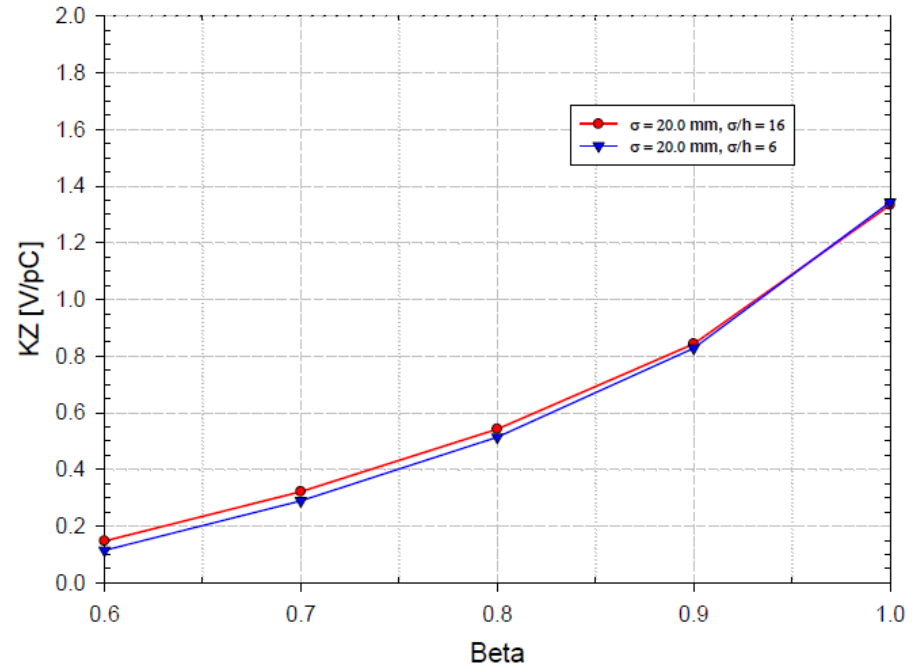
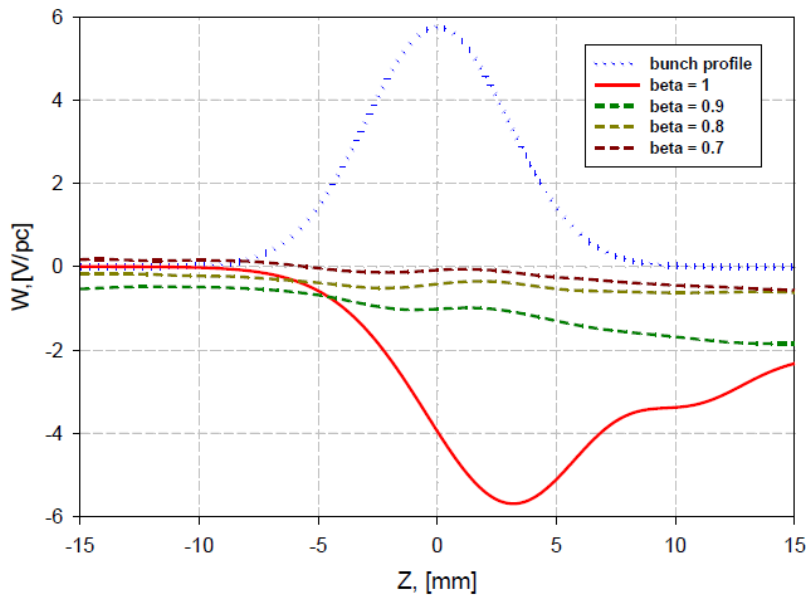


Wake potentials

Wakefield for non-relativistic bunch*:



The 650 MHz, $\beta=0.9$ elliptical accelerating cavity for PIP II



*S. Kurennoy

High-Order Modes in elliptical SRF cavities (long-range wakes)

❑ Possible issues:

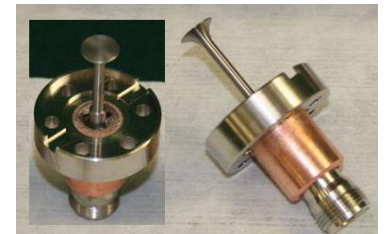
- Trapped modes;
- Resonance excitation of HOMs;
- Collective effects – transverse (BBU) and longitudinal (klystron-type instability);



- Additional cryo-losses;
- Emittance dilution (longitudinal and transverse).

- ## ❑ HOM damper is a vulnerable, expensive and complicated part of SC acceleration cavity (problems – heating, multipacting, etc; additional hardware – cables, feed-through, connectors, loads). HOM dampers may limit a cavity performance and reduce operation reliability;

“To damp, or not to damp?”

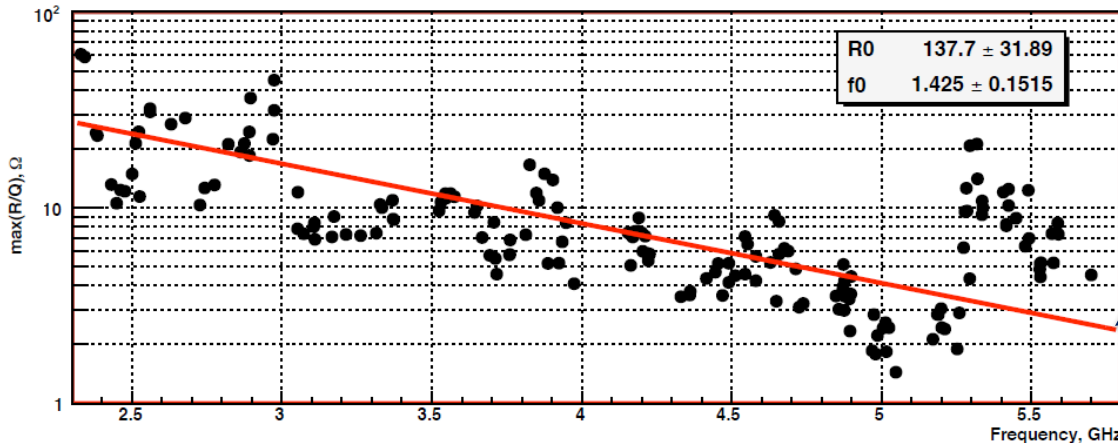


High-Order Modes in elliptical SRF cavities

- HOM energy gain dependence on frequency (see Lecture 7, slide 25)

$$V(r) \sim e^{kr/\beta\gamma}; \text{ or } V(0)/V(a) \sim e^{-ka/\beta\gamma}. \text{ It means that for HOMs } \frac{R}{Q} = \frac{V(0)^2}{\omega W} \sim e^{-2ka/\beta\gamma}$$

Example: $\beta = 0.9$, 650 MHz, 5-cell cavity.



$$\frac{R}{Q} = R_0 e^{-\frac{f}{f_0}}$$

- In proton linacs the HOM spectrum is limited in contrast to SRF cavities for electron linacs;
- R/Q of propagating modes having high frequencies is considerably small.

* **A. Sukhanov**, et al., "Higher Order Modes in Project-X Linac", Nuclear Instruments and Methods in Physics Research, Vol. 734, Part A, January 2014

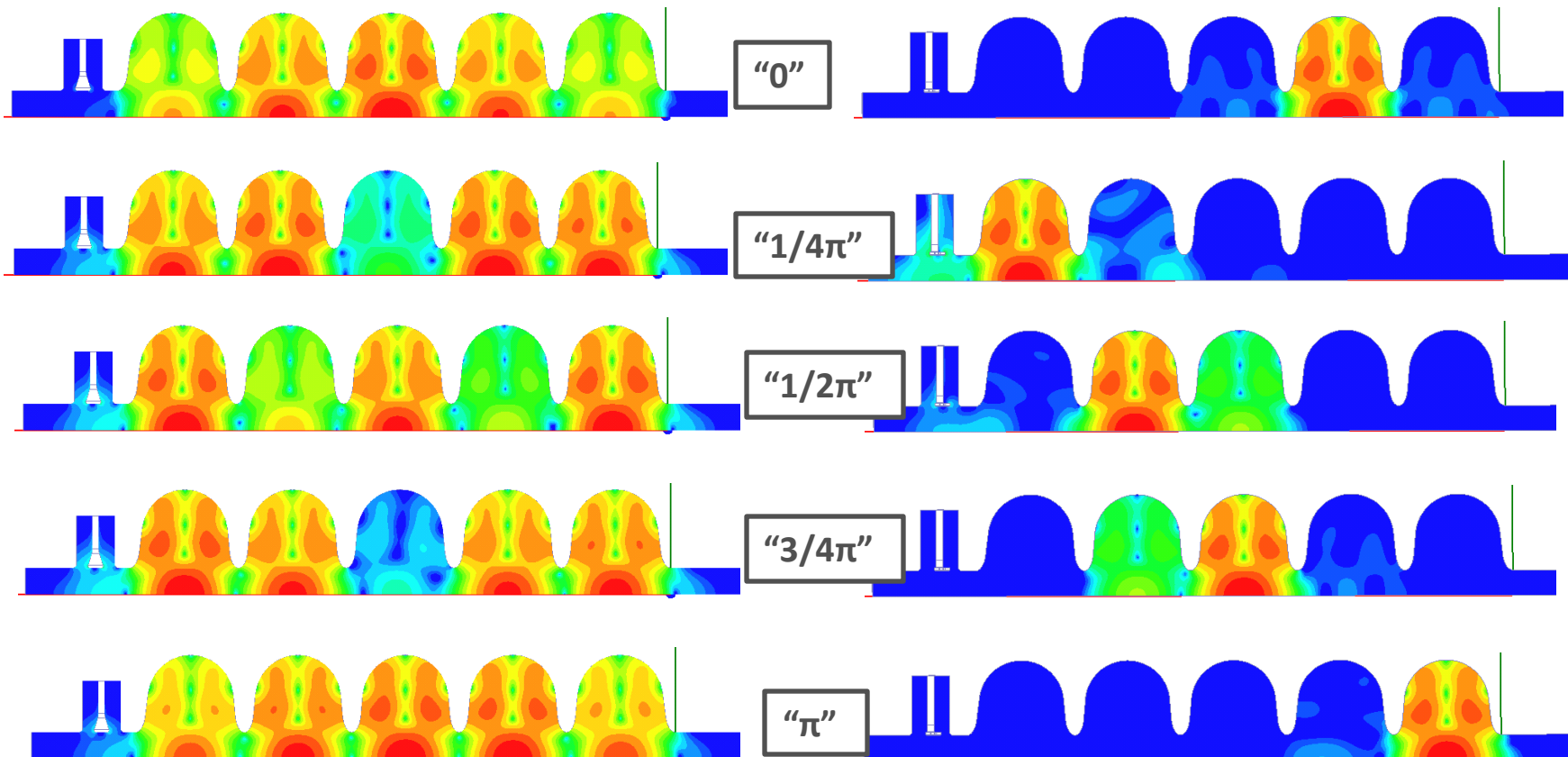
High-Order Modes in elliptical SRF cavities (long-range wakes)

- Specifics of Higher Order Mode effects in the elliptical cavities of proton linacs:
 - Non-relativistic beam;
 - Small current and small bunch population;
 - No feedback (linac);
 - Complicated beam timing structure (dense frequency spectrum).

Trapped Modes in elliptical SRF cavities

For some modes k (*coupling*) may be very small (electric coupling is compensated by magnetic coupling). Because of manufacturing errors, the field distribution may change, the mode will not be coupled to the FC or beam pipe and have high Q_{load} – so called trapped modes.

An example of a bad cavity design containing a trapped mode:

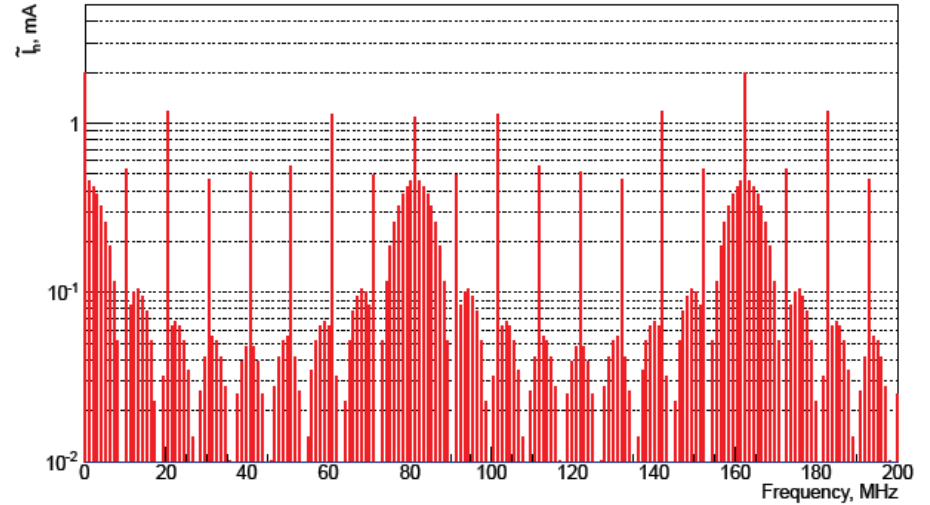
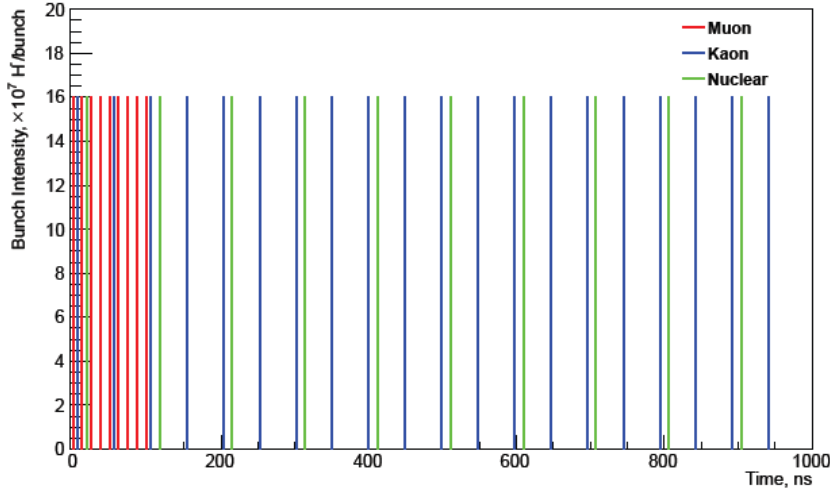


HOMs in an ideal cavity.

HOMs in a “realistic” cavity, i.e., in presence of misalignments.

In both cases the operating mode is tuned to correct frequency and field flatness.

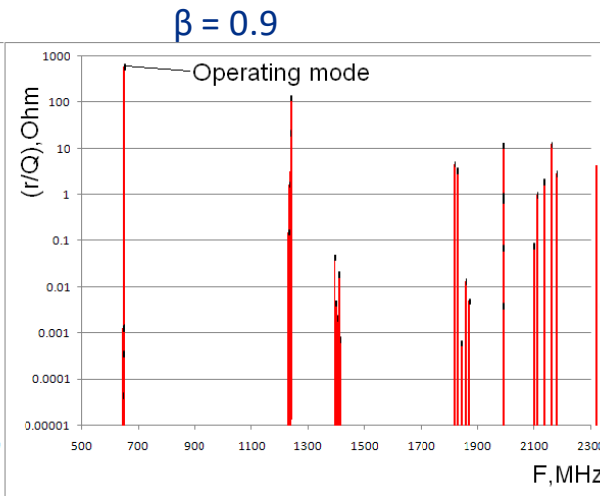
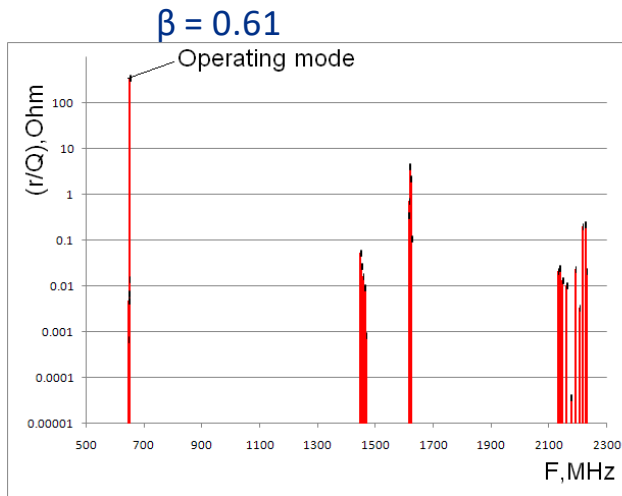
Resonance excitation of HOMs in elliptical SRF cavities



Example of the beam structure for multi-experimental proton driver (PIP II)

The beam current spectrum may be dense: for PIP II it contains

- ❖ • harmonics of the bunch sequence frequency of 10.15 MHz and
- ❖ • sidebands of the harmonics of 81.25 MHz separated by 1 MHz.



← R/Q spectrum of the cavities

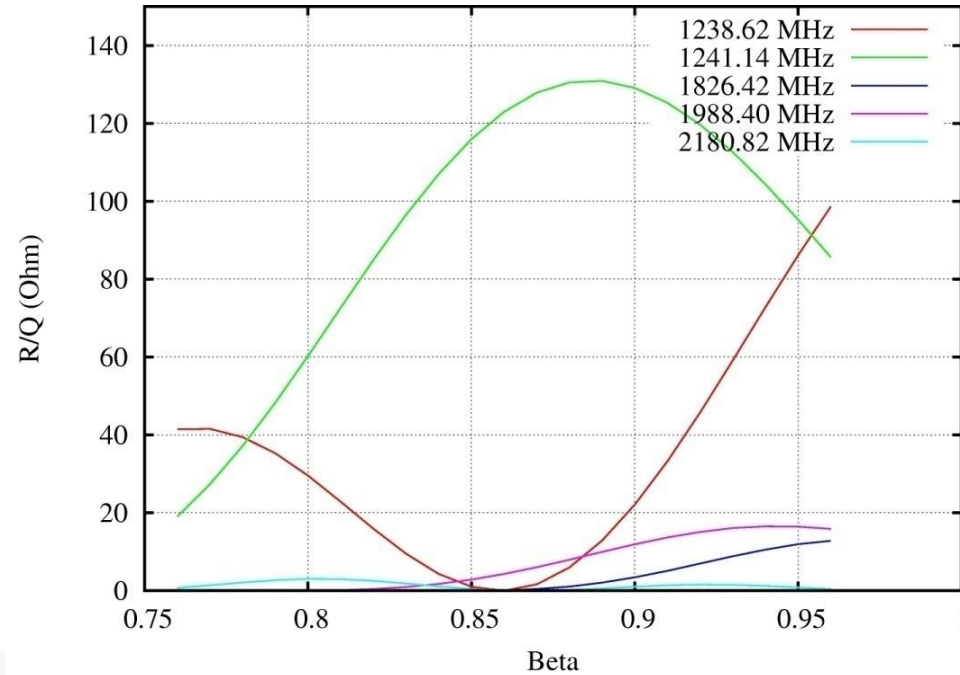
Resonance excitation of HOMs in elliptical SRF cavities

HOM have frequency spread caused by manufacturing errors:

- ❖ For 1.3 GHz ILC cavity r.m.s. spread σ_f of the resonance frequencies is 6-9 MHz depending on the pass band;

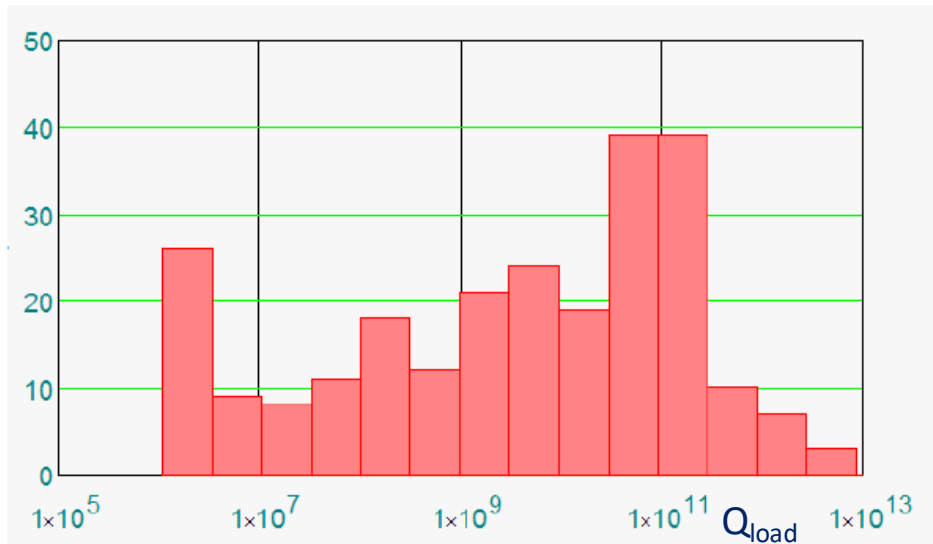
- ❖ Cornell: $\sigma_f \approx 10.9 \cdot 10^{-4} \times (f_{\text{HOM}} - f_0)$,

- ❖ SNS: $\sigma_f \approx (9.6 \cdot 10^{-4} - 13.4 \cdot 10^{-4}) \times (f_{\text{HOM}} - f_0)$;
 $\Delta f_{\text{max}} = |f_{\text{HOM,calculated}} - f_{\text{HOM,measured}}| \sim \sigma_f$



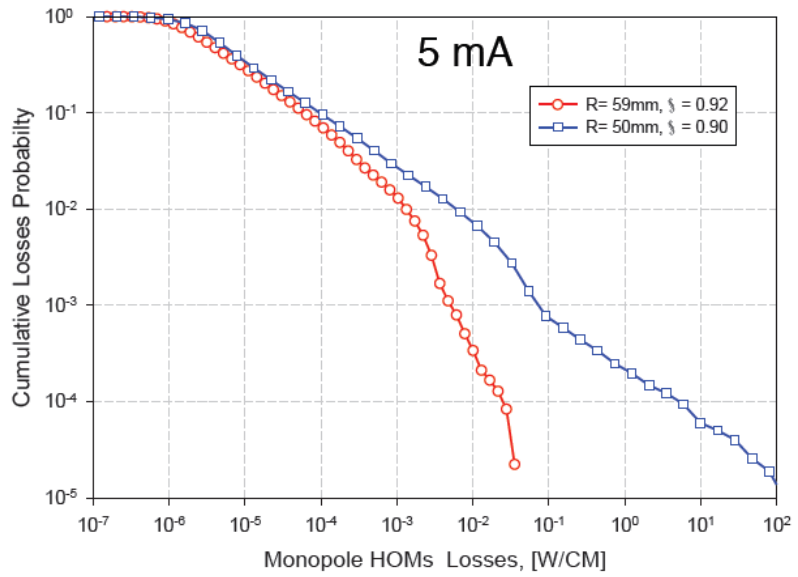
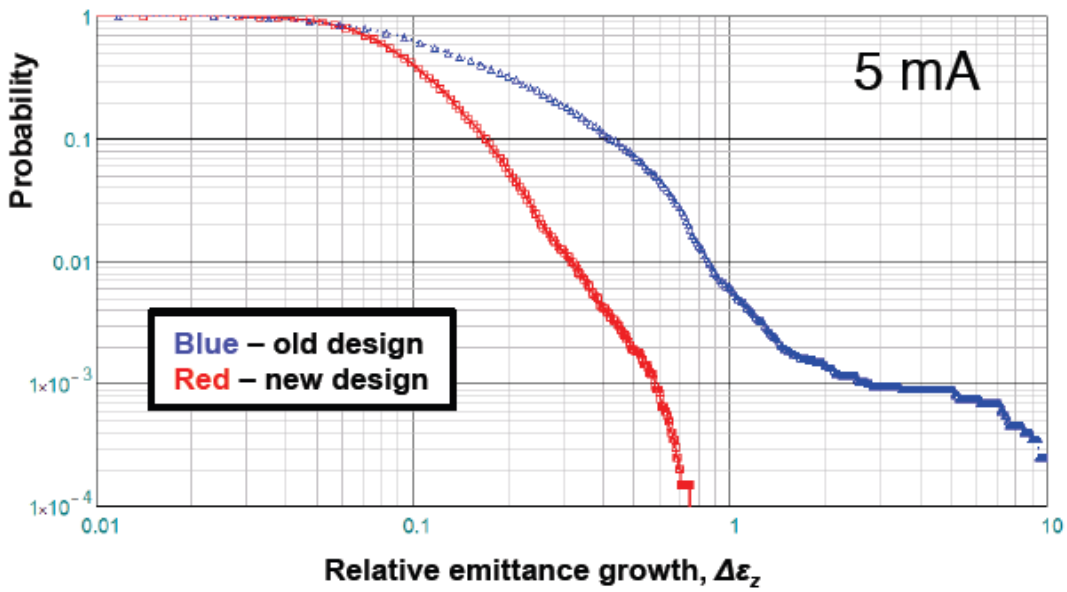
(R/Q) for HOM modes depends on the particle velocity β (650 MHz, $\beta=0.9$ cavity)

Variation of Q_{load} for 5th passband (650 MHz, $\beta=0.9$ cavity)



Resonance excitation of HOMs in elliptical SRF cavities (cont)

- Longitudinal emittance dilution does not take place if $\delta f \gg f \frac{\tilde{I}(R/Q)\sigma_t}{4\sqrt{2}\epsilon_z}$
 For typical parameters for proton linacs $\delta f \gg 10-100$ Hz.
- Transverse emittance dilution does not take place if $\delta f \ll \frac{cx_0\tilde{I}(R/Q)_1}{8\sqrt{2}\pi\beta\gamma U_0\sqrt{\epsilon/\beta_f}}$ **Not an issue!**
 For typical parameters for proton linacs $\delta f \gg 1-10$ Hz.



PIP II SRF linac

Cryo load caused by HOMS



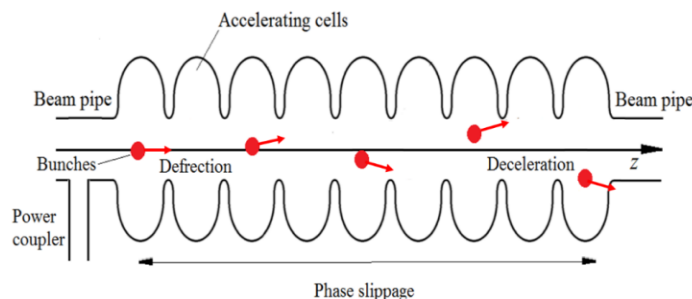
Resonance excitation of HOMs in elliptical SRF cavities (cont)

□ Regenerative instability, transverse (BBU):

- Regenerative BBU develops in one cavity and requires feedback; in SRF multi-cell cavities this feedback is caused by dipole partial travelling waves reflections from the cavity ends, which compose a HOM standing wave.
- The excitation mechanism :
 - Transverse kick in the beginning of the cavity; the $U_{kick} \sim V_{HOM}$, V_{HOM} is the HOM amplitude.
 - Deflecting in the cavity; deflection $x \sim V_{HOM}$
 - Phase slippage \rightarrow deceleration in the cavity end, $P_{beam} \sim x I_{beam} V_{HOM} \sim I_{beam} (V_{HOM})^2$
 - Instability condition: average power lost by the beam is equal or less to the loss power P_{loss} in the cavity: $P_{loss} \sim (V_{HOM})^2 / (r_{\perp} / Q \cdot Q_{load})$:

$$\langle P_{beam} \rangle = P_{loss} \quad (1)$$

- It gives the critical beam current: $I_{crit} = \kappa / (r_{\perp} / Q \cdot Q_{load})$. κ depends on the beam velocity and HOM field distribution, it is determined numerically. **It does not depend on the relationship between the HOM frequency and bunch spectrum line! “Instability selects its own frequency”**



For ultra-relativistic beam*:

$$I_{crit} \gtrsim \frac{\pi^3 p c / e}{2 k_{HOM} L \left(\frac{r_{\perp}}{Q} \right) Q_{load}}$$

*R.L. Gluckstern and H.S. Butler, “Transverse Beam Blow-Up in a Standing Wave Linac Cavity,” IEEE Transactions on Nuclear Science, vol. 12N, No3, 1965, pp. 605 – 612.

Resonance excitation of HOMs in elliptical SRF cavities (cont)

□ Regenerative instability, longitudinal (monotronic):

- The excitation mechanism :

- Velocity modulation in the beginning of the cavity; $\Delta\beta \sim V_{HOM}$, V_{HOM} is the HOM amplitude.

- Bunching in the cavity at the HOM frequency; the current harmonic $I_{HOM} \sim \Delta\beta I_{beam} \sim V_{HOM} I_{beam}$

- Phase slippage \rightarrow deceleration in the cavity end, $P_{beam} \sim I_{HOM} V_{HOM} \sim I_{beam} (V_{HOM})^2$

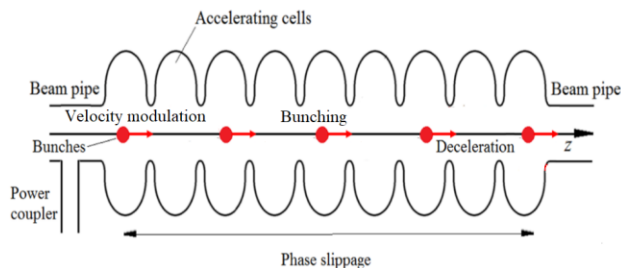
- Instability condition: average power lost by the beam is less or equal to the loss power P_{loss} in the cavity: $P_{loss} \sim (V_{HOM})^2 / (R/Q \cdot Q_{load})$:

$$\langle P_{beam} \rangle = P_{loss} \quad (2)$$

- It gives the critical beam current: $I_{crit} = \kappa_{||} / (R/Q \cdot Q_{load})$. $\kappa_{||}$ depends on the beam velocity and HOM field distribution, it is determined numerically from (2).

- **Similar to BBU, it does not depend on the relationship between the HOM frequency and bunch spectrum line! “Instability selects its own frequency”**

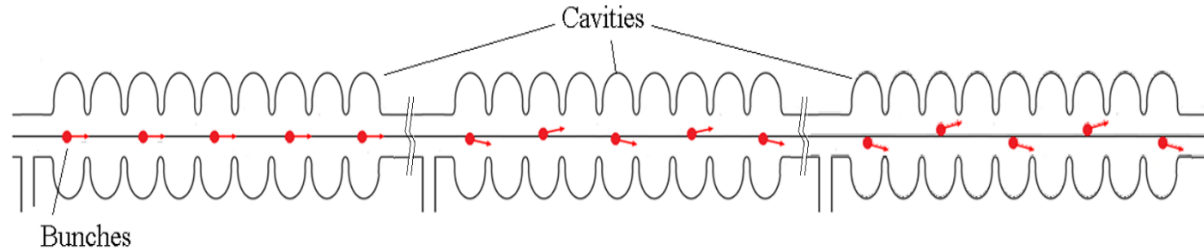
- **Typically, in proton accelerators I_{crit} is > 1 A. But it should be always checked!**



Resonance excitation of HOMs in elliptical SRF cavities (cont)

□ Cumulative BBU

- In contrast to regenerative BBU, cumulative BBU develops in the chain of the cavities.



- Mechanism:
 - Because of the initial transverse modulation on the beam, a dipole HOM is excited in the first accelerator cavity, which in turn provides transverse momentum modulation of the later bunches.
 - As a result, transverse momentum modulation converts in the downstream cavities to displacement modulation exciting there the dipole HOM, which in turn lead to further transverse displacement modulation, and therefore to the beam transverse emittance dilution, or even to the beam lost.
- The effect is coherent and cumulative as a function of length and time. As well as the regenerative instability, the cumulative instability is determined by the beam current I_{beam} and the cavity HOM parameters: resonance frequency f_{HOM} , transverse impedance r_{\perp}/Q and Q_{load} .

Resonance excitation of HOMs in elliptical SRF cavities (cont)

Why collective effects is not an issue for SRF proton linacs with elliptical cavities:

- No feedback as in ERLs (or CEBAF);
- Different cavity types with different frequencies and different HOM spectrum are used;
- Frequency spread of HOMs in each cavity type, caused by manufacturing errors;
- Velocity dependence of the (R/Q);
- Small – compared to electron linacs -beam current.

- No HOM dampers in SNS upgrade cavities ($I_{\text{beam}} = 26 \text{ mA}$);
- No HOM dampers in ESS cavities ($I_{\text{beam}} = 50 \text{ mA}$);
- No HOM dampers in PIP II cavities (I_{beam} up to 5 mA);
- Probably, HOM dampers will be necessary for future high – current drivers for ADS.

$$U_{\text{kick}} = i x_0 I_0 Q_{\text{ext}} \left(\frac{r_{\perp}}{Q} \right)$$

- Alignment!

Summary:

- ❑ Accelerated beam excites RF field in the cavity, which should be compensated by the RF source'
- ❑ The required power is determined by the beam current, voltage, cavities R/Q, loaded Q, cavity detune and the synchronous phase. There is the optimal coupling which provides minimal input power.
- ❑ Ultra-relativistic bunch radiates the field in the cavity, which may cause energy spread and transverse instability. Short-range wake changes the beam dynamics in the same bunch.
- ❑ Loss factor and kick factor limit the cavity aperture, that should be taken into account during the cavity design.
- ❑ Long-range wakes (= HOMs) may affect the beam dynamics (cumulative instabilities). The cavity should be optimized to get rid of trapped modes, and modes with high R/Q and Q_{load} . For proton linacs (pulsed and CW) HOMs typically are not the issue; for electron SRF linacs HOMs should be damped.
- ❑ Proper cavity alignment should be provided to mitigate or get rid of cumulative instabilities.

RF Accelerating Structures

Outline:

- 10. Architecture of SRF accelerators;
- 11. SRF around the world.

Chapter 10.

Architecture of SRF accelerators.

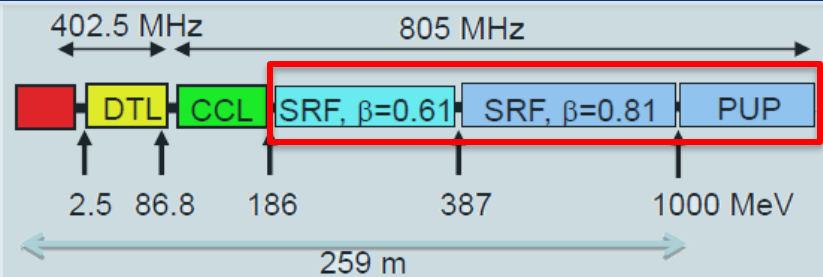
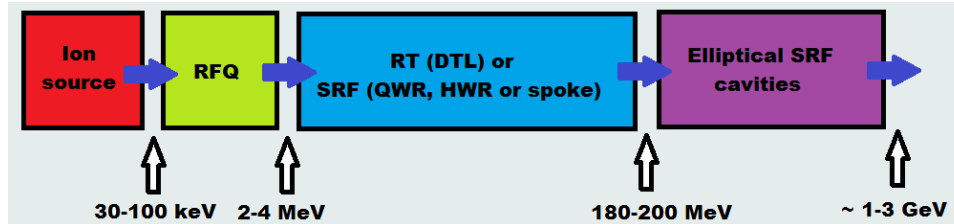
a. proton/ion SRF linacs:

- RT or SRF front end?
- choice of beamline elements;
- lattice design.

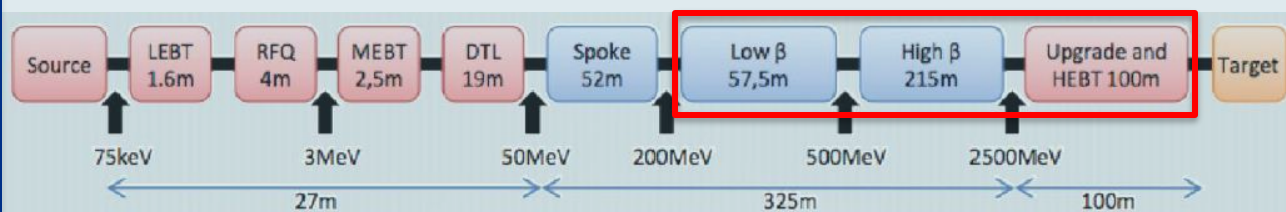
b. electron SRF linacs.

Architecture of a GeV-range proton SRF accelerator:

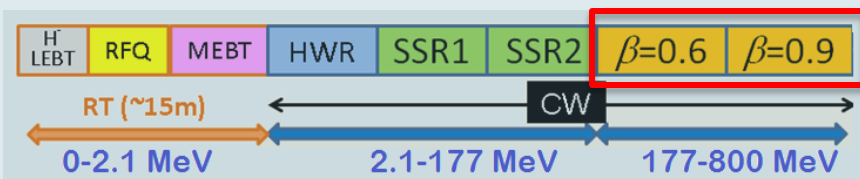
Layout of typical modern proton SRF accelerator.



SNS (ORNL): H^- , 1 GeV, 6% DF, 1.44 MW to accumulator ring
In operation



ESS (Lund): p^+ , 2.5 GeV, 4% DF, 5 MW to target
Under construction



PIP II (FNAL): H^- , 800 MeV, up to 100% DF, up to 1.6 MW
Design

Linac Design Philosophy:

❑ RT or SRF frontend?

- For low duty factor RT frontend (up to ~200 MeV) may be used
- For high DF or CW SRF is necessary from the beginning

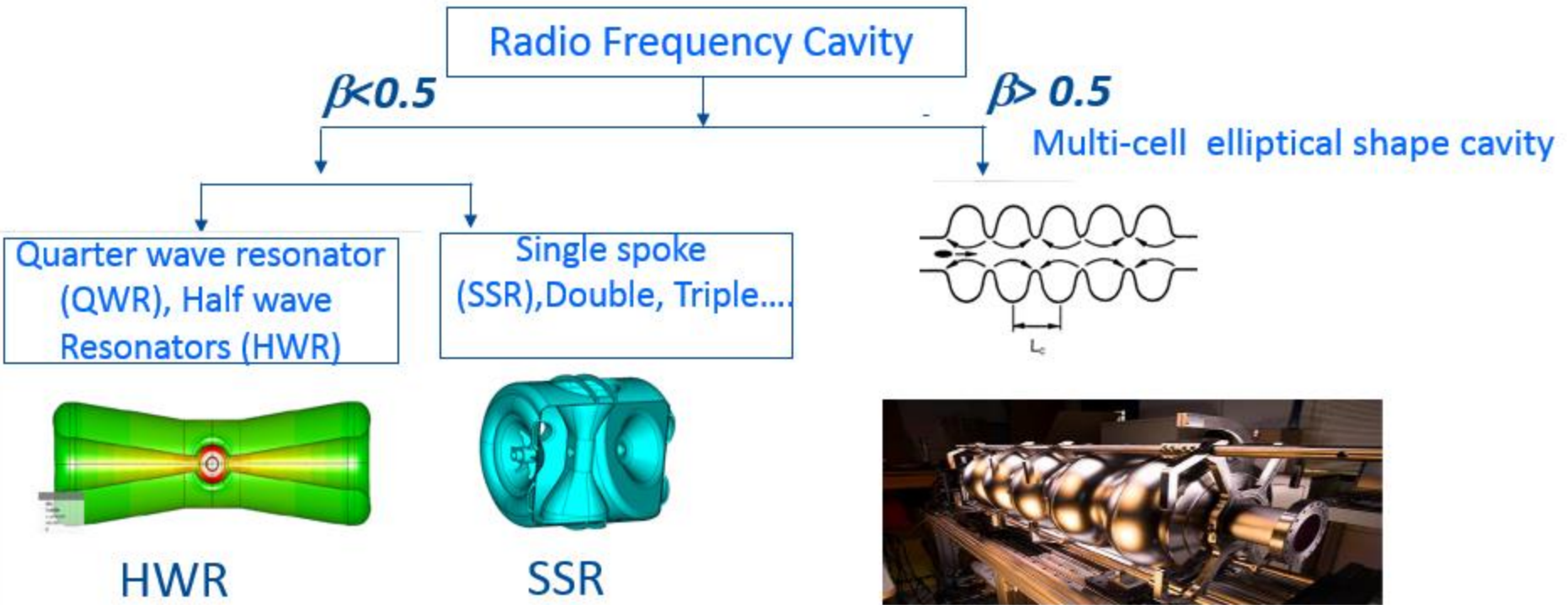
❑ Choice of beam line elements

- Accelerating RF Cavities
- Focusing Magnets

❑ Lattice Design

- Focusing Period
- Transition Energy between Sections

RF cavities:



- Lower RF frequency provides better interaction with beam.
- RF defocusing factor is inversely proportional to frequency.
- Lower frequency implies larger RF bucket and hence larger longitudinal acceptance.

RF cavities:

□ The frequency choices for multi-cell:

- Cavity length is about the same for the same β_G (the same number of couplers, tuners, etc). Typical length $\sim 0.8-1$ m depending on β_G (from iris to iris)
- Lower frequencies \rightarrow bigger size, higher cost, more difficult handling, microphonics but: lower losses per unit length (smaller R/Q , but lower R_s); larger aperture (current interception), smaller beam defocusing; smaller number of cells and therefore, smaller a/λ , smaller K_m and K_e and smaller numbers of cavity types.
- Typically , they use 650 – 800 MHz, and 5-7 cells/cavity:
 - SNS: 804 MHz, 6 cells/cavity (in operation)
 - ESS: 704 MHz, 5 cells/cavity (under construction)
 - PIP II: 650 MHz, 5 cells/cavity (under development)

□ The frequency choices for the front end:

- Subharmonics of the main frequency.

□ Acceleration gradient choice (high DF, CW):

- Quench, $B_{\text{peak}} \approx 70-80$ mT
- Field emission, $E_{\text{peak}} \approx 40$ MV/m
- Thermal breakdown typically is not an issue for proton linacs.

RF cavities:

- Selection of the maximum accelerating gradients in cavities are made on the basis of :
 - Peak surface magnetic field
 - Peak surface Electrical field
- Choices of peak magnetic fields are derived from:
 - Dynamics heat load due to accelerating mode
 - Cavity quenching.
- Choices of peak surface field is made to avoid field emission

CW Linac assumptions:

- 162.5 MHz: $H_{pk} < 50\text{mT}$
- 325 MHz: $H_{pk} < 60\text{mT}$
- 650 MHz: $H_{pk} < 70\text{mT}$
- $E_{pk} < 40 \text{ MV/m}$.

Accelerating Gradient in PIP-II Linac

	HWR	SSR1	SSR2	LB650	HB650
Gradient (MV/m)	9.7	10	11.4	15.9	17.8

Focusing elements:

- ❖ Normal conducting magnets are cheaper but superconducting magnets are:
 - Compact in size
 - Provide intense magnetic field with low power consumption.
- ❖ Low energy part of SRF linac typically has solenoidal focusing:
 - ❖ Provide radial focusing
- ❖ Intermediate and high energy section of linac use normal conducting doublet focusing.
 - ❖ Simplify cavity magnetic shielding requirements
- ❖ Correctors are built in each magnets.
- ❖ Solenoidal and doublet focussing keeps the beam round in transverse planes.

- *Focusing magnets in each section*

<u>Section</u>	HWR	SSR1	SSR2	LB650	HB650
<u>Magnet</u>	S	S	S	FD	FD

S – solenoid, FD – doublet (F : focusing and D: Defocusing quadrupole).

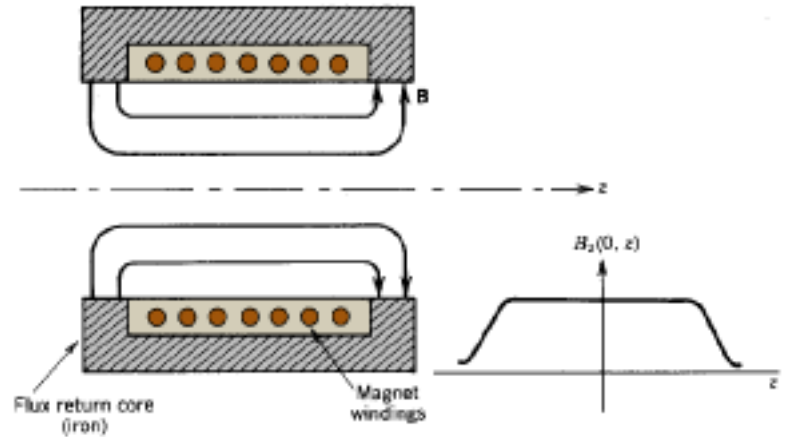
Focusing elements:

□ Solenoid:

Solenoid focal length f :
(non-relativistic case, T is a particle kinetic energy, $T=mv^2/2$.)

$$\frac{1}{f} = \frac{q^2}{8Tm} \int B_z^2 dz$$

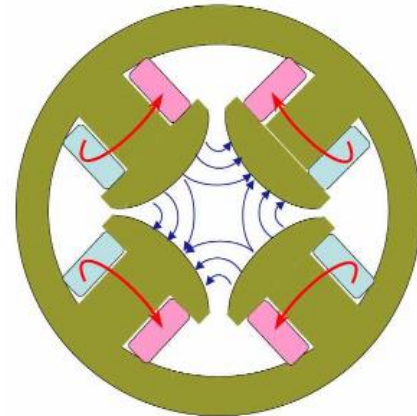
- Focal length is proportional to β^2 ;
- Focal length is inversed proportional to $B_z^2 L$, L is the solenoid length;
- Therefore, solenoid can be used for low β ($\beta < 0.5$). For higher β quad is used.



□ Quadrupole lens:

Quad focal length f :

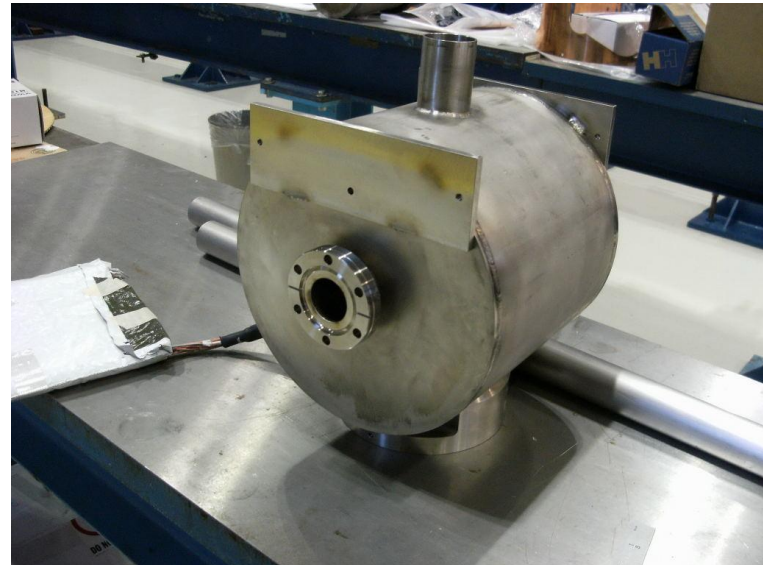
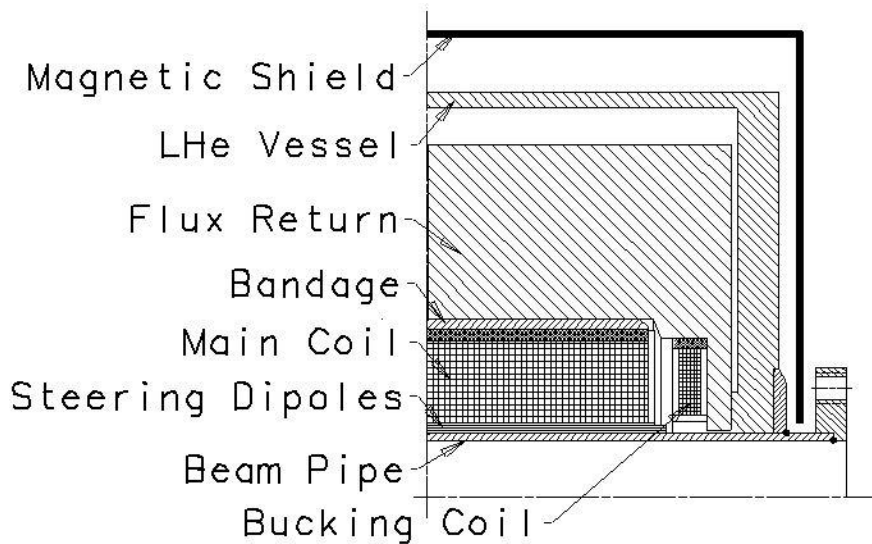
$$\frac{1}{f} = \frac{qB'L}{\gamma\beta mc^2}$$



Focusing elements:

For low section SC solenoids are used.

- Simple and inexpensive;
- Filed up to 6-8 T;
- SRF cavity should have < 10 mT on the SRF cavity surface: remnant solenoid field should be compensated
- Solenoid contains correction coils (steering dipoles)
- Alignment (typically < 0.3 - 0.5 mm, < 5 mrad tilt);
- Quench protection;
- Leads

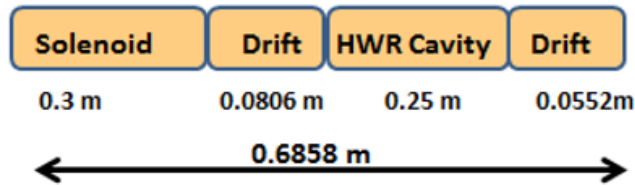


Lattice Design: Focusing Periods

- Length of the focusing period is kept short, especially in the low energy section where beam is non-relativistic and non-linear force may be significant.

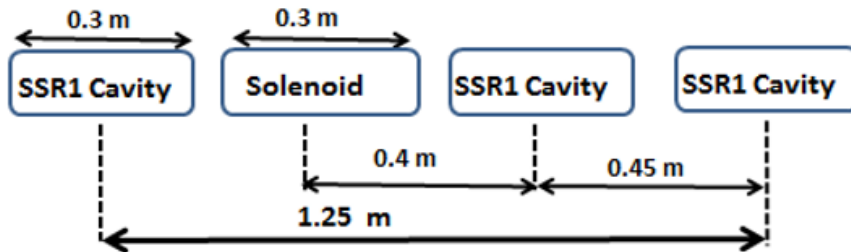
Cryomodule Arrangement

HWR Section :



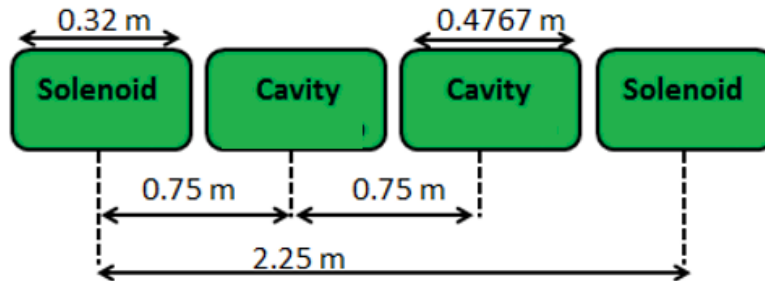
SC-SC-SC-SC-SC-SC-SC-SC

SSR1 Section :



CSC-CSC-CSC-CSC

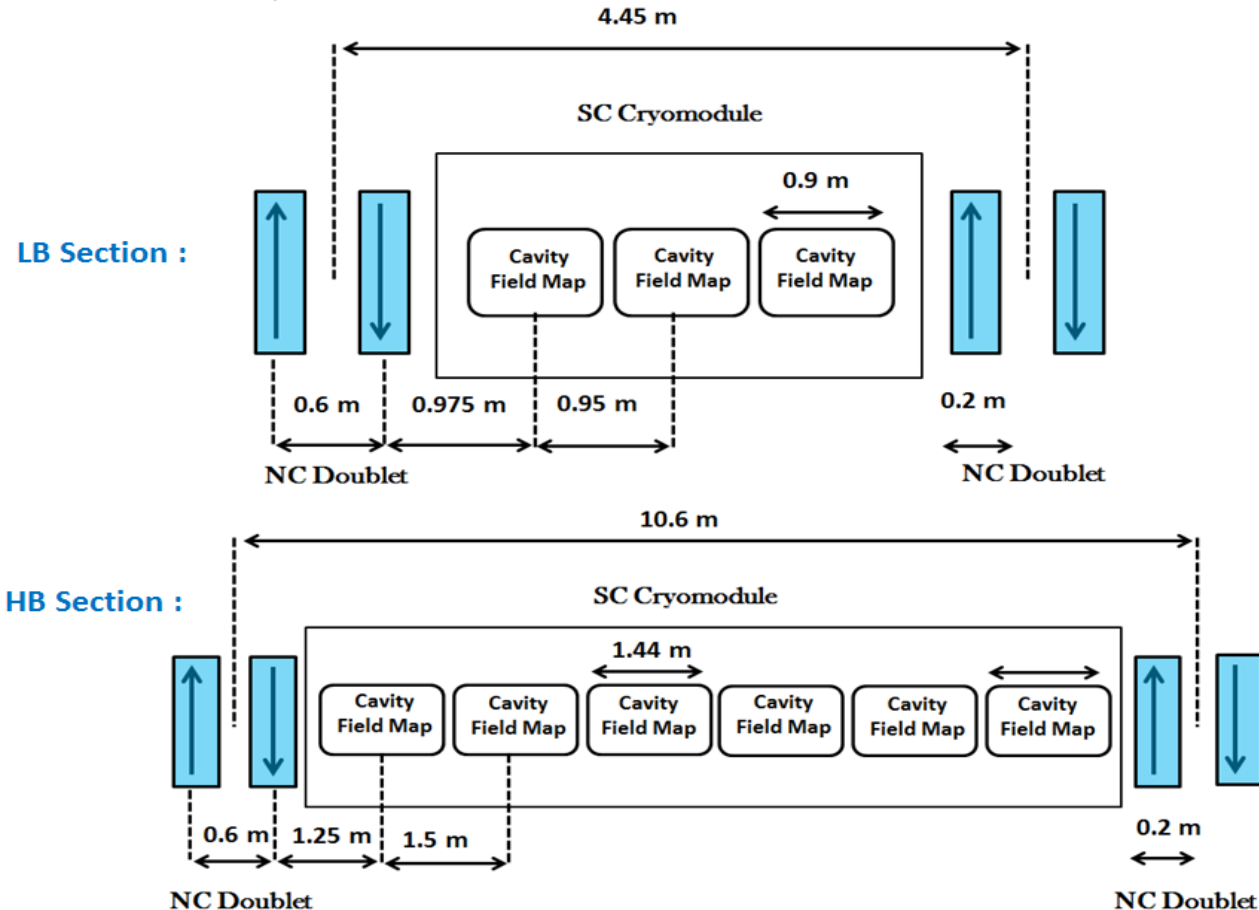
SSR2 Section :



SCC-SCC-SC

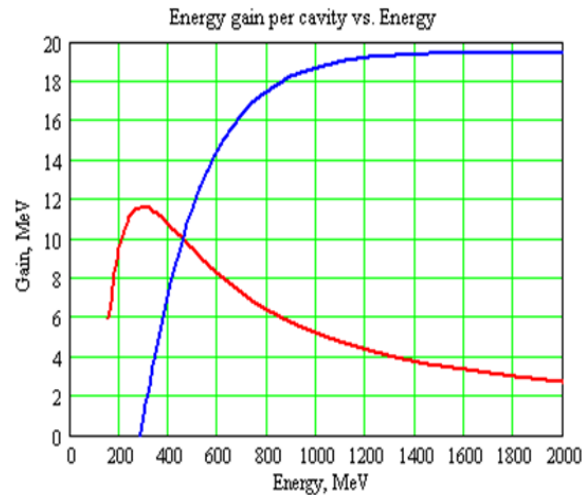
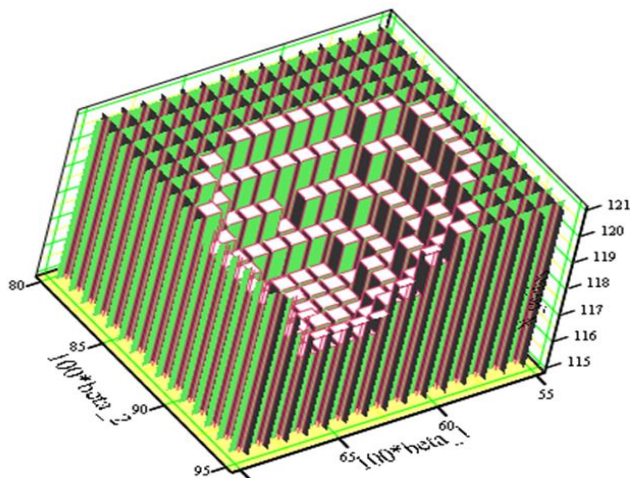
Lattice Design: Focusing Period in High Energy Section

- Frequency jump from 325 MHz to 650 MHz at LB650 MHz section
- Solenoidal focusing is replaced with quadrupole doublet.
- Same family of doublet is used in both LB650 and HB650 sections.



Transition Energy between Sections :

- Transition Energy between Sections (type cavity change). Optimization in order to minimize the number of cavities.
- Beam matching between sections and cryomodules are achieved using elements of each side of transitions. Avoiding abrupt changes in beam envelopes to reduce possibility of halo formations.
- Adiabatic variation in phase advance along linac. Reduces possibility of beam mismatch.

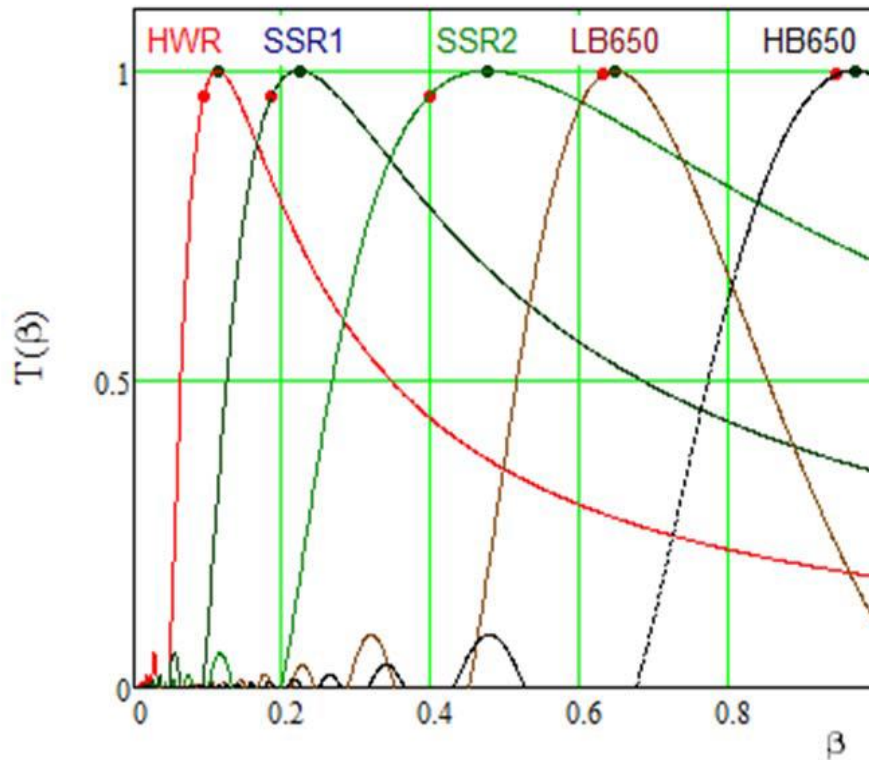


Number of cavities required for acceleration from 185 to 800 MeV versus cavity beta in the LB650 and HB650 sections (left) and the energy gain per cavity versus particle energy (right) for LB650 (red curve) and HB650 (blue curve) cavities.

Architecture of a GeV-range proton SRF accelerator:

Correct selections of transitional energy provide better optimization of real estate gradient and reduction in total number of beam line elements.

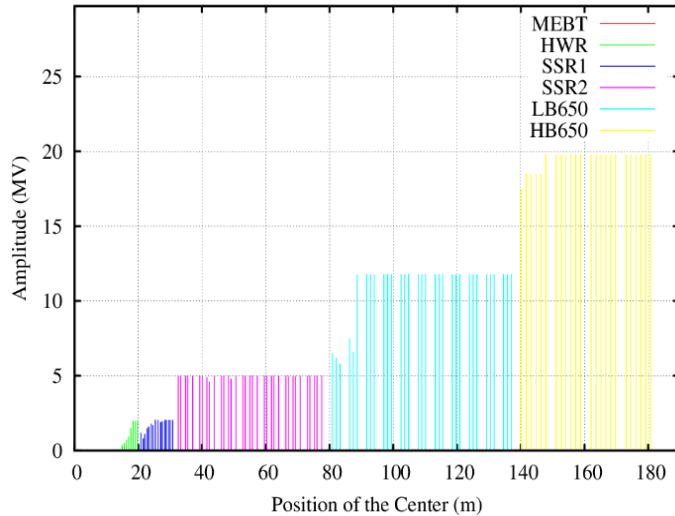
Transition time factor v/s beta



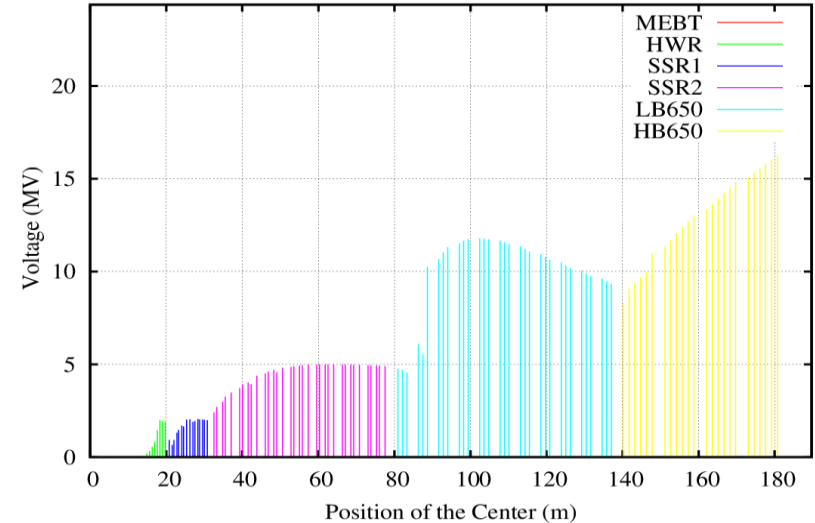
Sections	Initial Energy (MeV)	Design Beta	Beta range
HWR	2.1	0.094	0.067 -0.147
SSR1	10.3	0.186	0.147-0.266
SSR2	35	0.398	0.266-0.55
LB 650	185	0.61	0.55-0.758
HB 650	500	0.92	0.758-0.842

Acceleration voltage distribution

Voltage Amplitude in Cavities

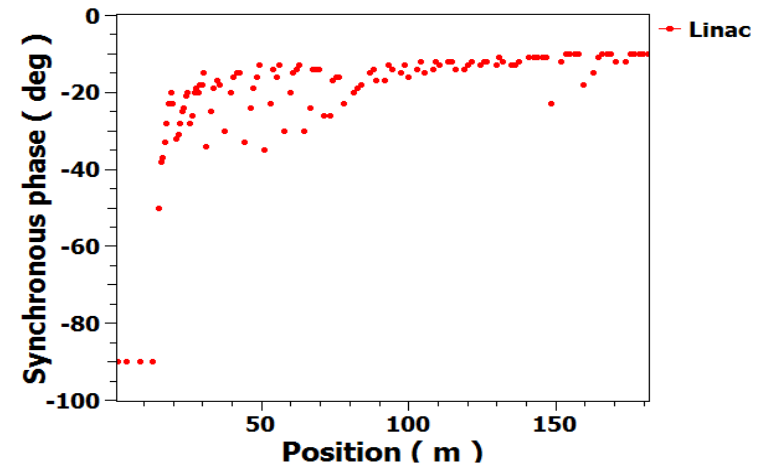


Voltage gain by beam



- Maximum Energy gain in PIP-II SC cavities

	HWR	SSR1	SSR2	LB650	HB650
Max. Egain (MeV)	2	2.05	5	11.9	19.9



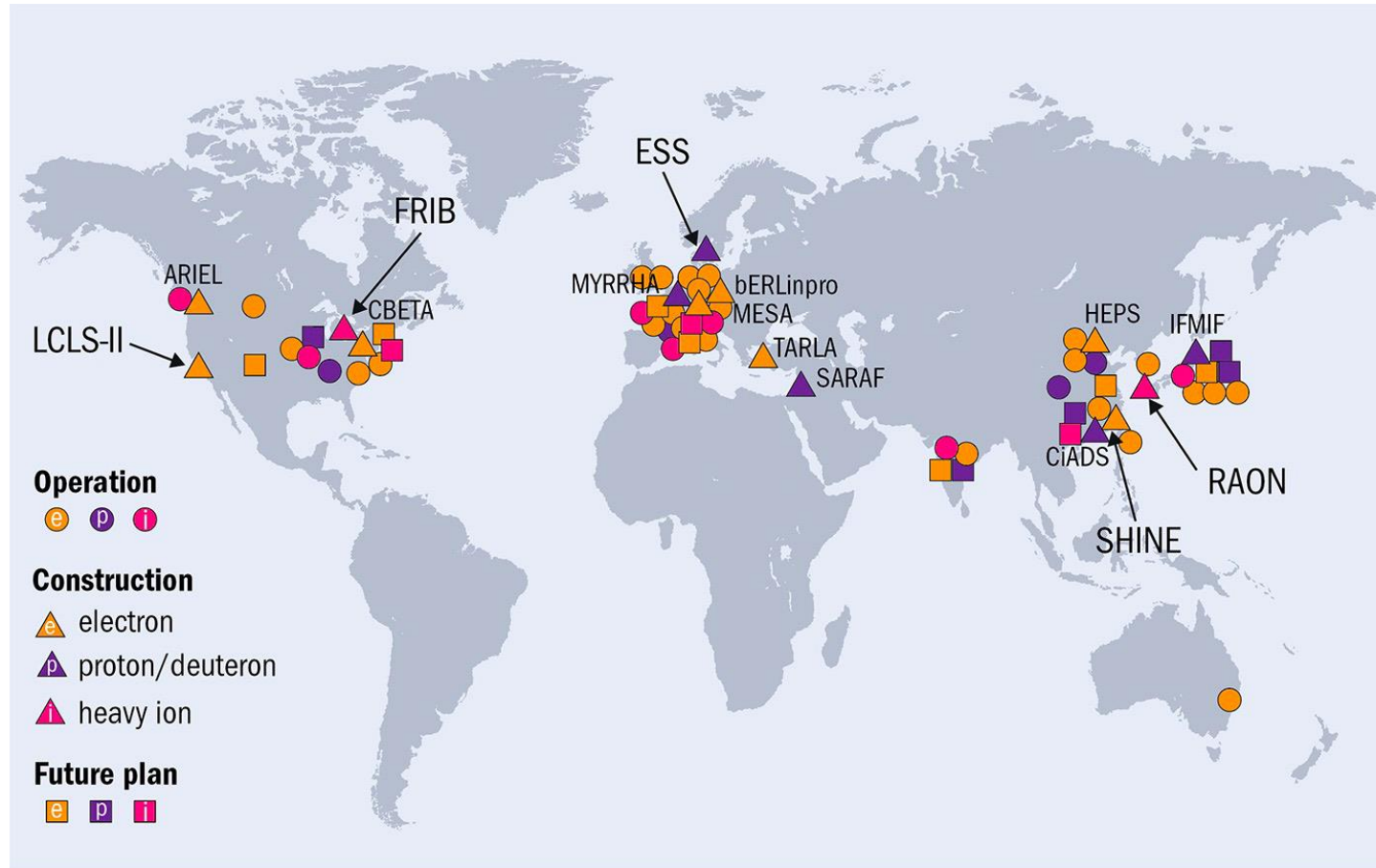
Summary:

- ❑ Architecture of a big SRF linac is determined by:
 - accelerated particles – electrons, protons or ions;
 - accelerator operation regime – pulsed or CW;
 - accelerator parameters – energy and power.
- ❑ For a proton accelerator the choice of the front end – RT or SRF – depends on the operation regime, pulsed or CW.
- ❑ The frequencies and cavity types for a proton or an ion accelerator should be determined;
- ❑ The types of the focusing elements should be selected.
- ❑ The lattice should be designed, which provides
 - acceleration
 - focusing
 - bunching.
- ❑ Break points between the section with different cavity types should be optimized;
- ❑ The sections should be matched to each other to provide required beam quality.

Chapter 11.

SRF around the world

SRF around the world



Global view Distribution of superconducting particle accelerators using SRF structures for electrons (orange), protons (purple) and heavy ions (pink). More than 30 SRF accelerators are in operation (circles), approximately 15 are presently under construction (triangles) and more than 10 future projects are under consideration (squares). *Credit: CERN*

Big SRF Accelerator Facilities:

Linac	Laboratory	Application	Acc. Particle	Operation	Status
SNS	ORNL, USA	Neutron Source	H⁻	pulsed	Operation
ESS	ESS, Sweden	Neutron Source	p	pulsed	Construction
CIADS	IMP, China	ADS	p	CW	R&D
ISNS	Indore, India	Neutron Source	p	pulsed	R&D
ADSS	BARC, India	ADS	p	CW	R&D
PIP II	FNAL, USA	Neutrino/Muons	H ⁻	CW/pulsed	Construction
FRIB	MSU, USA	Nucellar physics	Ions	CW	Operation
RAON	RISP, S.Korea	Nucellar physics	Ions	CW	Construction
CEBAF	JLAB, USA	Nucellar physics	e⁻	CW	Operation
XFEL	DESY, Germany	FEL	e⁻	pulsed	Operation
SHINE	SINAP, China	FEL	e ⁻	CW	Construction
LCLS II	SLAC, USA	FEL	e ⁻	CW	Construction

New large SRF accelerator installations

CEBAF Upgrade - JLAB Upgrade 6.5 GeV => 12 GeV electrons	80 cavities	Electrons
XFEL – Hamburg, Germany 17.5 GeV electrons – Pulsed X-ray FEL	840 cavities	
LCLS-II (+ LCLS-II-HE) – SLAC 4 GeV electrons – CW X-ray FEL	296 (+184) cavities	
SPIRAL-II – France 30 MeV, 5 mA protons -> Heavy Ions	28 cavities	Ions
FRIB – MSU 400 kW, heavy ion beams for nuclear astrophysics	340 cavities	
RISP - Daejeon, South Korea 400 kW, heavy ion beams for nuclear astrophysics	340 cavities	
ESS – Sweden 1 – 2 GeV, 5 MW Pulsed spallation source	150 cavities	Protons
PIP-II – Fermilab 800 MV High intensity proton linac for neutrino beams	115 cavities	

Coming up: *SHINE* in China, *EIC* at BNL, *ILC* in Japan, *FCC-ee/FCC-hh* at CERN, *CEPC-SPPC* in China, *Accelerator complex upgrade to 2.4 MW* at Fermilab

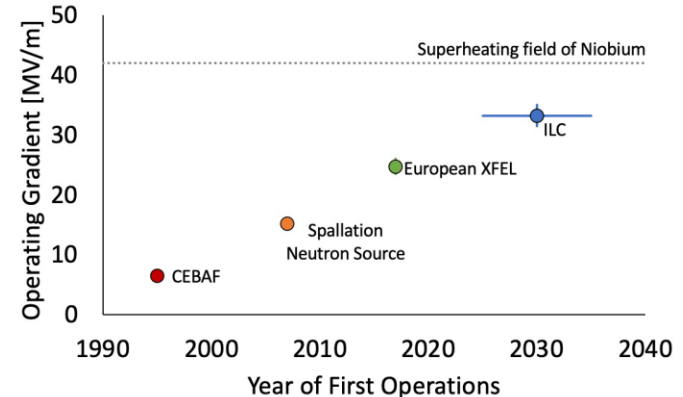
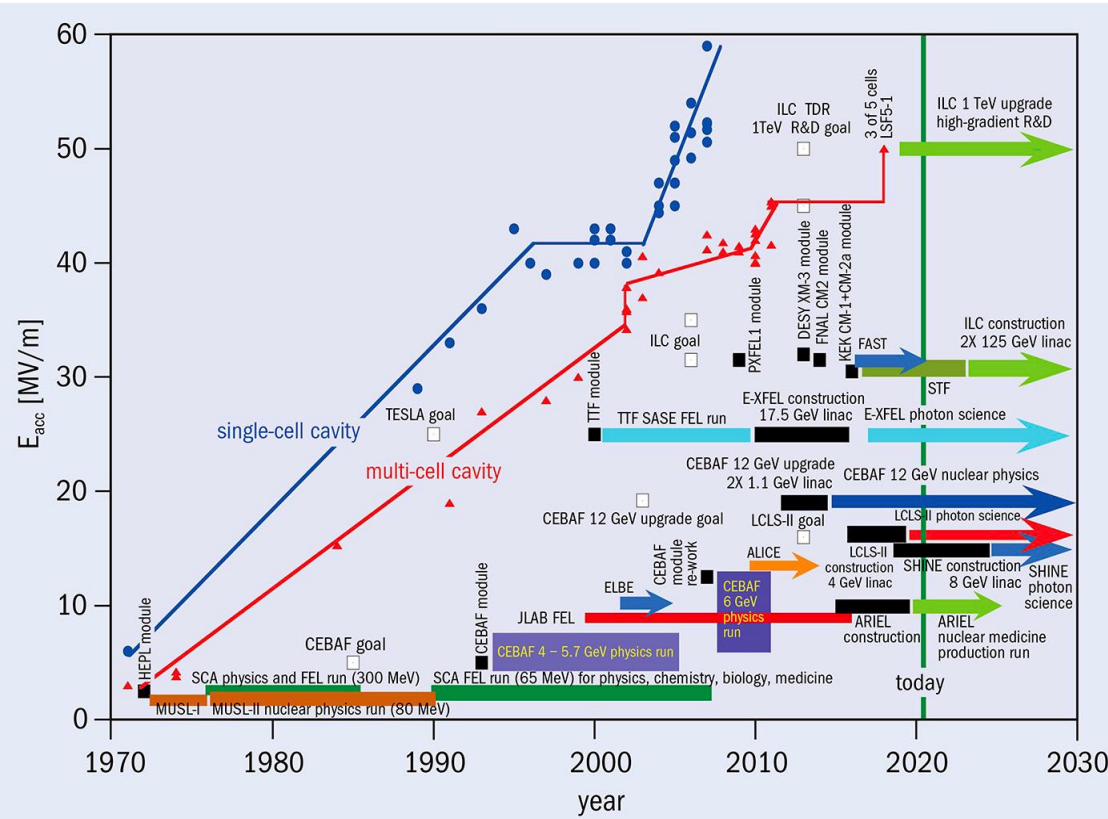
SRF gradient achievements and applications

Gradient growth SRF linac accelerating gradient achievements and application specifications since 1970.

CW SRF Linacs – SCA: Stanford Superconducting Accelerator; MUSL: Illinois Microtron Using a Superconducting Linac; CEBAF: Continuous Electron Beam Accelerator Facility; JLab FEL: JLab Free Electron Laser; ELBE: HZDR Electron Linear accelerator with high Brilliance and Low Emittance; ALICE: STFC Accelerators and Lasers In Combined Experiments; ARIEL: TRIUMF Advanced Rare Isotope Laboratory; LCLS-II:

Linac Coherence Light Source extension; SHINE: Shanghai High Brightness Photon Facility.

Pulsed SRF Linacs – FAST: Fermilab Accelerator Science and Technology Facility; STF: KEK Superconducting RF Test Facility; E-XFEL: European X-ray Free Electron Laser; ILC: International Linear Collider.



Credit: Source: R Geng/ORNL



Fermilab PIP-II



(115 Cavities)



Half Wave



Spokes

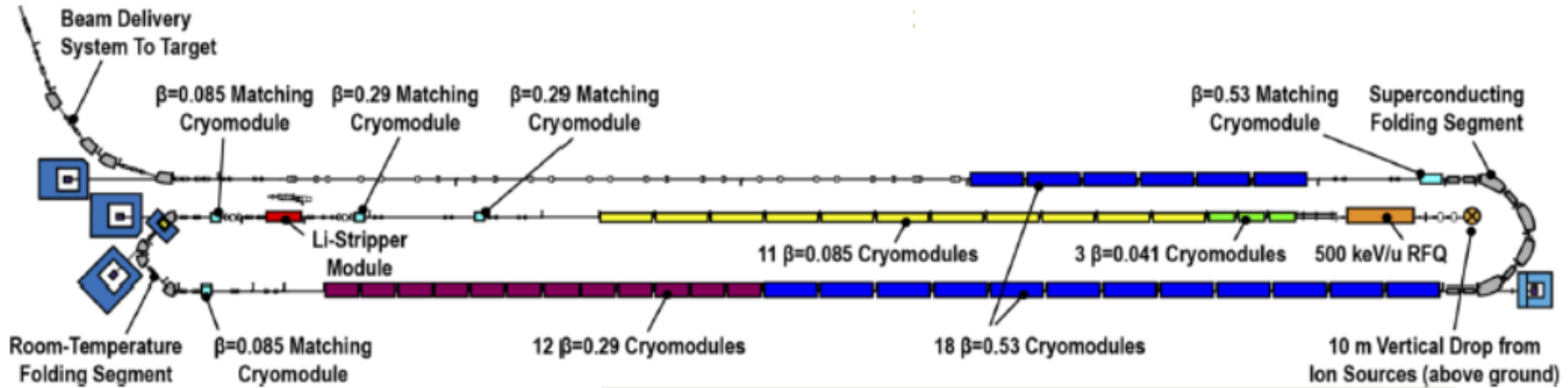


Medium-Beta Elliptical Cavities

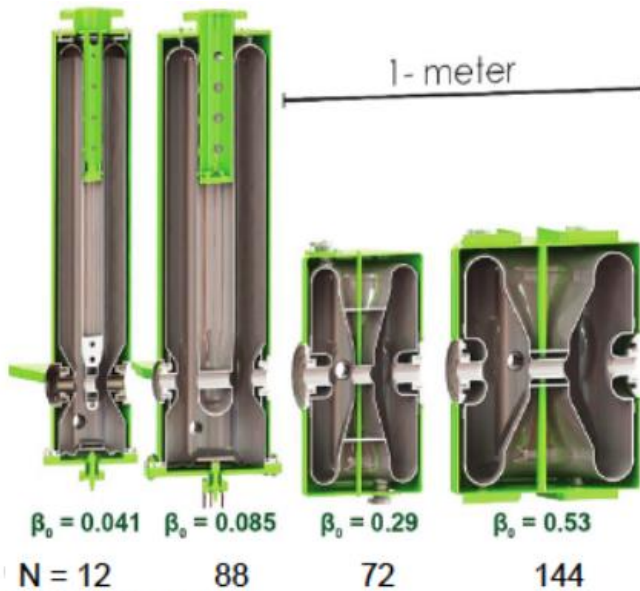


High-Beta Elliptical Cavities

Architecture of Facility for Rare Isotope Beams (FRIB, MSU)



K. Saito, September 2014 LINAC14 THIOA02,



316 cavities need,
total 347 including matching module, spares

FRIB cavities

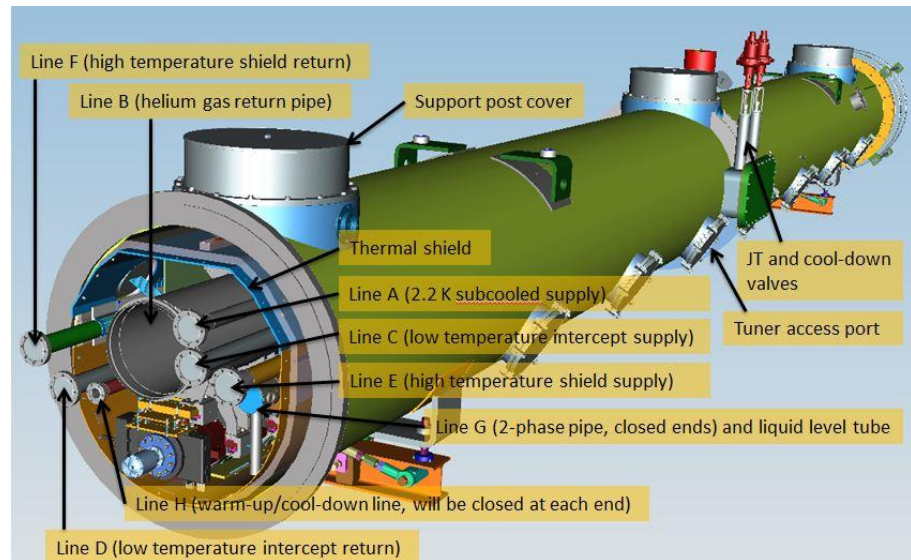
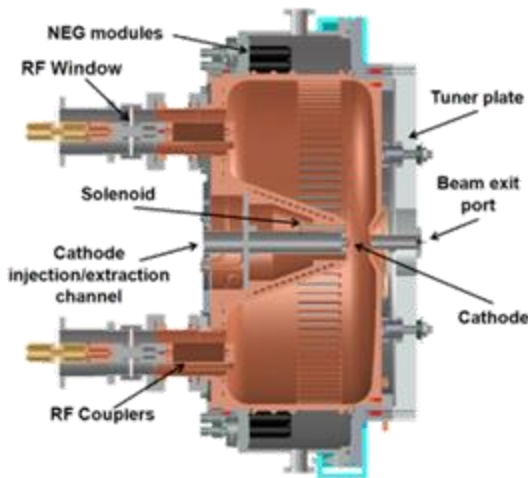
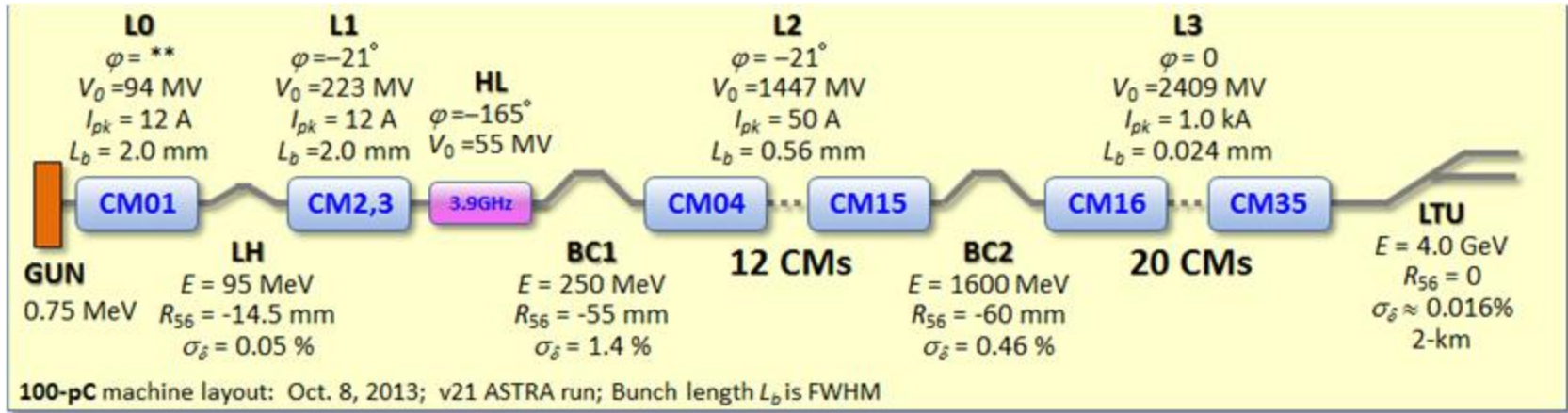
Cavity Type	QWR	QWR	HWR	HWR
β_0	0.041	0.085	0.285	0.53
f [MHz]	80.5	80.5	322	322
V_a [MV]	0.810	1.80	2.09	3.70
E_{acc} [MV/m]	5.29	5.68	7.89	7.51
E_p/E_{acc}	5.82	5.89	4.22	3.53
B_p/E_{acc} [mT/(MV/m)]	10.3	12.1	7.55	8.41
R/Q [Ω]	402	455	224	230
G [Ω]	15.3	22.3	77.9	107
Aperture [m]	0.036	0.036	0.040	0.040
$L_{eff} \equiv \beta\lambda$ [m]	0.153	0.317	0.265	0.493
Lorenz detuning [Hz/(MV/m) ²]	< 4	< 4	< 4	< 4
Specific $Q_0@VT$	1.4E+9	2.0E+9	5.5e+9	9.2E+9
Q_L	6.3E+6	1.9E+6	5.6E+6	9.7E+6

FRIB linac is successfully commissioned in May 2021!



5-cell 644 MHz cavities for FRIB upgrade

Architecture of LCLS II (electron SRF Linac for FEL)



European XFEL

View Along the 1 km Long
Superconducting Accelerator

- EXFEL is the world largest SRF application at 17.5 GeV (800 cavities).
- Operating gradient is 23.5 MV/m.
- Construction is complete, commissioning has started.
- First lasing in May 2017!

IPAC '17, 15.5.2017
Winnl Decking, DESY



Επιλογος

“The internal machinery of life, the chemistry of the parts, is something beautiful. And it turns out that all life is interconnected with all other life.”
Richard Feynman

- ❖ SRF Liner Accelerator is self-consistent system, parts of it strongly depend on each other. Deep understanding and careful analysis of subsystems and components as well as their interaction are necessary to achieve required beam parameters and facility reliability at minimal capital and operation cost.
- ❖ The design process will never be reduced to just a few simple rules or recipes. Using an existing design as a base for developing a new system is OK and can shorten the new system development time, but the system designers should be aware that even seemingly small changes could bring big consequences.
- ❖ As accelerator application demands continue to increase (higher energy, higher luminosity, brighter beams, more efficient accelerators, ...) there will be no shortage of new challenges to tackle in the future.
- ❖ The field of RF superconductivity is very active. The SRF technology is the technology of choice for many types of accelerators.

There will always be ample opportunities for imagination, originality, and common sense.



The end

Appendixes

Appendix 1, Vector calculus

$\nabla \cdot (\psi \mathbf{A}) = \mathbf{A} \cdot \nabla \psi + \psi \nabla \cdot \mathbf{A}$	$\text{div}(\psi \mathbf{A}) = \mathbf{A} \cdot \text{grad} \psi + \psi \text{div} \mathbf{A}$
$\nabla \times (\psi \mathbf{A}) = \nabla \psi \times \mathbf{A} + \psi \nabla \times \mathbf{A}$	$\text{curl}(\psi \mathbf{A}) = \text{grad} \psi \times \mathbf{A} + \psi \text{curl} \mathbf{A}$
$\nabla(\mathbf{A} \cdot \mathbf{B}) = (\mathbf{A} \cdot \nabla) \mathbf{B} + (\mathbf{B} \cdot \nabla) \mathbf{A} + \mathbf{A} \times (\nabla \times \mathbf{B}) + \mathbf{B} \times (\nabla \times \mathbf{A})$	$\text{grad}(\mathbf{A} \cdot \mathbf{B}) = (\mathbf{A} \cdot \nabla) \mathbf{B} + (\mathbf{B} \cdot \nabla) \mathbf{A} + \mathbf{A} \times \text{curl} \mathbf{B} + \mathbf{B} \times \text{curl} \mathbf{A}$
$\frac{1}{2} \nabla A^2 = \mathbf{A} \times (\nabla \times \mathbf{A}) + (\mathbf{A} \cdot \nabla) \mathbf{A}$	$\frac{1}{2} \text{grad} A^2 = \mathbf{A} \times (\text{curl} \mathbf{A}) + (\mathbf{A} \cdot \nabla) \mathbf{A}$
$\nabla \cdot (\mathbf{A} \times \mathbf{B}) = \mathbf{B} \cdot \nabla \times \mathbf{A} - \mathbf{A} \cdot \nabla \times \mathbf{B}$	$\text{div}(\mathbf{A} \times \mathbf{B}) = \mathbf{B} \cdot \text{curl} \mathbf{A} - \mathbf{A} \cdot \text{curl} \mathbf{B}$
$\nabla \times (\mathbf{A} \times \mathbf{B}) = \mathbf{A}(\nabla \cdot \mathbf{B}) - \mathbf{B}(\nabla \cdot \mathbf{A}) + (\mathbf{B} \cdot \nabla) \mathbf{A} - (\mathbf{A} \cdot \nabla) \mathbf{B}$	$\text{curl}(\mathbf{A} \times \mathbf{B}) = \mathbf{A}(\text{div} \mathbf{B}) - \mathbf{B}(\text{div} \mathbf{A}) + (\mathbf{B} \cdot \nabla) \mathbf{A} - (\mathbf{A} \cdot \nabla) \mathbf{B}$

P.W.

*

Appendix 1. Vector calculus

$$\nabla\psi = \text{grad } \psi$$

$$\nabla \cdot \mathbf{A} = \text{div } \mathbf{A}$$

$$\nabla \times \mathbf{A} = \text{curl } \mathbf{A} \equiv \text{rot } \mathbf{A}$$

$$\Delta = \nabla^2 = \nabla \cdot \nabla$$

$$\nabla \times (\nabla\psi) = 0$$

$$\text{curl}(\text{grad } \psi) = 0$$

$$\nabla \cdot (\nabla \times \mathbf{A}) = 0$$

$$\text{div}(\text{curl } \mathbf{A}) = 0$$

$$\Delta \psi = \nabla \cdot (\nabla\psi) = \nabla^2 \psi$$

$$\Delta \psi = \text{div}(\text{grad } \psi)$$

$$\nabla \times \nabla \times \mathbf{A} = \nabla(\nabla \cdot \mathbf{A}) - \nabla^2 \mathbf{A}$$

$$\text{curl}(\text{curl } \mathbf{A}) = \text{grad}(\text{div } \mathbf{A}) - \Delta \mathbf{A}$$

$$\nabla = \frac{\partial}{\partial x} \vec{i} + \frac{\partial}{\partial y} \vec{j} + \frac{\partial}{\partial z} \vec{k},$$

$$\int \text{curl } \mathbf{F} \cdot d\mathbf{S} = \oint \mathbf{F} \cdot d\mathbf{l}, \quad \int \text{div } \mathbf{F} dV = \int \mathbf{F} \cdot d\mathbf{S}$$

Stokes theorem

Gauss theorem

Appendix 1. Vector calculus

Differential operators in different coordinates:

Cartesian

Cylindrical

Spherical

\mathbf{A}	$A_x \hat{\mathbf{x}} + A_y \hat{\mathbf{y}} + A_z \hat{\mathbf{z}}$	$A_\rho \hat{\boldsymbol{\rho}} + A_\varphi \hat{\boldsymbol{\varphi}} + A_z \hat{\mathbf{z}}$	$A_r \hat{\mathbf{r}} + A_\theta \hat{\boldsymbol{\theta}} + A_\varphi \hat{\boldsymbol{\varphi}}$
∇f	$\frac{\partial f}{\partial x} \hat{\mathbf{x}} + \frac{\partial f}{\partial y} \hat{\mathbf{y}} + \frac{\partial f}{\partial z} \hat{\mathbf{z}}$	$\frac{\partial f}{\partial \rho} \hat{\boldsymbol{\rho}} + \frac{1}{\rho} \frac{\partial f}{\partial \varphi} \hat{\boldsymbol{\varphi}} + \frac{\partial f}{\partial z} \hat{\mathbf{z}}$	$\frac{\partial f}{\partial r} \hat{\mathbf{r}} + \frac{1}{r} \frac{\partial f}{\partial \theta} \hat{\boldsymbol{\theta}} + \frac{1}{r \sin \theta} \frac{\partial f}{\partial \varphi} \hat{\boldsymbol{\varphi}}$
$\nabla \cdot \mathbf{A}$	$\frac{\partial A_x}{\partial x} + \frac{\partial A_y}{\partial y} + \frac{\partial A_z}{\partial z}$	$\frac{1}{\rho} \frac{\partial (\rho A_\rho)}{\partial \rho} + \frac{1}{\rho} \frac{\partial A_\varphi}{\partial \varphi} + \frac{\partial A_z}{\partial z}$	$\frac{1}{r^2} \frac{\partial (r^2 A_r)}{\partial r} + \frac{1}{r \sin \theta} \frac{\partial}{\partial \theta} (A_\theta \sin \theta) + \frac{1}{r \sin \theta} \frac{\partial A_\varphi}{\partial \varphi}$
$\nabla \times \mathbf{A}$	$\begin{pmatrix} \frac{\partial A_z}{\partial y} - \frac{\partial A_y}{\partial z} \\ \frac{\partial A_x}{\partial z} - \frac{\partial A_z}{\partial x} \\ \frac{\partial A_y}{\partial x} - \frac{\partial A_x}{\partial y} \end{pmatrix} \begin{matrix} \hat{\mathbf{x}} \\ \hat{\mathbf{y}} \\ \hat{\mathbf{z}} \end{matrix} +$	$\begin{pmatrix} \frac{1}{\rho} \frac{\partial A_z}{\partial \varphi} - \frac{\partial A_\varphi}{\partial z} \\ \frac{\partial A_\rho}{\partial z} - \frac{\partial A_z}{\partial \rho} \\ \frac{1}{\rho} \left(\frac{\partial (\rho A_\varphi)}{\partial \rho} - \frac{\partial A_\rho}{\partial \varphi} \right) \end{pmatrix} \begin{matrix} \hat{\boldsymbol{\rho}} \\ \hat{\boldsymbol{\varphi}} \\ \hat{\mathbf{z}} \end{matrix} +$	$\begin{matrix} \frac{1}{r \sin \theta} \left(\frac{\partial}{\partial \theta} (A_\varphi \sin \theta) - \frac{\partial A_\theta}{\partial \varphi} \right) \hat{\mathbf{r}} + \\ \frac{1}{r} \left(\frac{1}{\sin \theta} \frac{\partial A_r}{\partial \varphi} - \frac{\partial}{\partial r} (r A_\varphi) \right) \hat{\boldsymbol{\theta}} + \\ \frac{1}{r} \left(\frac{\partial}{\partial r} (r A_\theta) - \frac{\partial A_r}{\partial \theta} \right) \hat{\boldsymbol{\varphi}} \end{matrix}$
$\Delta f = \nabla^2 f$	$\frac{\partial^2 f}{\partial x^2} + \frac{\partial^2 f}{\partial y^2} + \frac{\partial^2 f}{\partial z^2}$	$\frac{1}{\rho} \frac{\partial}{\partial \rho} \left(\rho \frac{\partial f}{\partial \rho} \right) + \frac{1}{\rho^2} \frac{\partial^2 f}{\partial \varphi^2} + \frac{\partial^2 f}{\partial z^2}$	$\frac{1}{r^2} \frac{\partial}{\partial r} \left(r^2 \frac{\partial f}{\partial r} \right) + \frac{1}{r^2 \sin \theta} \frac{\partial}{\partial \theta} \left(\sin \theta \frac{\partial f}{\partial \theta} \right) + \frac{1}{r^2 \sin^2 \theta} \frac{\partial^2 f}{\partial \varphi^2}$
$\Delta \mathbf{A}$	$\Delta A_x \hat{\mathbf{x}} + \Delta A_y \hat{\mathbf{y}} + \Delta A_z \hat{\mathbf{z}}$	$\begin{pmatrix} \left(\Delta A_\rho - \frac{A_\rho}{\rho^2} - \frac{2}{\rho^2} \frac{\partial A_\varphi}{\partial \varphi} \right) \hat{\boldsymbol{\rho}} + \\ \left(\Delta A_\varphi - \frac{A_\varphi}{\rho^2} + \frac{2}{\rho^2} \frac{\partial A_\rho}{\partial \varphi} \right) \hat{\boldsymbol{\varphi}} + \\ (\Delta A_z) \hat{\mathbf{z}} \end{pmatrix}$	$\begin{pmatrix} \left(\Delta A_r - \frac{2A_r}{r^2} - \frac{2}{r^2 \sin \theta} \frac{\partial (A_\theta \sin \theta)}{\partial \theta} - \frac{2}{r^2 \sin \theta} \frac{\partial A_\varphi}{\partial \varphi} \right) \hat{\mathbf{r}} + \\ \left(\Delta A_\theta - \frac{A_\theta}{r^2 \sin^2 \theta} + \frac{2}{r^2} \frac{\partial A_r}{\partial \theta} - \frac{2 \cos \theta}{r^2 \sin^2 \theta} \frac{\partial A_\varphi}{\partial \varphi} \right) \hat{\boldsymbol{\theta}} + \\ \left(\Delta A_\varphi - \frac{A_\varphi}{r^2 \sin^2 \theta} + \frac{2}{r^2 \sin \theta} \frac{\partial A_r}{\partial \varphi} + \frac{2 \cos \theta}{r^2 \sin^2 \theta} \frac{\partial A_\theta}{\partial \varphi} \right) \hat{\boldsymbol{\varphi}} \end{pmatrix}$

Appendix 2

□ Focusing. Panofsky-Wenzel theorem

Let's consider the particle transverse momentum change caused by the cavity RF field. The particle moves on the trajectory $z=vt$ parallel to the axis, but is displaced from it by \vec{r}_\perp .

Force acting on the particle is

$$\vec{F}(\vec{r}) = e \left[\vec{E}(\vec{r}) + \vec{v} \times \vec{B}(\vec{r}) \right] e^{i\omega t}.$$

From Maxwell equation $\text{curl} \vec{E}(\vec{r}) = -i\omega \vec{B}(\vec{r})$ one has:

$$\vec{F}(\vec{r}) = e \left[\vec{E}(\vec{r}) + \vec{v} \times \frac{i}{\omega} \text{curl} \vec{E}(\vec{r}) \right] e^{i\omega t} = e \left[\vec{E}(\vec{r}) + \frac{i}{\omega} \vec{\nabla} (\vec{v} \cdot \vec{E}(\vec{r})) - (\vec{v} \cdot \vec{\nabla}) \cdot \vec{E}(\vec{r}) \right] e^{i\omega t}.$$

If $\vec{v} = \vec{i}_z v$, then

$$F_z(\vec{r}) = e E_z(\vec{r}) e^{i\omega t}$$

$$F_\perp(\vec{r}) = e \left[\vec{E}_\perp(\vec{r}) + v \frac{i}{\omega} \left(\vec{\nabla}_\perp E_z(\vec{r}) - \frac{\partial \vec{E}_\perp(\vec{r})}{\partial z} \right) \right] e^{i\omega t}$$

The differential operator $\vec{\nabla}_\perp$ acts on the transverse coordinates \vec{r}_\perp only.

Appendix 2

If the particle velocity and particle transverse coordinates do not change significantly in the cavity, longitudinal and transverse momentum changes are:

$$\Delta p_{\parallel} = e \int_{-\infty}^{\infty} E_z(\vec{r}) e^{i\omega t} dt \Big|_{t=z/v} = \frac{e}{v} \int_{-\infty}^{\infty} E_z(\vec{r}) e^{i\omega z/v} dz;$$

$$\Delta \vec{p}_{\perp} = e \int_{-\infty}^{\infty} \left[\vec{E}_{\perp}(\vec{r}) + \frac{iv}{\omega} \vec{\nabla}_{\perp} E_z(\vec{r}) - \frac{iv}{\omega} \frac{\partial \vec{E}_{\perp}(\vec{r})}{\partial z} \right] e^{i\omega t} dt \Big|_{t=z/v}$$

However,

$$\frac{iv}{\omega} \int_{-\infty}^{\infty} \frac{\partial \vec{E}_{\perp}(\vec{r})}{\partial z} e^{i\omega t} dt \Big|_{t=z/v} = \frac{i}{\omega} \int_{-\infty}^{\infty} \frac{\partial \vec{E}_{\perp}(\vec{r})}{\partial z} e^{i\omega z/v} dz = \frac{1}{v} \int_{-\infty}^{\infty} \vec{E}_{\perp}(\vec{r}) e^{i\omega z/v} dz = \int_{-\infty}^{\infty} \vec{E}_{\perp}(\vec{r}) e^{i\omega t} dt \Big|_{t=z/v}$$

and

$$\Delta \vec{p}_{\perp} = e \frac{iv}{\omega} \int_{-\infty}^{\infty} \vec{\nabla}_{\perp} E_z(\vec{r}) e^{i\omega t} dt \Big|_{t=z/v} = e \frac{i}{\omega} \int_{-\infty}^{\infty} \vec{\nabla}_{\perp} E_z(\vec{r}) e^{i\omega z/v} dz$$

Finally, we have:

$$\Delta \vec{p}_{\perp} = \frac{iv}{\omega} \vec{\nabla}_{\perp} (\Delta p_{\parallel}).$$

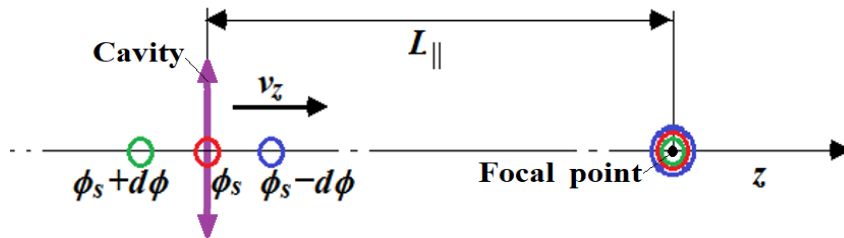
This relation between transverse and longitudinal momentum changes in an RF field is known as Panofsky – Wenzel theorem.

Appendix 2.

□ Bunching

Because a particle velocity depends on its energy, the cavity RF field provides the beam bunching. If the particle in the bunch center has the RF phase of ϕ_s (ϕ_s is a so-called synchronous phase), the particles next to the bunch center will have the same longitudinal coordinate at the same time at the distance L_z from the cavity (see Figure below), if

$$d(v(\phi) \cdot t(\phi))/d\phi|_{\phi=\phi_s} = 0. \quad (1)$$



Here $v(\phi)$ is the particle velocity after it leaves the cavity, and $t(\phi)$ is time necessary for the particle to reach the distance $L_{||}$ – “longitudinal focusing distance”:

$$t(\phi) = L_{||}/v(\phi_s) - (\phi - \phi_s)/\omega. \quad (2)$$

On the other hand, one has (Lecture 11, Slide 28):

$$\Delta W(r) = e \left| V_{0,z} \left(\frac{k}{\beta} \right) \right| I_0 \left(\frac{kr}{\beta\gamma} \right) \cos \phi, \quad (3)$$

Appendix 2.

From (1), (2) and (3) it follows for the particle next to the axis ($kr/\beta\gamma \ll 1$) that

$$L_{||} = \left[\frac{v(\phi)^2}{\omega} \cdot \frac{dW/dv}{dW/d\phi} \right]_{\phi=\phi_s} = - \frac{v(\phi_s)^2}{\omega} \cdot \frac{dW/dv|_{\phi=\phi_s}}{\Delta W_{max}(0) \cdot \sin\phi_s} \quad (4)$$

For a linear accelerator one has

$$\frac{dW}{dv} = \frac{d(mc^2\gamma)}{dv} = mv\gamma^3, \quad (5)$$

where m is the particle mass, and therefore

$$L_{||} = - \frac{(mc^2/e)\beta(\phi_s)^3 \gamma(\phi_s)^3}{k\Delta W_{max}(0) \cdot \sin\phi_s} = - \frac{(mc^2/e)\beta(\phi_s)^3 \gamma(\phi_s)^3}{kV_{max}(0) \cdot \sin\phi_s} \quad (6)$$

For bunching one needs $L_{||} > 0$, and therefore, $\phi_s < 0$. Note that $L_{||} \sim 1/k$. Note that for small energy (and therefore small β) the bunching may be too strong, and low RF frequency is to be used for acceleration.

Appendix 3. Eigen modes properties:

Eigenmodes in a cavity.

$$\begin{aligned} \text{curl} \vec{E} &= -i\omega\mu_0 \vec{H}, \text{curl} \vec{H} = i\omega\varepsilon_0 \vec{E}, \\ \text{curlcurl} \vec{E} - k^2 \vec{E} &= 0, \text{curlcurl} \vec{H} - k^2 \vec{H} = 0, \end{aligned} \quad (1)$$

Here $k^2 = \omega^2 \varepsilon_0 \mu_0$

Boundary conditions: $\vec{E}_t = 0, \vec{H}_n = 0$ or $\vec{n} \times \vec{E} = 0, \vec{n} \cdot \vec{H} = 0$.

Equations (1) has non-trivial solutions only for defined k_m^2 , eigenvalues.

Corresponding solutions $\vec{E}_m(x, y, z)$ and $\vec{H}_m(x, y, z)$ -eigenfunctions. There are infinite number of eigenvalues.

Eigenvalues are **real** and **positive**. From (1) and vector theorem (App.1)

$$\text{div}(\vec{A} \times \vec{B}) = \vec{B} \cdot \text{curl} \vec{A} - \vec{A} \cdot \text{curl} \vec{B} \quad (2)$$

one has:

$$\text{div}(\vec{H}_m^* \times \text{curl} \vec{H}_m) = \text{curl} \vec{H}_m \cdot \text{curl} \vec{H}_m^* - \vec{H}_m^* \cdot \text{curlcurl} \vec{H}_m = |\text{curl} \vec{H}_m|^2 - k_m^2 |\vec{H}_m|^2$$

$$k_m^2 \int_V |\vec{H}_m|^2 dV = \int_V |\text{curl} \vec{H}_m|^2 dV - \oint_S (\vec{H}_m^* \times \text{curl} \vec{H}_m) \cdot \vec{n} dS. \quad \Rightarrow \quad k_m^2 = \frac{\int_V |\text{curl} \vec{H}_m|^2 dV}{\int_V |\vec{H}_m|^2 dV}$$

Appendix 3. Eigen modes properties

Eigenmodes are orthogonal:

$$\text{curlcurl}\vec{E}_m - k_m^2\vec{E}_m = 0, \quad (3)$$

$$\text{curlcurl}\vec{E}_n - k_n^2\vec{E}_n = 0, \quad k_m^2 \neq k_n^2$$

Let's calculate using (2)

$$\begin{aligned} \text{div}(\vec{E}_n \times \text{curl}\vec{E}_m) - \text{div}(\vec{E}_m \times \text{curl}\vec{E}_n) &= \text{curl}\vec{E}_m \cdot \text{curl}\vec{E}_n - \vec{E}_n \text{curlcurl}\vec{E}_m - \\ \text{curl}\vec{E}_n \cdot \text{curl}\vec{E}_m + \vec{E}_m \text{curlcurl}\vec{E}_n &= \vec{E}_m \text{curlcurl}\vec{E}_n - \vec{E}_n \text{curlcurl}\vec{E}_m. \end{aligned}$$

Using (3) we have:

$$\text{div}(\vec{E}_n \times \text{curl}\vec{E}_m) - \text{div}(\vec{E}_m \times \text{curl}\vec{E}_n) = (k_n^2 - k_m^2) \vec{E}_m \cdot \vec{E}_n \rightarrow 0$$

$$(k_n^2 - k_m^2) \int_V \vec{E}_m \cdot \vec{E}_n dV = \oint_S \left(\text{div}(\vec{E}_n \times \text{curl}\vec{E}_m) - \text{div}(\vec{E}_m \times \text{curl}\vec{E}_n) \right) \vec{n} dS.$$

$$(k_n^2 - k_m^2) \int_V \vec{E}_m \cdot \vec{E}_n dV = 0, \quad \leftarrow k_m^2 \neq k_n^2$$

$$\int_V \vec{E}_m \cdot \vec{E}_n dV = 0,$$

$$\int_V \vec{H}_m \cdot \vec{H}_n dV = 0,$$

Appendix 3. Eigen modes properties

Let's consider again the equation we got

$$k_m^2 \int_V |\vec{H}_m|^2 dV = \int_V |\text{curl} \vec{H}_m|^2 dV$$

Taking into account $\text{curl} \vec{H}_m = i\omega_m \epsilon_0 \vec{E}_m$ and $k_m^2 = \omega_m^2 \epsilon_0 \mu_0$, we have:

$$\frac{1}{4} \int_V \mu_0 |\vec{H}_m|^2 dV = \frac{1}{4} \int_V \epsilon_0 |\vec{E}_m|^2 dV$$

The time-average electrical stored energy is equal to the time-average magnetic stored energy.

Appendix 3. Eigen modes properties:

Variation properties of the eigenmodes:

Let's consider expression for k^2 :

$$k^2 = \frac{\int_V |\text{curl}\vec{H}|^2 dV}{\int_V |\vec{H}|^2 dV}. \quad (1)$$

Variation of (1) gives:

$$\delta k^2 \int_V |\vec{H}|^2 dV + 2k^2 \int_V \vec{H} \cdot \delta\vec{H} dV = 2 \int_V \text{curl}\vec{H} \cdot \text{curl}\delta\vec{H} dV$$

Using the and vector theorem (2)

$\text{div}(\delta\vec{H} \times \text{curl}\vec{H}) = \text{curl}\vec{H} \cdot \text{curl}\delta\vec{H} - \delta\vec{H} \cdot \text{curlcurl}\vec{H}$, we have

$$\delta k^2 \int_V |\vec{H}|^2 dV = 2 \int_V (\text{curlcurl}\vec{H} - k^2\vec{H}) \cdot \delta\vec{H} dV + 2 \int_V \text{div}(\delta\vec{H} \times \text{curl}\vec{H}) dV.$$

Using Gauss theorem, we get

$$\delta k^2 \int_V |\vec{H}|^2 dV = 2 \int_V (\text{curlcurl}\vec{H} - k^2\vec{H}) \cdot \delta\vec{H} dV + 2 \oint_S (\delta\vec{H} \times \text{curl}\vec{H}) \cdot \vec{n} dS.$$

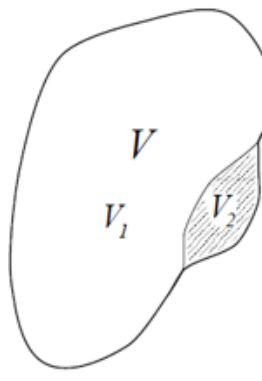
Taking into account that $\text{curl curl}\vec{H} - k^2\vec{H} = 0$ and boundary condition

$\vec{n} \times \text{curl}\vec{H} = 0$ on S , and we finally get

$$\delta k^2 = 0$$

Appendix 3.

Small perturbations of the cavity geometry:



$$k^2 = \frac{\int_{V_1} |\text{curl} \vec{H}^{(2)}|^2 dV}{\int_{V_1} |\vec{H}^{(2)}|^2 dV} \approx \frac{\int_{V_1} |\text{curl} \vec{H}^{(1)}|^2 dV}{\int_{V_1} |\vec{H}^{(1)}|^2 dV} = \frac{\int_V |\text{curl} \vec{H}^{(1)}|^2 dV}{\int_V |\vec{H}^{(1)}|^2 dV} - \frac{\int_{V_2} |\text{curl} \vec{H}^{(1)}|^2 dV}{\int_{V_2} |\vec{H}^{(1)}|^2 dV} =$$

$$= k_1^2 \left\{ 1 + \frac{\int_{V_2} |\vec{H}^{(1)}|^2 dV}{\int_V |\vec{H}^{(1)}|^2 dV} - \frac{\int_{V_2} |\text{curl} \vec{H}^{(1)}|^2 dV}{\int_V |\text{curl} \vec{H}^{(1)}|^2 dV} \right\} = k_1^2 \left(1 + \frac{\Delta W_E - \Delta W_H}{W_0} \right)$$

$$\frac{k^2 - k_1^2}{k_1^2} = \frac{\Delta W_E - \Delta W_H}{W_0} \approx \frac{2\Delta\omega}{\omega_1} = \frac{(w_E - w_H) \cdot \Delta V}{W_0} \quad \leftarrow \text{Slater theorem}$$

On the other hand, $\frac{1}{2}(w_H - w_E)\Delta V = p \Delta V = -\Delta W_0$ and

$$\frac{\Delta\omega}{\omega_0} = \frac{\Delta W_0}{W_0},$$



$$\boxed{\frac{W_0}{\omega_0} = \text{const}} \quad (\text{compare to } E = \nu h)$$

Appendix 4: Accelerating voltage and transit time factor:

For arbitrary axial distribution of the axisymmetric accelerating field the voltage

$V(\varphi)$ at arbitrary phase φ is the following:

$$\begin{aligned} V(\varphi) &= \operatorname{Re} \int_{-\infty}^{\infty} E_z(\rho = 0, z) e^{i(k_z z + \varphi)} dz = \\ &= \int_{-\infty}^{\infty} \operatorname{Re}[E_z(\rho = 0, z)] \cos(k_z z + \varphi) dz - \int_{-\infty}^{\infty} \operatorname{Im}[E_z(\rho = 0, z)] \sin(k_z z + \varphi) dz = \\ &= \int_{-\infty}^{\infty} \operatorname{Re}[E_z(\rho = 0, z)] \cos(k_z z + \varphi) dz - \int_{-\infty}^{\infty} \operatorname{Im}[E_z(\rho = 0, z)] \sin(k_z z + \varphi) dz = \\ &= \cos(\varphi) \left(\int_{-\infty}^{\infty} \operatorname{Re}[E_z(\rho = 0, z)] \cos(k_z z) dz - \int_{-\infty}^{\infty} \operatorname{Im}[E_z(\rho = 0, z)] \sin(k_z z) dz \right) - \\ &\quad - \sin(\varphi) \left(\int_{-\infty}^{\infty} \operatorname{Re}[E_z(\rho = 0, z)] \sin(k_z z) dz - \int_{-\infty}^{\infty} \operatorname{Im}[E_z(\rho = 0, z)] \cos(k_z z) dz \right) \end{aligned}$$

Maximal voltage V is, therefore,

$$\begin{aligned} V &= \left[\left(\int_{-\infty}^{\infty} \operatorname{Re}[E_z(\rho = 0, z)] \cos(k_z z) dz - \int_{-\infty}^{\infty} \operatorname{Im}[E_z(\rho = 0, z)] \sin(k_z z) dz \right)^2 \right. \\ &\quad \left. + \left(\int_{-\infty}^{\infty} \operatorname{Re}[E_z(\rho = 0, z)] \sin(k_z z) dz - \int_{-\infty}^{\infty} \operatorname{Im}[E_z(\rho = 0, z)] \cos(k_z z) dz \right)^2 \right]^{1/2} \end{aligned}$$

If $E_z(\rho, z)$ is real,
$$V = \left[\left(\int_{-\infty}^{\infty} E_z(\rho = 0, z) \cos(k_z z) dz \right)^2 + \left(\int_{-\infty}^{\infty} E_z(\rho = 0, z) \sin(k_z z) dz \right)^2 \right]^{1/2}$$

Appendix 5. Modes in a pillbox cavity:

In a pillbox cavities resonance field satisfies wave equations:

$$\Delta \vec{E} + k^2 \vec{E} = 0, \Delta \vec{H} + k^2 \vec{H} = 0, \text{ where } k = \frac{\omega}{c} - \text{wavenumber.}$$

For an ideally conductive wall components of electric field tangential to the surface is zero. The pillbox cavity may be considered as a part of a waveguide having circular cross section, shortened at both ends. The fields in this waveguide may be described in cylindrical coordinates, (r, φ, z) . In cylindrical coordinates longitudinal field components satisfy scalar wave equations:

$$\Delta E_z + k^2 E_z = 0, \Delta H_z + k^2 H_z = 0 \quad (1)$$

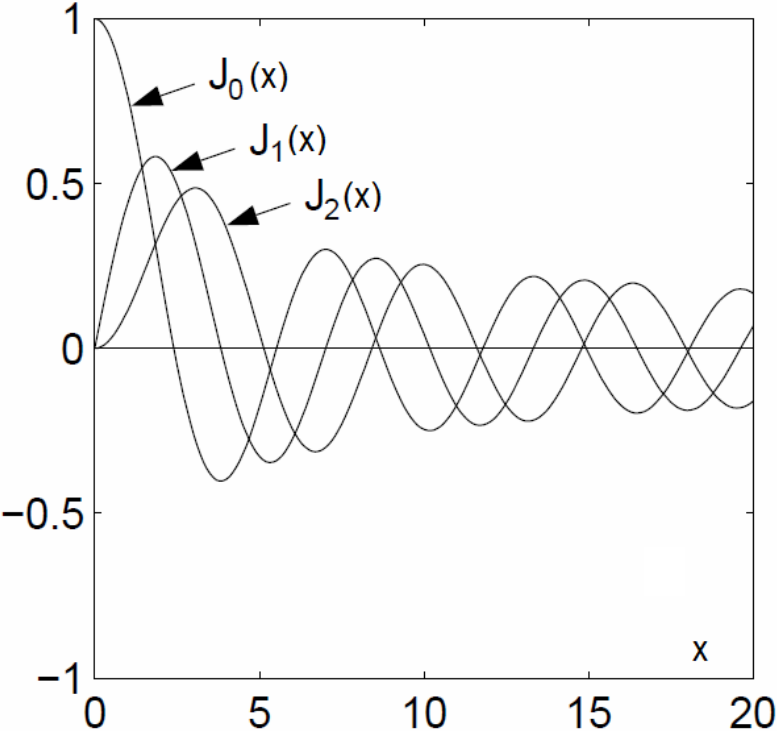
For the waveguide, the fields have translation symmetry along \vec{z} , i.e., in two points having the same transverse coordinate, but different z , the fields differ by phase $\psi = k_z z$; i.e., $\vec{E}, \vec{H} \sim e^{ik_z z}$. In this case:

- Equations (1) have solution

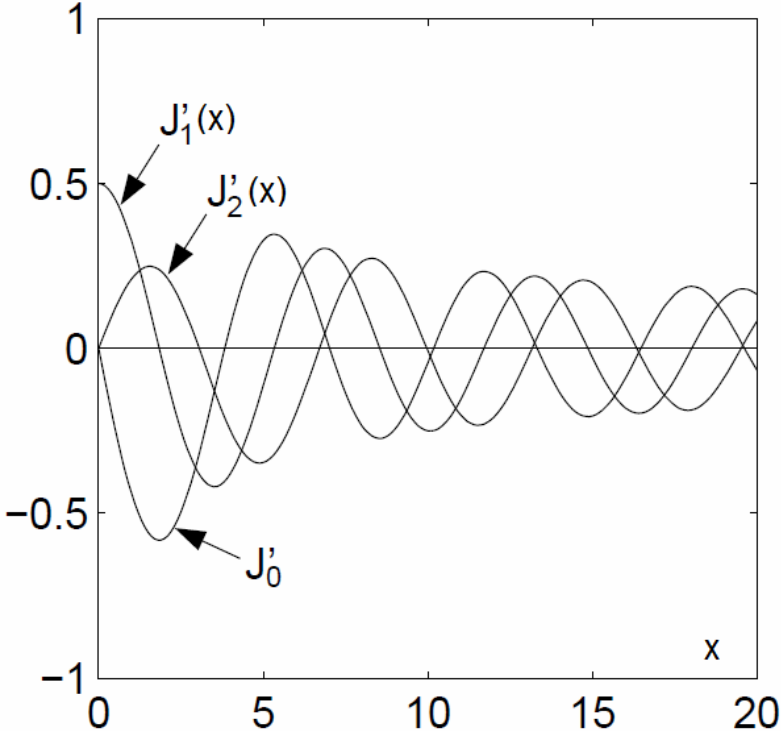
$$E_z(r, \varphi, z), H_z(r, \varphi, z) = J_m(k_r r) e^{im\varphi} e^{ik_z z}; J_m(k_r r) \text{ are Bessel functions;}$$

- $k_r^2 + k_z^2 = k^2$;
- All transverse components (E_r, E_φ, H_r and H_φ) may be expressed through the longitudinal field components, E_z and H_z ;
- At $r=b$ (b is the waveguide radius) $E_z=0$ and $\frac{\partial H_z}{\partial n} = 0$. \vec{n} is normal to the waveguide surface.

Appendix 5.



(a)



(b)

Bessel functions and their derivatives

Appendix 5.

E_z and H_z satisfy the same equation, but have different boundary conditions, and therefore, different k_r :

Electric field:

Equation:

$$\Delta E_z + k^2 E_z = 0$$

Boundary condition: $E_z(r, \varphi, z) = 0, r = a$;

or $J_m(k_r b) = 0$;

and $k_r = \frac{\nu_{mn}}{b}$; $J_m(\nu_{mn}) = 0$;

Magnetic field:

$$\Delta H_z + k^2 H_z = 0$$

$\partial H_z(r, \varphi, z) / \partial r = 0, r = a$

$$J'_m(k_r b) = 0,$$

$$k_r = \frac{\mu_{mn}}{b}; J'_m(\mu_{mn}) = 0.$$

For the pillbox cavity having end walls at $z=0$ and $z=d$; therefore $k_z d = \pi p$ and

$$E_z = C J_m(k_r r) e^{im\varphi} \cos(\pi p z / d); H_z = J_m(k_r r) e^{im\varphi} \sin(\pi p z / d),$$

and resonant frequencies are:

$$\frac{\omega}{c} = \sqrt{\left(\frac{\nu_{mn}}{b}\right)^2 + \left(\frac{\pi p}{d}\right)^2};$$

$$m = 0, 1, \dots, \infty;$$

$$n = 1, 2, \dots, \infty;$$

$$p = 0, 1, \dots, \infty;$$

TM_{mnp}-modes

$$\frac{\omega}{c} = \sqrt{\left(\frac{\mu_{mn}}{b}\right)^2 + \left(\frac{\pi p}{d}\right)^2}$$

$$m = 0, 1, \dots, \infty;$$

$$n = 1, 2, \dots, \infty;$$

$$p = 1, 2, \dots, \infty;$$

TE_{mnp}-modes

Appendix 5.

Roots of $J'_m(x) = 0$.

m	μ_{m1}	μ_{m2}	μ_{m3}	μ_{m4}
0	3.832	7.016	10.174	13.324
1	1.841	5.331	8.536	11.706
2	3.054	6.706	9.970	13.170
3	4.201	8.015	11.346	14.586
4	5.318	9.282	12.682	15.964
5	6.416	10.520	13.987	17.313

Roots of $J_m(x) = 0$.

m	ν_{m1}	ν_{m2}	ν_{m3}	ν_{m4}
0	2.405	5.520	8.654	11.792
1	3.832	7.016	10.174	13.324
2	5.135	8.417	11.620	14.796
3	6.380	9.761	13.015	16.223
4	7.588	11.065	14.373	17.616
5	8.771	12.339	15.700	18.980

$$\mu_{0n} = \nu_{1n}!$$

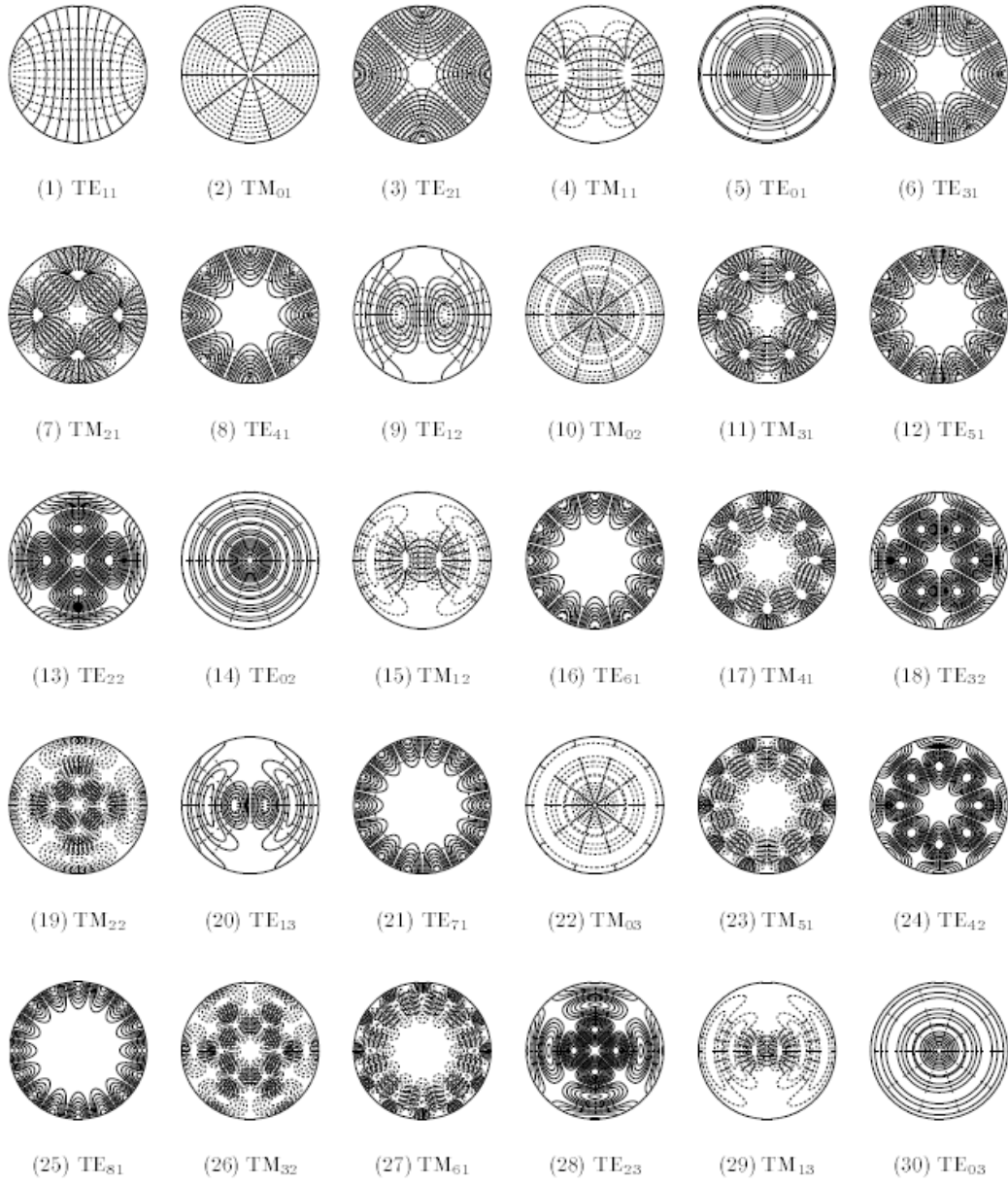
TM_{1np} and TE_{0np}
are degenerated!

$n=1,2,\dots,\infty;$

$p=1,2,\dots,\infty^*$

*Note that TE_{0n0} does not exist because of boundary conditions for magnetic field on the end walls.

Appendix 5.



Field plots for the pillbox modes

Appendix 6: RF cavity excitation by the beam:

- RF cavity having eigenmodes: eigen fields satisfy Maxwell equations:

$$\text{curl} \mathbf{E}_s = -i\omega_s \mu \mathbf{H}_s, \quad \text{curl} \mathbf{H}_s = i\omega_s \varepsilon \mathbf{E}_s. \quad (1)$$

- The field excited by the beam:

$$\text{curl} \mathbf{E} = -i\omega \mu \mathbf{H}, \quad (2)$$

$$\text{curl} \mathbf{H} = i\omega \varepsilon \mathbf{E} + \mathbf{J}_e$$

- The excited field may be expanded over the eigenmodes:

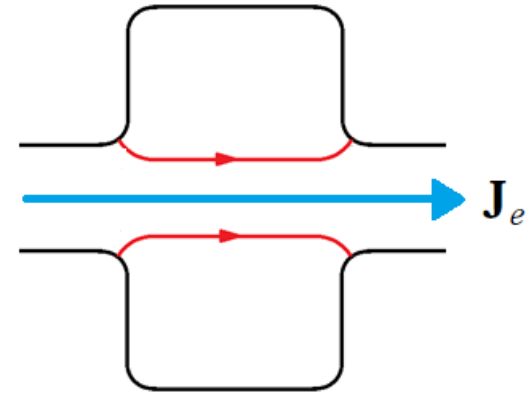
$$\mathbf{E} = \sum A_s \mathbf{E}_s - \text{grad} \varphi_e, \quad \mathbf{H} = \sum B_s \mathbf{H}_s \quad (3)$$

Here φ_e is space charge potential, typically its impact is small.

- From (1) and (2) one has:

$$\begin{aligned} \text{div} (\mathbf{E}_s^* \times \mathbf{H}) &= \mathbf{H} \cdot (i\omega_s \mu \mathbf{H}_s^*) - \mathbf{E}_s^* \cdot (i\omega \varepsilon \mathbf{E} + \mathbf{J}_e) = \\ &= i\omega_s \mu \mathbf{H} \cdot \mathbf{H}_s^* - i\omega \varepsilon \mathbf{E} \cdot \mathbf{E}_s^* - \mathbf{J}_e \cdot \mathbf{E}_s^*, \end{aligned} \quad (4)$$

$$\begin{aligned} \text{div} (\mathbf{E} \times \mathbf{H}_s^*) &= \mathbf{H}_s^* \cdot (-i\omega \mu \mathbf{H}) - \mathbf{E} \cdot (-i\omega_s \varepsilon \mathbf{E}_s^*) = \\ &= -i\omega \mu \mathbf{H} \cdot \mathbf{H}_s^* + i\omega_s \varepsilon \mathbf{E} \cdot \mathbf{E}_s^*. \end{aligned}$$



\mathbf{J}_e – the beam current density spectrum component oscillating at the frequency ω

All the fields have zero tangential electric field components on the wall.

Appendix 6:

Substituting (3) to (4) one has:

$$A_s = -\frac{\omega}{i(\omega^2 - \omega_s^2)} \cdot \frac{\int_V \mathbf{J}_e \mathbf{E}_s^* dV}{\mu \int_V \mathbf{H}_s \cdot \mathbf{H}_s^* dV}, \quad B_s = -\frac{\omega_s}{i(\omega^2 - \omega_s^2)} \cdot \frac{\int_V \mathbf{J}_e \mathbf{E}_s^* dV}{\mu \int_V \mathbf{H}_s \cdot \mathbf{H}_s^* dV},$$

Note that

$$\mu \int_V \mathbf{H}_s \cdot \mathbf{H}_s^* dV = 2W_s$$

If there are wall losses, $\omega_s^2 \rightarrow \omega_s^2 \left(1 + \frac{i}{Q_0}\right)$

and for thin beam having the average current I_0 on the axis one has:

$$A_s = -\frac{i\omega}{\omega^2 - \omega_s^2 - i\frac{\omega\omega_s}{Q_s}} \times \frac{\int \mathbf{J}_e \mathbf{E}_s dV}{2W_s} = -\frac{i\omega}{\omega^2 - \omega_s^2 - i\frac{\omega\omega_s}{Q_s}} \times \frac{I_0 \left| \int_{-\infty}^{\infty} E_{sz}(z) e^{ikz} dz \right|}{W_s}, \quad k = \frac{\omega_s}{c} \quad (5)$$

From (5) and (3) one has for the cavity voltage on the axis for the s^{th} mode:

$$V_s = \frac{\Delta p_{\parallel} c}{e} = \int_{-\infty}^{\infty} E_{sz} e^{ikz} dz \approx \frac{i\omega_s^2}{\omega^2 - \omega_s^2 - i\frac{\omega\omega_s}{Q_s}} \cdot \frac{I_0 \left| \int_{-\infty}^{\infty} E_{sz}(z) e^{ikz} dz \right|^2}{\omega_s W_s} = \frac{i\omega_s^2}{\omega^2 - \omega_s^2 - i\frac{\omega\omega_s}{Q_s}} \cdot I_0 \left(\frac{R}{Q} \right)_s$$

Appendix 6:

here

$$\left(\frac{R}{Q}\right)_s = \frac{\left|\int_{-\infty}^{\infty} E_{sz}(z)e^{ikz} dz\right|^2}{\omega_s W_s}$$

At the resonance one has

$$V_s = -Q_s I_0 \left(\frac{R}{Q}\right)_s = -I_0 R_s$$

where

$$R_s = Q_s \left(\frac{R}{Q}\right)_s$$

is a shunt impedance of the s^{th} mode.

Appendix 6:

- This coincides to the voltage excited by the AC current $I = -2I_0$ in a parallel resonance circuit.
- Note that for a short bunch the beam current spectrum is
$$I(\omega) \approx I_0 + 2I_0 \sum \delta(\omega_s),$$
 ω_s is the bunch sequence frequency; the equivalent circuit describes the cavity excitation by imaginary current, it gives the sign “-”.
- From Kirchhoff theorem one has

$$I_C + I_L + I_R = iV\omega C + V/R + V/i\omega L = -2I_0,$$

and taking into account that $\omega_s = (LC)^{-1/2}$, we get

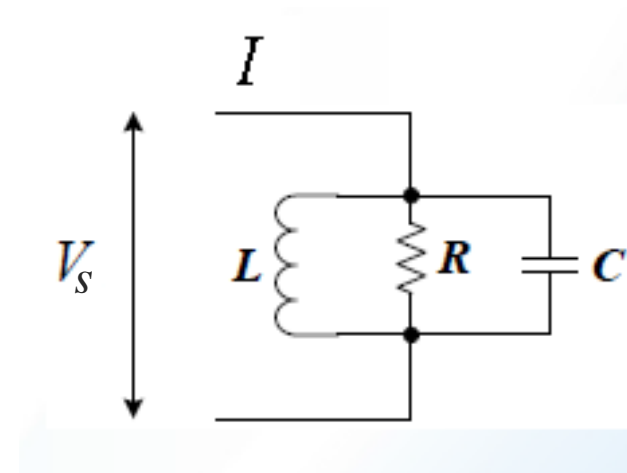
$$V_s = \frac{i\omega_s^2}{\omega^2 - \omega_s^2 - i\frac{\omega\omega_s}{Q_s}} \cdot I_0 \left(\frac{R}{Q} \right)_s,$$

if $\omega_s \approx \omega$. Here are the equivalent circuit parameters:

$$L = (R/Q)_s / 2\omega;$$

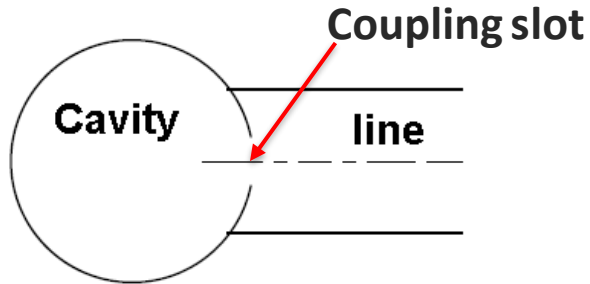
$$C = 2/\omega(R/Q)_s;$$

$$R = (R/Q)_s Q_s / 2.$$

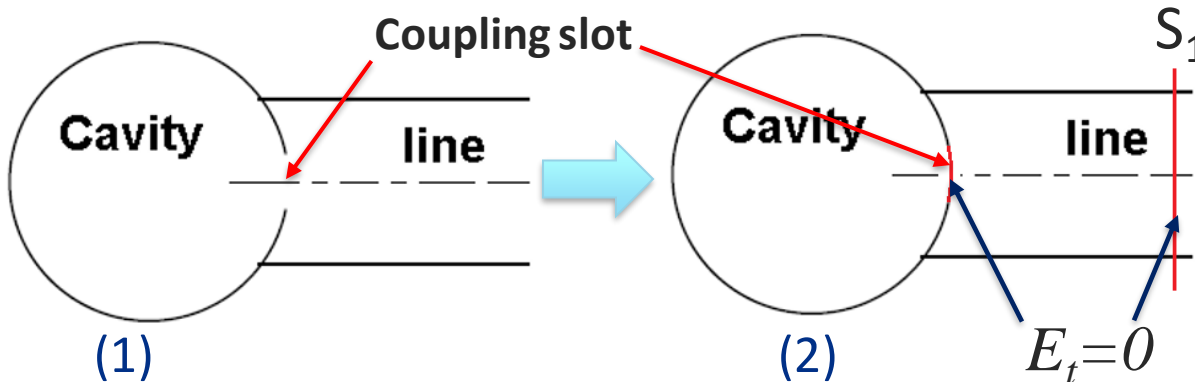


Appendix 7: The cavity coupled to the line.

Let's consider the cavity coupled to the feeding line:



Consider another problem – the cavity coupled to the line shortened by a perfectly conducting plane S_1 placed such a way, that the electric field at the coupling slot has no tangential component:



- The eigenfrequency of the new problem will be the same as for uncoupled cavity;
- The fields inside the cavity will be the same as for uncoupled cavity;
- The magnetic field on S_1 will be proportional to WG magnetic transverse eigenfunction h , $H_t = ikh(x, y)$; k is coefficient (real for convenience). Tangential electric field is zero.

Appendix 7:

For the cavity excited by the line (problem 1) one has on S_1 for transverse fields:

$$E_t = U \cdot \mathbf{e}(x, y), H_t = I \cdot \mathbf{h}(x, y), \quad (1)$$

where $\mathbf{e}(x, y)$ and $\mathbf{h}(x, y)$ are the electric and magnetic WG transverse eigenfunction, $\int_{S_1} (\mathbf{e} \times \mathbf{h}) d\mathbf{S} = 1$.

The field in the cavity \mathbf{H} is proportional to the eigenfunction \mathbf{H}_s of the cavity coupled to the shortened line (see previous slide):

$$\mathbf{H} = B \cdot \mathbf{H}_s = ikB \mathbf{h}(x, y) \quad (2)$$

From (1) and (2) one can find that

$$I = ikB \quad (3)$$

Following the procedure from Appendix 11, we have, see Formulas 1, 2 and 3 from this Appendix 11 and (1-3):

$$B = \frac{i\omega_s}{\omega^2 - \omega_s^2} \cdot \frac{\int_{S_1} (\vec{E} \times \vec{H}_s^*) \cdot d\mathbf{S}}{2W_s} = - \frac{\omega_s}{\omega^2 - \omega_s^2} \cdot \frac{Uk}{2W_s}$$

and

$$I = - \frac{i\omega_s}{\omega^2 - \omega_s^2} \cdot \frac{Uk^2}{2W_s}$$

(4)

Appendix 7:

If there is wall loss in the cavity, $\omega_s^2 \rightarrow \omega_s^2 \left(1 + \frac{i}{Q_0}\right)$ and

$$I = -\frac{i\omega_s}{\omega^2 - \omega_s^2 - \frac{i\omega_s^2}{Q_0}} \cdot \frac{Uk^2}{2W_s}$$

The cavity impedance at S_1 is therefore

$$Z_1 = \frac{U}{I} = -R_1 Q_0 \left(\frac{\omega^2 - \omega_s^2 - \frac{i\omega_s^2}{Q_0}}{i\omega_s^2} \right) \approx R_1 (1 + iQ_0 x),$$

where

$$R_1 = \frac{2\omega_s W_s}{Q_0 k^2}, \quad x = \frac{\omega^2}{\omega_s^2} - 1 \approx \frac{2(\omega - \omega_s)}{\omega_s}$$

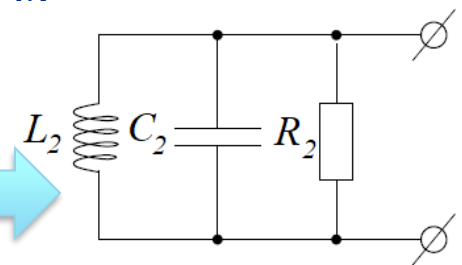
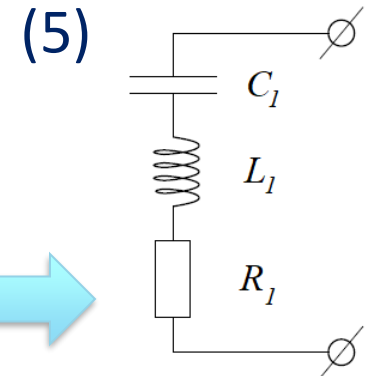
The impedance (5) coincides to the impedance of a serial resonance circuit . At the distance of

$\Lambda/4$ (Λ is wavelength in the WG) the cavity impedance is

$$Z_2 = \frac{Z_0^2}{Z_1} = \frac{Z_0^2}{R_1 (1 + iQ_0 x)} = \frac{R_2}{(1 + iQ_0 x)}, \quad R_2 = \frac{Z_0^2 Q_0 k^2}{2\omega_s W_s} \quad (6)$$

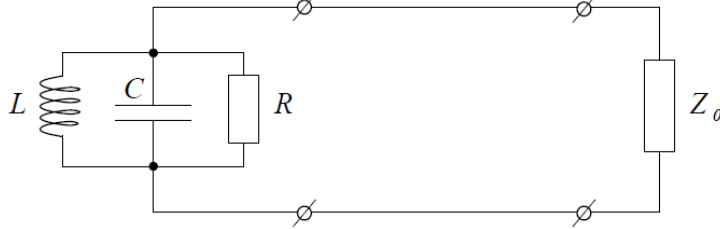
It is the impedance of a parallel resonance circuit

(Z_0 is the WG impedance).



Appendix 7:

If the line is matched, the equivalent circuit is



- Power P_R dissipated in R corresponds to the Ohmic losses in the cavity walls;
- Power P_{Z_0} dissipated in Z_0 corresponds to radiation in the line.

One can see:

$$\frac{P_{Z_0}}{P_R} = \frac{R}{Z_0} = \frac{Q_0}{Q_{ext}},$$

External quality factor, Q_{ext} describes radiation to the line:

$$Q_{ext} = \frac{\omega_s W_s}{P_{Z_0}}$$

Note that $Q_0 = \frac{\omega_s W_s}{P_R}$. The total loss is described by the loaded quality factor, Q_{load}

$$\frac{1}{Q_{load}} = \frac{P_{Z_0} + P_R}{\omega_s W_s} = \frac{1}{Q_{ext}} + \frac{1}{Q_0} \quad (7)$$

Ratio of Q_0 to Q_{ext} is called coupling, β :

$$\frac{Q_0}{Q_{ext}} = \frac{R}{Z_0} \equiv \beta \quad (8)$$

Appendix 7:

Let's estimate the reflection coefficient Γ of the parallel resonance circuit connected to the line:

$$\Gamma = \frac{Z - Z_0}{Z + Z_0},$$

According to (6)

$$Z = \frac{R}{(1 + iQ_0x)}$$

At resonance ($x=0$)

$$\Gamma_0 = \frac{R - Z_0}{R + Z_0} = \frac{\frac{R}{Z_0} - 1}{\frac{R}{Z_0} + 1} = \frac{\beta - 1}{\beta + 1}.$$

For $x \neq 0$ one has

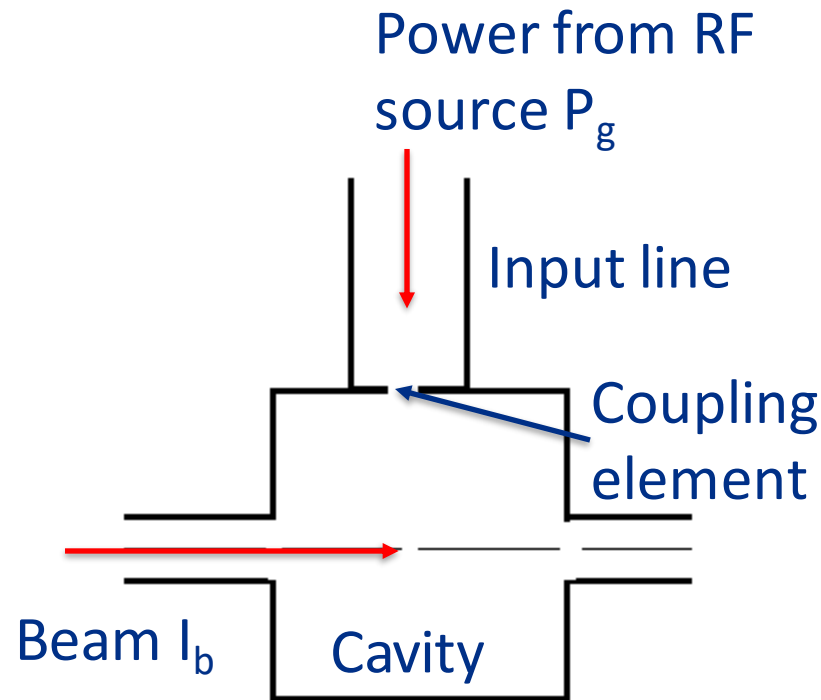
$$\Gamma = \frac{R - Z_0(1 + iQ_0x)}{R + Z_0(1 + iQ_0x)} = \frac{\Gamma_0 + 1}{1 + iQ_0x/(1 + \beta)} - 1 = \frac{\Gamma_0 + 1}{1 + iQ_{load}x} - 1$$

(from (7) and (8) it follows that $Q_0/(1 + \beta) = Q_{load}$).

The power P dissipated in the cavity excited by the input power P_{in} is the following:

$$P = P_{in}(1 - |\Gamma|^2) = P_{in} \frac{1 - \Gamma_0^2}{1 + Q_{load}^2 x^2}.$$

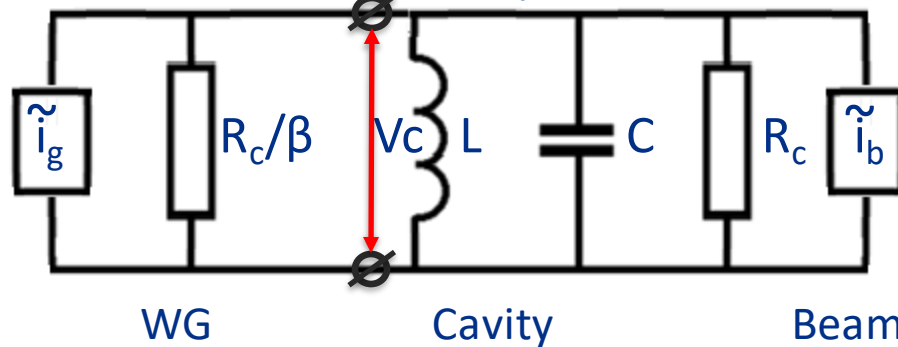
Appendix 8: Beam Loading



- RF source and beam $\omega_g = \omega_b = \omega$;
- Cavity: ω_0
- Cavity voltage : V_c
- Shunt impedance: R_{sh}
- Losses: $P_c = V_c^2 / R_{sh} = V_c^2 / (Q_0 \cdot R / Q)$
- Radiation to the line: $V_c^2 / (Q_{ext} \cdot R / Q)$
- Coupling: $\beta = Q_0 / Q_{ext}$
- Loaded Q: $Q_L = Q_0 / (1 + \beta)$
- Average beam current: I_b
- Synchronous phase: φ
- Power consumed by the beam: $P_b = I_b V_c \cos \varphi$
- Input power P_g
- Reflected power: $P_r = P_g - P_c - P_b$

Appendix 8:

Equivalent circuit for the cavity excited by a WG and loaded by the beam (transformed to the cavity):



$$L = R/Q / (2\omega_0)$$

$$C = 2 / (R/Q \cdot \omega_0)$$

$$R_c = R/Q \cdot Q_0/2$$

$$\tilde{i}_b = -2I_b$$

$$\beta = Q_0/Q_{ext}$$

- The WG impedance transformed to the cavity is $Z_{WG} = R_c/\beta$ (radiated power is $\frac{V_c^2}{R_c/\beta}$);
 - The WG is terminated by the cavity impedance* $Z_0 = \frac{R_c}{1+iQ_0x}$ in parallel to the beam impedance $Z_b = \frac{V_c}{I_b e^{i\varphi}}$, φ is the beam phase versus the voltage V_c .
 - The total load impedance is $Z = \left(\frac{1}{Z_0} + \frac{1}{Z_b} \right)^{-1} = \left(\frac{1+iQ_0x}{R_c} + \frac{I_b e^{i\varphi}}{V_c} \right)^{-1}$.
 - Reflection for this load is $\Gamma = \frac{V_{ref}}{V_{forw}} = \frac{Z - Z_{WG}}{Z + Z_{WG}} = \frac{1 - Z_{WG}/Z}{1 + Z_{WG}/Z}$.
 - The cavity voltage is $V_c = V_{ref} + V_{forw} = V_{forw}(1 + \Gamma) = V_{forw} \frac{2}{1 + Z_{WG}/Z}$ and
- $$V_{forw} = \frac{V_c}{(1+\Gamma)} = \frac{V_c}{2} \left(1 + Z_{WG}/Z \right).$$

*See Formulas (5-6), Appendix 7

Appendix 8:

Therefore, the input power is:

$$P_g = \frac{|V_{forw}|^2}{Z_{WG}} = \frac{V_c^2}{4Z_{WG}} \left| 1 + Z_{WG}/Z \right|^2 =$$
$$\approx \frac{V_c^2(1+\beta)^2}{4\left(\frac{R}{Q}\right)\beta Q_0} \left[\left(1 + \frac{I_b \cos\varphi \left(\frac{R}{Q}\right) Q_0}{(1+\beta)V_c} \right)^2 + \left(\frac{Q_0}{1+\beta} \cdot \frac{2\Delta f}{f} + \frac{I_b \sin\varphi \left(\frac{R}{Q}\right) Q_0}{1+\beta} \right)^2 \right].$$

The formula works next to resonance: approximation is used for x :

$$x = \frac{\omega^2}{\omega_0^2} - 1 \approx \frac{2(\omega - \omega_0)}{\omega_0} = \frac{2(f - f_0)}{f_0} \approx \frac{2(f - f_0)}{f} = \frac{2\Delta f}{f}.$$

Note that $P_g = \frac{|V_{forw}|^2}{Z_{WG}}$ does not contain factor of 2 in the denominator because of the cavity impedance $\left(\frac{R}{Q}\right)$ definition.

Appendix 9: Transverse impedance:

Let's consider a cavity excited by a beam current I_0 having offset x_0 . If \vec{E} is a dipole eigenmode, the field \vec{E} in the cavity in one-mode approximation may be expressed as $\vec{E} \approx A(\omega, \omega_0)\vec{E}$, where ω is the bunch sequence harmonic frequency, ω_0 is the resonant frequency, and

$$A = -\frac{i\omega}{\omega^2 - \omega_0^2 - i\frac{\omega\omega_0}{Q}} \times \frac{\int \vec{j} \cdot \vec{E} dV}{2W} = -\frac{i\omega}{\omega^2 - \omega_0^2 - i\frac{\omega\omega_0}{Q}} \times \frac{I_0 \left| \int_{-\infty}^{\infty} E_z(x, y, z) e^{ikz} dz \right|}{W}.$$

where $W = \frac{\epsilon_0}{2} \int |\vec{E}|^2 dV$ and I_0 is an average current

Appendix 10:

RF-kick at $x=x_0$ and $y=0$ may be obtained using Panofsky-Wenzel theorem:

$$\begin{aligned}
 U_{kick} &= \frac{\Delta p_{\perp} c}{e} = \frac{ic}{\omega} \left| \nabla_{\perp} \int_{-\infty}^{\infty} E_z e^{ikz} dz \right| \approx \frac{c}{x_0 \left(\omega^2 - \omega_0^2 - i \frac{\omega \omega_0}{Q} \right)} \times \frac{I_0 \left| \int_{-\infty}^{\infty} E_z(x_0, 0, z) e^{ikz} dz \right|^2}{W} \\
 &\approx \frac{c \omega_0}{\left(\omega^2 - \omega_0^2 - i \frac{\omega \omega_0}{Q} \right)} \times \frac{x_0 I_0 \left| \int_{-\infty}^{\infty} \left(\frac{\partial E_z(x, 0, z)}{\partial x} \right)_{x=x_0} e^{ikz} dz \right|^2}{W \omega_0} = \frac{\omega_0^2}{\left(\omega^2 - \omega_0^2 - i \frac{\omega \omega_0}{Q} \right)} \times \left(\frac{x_0}{k} \right) I_0 \left(\frac{r_{\parallel}}{Q} \right)
 \end{aligned}$$

where $\left(\frac{r_{\parallel}}{Q} \right) \equiv \frac{\left| \int_{-\infty}^{\infty} \left(\frac{\partial E_z(x, 0, z)}{\partial x} \right)_{x=x_0} e^{ikz} dz \right|^2}{W \omega_0}$

is dipole longitudinal impedance. and $k = \omega_0/c$. **Dipole** $\left(\frac{r_{\parallel}}{Q} \right)$ is measured in Ohm/m².

Appendix 10:

RF-kick may be expressed through the transverse impedance:

$$U_{kick} = \frac{\omega_0^2}{\left(\omega^2 - \omega_0^2 - i\frac{\omega\omega_0}{Q}\right)} \times x_0 I_0 \left(\frac{r_{\perp}}{Q}\right),$$

where $\left(\frac{r_{\perp}}{Q}\right) \equiv \left(\frac{r_{\parallel}}{Q}\right) \times \frac{1}{k} = \frac{\left| \int_{-\infty}^{\infty} \left(\frac{\partial E_z(x, 0, z)}{\partial x}\right)_{x=x_0} e^{ikz} dz \right|^2}{kW\omega_0}$.

Note that $\left(\frac{r_{\perp}}{Q}\right)$ is measured in Ohm/m.

At resonance

$$U_{kick} = i \left(\frac{x_0}{k}\right) I_0 Q \left(\frac{r_{\parallel}}{Q}\right) = ix_0 I_0 Q \left(\frac{r_{\perp}}{Q}\right).$$

Appendix 10:

Sometimes they use other transverse impedance, that is determined as:

$$\left(\frac{r_{\perp}}{Q}\right)_1 = \frac{|U_{kick}|^2}{\omega_0 W_0},$$

where W_0 is the energy, stored in the cavity at the RF field amplitude which provides given transverse kick U_{kick} , $W_0 = |A|^2 W$. At the resonance one has

$$|A|^2 = \frac{\left| x_0 I_0 Q \int_{-\infty}^{\infty} \left(\frac{\partial E_z(x, 0, z)}{\partial x} \right)_{x=x_0} e^{ikz} dz \right|^2}{(W \omega_0)^2} = \left(\frac{r_{\parallel}}{Q}\right) \frac{(x_0 I_0 Q)^2}{W \omega_0}$$

and

$$\omega_0 W_0 = \omega_0 W |A|^2 = \left(\frac{r_{\parallel}}{Q}\right) (x_0 I_0 Q)^2. \text{ On the other hand, } |U_{kick}|^2 = \frac{1}{k^2} \left(x_0 I_0 Q \left(\frac{r_{\parallel}}{Q}\right) \right)^2$$

and

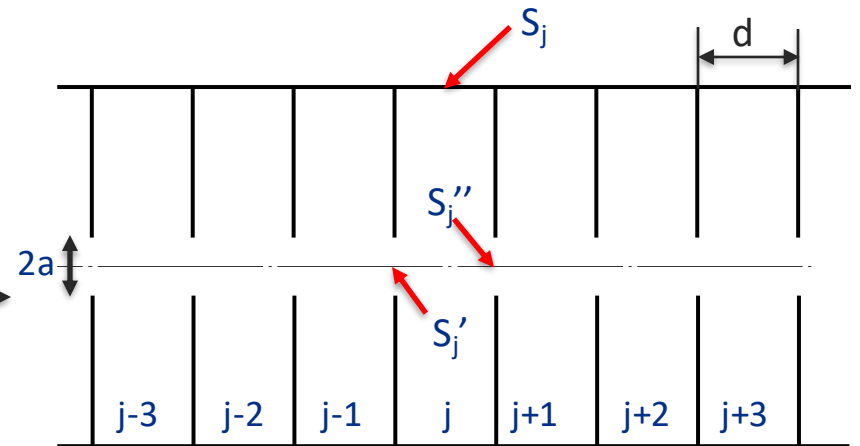
$$\left(\frac{r_{\perp}}{Q}\right)_1 = \frac{|U_{kick}|^2}{\omega_0 W_0} = \left(\frac{r_{\parallel}}{Q}\right) \times \frac{1}{k^2}.$$

$\left(\frac{r_{\perp}}{Q}\right)_1$ is measured in **Ohm**. Note that

$$U_{kick} = i(kx_0) I_0 Q \left(\frac{r_{\perp}}{Q}\right)_1$$

Appendix 11: Travelling–Wave acceleration structures:

- Each previous cell exits EM field in a current cell, which in turn excites the field in the next cell.
- Pillbox cells with thin walls



S_i is the cell metallic surface, S'_j and S''_j are the coupling holes; V is the cell volume.

\vec{E}_j, \vec{H}_j - fields in the j^{th} pillbox cell oscillate at frequency ω ;

$\vec{E}_{j,n}, \vec{H}_{j,n}$ - eigenmodes in the j^{th} pillbox cell oscillate at frequency ω_n ;

All the fields satisfy Maxwell Equations. Boundary conditions:

$$\vec{E}_j \times n = 0 \text{ on } S_j; \vec{E}_{j,n} \times n = 0 \text{ on } S_j + S'_j + S''_j.$$

Appendix 11: Travelling–Wave acceleration structures.

We consider the following:

$$\begin{aligned} \int_{V_j} \vec{\nabla} \cdot (\vec{E}_j \times \vec{H}_{j,n}^*) dV &= \int_{V_j} [\vec{H}_{j,n}^* \cdot (\vec{\nabla} \times \vec{E}_j) - \vec{E}_j \cdot (\vec{\nabla} \times \vec{H}_{j,n}^*)] dV \\ &= \int_{V_j} [-i\omega\mu_0 \vec{H}_j \cdot \vec{H}_{j,n}^* - i\omega_n \epsilon_0 \cdot \vec{E}_{j,n}^* \cdot \vec{E}_j] dV \end{aligned}$$

Using Gauss theorem and boundary conditions we have

$$\omega_n \epsilon_0 \int_{V_j} \vec{E}_{j,n}^* \cdot \vec{E}_j dV - \omega \mu_0 \int_{V_j} \vec{H}_j \cdot \vec{H}_{j,n}^* dV = \frac{1}{i} \int_{S'_j + S''_j} (\vec{E}_j \times \vec{H}_{j,n}^*) \cdot dS \quad (1)$$

Similarly, by considering

$$\int_{V_j} \vec{\nabla} \cdot (\vec{H}_j \times \vec{E}_{j,n}^*) dV$$

we have

$$\omega \epsilon_0 \int_{V_j} \vec{E}_{j,n}^* \cdot \vec{E}_j dV - \omega_n \mu_0 \int_{V_j} \vec{H}_j \cdot \vec{H}_{j,n}^* dV = 0 \quad (2)$$

The eigenmode expansion:

$$\begin{aligned} \vec{E}_j &= \sum X_{j,n} \vec{E}_{j,n} \\ \vec{H}_j &= \sum Y_{j,n} \vec{H}_{j,n} \end{aligned}$$

Appendix 11: Travelling–Wave acceleration structures:

By using (1) and (2) we obtain

$$X_{j,n} = -\frac{i\omega_n}{\omega^2 - \omega_n^2} \cdot \frac{\int_{S'_j+S''_j} (\vec{E}_j \times \vec{H}_{j,n}^*) \cdot dS}{2W_{j,n}} \quad (3)$$

$$Y_{j,n} = \frac{i\omega}{\omega^2 - \omega_n^2} \cdot \frac{\int_{S'_j+S''_j} (\vec{E}_j \times \vec{H}_{j,n}^*) \cdot dS}{2W_{j,n}}$$

The eigenmode amplitudes are determined by tangential electric field on the holes, E_{rj}

How to find E_{rj} for small holes?

1. Quasi-static approximation:

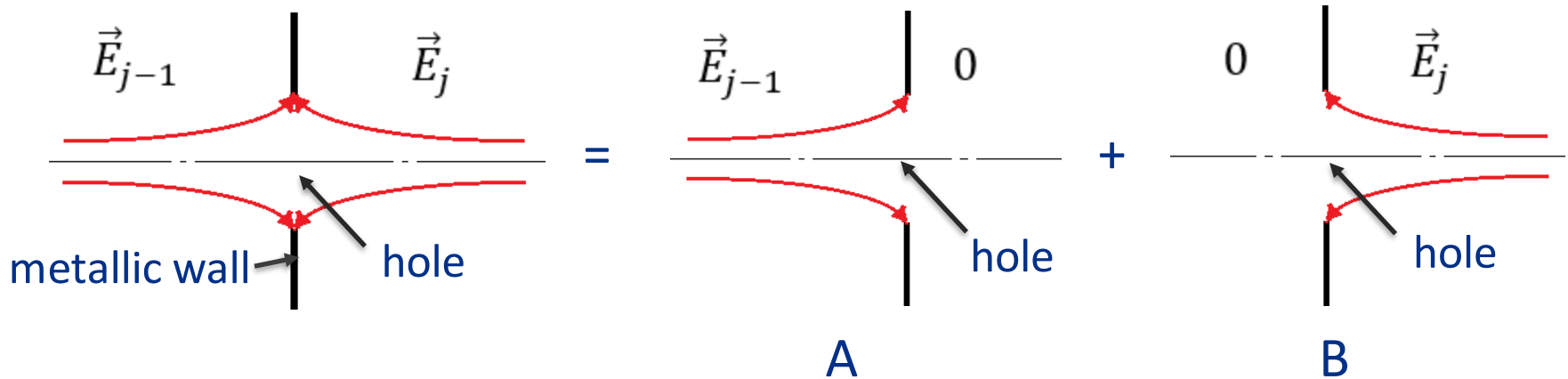
We have: $\Delta \vec{E}_j + k^2 \vec{E}_j = 0$, $k^2 = \frac{\omega^2}{c^2}$

For a small hole, $a \ll \lambda_n$. It means that $\Delta \vec{E}_j \sim \frac{\vec{E}_j}{a^2} \gg k^2 \vec{E}_j = \left(\frac{\omega}{c}\right)^2 \vec{E}_j$ and $\Delta \vec{E}_j \approx 0$ i.e., it means that $\vec{E}_j = \vec{\nabla} \Phi$, $\Delta \Phi = 0$ or electric field is quasi-static.

Far from the holes electric field has only longitudinal (accelerating) component!

Appendix 11: Travelling–Wave acceleration structures:

2. Superposition:



3. Electrostatic problem: conducting sheet at $z=0$ with a circular hole of the radius a , at $z=-\infty$ the field is homogeneous, $E_z=E_0$; at $z=\infty$ the field $E=0$: problem A above. The problem has analytical solution.*

We need to define the radial electric field at the hole, or at $z=0$.

* W.R. Smythe, Static and Dynamic Electricity, 1939, p. 159

Appendix 11: Travelling-Wave acceleration structures:

Oblate spheroidal coordinates:

$$\frac{z^2}{\zeta^2} + \frac{r^2}{1 + \zeta^2} = a^2 \quad \text{spheroids}$$

$$-\frac{z^2}{\xi^2} + \frac{r^2}{1 - \xi^2} = a^2 \quad \text{hyperboloids}$$

$$r = a[(1 + \zeta^2)(1 - \xi^2)]^{1/2}$$

$$z = a\zeta\xi$$

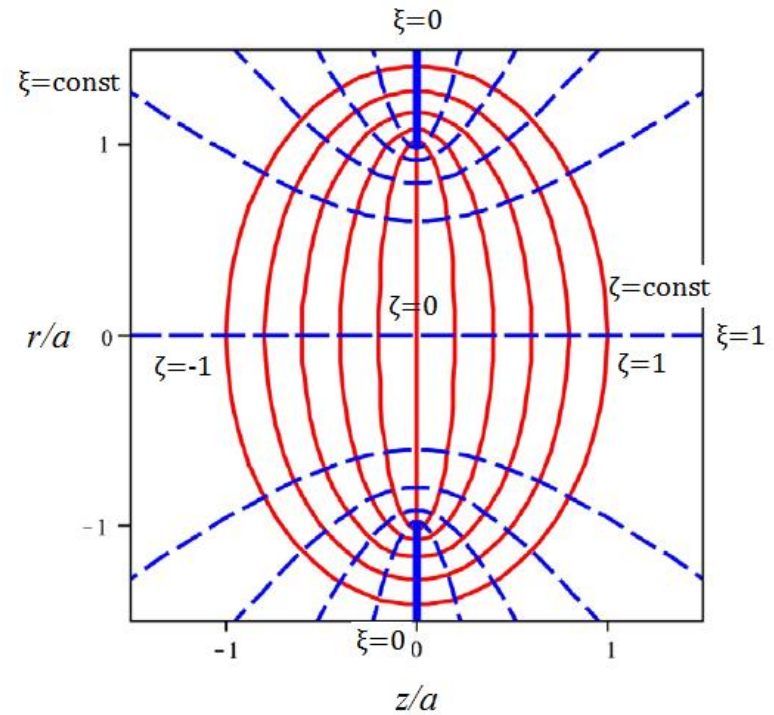
$$\Delta\Phi = 0$$



$$\Phi(\xi, \zeta) = aE_0\xi \left[\zeta - \frac{1}{\pi}(\zeta \cot^{-1}\zeta - 1) \right]$$

$$E_r(r, 0) = \frac{1}{h_1} \nabla_\xi(\Phi(\xi, \zeta)|_{\zeta=0}) = E_0 \frac{(1 - \xi^2)^{1/2}}{\pi\xi} = E_0 \frac{r}{\pi(a^2 - r^2)^{1/2}}$$

$$E_z(r, 0) = \frac{1}{h_2} \nabla_\zeta(\Phi(\xi, \zeta)|_{\zeta=0}) = \frac{1}{2}E_0$$



Lamet coefficients

$$h_1 = a \left(\frac{\xi^2 - \zeta^2}{1 - \xi^2} \right)^{1/2}$$

$$h_2 = a \left(\frac{\xi^2 - \zeta^2}{1 + \zeta^2} \right)^{1/2}$$

Appendix 11: Travelling–Wave acceleration structures:

For TM_{010} mode in a pillbox near the axis (see slide 110):

$$E_{j,r}(r)|_{S'_j} = E_0 \frac{r}{\pi(a^2 - r^2)^{1/2}} [X_{j-1} - X_j]$$

$$E_{j,r}(r)|_{S''_j} = E_0 \frac{r}{\pi(a^2 - r^2)^{1/2}} [X_j - X_{j+1}]$$

$$H_{j,\varphi}(r) \approx -iE_0 \frac{(\frac{\omega_0}{c})r}{2Z_0}$$

and from (3), slide 108, we have:

$$X_j \left[1 - (1 + K) \frac{\omega_0^2}{\omega^2} \right] + \frac{1}{2} K \frac{\omega_0^2}{\omega^2} [X_{j-1} + X_{j+1}] = 0 \quad (4)$$

where K is the coupling, dimensionless parameter:

$$K = \frac{2E_0^2 a^3}{3Z_0 W_0 c} = \frac{2}{3} \cdot \frac{R/Q}{Z_0} \cdot \frac{k_0 a^3}{d^2 T^2} \quad k_0 = \frac{\omega_0}{c}$$

$K \sim a^3$. For a thick wall $K \sim a^\eta$, $\eta > 3$ (field decays in the coupling hole).

THE PHYSICAL REVIEW

A journal of experimental and theoretical physics established by E. L. Nichols in 1893

SECOND SERIES, VOL. 66, Nos. 7 AND 8

OCTOBER 1 AND 15, 1944

Theory of Diffraction by Small Holes

H. A. BETHE

Department of Physics, Cornell University, Ithaca, New York

(Received January 26, 1942)

Appendix 11: Travelling–Wave acceleration structures:

In the infinite chain of cavities equation (4) has solution (travelling wave):

$$X_j = X e^{ij\varphi}$$

and

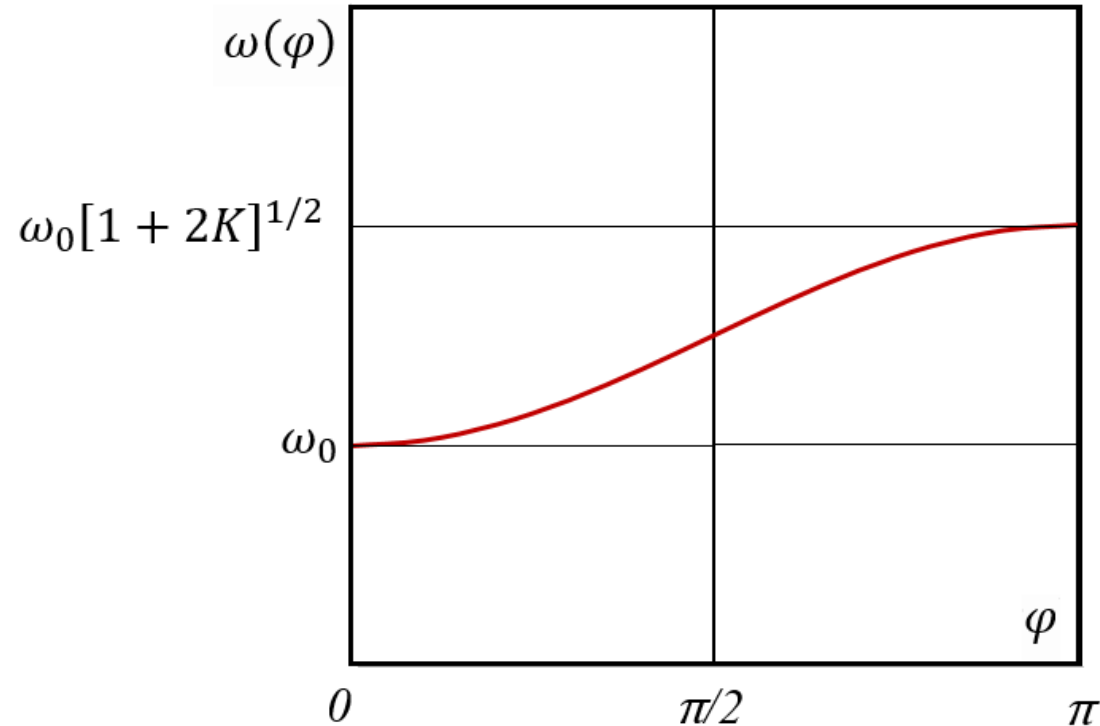
$$\omega(\varphi) = \omega_0 [1 + K(1 - \cos\varphi)]^{1/2}$$

For small K we have:

$$\omega(\varphi) \approx \omega_0 [1 + \frac{1}{2}K(1 - \cos\varphi)]$$

One can see that

$$K = \frac{\omega(\pi) - \omega(0)}{\omega(0)}$$



Appendix 11: Travelling–Wave acceleration structures.

The 2d Bell theorem, illustration:

For a pillbox structure:

The fields on the hole are equal to

$$E_{j,r}(r)|_{S'_j} = E_0 \frac{r}{\pi(a^2 - r^2)^{1/2}} [X_{j-1} - X_j]$$

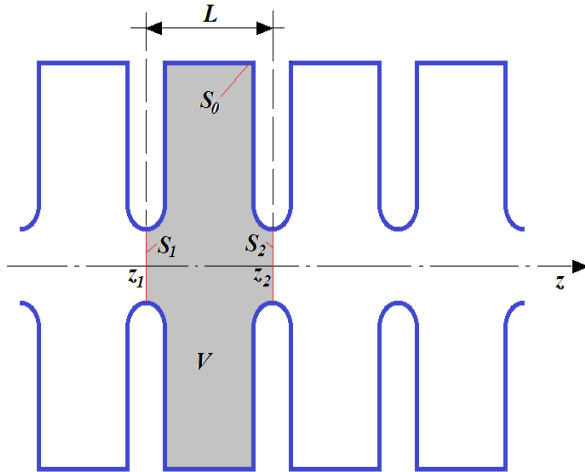
$$H_{j,\phi}(r)|_{S'_j} \approx -iE_0 \frac{\left(\frac{\omega_0}{c}\right) r}{4Z_0} [X_{j-1} + X_j]$$

(E_z and H_ϕ on the hole are two times smaller than in the cell center, see slides 110-111).

Therefore, we have

$$\begin{aligned} v_{gr} &= \frac{P}{\frac{|X_j|^2 W_0}{d}} = \frac{\frac{1}{2} \text{Re} \int E_r H_\phi^* dS}{\frac{|X_j|^2 W_0}{d}} = \frac{\omega_0 E_0^2 a^3 d}{6Z_0 W_0 c} \text{Re}[i(X_{j-1} - X_j)(X_{j-1}^* + X_j^*)] = \\ &= \frac{\omega_0 E_0^2 a^3 d}{3Z_0 W_0 c} \sin(\varphi) = \frac{\omega_0 d}{2} K \sin(\varphi) = c \frac{\pi K d}{\lambda} \sin(\varphi) = \frac{d\omega}{dk_z} \end{aligned}$$

Bell theorems for periodic acceleration structures, proof



I. Floquet Theorem

“For a given mode of propagation in a periodic system at given steady-state frequency the fields at one cross section differ from that one period away only by complex constant”.

$$\begin{aligned}\vec{E}(x, y, z_2) &= \vec{E}(x, y, z_1)e^{-ik_z L} \\ \vec{H}(x, y, z_2) &= \vec{H}(x, y, z_1)e^{-ik_z L} \\ z_2 &= z_1 + L\end{aligned}\quad (1)$$

II. 1st Bell Theorem

“The time-average electrical stored energy per period is equal to the time-average magnetic stored energy per period in the passband”.

Consider the periodic structure to be divided by a series of surfaces perpendicular to the axis spaced by the periodic distance L . One cell of the structure having the volume V is surrounded by these surfaces S_1 and S_2 and the ideal metal boundary S_0 . Let's consider the integral over the surface surrounding the cell, which equals to zero:

$$\oint \vec{E} \times \vec{H}^* \cdot d\vec{s} = \int_{S_0} \vec{E} \times \vec{H}^* \cdot d\vec{s} + \int_{S_1} \vec{E} \times \vec{H}^* \cdot d\vec{s} + \int_{S_2} \vec{E} \times \vec{H}^* \cdot d\vec{s} = 0 \quad (2)$$

This is because we have

$$\int_{S_0} \vec{E} \times \vec{H}^* \cdot d\vec{s} = 0 \text{ because } E_t = 0 \text{ on } S_0$$

$$\text{and } \int_{S_1} \vec{E} \times \vec{H}^* \cdot d\vec{s} + \int_{S_2} \vec{E} \times \vec{H}^* \cdot d\vec{s} = 0 \text{ because of (1) and } d\vec{s}_2 = -d\vec{s}_1$$

Bell theorems for periodic acceleration structures, proof

From Maxwell equations

$$\text{curl} \vec{E} = -i\omega\mu_0 \vec{H} \quad (3)$$

$$\text{curl} \vec{E}^* = i\omega\mu_0 \vec{H}^*$$

and (2) we have

$$\oint \vec{E} \times \text{curl} \vec{E}^* \cdot d\vec{s} = 0$$

Applying Gauss's theorem, we get:

$$\int_V \text{div}(\vec{E} \times \text{curl} \vec{E}^*) dv = 0. \quad (4)$$

Using the vector theorem (see Appendix 1)

$$\text{div}(\vec{A} \times \vec{B}) = \vec{B} \cdot \text{curl} \vec{A} - \vec{A} \cdot \text{curl} \vec{B}, \quad (5)$$

we get:

$$\int_V (\text{curl} \vec{E}^*) \cdot (\text{curl} \vec{E}) dv - \int_V \vec{E} \cdot (\text{curl}(\text{curl} \vec{E}^*)) dv = 0.$$

Using Maxwell's equations (3) and the homogenous wave equation derived therefrom (see Lecture 10)

$$\text{curl}(\text{curl} \vec{E}^*) = \omega^2 \mu_0 \varepsilon_0 \vec{E}^* \quad (6)$$

we get

$$\int_V (-i\omega\mu_0 \vec{H}) \cdot (i\omega\mu_0 \vec{H}^*) dv - \int_V \vec{E} \cdot (\omega^2 \mu_0 \varepsilon_0 \vec{E}^*) dv = 0$$

Dividing through $4\omega^2 \mu_0$ yields:

$$\frac{1}{4} \int_V \mu_0 |\vec{H}|^2 dv = \frac{1}{4} \int_V \varepsilon_0 |E|^2 dv = W/2,$$

quod erat demonstrandum.

Here W is total energy of electromagnetic field per period,

$$W = \frac{1}{2} \int_V \varepsilon_0 \vec{E} \cdot \vec{E}^* dv = \frac{1}{2} \int_V \mu_0 \vec{H} \cdot \vec{H}^* dv$$

Bell theorems for periodic acceleration structures, proof

III. 2^d Bell Theorem

“The time-average power flow in the pass band is equal to the group velocity times time-average electro-magnetic stored energy per period divided by the period.”

Consider (4) wherein \vec{E} and \vec{E}^* are functions of frequency ω . Differentiate with respect to frequency:

$$\frac{\partial}{\partial \omega} \int_V \operatorname{div}(\vec{E} \times \operatorname{curl} \vec{E}^*) dv = 0.$$

It gives:

$$\int_V \operatorname{div} \left(\frac{\partial \vec{E}}{\partial \omega} \times \operatorname{curl} \vec{E}^* \right) dv + \int_V \operatorname{div} \left(\vec{E} \times \operatorname{curl} \frac{\partial \vec{E}^*}{\partial \omega} \right) dv = 0.$$

Using the vector identity equation (5), we get

$$\begin{aligned} & \int_V (\operatorname{curl} \vec{E}^*) \cdot \left(\operatorname{curl} \frac{\partial \vec{E}}{\partial \omega} \right) dv - \int_V \frac{\partial \vec{E}}{\partial \omega} \cdot (\operatorname{curl}(\operatorname{curl} \vec{E}^*)) dv + \\ & + \int_V (\operatorname{curl} \vec{E}) \cdot \left(\operatorname{curl} \frac{\partial \vec{E}^*}{\partial \omega} \right) dv - \int_V \vec{E} \cdot \left(\operatorname{curl}(\operatorname{curl} \frac{\partial \vec{E}^*}{\partial \omega}) \right) dv = 0 \end{aligned} \quad (7)$$

Differentiation (6) with respect to ω gives

$$\operatorname{curl}(\operatorname{curl} \frac{\partial \vec{E}^*}{\partial \omega}) = 2\omega \mu_0 \epsilon_0 \vec{E}^* + \omega^2 \mu_0 \epsilon_0 \frac{\partial \vec{E}^*}{\partial \omega}$$

Using this in the second and fourth integrals of (7)

$$\begin{aligned} & \int_V (\operatorname{curl} \vec{E}^*) \cdot \left(\operatorname{curl} \frac{\partial \vec{E}}{\partial \omega} \right) dv - \omega^2 \mu_0 \epsilon_0 \int_V \frac{\partial \vec{E}}{\partial \omega} \cdot \vec{E}^* dv + \\ & + \int_V (\operatorname{curl} \vec{E}) \cdot \left(\operatorname{curl} \frac{\partial \vec{E}^*}{\partial \omega} \right) dv - 2\omega \mu_0 \epsilon_0 \int_V \vec{E} \cdot \vec{E}^* dv - \omega^2 \mu_0 \epsilon_0 \int_V \frac{\partial \vec{E}^*}{\partial \omega} \cdot \vec{E} dv = 0 \end{aligned}$$

which is

$$2\operatorname{Re} \left\{ \int_V (\operatorname{curl} \vec{E}^*) \cdot \left(\operatorname{curl} \frac{\partial \vec{E}}{\partial \omega} \right) dv - \int_V \frac{\partial \vec{E}}{\partial \omega} \cdot (\operatorname{curl}(\operatorname{curl} \vec{E}^*)) dv \right\} - 2\omega \mu_0 \epsilon_0 \int_V \vec{E} \cdot \vec{E}^* dv = 0.$$

Bell theorems for periodic acceleration structures, proof

Using (5) in reverse,

$$2\text{Re} \left\{ \int_V \text{div} \left(\frac{\partial \vec{E}}{\partial \omega} \times \text{curl} \vec{E}^* \right) dv \right\} - 2\omega \mu_0 \epsilon_0 \int_V \vec{E} \cdot \vec{E}^* dv = 0.$$

and using Gauss's theorem on the first term,

$$2\text{Re} \left\{ \oint \frac{\partial \vec{E}}{\partial \omega} \times \text{curl} \vec{E}^* \cdot d\vec{s} \right\} - 2\omega \mu_0 \epsilon_0 \int_V \vec{E} \cdot \vec{E}^* dv = 0. \quad (8)$$

Integral $\int_{S_0} \frac{\partial \vec{E}}{\partial \omega} \times \text{curl} \vec{E}^* \cdot d\vec{s} = 0$ because of boundary conditions on the ideal metal surface.

From Floquet theorem (1) the following relation hold:

$$\begin{aligned} \vec{E}(x, y, z_2) &= \vec{E}(x, y, z_1) e^{-ik_z L} \\ \text{curl} \vec{E}^*(x, y, z)|_{z=z_2} &= \text{curl} \vec{E}^*(x, y, z)|_{z=z_1} e^{ik_z L} \end{aligned} \quad (9)$$

$$\vec{E}^*(x, y, z_2) = \vec{E}^*(x, y, z_1) e^{ik_z L}$$

$$\frac{\partial \vec{E}(x, y, z_2)}{\partial \omega} = \frac{\partial \vec{E}(x, y, z_1)}{\partial \omega} e^{-ik_z L} - iL \frac{dk_z}{d\omega} \vec{E}(x, y, z_1) e^{-ik_z L}$$

Separating the surface integral of (8)

$$2\text{Re} \left\{ \int_{S_1} \frac{\partial \vec{E}(x, y, z_1)}{\partial \omega} \times \text{curl} \vec{E}^*(x, y, z)|_{z=z_1} \cdot d\vec{s} + \int_{S_2} \frac{\partial \vec{E}(x, y, z_2)}{\partial \omega} \times \text{curl} \vec{E}^*(x, y, z)|_{z=z_2} \cdot d\vec{s} \right\} -$$

$$2\omega \mu_0 \epsilon_0 \int_V \vec{E} \cdot \vec{E}^* dv = 0$$

and substituting equations (9)

$$2\text{Re} \left\{ \int_{S_1} \frac{\partial \vec{E}(x, y, z_1)}{\partial \omega} \times \text{curl} \vec{E}^*(x, y, z)|_{z=z_1} \cdot d\vec{s} +$$

$$\int_{S_2} \frac{\partial \vec{E}(x, y, z_1)}{\partial \omega} \times \text{curl} \vec{E}^*(x, y, z)|_{z=z_1} \cdot d\vec{s} - iL \frac{dk_z}{d\omega} \int_{S_2} \vec{E}(x, y, z_1) \times \text{curl} \vec{E}^*(x, y, z)|_{z=z_1} \cdot d\vec{s} \right\} -$$

$$2\omega \mu_0 \epsilon_0 \int_V \vec{E} \cdot \vec{E}^* dv = 0$$

Bell theorems for periodic acceleration structures, proof

Since $d\vec{s}_2 = -d\vec{s}_1$ the first two integrals cancel. Using Maxwell equation (3) and condition s (9) we get

$$2\text{Re} \left\{ \omega \mu_0 L \frac{dk_z}{d\omega} \int_{S_2} \vec{E}(x, y, z_2) \times \vec{H}^*(x, y, z_2) \cdot d\vec{s} \right\} - 2\omega \mu_0 \varepsilon_0 \int_V \vec{E} \cdot \vec{E}^* dv = 0$$

Multiplying by $\frac{1}{4\omega \mu_0 L} \frac{d\omega}{dk_z}$ we finally have

$$\frac{1}{2} \text{Re} \left\{ \int_{S_2} \vec{E}(x, y, z_2) \times \vec{H}^*(x, y, z_2) \cdot d\vec{s} \right\} = \frac{d\omega}{dk_z} \cdot \frac{1}{L} \cdot \frac{1}{2} \int_V \varepsilon_0 \vec{E} \cdot \vec{E}^* dv = 0$$

or

$$P = v_{gr} w,$$

here

$P = \frac{1}{2} \text{Re} \left\{ \int_{S_2} \vec{E}(x, y, z_2) \times \vec{H}^*(x, y, z_2) \cdot d\vec{s} \right\}$ is the time averaged power flow in the passbands;

$v_{gr} = \frac{d\omega}{dk_z}$ is a group velocity;

$w = \frac{1}{L} \cdot \frac{1}{2} \int_V \varepsilon_0 \vec{E} \cdot \vec{E}^* dv = \frac{1}{L} \cdot \frac{1}{2} \int_V \mu_0 \vec{H} \cdot \vec{H}^* dv = \frac{W}{L}$ is the time-averaged stored electromagnetic energy per unit length.

[1] J.S. Bell, "Group velocity and energy velocity in periodic waveguides," Harwell, AERE-T-R-858 (1952)

[2] D.A. Watkins, Topics in Electromagnetic Theory, John Willey & Sons, Inc. London, 1958

[3] E. A. Burshtein, and G. B. Voskresensky, The Intensive Beam Electron Linear Accelerators, Atomizdat, Moscow, 1970.

Appendix 12: Standing –Wave acceleration structures.

Perturbation theory.

In matrix form Eq(1), see Lecture 8, Slide 31:

$$M\hat{X} - \frac{\omega_0^2}{\omega^2}\hat{X} = 0$$

here $M_{jj} = 1; j = 0, 1, \dots, N;$

$$M_{jj-1} = \frac{K}{2W(j)}; j = 1, 2, \dots, N; M_{jj+1} = \frac{K}{2W(j)}; j = 0, 1, \dots, N - 1.$$

and $W(j) = 1, j = 1, 2, \dots, N - 1$ $W(j) = \frac{1}{2}, j = 0, N$

Eigenvectors and eigenvalues:

$$\hat{X}_j^q = \cos \frac{\pi q j}{N}; \omega_q^2 = \frac{\omega_0^2}{1 + K \cos \frac{\pi q}{N}}, q = 0, 1, \dots, N$$

Orthogonality:

$$\hat{X}^q \cdot \hat{X}^r \equiv \sum_{j=0}^N W(j) \hat{X}_j^q \hat{X}_j^r = \frac{N \delta_{qr}}{2W(q)}, \delta_{qq} = 1, \text{ and } \delta_{qr} = 0, \text{ if } q \neq r$$

Appendix 12: Standing –Wave acceleration structures.

Perturbation theory

- Perturbation of the cell resonance frequencies causes perturbation of the mode resonance frequencies $\delta\omega_q$;
- the field distribution $\delta\hat{X}^q$.

$$\omega_{0j}^{2'} = \omega_0^2 + \delta\omega_{0j}^2 \rightarrow \hat{X}^{q'} = \hat{X}^q + \delta\hat{X}^q, \quad \hat{X}^q \cdot \delta\hat{X}^q$$

Variation of the equation (1), see previous

slide, gives $M\delta\hat{X}^q = \frac{\omega_0^2}{\omega_q^2} \left[\delta\hat{X}^q + \Omega\hat{X}^q - \frac{\delta\omega_q^2}{\omega_q^2} \hat{X}^q \right]$, where $\Omega = \begin{bmatrix} \frac{\delta\omega_{01}^2}{\omega_0^2} & \dots & 0 \\ \vdots & \ddots & \vdots \\ 0 & \dots & \frac{\delta\omega_{0N}^2}{\omega_0^2} \end{bmatrix}$

$$\frac{\delta\omega_q^2}{\omega_q^2} = [2W(q)/N] \cdot \hat{X}^q \Omega \hat{X}^q;$$

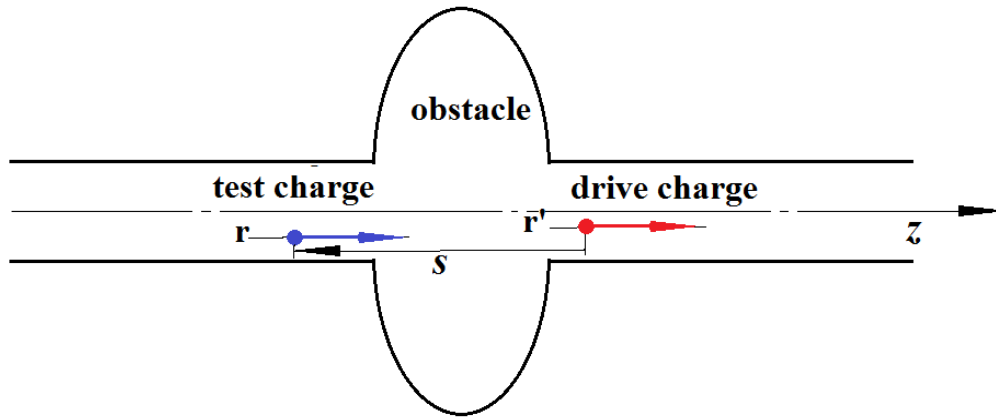
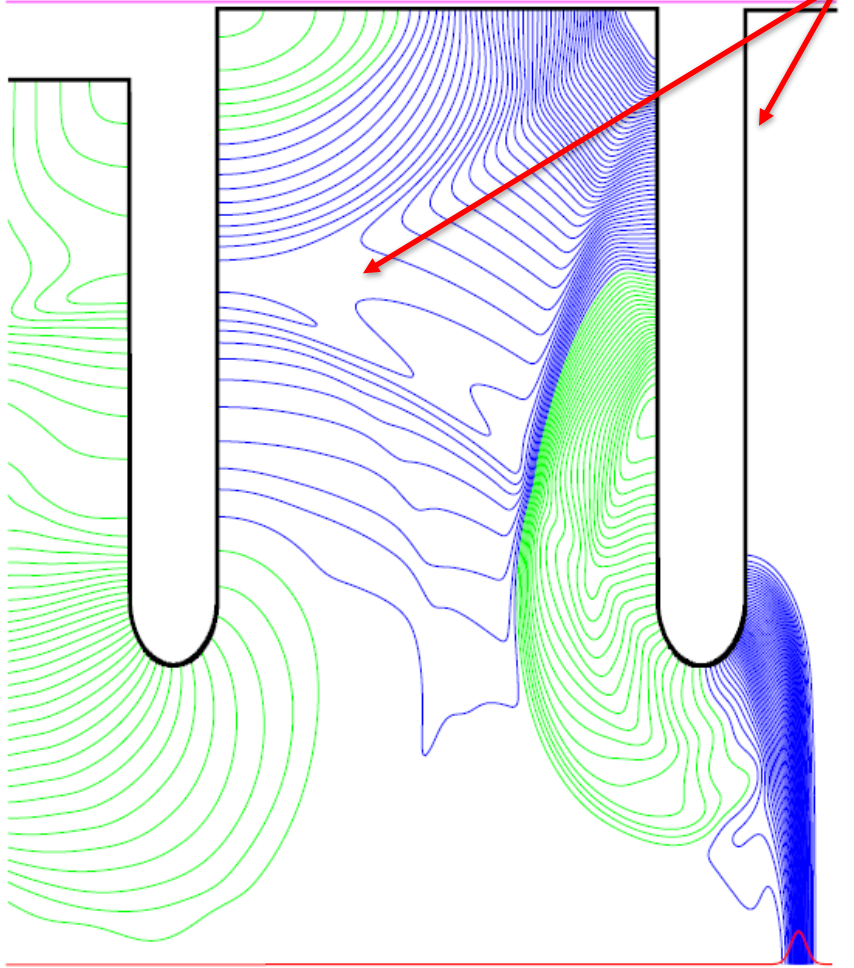
$$\delta\hat{X}^q = \sum_{q' \neq q} \frac{2W(q') \hat{X}^q \Omega \hat{X}^q}{N \left(\frac{\omega_q^2}{\omega_{q'}^2} - 1 \right)} \hat{X}^{q'}$$

$$|\delta\hat{X}^q| \sim \frac{|\delta\omega_{0j}|_{av}}{|\omega_q - \omega_{q\pm 1}|}$$

Appendix 13: Wake potentials

Acceleration cells

Radiation fields in the TW acceleration structure



$$W_z(\vec{r}, \vec{r}', s) = -\frac{1}{q} \int_{z_1}^{z_2} dz [E_z(\vec{r}, z, t)]_{t=(z+s)/c}$$

$$\vec{W}_\perp(\vec{r}, \vec{r}', s) = \frac{1}{q} \int_{z_1}^{z_2} dz [\vec{E}_\perp + c(\hat{z} \times \vec{B})]_{t=(z+s)/c}$$

A. Novokhatski

Blue – deceleration
Green - acceleration

bunch

$$W_z=0, W_\perp=0 \text{ for } s < 0$$

Appendix 13: Wake potentials

Loss and kick distribution along the bunch $V_z(s)$ and $V_{\perp}(s)$:

$$V_z(s) = \int_0^{\infty} ds' \lambda(s-s') W_z(s') = \int_{-\infty}^s ds' \lambda(s') W_z(s-s'),$$

$$\vec{V}_{\perp}(s) = \int_0^{\infty} ds' \lambda(s-s') \vec{W}_{\perp}(s') = \int_{-\infty}^s ds' \lambda(s') \vec{W}_{\perp}(s-s').$$

$\lambda(s)$ is the charge distribution along the bunch.

Total losses and kick:

$$\Delta U = \int_{-\infty}^{\infty} ds \lambda(s) V_z(s), \quad k_{\ell} = \frac{\Delta U}{q^2} \equiv \frac{1}{q^2} \int_{-\infty}^{\infty} ds \lambda(s) V_z(s) \quad k_{\ell} - \text{loss factor}$$

$$k_{HOM} = k_{\ell} - \frac{1}{4} R/Q \cdot \omega |_{\text{acc. mode}}$$

$$\vec{p}_{\perp} = q^2 \vec{k}_{\perp} / c \quad \vec{k}_{\perp} \equiv \frac{1}{q^2} \int_{-\infty}^{\infty} ds \lambda(s) \vec{V}_{\perp}(s) \quad \vec{k}_{\perp} - \text{kick factor}$$

Appendix 13: Wake potentials

Panofsky-Wenzel theorem for wakes:

$$\frac{\partial \vec{W}_\perp}{\partial s} = \frac{c}{eq} \frac{\partial \vec{p}_\perp}{\partial s} = -\frac{1}{q} \int_0^L dz \left[\vec{\nabla}_\perp E_z(z, t) \right]_{t=(s+z)/c} = \vec{\nabla}_\perp W_z .$$

Relation between wake and impedance:

$$Z(\omega) = \int_0^\infty W_z(\tau) \exp\{-i\omega\tau\} d\tau \equiv \widetilde{W}_z(\tau) ,$$

$$s = c\tau = ct - z$$

$$Z(k) = \int_0^\infty W_z(s) \exp\{-iks\} ds \equiv \widetilde{W}_z(s) = c[Z(\omega)]_{\omega=kc}$$

and

$$k_\ell = \frac{\Delta U}{q^2} = \frac{1}{\pi q^2} \int_0^\infty Z_R(\omega) I^2(\omega) d\omega .$$